Historical Trends and Future Projections of Climate and Streamflow in the Willamette Valley and Rogue River Basins

June 2015

A Report to the US Army Corps of Engineers Portland District Office

Prepared by
The Oregon Climate Change Research Institute

Detroit Dam and Detroit Reservoir-Oregon, August 2011. Photo by Doug Kerr under Creative Commons License (CC BY-SA 2.0)

Historical Trends and Future Projections of Climate and Streamflow in the Willamette Valley and Rogue River Basins

A report to the US Army Corps of Engineers Portland District Office

Prepared by:
Meghan Dalton, David Rupp, Kathie Dello, Philip Mote
Oregon Climate Change Research Institute
College of Earth, Ocean, and Atmospheric Sciences
104 CEAOS Admin Building
Oregon State University
Corvallis, OR 97331

Information and guidance provided by the following list of USACE PDT:
Alan Donner (NWP)
Keith Duffy (NWP)
Laurie Nicholas (NWP)
Mary Karen Scullion (NWP)
Kathryn Tackley (NWP)
Daniel Turner (NWP)
Jason Ward (NWD)
Kathryn Warner (NWP)

June 2015

Table of Contents

LIST OF FIGURES 1

LIST OF TABLES 4

EXECUTIVE SUMMARY 5

INTRODUCTION 10

OBSERVED DATASETS & METHODS 12

Temperature & Precipitation 12
Snow Water Equivalent (SWE) 13
Streamflow 14
Historical Trend Analysis Methods 17

MODELED DATASETS & METHODS 18

Global Climate Models 18
Emissions Scenarios 18
Climate & SWE Simulations 21
Climate Projections Methods 22
Streamflow Simulations 22
Streamflow Projections Methods 25

RESULTS 26

Temperature 26
Precipitation 31
Snow Water Equivalent (SWE) 35
Wind Speed 43
Cloud Cover 44
Streamflow Volumes 45
Flow-Duration-Frequency 80

CONCLUSIONS 86

Historical Observed Changes 86
Future Climate Projections 87
Future Streamflow Projections 88
Implications 91
Uncertainties & Limitations 92
Data Gaps 93

REFERENCES 94

APPENDIX A. GLOBAL CLIMATE MODELS 99

APPENDIX B. DATASETS 101

APPENDIX C. TEMPERATURE PROJECTIONS 102

APPENDIX D. PRECIPITATION PROJECTIONS 118

APPENDIX E. SNOW WATER EQUIVALENT PROJECTIONS 126

APPENDIX F. PROJECTIONS OF FUTURE STREAMFLOW 142

APPENDIX G. PROJECTED CHANGES TO FLOW-DURATION-FREQUENCY CURVES OF ANNUAL MAXIMUM FLOWS 186

List of Figures

Figure 1 The Willamette River Basin with USACE Projects 12
Figure 2 Rogue River Basin Projects 13
Figure 3 Fossil fuel emissions and carbon dioxide concentrations driving the four scenarios of future climate and hydrology projections used in this project. Data: live.magicc.org (Meinhauser et al., 2011) 21
Figure 4 Location of Columbia Basin Climate Change Scenarios Project (CBCCSP) routed streamflow projections in the Willamette Basin. Labeled sites in red have complete datasets available. 24
Figure 5 Annual trends in maximum (left) and minimum (right) temperature for 10 USHCN stations in the Willamette and Rogue. Large circles denote statistically significant trends. 29
Figure 6 Annual and seasonal multi-model mean projections in maximum temperature for RCP4.5 and RCP8.5 31
Figure 7 Annual precipitation trends from 10 USHCN stations in the Willamette and Rogue Basins. Large circles denote statistically significant trends 33
Figure 8 Annual and seasonal multi-model mean projected changes in precipitation for RCP4.5 and RCP8.5 35
Figure 9 April 1 SWE trends (cm/year) from 1960-2014 at SNOTEL/Snow Course sites in the Willamette and Rogue. Large circles denote statistically significant trends. 38
Figure 10 Simulated historic and future basin-averaged, 30-year mean snow water equivalent (SWE) on the first day of the month as a percentage of accumulated water year precipitation for the North Santiam basin (17090005; upper panel) and Middle Willamette basin (17090007; lower panel). The solid line and shading give the mean and 5th to 95th percentile range, respectively, of simulations from 10 GCMs 39
Figure 11 "Box and whisker" plots showing changes in SWE/P. For each season, the figures indicate the distribution of projections from different GCMs of basin-averaged, 30-year mean snow water equivalent (SWE) on the first day of the month as a percentage of accumulated water year precipitation for the North Santiam basin (17090005). Individual GCM projections are given by the circles, and the box and whiskers show the median, inner quartile range, and 5th and 95th percentiles. 40
Figure 12 Seasonal mean change from simulated historical to future basin-averaged, 30-year mean snow water equivalent (SWE) on the first day of the month as a percentage of accumulated water year precipitation. Changes are averaged over simulations from 10 GCMS and are calculated as relative differences. Non-shaded basins have less than a 1% mean SWE/P over the baseline period. 42
Figure 13 Average wind speed monthly climatology for simulated historic (1970-1999) and future (2030-2059) for the Lower Willamette basin (17090012). The solid line and shading give the mean and 5th to 95th percentile range, respectively, of simulations from 20 GCMs. 43
Figure 14 Projected changes by 2030-2059 in monthly cloud cover for Middle Fork Willamette (17090001). Percent of days in each month, in which skies are clear, scattered, broken, or overcast as defined in Table 5. Solid lines and shading denote the multi-model mean and 5th to 95th percentile range across 20 GCMs, respectively. 45

Figure 15 5th, 50th, and 95th percentiles of monthly observed streamflow Willamette River at Albany (1892-2014; top) and Rogue River at Raygold (1905-2014; bottom). 46
Figure 16 Historical streamflow for selected gages in the Willamette and Rogue River Basins reflecting conditions in the periods 1941-1970 and 1981-2010. 48
Figure 17 Mean annual hydrograph of daily simulated, bias-corrected, naturalized streamflow at North Santiam River below Boulder Creek near Detroit (NOSAN 4056, USGS 14178000) for the historical period and hybrid-delta A1B and B1 future scenarios. Thin lines show each of the 19 individual simulations. 53
Figure 18 Mean annual hydrograph of monthly simulated, bias-corrected, naturalized streamflow at North Santiam River below Boulder Creek near Detroit (NOSAN 4056, USGS 14178000) for the historical period and hybrid-delta A1B and B1 future scenarios..... 54
Figure 19 5th, 50th, and 95th percentiles of monthly simulated, bias-corrected, naturalized streamflow at North Santiam River below Boulder Creek near Detroit (NOSAN 4056, USGS 14178000) for the historical period and the A1B and B1 future scenarios. 55
Figure 20 5th, 50th, and 95th percentiles of winter (DJF) and summer (JJAS) simulated, bias-corrected, naturalized streamflow at North Santiam River below Boulder Creek near Detroit (NOSAN 4056, USGS 14178000) for the historical period and hybrid-delta A1B and B1 future scenarios. 56
Figure 21 Mean annual hydrograph of daily simulated, bias-corrected, naturalized streamflow at Row River above Pitcher Creek near Dorena (ROPIT 4035, USGS 14154500) for the historical (1970-1999) and A1B and B1 future scenarios (2030-2059)..... 58
Figure 22 Mean annual hydrograph of monthly simulated, bias-corrected, naturalized streamflow at Row River above Pitcher Creek near Dorena (ROPIT 4035, USGS 14154500) for the historical (1970-1999) and A1B and B1 future scenarios (2030-2059)..... 59
Figure 23 5th, 50th, and 95th percentiles of monthly simulated, bias-corrected, naturalized streamflow at Row River above Pitcher Creek near Dorena (ROPIT 4035, USGS 14154500) for the historical period and the A1B and B1 future scenarios..... 60
Figure 24 5th, 50th, and 95th percentile of winter (DJF) and summer (JJAS) simulated, bias-corrected, naturalized streamflow at Row River above Pitcher Creek near Dorena (ROPIT 4035, USGS 14154500) for the historical period and hybrid-delta A1B and B1 future scenarios..... 61
Figure 25 Mean annual hydrograph of daily simulated, bias-corrected, naturalized streamflow at Middle Fork Willamette River below North Fork near Oakridge (WILNF 4048, USGS 14148000) for the historical period and hybrid-delta A1B and B1 future scenarios. Thin lines show each of the 19 individual simulations. 63
Figure 26 Mean annual hydrograph of monthly simulated, bias-corrected, naturalized streamflow at Middle Fork Willamette River below North Fork near Oakridge (WILNF 4048, USGS 14148000) for the historical (1970-1999) and A1B and B1 future scenarios (2030-2059)..... 64
Figure 27 5th, 50th, and 95th percentiles of monthly simulated, bias-corrected, naturalized streamflow at Row River above Pitcher Creek near Dorena (ROPIT 4035, USGS 14154500) for the historical period and the A1B and B1 future scenarios..... 65

Figure 28 5th, 50th, and 95th percentile of winter (DJF) and summer (JJAS) simulated, bias-corrected, naturalized streamflow at Row River above Pitcher Creek near Dorena (ROPIT 4035, USGS 14154500) for the historical period and hybrid-delta A1B and B1 future scenarios..... 66
Figure 29 Mean annual hydrograph of daily simulated, bias-corrected, naturalized streamflow at McKenzie River near Vida (MCKVI 4036, USGS 14162500) for the historical period and hybrid-delta A1B and B1 future scenarios. Thin lines show each of the 19 individual simulations..... 68
Figure 30 Mean annual hydrograph of monthly simulated, bias-corrected, naturalized streamflow at McKenzie River near Vida (MCKVI 4036, USGS 14162500) for the historical (1970-1999) and A1B and B1 future scenarios (2030-2059)..... 69
Figure 31 5th, 50th, and 95th percentiles of monthly simulated, bias-corrected, naturalized streamflow at McKenzie River near Vida (MCKVI 4036, USGS 14162500) for the historical period and the A1B and B1 future scenarios..... 70
Figure 32 5th, 50th, and 95th percentile of winter (DJF) and summer (JJAS) simulated, bias-corrected, naturalized streamflow at McKenzie River near Vida (MCKVI 4036, USGS 14162500) for the historical period and hybrid-delta A1B and B1 future scenarios..... 71
Figure 33 Mean annual hydrograph of daily simulated, bias-corrected, naturalized streamflow at South Santiam at Waterloo (SANWA 4059, USGS 14187500) for the historical period and hybrid-delta A1B and B1 future scenarios. Thin lines show each of the 19 individual simulations..... 73
Figure 34 Mean annual hydrograph of monthly simulated, bias-corrected, naturalized streamflow at South Santiam at Waterloo (SANWA 4059, USGS 14187500) for the historical (1970-1999) and A1B and B1 future scenarios (2030-2059)..... 74
Figure 35 5th, 50th, and 95th percentiles of monthly simulated, bias-corrected, naturalized streamflow at South Santiam at Waterloo (SANWA 4059, USGS 14187500) for the historical period and the A1B and B1 future scenarios..... 75
Figure 36 5th, 50th, and 95th percentile of winter (DJF) and summer (JJAS) simulated, bias-corrected, naturalized streamflow at South Santiam at Waterloo (SANWA 4059, USGS 14187500) for the historical period and hybrid-delta A1B and B1 future scenarios..... 76
Figure 37 Change from historical to future (A1B and B1) in the mean and 5th, 50th, and 95th percentiles of seasonal, simulated, bias-corrected, naturalized streamflow at 11 locations in the Willamette Basin. Sites are ordered by magnitude of change (low to high; A1B) in winter (Dec-Feb) streamflow..... 79
Figure 38 Flow-duration-frequency curves for annual maxima streamflow of 1-, 3-, 5-, 7-, and 15-day durations for the historical and future periods at North Santiam River below Boulder Creek near Detroit (NOSAN 4056, USGS 14178000)..... 82
Figure 39 Relative change in flow in FDF curves of annual maximum from the historical to future periods at North Santiam River below Boulder Creek near Detroit (NOSAN 4056, USGS 14178000)..... 83
Figure 40 Flow-duration-frequency curves for annual maxima streamflow of 1-, 3-, 5-, 7-, and 15-day durations for the historical and future periods at Row River above Pitcher Creek near Dorena (ROPIT 4035, USGS 14154500)..... 84
Figure 41 Relative change in flow in FDF curves of annual maximum from the historical to future periods at Row River above Pitcher Creek near Dorena (ROPIT 4035, USGS 14154500)..... 85

Figure 42 Relative change in the 2-year return period annual maximum flow from the historical to future periods..... 86

List of Tables

Table 1 Location of USHCN stations in the Willamette and Rogue Basins. 14
Table 2 SNOTEL (ST)/Snow Course (SC) stations analyzed..... 15
Table 3 Streamflow gage sites used for historical and future analysis in the Willamette and Rogue Basins. Future streamflow projections are available for sites highlighted in orange. The CBCCSP IDs for Willamette sites are given. 16
Table 4 Summary of observed data used in this project 18
Table 5 Definition of state of weather codes to define categories of cloud cover based on percent of maximum daily solar insolation (%$RSDS_{max}$). 23
Table 6 Summary of modeled data used in this project 26
Table 7 Annual and seasonal trends in maximum temperature (°F/century) for 1901-2013. Statistically significant trends at the 95% level are denoted by an asterisk and shaded pink for positive trends or blue for negative trends. 28
Table 8 Annual and seasonal trends in minimum temperature (°F/century). Statistically significant trends at the 95% level are denoted by an asterisk and shaded pink for positive trends or blue for negative trends..... 28
Table 9 Mean and range across all models, scenarios, and sub-basins of projected changes in minimum and maximum temperature for the 2040s compared with simulated historical baseline (1970-1999). 30
Table 10 Annual and seasonal precipitation trends (inches/century) over 1901-2013. Statistically significant trends are denoted by an asterisk and shaded pink for negative trends or blue for positive trends..... 32
Table 11 Mean and range across all models, scenarios, and sub-basins of projected changes in precipitation for the 2040s compared with simulated historical baseline (1970-1999)..... 34
Table 12 Trends in April 1 SWE from 1960-2014 ordered by largest to smallest relative decrease. Sites with statistically significant trends are denoted with an asterisk..... 37
Table 13 Range across all models and scenarios of projected sub-basin averaged seasonal changes in snow water equivalent on the first day of the month as a percentage of accumulated water year precipitation (SWE/P). Rogue River sub-basins are shaded. Changes are given as relative differences (%). Asterisk denotes basins/seasons with little snow accumulation (at least one simulation of historical period with mean SWE/P < 1%)..... 41
Table 14 Mean and range across all models, scenarios, and sub-basins of projected changes in average wind speed for the 2040s compared with simulated historical baseline (1970-1999). 44
Table 15 USACE Projects in the Willamette and Rogue Basins and associated CBCCSP locations with bias-corrected normalized streamflow projections 50
Table 16 Relative differences in mean seasonal streamflow volume between the historical (1970-1999) and A1B and B1 future scenarios (2030-2059) for selected CBCCSP locations..... 78

Executive Summary

Regional warming and changing precipitation patterns are affecting water supply with implications for water management under future climate change. The US Army Corps of Engineers (USACE) Portland District manages dams, reservoirs, and projects (e.g. fish facilities) in the Willamette and Rogue River Basins and must balance multiple objectives of providing reservoir storage space to minimize flood risk, refilling reservoirs for conservation storage, meeting environmental objectives, and maximizing hydropower. This balancing act may become more challenging under future climate conditions.

This report examines observed changes in temperature, precipitation, snowpack, and streamflow in the Willamette and Rogue River Basins and provides projections of future changes in these variables based on global climate model simulations.

Observed Changes

Annual and seasonal—winter (DJF), spring (MAM), summer (JJA), and fall (SON)—trends in maximum temperature, minimum temperature and precipitation were analyzed using US Historical Climate Network (USHCN) stations, and April 1 snow water equivalent (SWE) trends using SNOTEL and Snow Course sites located in the Willamette and Rogue Basins.

Minimum and maximum temperature increased annually for most stations over the period 1901-2013 with warming rates ranging from 0.5°F to 3.9°F per century. Stations tended to warm less in winter and spring, and more in summer and fall.

Water year and seasonal precipitation exhibited large natural variability over the period 1901-2013. Spring and summer precipitation increased for most stations and precipitation increased annually and in winter and fall for approximately half of stations.

Snow water equivalent decreased at virtually all sites with a range of –3% to –60% over the period 1960-2014, with the largest decreases generally at lower elevations (2,500 to 5,000 feet) that hover near freezing during winter.

Changes in streamflow hydrographs based on data from USGS gages in the Willamette and Rogue basins were analyzed for two time periods: 1941-1970 and 1981-2010. The streamflow hydrographs at sites in rain-dominated basins changed between the two periods in a way that indicates current flood control management: winter streamflow decreased and summer streamflow increased. In basins with a snowmelt component, the winter and early summer peaks in streamflow shifted toward relatively stable flows during December through May, consistent with expected warming.

Climate Projections

Future projections of temperature, precipitation, snow water equivalent, wind, and cloud cover are based on 20 global climate models (GCMs) from the 5th phase of the Coupled Model Intercomparison Project (CMIP5) driven by a moderate and high future emissions scenario (representative concentration pathways (RCP) 4.5 and 8.5, respectively). The GCM meteorological data was statistically downscaled to a 6-km grid and served as input to the Variable Infiltration Capacity (VIC) hydrological model to produce future SWE projections. Aggregating data within each sub-basin of the Willamette and Rogue River Basins, changes in these variables were examined between the simulated historic (1970-1999) and future (2030-2059) periods.

With a high degree of confidence (as indicated by the fact that all models agree), both minimum and maximum temperature is projected to increase year-round with greater warming in summer (JJA). Annual average increases in minimum and maximum temperature range from 0.8°F-5.3°F and 1.1°-5.5°F, respectively, depending on basin and scenario.

Projections of precipitation are a different matter. In each season, some models project increases, and some decreases: therefore, even the sign of projected change is uncertain. The multi-model average projection is small in each season, and is slightly positive in winter and slightly negative in summer.

Snowpack (SWE) as a proportion of cumulative precipitation (P) is expected to decline markedly across the region. Those sub-basins that historically receive the most snow such as North Santiam show projected winter (DJF) declines of 27%-67% in SWE/P. Sub-basins with little snow currently, such as Middle Willamette, are projected to receive virtually no snow in the future. The small projected increases in total winter precipitation provide little offset to the loss in snow due to projected warming.

Wind speed and cloud cover projections are highly uncertain because, as with precipitation, the models disagree on the sign of change. However, the multi-model mean suggests small decreases in average wind speed annually and for most seasons. Projected changes in cloud cover suggest an enhancement of the annual cycle, with decreased cloud cover in summer and increased cloud cover in winter.

Streamflow Projections

Streamflow projections are based on 10 GCMs from the 3rd phase of CMIP (CMIP3) driven by a low (B1) and high (A1B) future emissions scenario. The GCM meteorological data was statistically downscaled and run through the VIC hydrological model and routed to 30 locations in the Willamette Basin as part of the Columbia Basin Climate Change Scenarios

Project (CBCCSP). Changes in mean annual and seasonal streamflow hydrographs, peak flows, and flow frequencies were examined comparing the simulated historic (1970-1999) and future (2030-2059) periods.

Future streamflow changes are driven primarily by warming-induced decreases in snow accumulation and secondarily by seasonal variation in precipitation change. All basins are projected to have increased mean flows in winter and decreased flows in summer, while the magnitude of these changes is largely determined by a basin's sensitivity to a decline in snow accumulation. For example, in the North Santiam with its historically significant snowpack, mean flow is projected to increase substantially during winter and decrease in spring and summer. In basins with little snowmelt component, such as the Middle Fork Willamette, winter flows are projected to increase slightly (<7%) with small *absolute* changes during the rest of the year. Projected increases in winter (DJF) mean flow range from 2% to 26% and projected decreases in summer (JJAS) mean flow range from -15% to -38% depending on gaging site and future emissions scenario. Total water year flow volumes are projected to increase only slightly (0.4% to 3.5%).

In addition to mean winter flow, annual peak flows are projected to increase in the future. The magnitude of peak flows of any duration (1- to 15-day) with lower return periods (e.g., 2-year) tend to increase more than those with higher return periods. Longer flow durations (e.g., 15-day) show smaller changes in peak flow magnitudes than shorter flow durations (e.g., 1-day). Annual peak flows of 1- to 5-day durations are projected to occur 0-5 days earlier in the water year at the majority of gauges, and up to 2 weeks earlier for the basins with larger snowmelt component.

Implications

Will climate change lead to revised project rule curves?

Projected increases in winter flooding and summer hydrological drought create additional stressors to management of USACE projects in the Willamette and Rogue Basins. These stressors are competing, in the sense that attempting to ameliorate increased winter flow only further stresses the ability to manage for summer drought.

Are current operations flexible enough to accommodate projected future changes in hydrology?

Whether current operations are flexible enough to accommodate such climate and hydrological changes is beyond our expertise to answer.

Should refill be adjusted due to shifting snowpack in the basins?

Recent work by Moore (2015) in the Willamette Basin showed how a project's rule curve could be optimized to accommodate climate change impacts, which are primarily the shifting snowpack, and to a lesser degree the increase in winter precipitation. This would

mean beginning the reservoir fill earlier, but at a slower rate to balance flood risk with summer water demand (Jung and Chang, 2011; Moore 2015). However, the study by Moore (2015) also indicated that the USACE rule curves in the Willamette Basin already favor summer water demand for recreation over flood protection, based on their economic analysis of the value of flood protection and recreation. In effect, the rule curves already have an earlier refill than what is optimal based on economic considerations. The implication is that the USACE may not have much cushion in terms of shifting to an earlier refill, especially if the value of flood protection increases with increasing development along the rivers downstream.

Will climate change require structural changes to dams?

Peak flows are projected to increase roughly between 10%-20%, though uncertainty is high. Whether structural changes may need to be made to the dams to account for future changes in peak flows depends on both the magnitude of the changes and the design specifications of the individual structures. Without knowledge of the latter, this report is unable to fully address this question. There is a suggestion in the hydrological simulations that future peak flow magnitudes with the largest return periods will increase proportionally less than more frequent, smaller peak flows magnitudes. This would imply favoring the modification of operations over costly structural changes. However, this pattern in the hydrological simulations may be an artifact of the chosen downscaling methodology. Given the costly implications of these particular findings, it is recommended that this topic be investigated further.

Will back-to-back large storm events increase in the future leading to more, high flood risk situations?

Changes in the 15-day duration peak flow relative to changes in shorter duration peak flows were used as a proxy for assessing the hydrological consequences of any increased frequency of back-to-back large storm events. While changes in the 15-day duration peak flow are projected to increase, their increase is less than those of peak flows of shorter durations. This suggests that increases in 15-day duration peak flow arise largely from higher volumes of flow overall in the winter and not from a greater frequency of back-to-back events. However, the downscaling methodology used for this study is not well-suited for detecting changes in the timing of precipitation events because it maintains the timing (though not the magnitude) of the daily historical precipitation; therefore, simulated changes in the frequency of large back-to-back flow events would only arise from the interaction of precipitation with processes affected by changes in temperature (e.g., snowfall and rain-on-snow events). A more direct assessment of back-to-back events would use a downscaling method that explicitly maintains the projected changes (if present) in the distribution of storm inter-arrival periods.

How will climate change affect water management operations, which are focused on environmental objectives, such as water quality?

Projected increases in air temperature can result in higher in-stream temperatures (Isaak et al., 2010) and declines in dissolved oxygen threatening the health of endangered aquatic species (Raymondi et al., 2013). In addition, increased wildfire activity, related to increasing temperatures and drought conditions, can increase sediment and nutrient loads in streams (Cannon et al., 2010; Chang et al., 2010).

Will the risk of drought increase under future climate change?

Even though total water year precipitation is projected to increase slightly in the Willamette and Rogue basins, and across the Northwest as a whole, the region can expect to experience warmer, wetter winters, warmer, drier summers, and a diminishing snowpack in the future under rising greenhouse gas concentrations. Therefore, if drought is defined as prolonged periods of demand exceeding supply, the risk of drought is projected to increase under future climate change.

Will there be a significant shift in peak annual flow timing under future climate change?

In addition to projected increases in the magnitude of peak flows, the streamflow simulations also show shifts in the mean timing of peak flows. Annual maximum flows of 1- to 5-day durations are projected to occur 0-5 days earlier in the water year at the majority of gauges, and up to 2 weeks earlier at locations with larger snowmelt influence, such as the gage on the North Santiam River.

Introduction

Global climate is warming primarily as a result of the accumulation of greenhouse gases in the atmosphere from human activities (IPCC 2013). Regional warming and changing precipitation patterns are affecting the water cycle with implications for water management under future climate change (Dalton et al., 2013). The US Army Corps of Engineers (USACE) Portland District, which manages projects that have multiple functions, including flood damage reduction, hydropower, irrigation, power, water supply and recreation in Oregon watersheds, teamed up with the Oregon Climate Change Research Institute (OCCRI) to assess the potential impacts of climate change on USACE water management practices in the Willamette Valley and Rogue River basins.

The District manages 13 multi-purpose dams and reservoirs in the Willamette River Basin (Figure 1) and 2 projects in the Rogue Basin (Figure 2). The District must balance multiple objectives of providing reservoir storage space to minimize flood risk, refilling reservoirs for conservation storage, meeting environmental objectives, and maximizing hydropower. Successfully meeting these objectives now and into the future will require regular evaluations of the current rules and operations as climate continues to change. The Corps would like to understand better the potential implications of future climate change on water management operations in the Willamette and Rogue basins in the context of historical trends and variability in order to more effectively manage projects in the future.

The Corps is actively seeking answers to the following salient questions:

1. Will climate change lead to revised project rule curves?
2. Will back-to-back large storm events increase in the future leading to more, high flood risk situations?
3. Should refill be adjusted due to shifting snowpack in the basins?
4. Will climate change require structural changes to dams?
5. Are current operations flexible enough to accommodate projected future changes in hydrology?
6. How will climate change affect water management operations, which are focused on environmental objectives, such as water quality?
7. Will the risk of drought increase under future climate change?

Toward informing answers to these questions, historical trends and future projections in the following climate and streamflow metrics relevant to USACE water management are discussed:

1. Annual streamflow hydrograph
2. The 5th, 50th, and 95th percentiles of monthly streamflow

3. Mean, 5th, 50th, and 95th percentiles of winter (DJF) and summer (JJAS) streamflow
4. Flow-duration-frequency curves for annual maximum streamflow at 1-, 3-, 5-, 7-, and 15-day durations
5. Monthly ratios of snow water equivalent (SWE) to accumulated precipitation
6. Seasonal temperature and precipitation
7. Monthly wind speed and cloud cover

Figure 1 The Willamette River Basin with USACE Projects

Figure 2 Rogue River Basin Projects

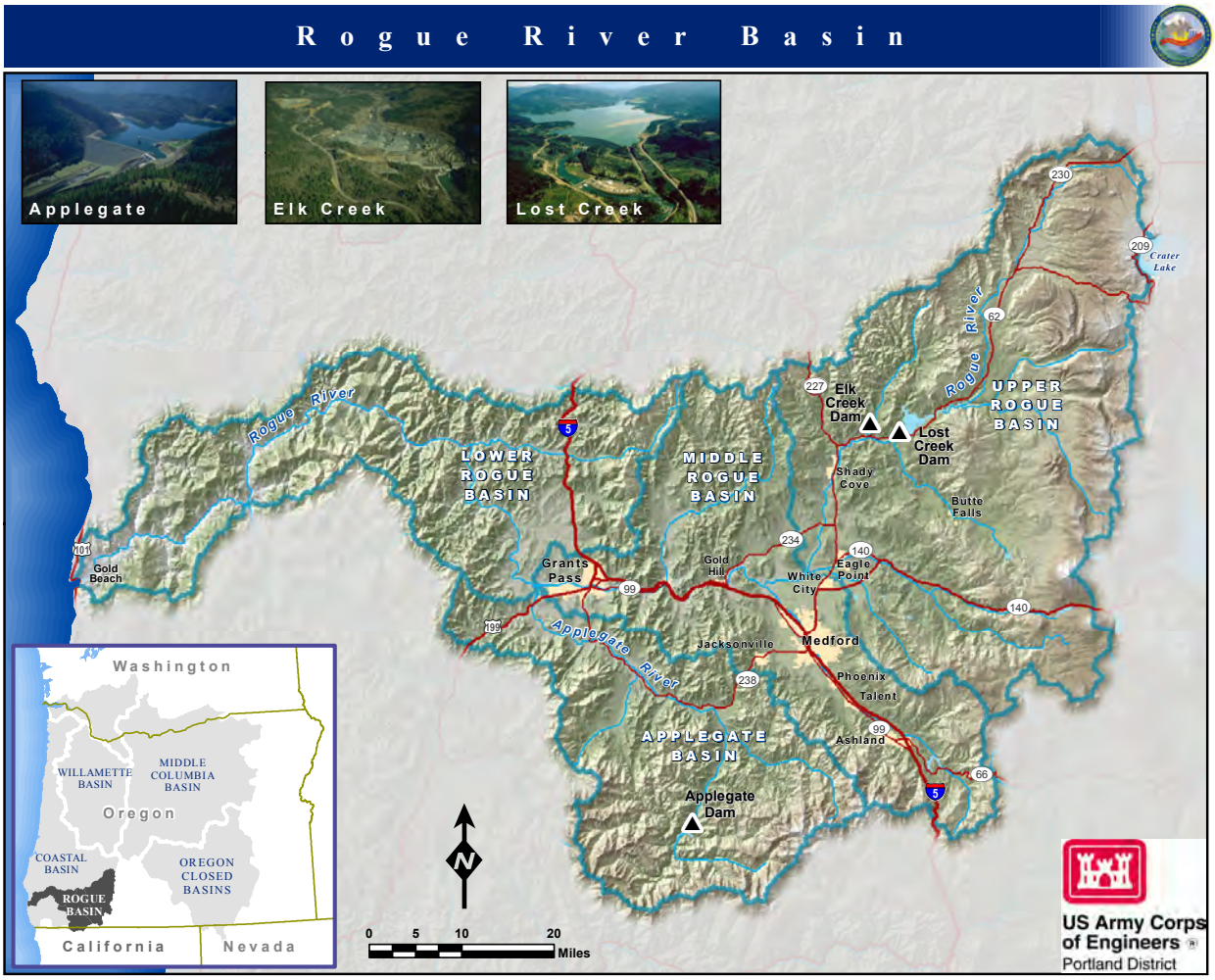

Observed Datasets & Methods

Temperature & Precipitation

Observed trends in temperature and precipitation were analyzed using the US Historical Climate Network (USHCN) Version 2.5. The USHCN is a subset of the National Weather Service Cooperative Observer Program (NWS Coop) network selected for its length of record and data completeness. The USHCN stations have been quality controlled and bias-corrected to remove non-climatic influences such as site moves, canopy changes, and instrumentation changes (Menne et al., 2009). It is the best quality data for long-term trend analysis.

Monthly summaries of minimum temperature, maximum temperature, and precipitation from Version 2.5 were obtained from the Carbon Dioxide Information Analysis Center

(CDIAC) for station start year through 2013 for the 6 stations in the Willamette Basin and the 4 stations in the Rogue Basin (Table 1). These stations began recording data in the 1880s and 1890s, but early records contained some missing data. Starting in year 1901, all stations and variables had complete data through the remainder of the record. Thus, trends were analyzed over the period 1901-2013. Stations are located throughout the basins at elevations ranging from 180 to nearly 6500 feet.

Table 1 Location of USHCN stations in the Willamette and Rogue Basins.

Station ID	Location	Sub-Basin	Lat.	Lon.	Elev. (ft)
Willamette River Basin					
USH00351862	Corvallis	Upper Will.	44.63	-123.19	225.1
USH00351897	Cottage Grove	Coast Fork Will.	43.79	-123.03	595.1
USH00355384	McMinnville	Yamhill	45.22	-123.16	154.9
USH00352997	Forest Grove	Tualatin	45.52	-123.10	180.1
USH00358466	Three Lynx	Clackamas	45.12	-122.07	1120.1
USH00355362	McKenzie Brg Res	McKenzie	44.18	-122.12	1478.0
Rogue River Basin					
USH00350304	Ashland	Middle	42.21	-122.71	1746.1
USH00351946	Crater Lake NPS HQ	Upper	42.90	-122.13	6475.1
USH00353445	Grants Pass	Middle	42.42	-123.32	930.1
USH00356907	Prospect	Upper	42.73	-122.52	2482.0

Snow Water Equivalent (SWE)

Observed trends in April 1 snow water equivalent (SWE) were analyzed using SNOTEL and Snow Course data collected by the Natural Resources Conservation Service (NRCS). Trends were estimated over the period 1960-2014 (Mote and Sharp, 2014) for 10 stations in the Willamette Basin and 13 stations in the Rogue Basin (Table 2). SNOTEL sites began recording data in the 1980s, so NRCS uses data from existing Snow Course sites to extend the record backward by using statistical relationships between co-located, overlapping SNOTEL and Snow Course data. The number of stations increases with start year. In order to maximize both the length of record and number of stations that could be included, the period 1960-2014 was chosen for analysis. Most stations are located along the western slopes of the Cascade Mountains at elevations ranging from 2500 to 6500 feet.

Table 2 SNOTEL (ST)/Snow Course (SC) stations analyzed.

Station Name	Sub-Basin	Lat.	Lon.	Elev. (ft)
	Willamette River Basin			
CascadeSummit_ST	Middle Fork Will.	43.59	-122.06	5100
HoggPass_ST	McKenzie	44.42	-121.86	4790
IrishTaylor_ST	McKenzie/Middle Fork	43.80	-121.95	5540
JumpOffJoe_ST	McKenzie/South Santiam	44.39	-122.17	3520
MarionForks_ST	North Santiam/South Santiam	44.59	-121.97	2590
MarysPeak_SC	Upper Will.	44.51	-123.56	3580
PeavineRidge_ST	Clackamas	45.04	-121.93	3420
RoaringRiver_ST	McKenzie/Middle Fork Will.	43.90	-122.03	4950
SaltCreekFalls_ST	Middle Fork Will.	43.61	-122.12	4220
SummitLake_ST	Middle Fork Will.	43.45	-122.14	5610
	Rogue River Basin			
AnnieSprings_ST	Upper	42.87	-122.17	6010
BeaverDamCreek_SC	Upper	42.30	-122.29	5120
BigRedMountain_ST	Applegate	42.05	-122.85	6050
BillieCreekDivide_ST	Upper	42.41	-122.27	5280
ColdSpringsCamp_ST	Upper	42.53	-122.18	5940
DeadwoodJunction_SC	Upper	42.29	-122.38	4660
DiamondLake_ST	Upper	43.19	-122.14	5280
FishLk._ST	Upper	42.38	-122.35	4660
FourmileLake_ST	Upper	42.44	-122.23	5970
HowardPrairie_SC	Upper	42.21	-122.37	4580
ParkH.q.Rev_SC	Upper	42.90	-122.14	6570
SilverBurn_SC	Upper	42.93	-122.40	3680
SiskiyouSummit_SC	Middle	42.07	-122.61	4560

Streamflow

Observed mean daily and monthly streamflow data were obtained from the Oregon Water Resources Department Historical Streamflow and Lake Level Data website, which has a simple interface to download the same data available from the USGS Water Data website. For consistency in presentation of results between historic and future climate change projections, the 31 sites in the Willamette where future climate change streamflow projections from the Columbia Basin Climate Change Scenario Project (CBCCSP) are also available were chosen for the historical analysis (Table 3). In the Rogue River Basin, where future flows are unavailable, 12 active sites with at least 60 years of data were selected (Table 3).

Table 3 Streamflow gage sites used for historical and future analysis in the Willamette and Rogue Basins. Future streamflow projections are available for sites highlighted in orange. The CBCCSP IDs for Willamette sites are given.

USGS ID	Location Name	Sub-Basin	Lat.	Lon.
	Willamette River Basin			
14170000	LONTO 4037: Long Tom River At Monroe	Upper W.	44.31	-123.30
14169000	TOMAL 4054: Long Tom River Near Alvadore	Upper W.	44.12	-123.28
14190500	LUCKI 4041: Luckiamute River Near Suver	Upper W.	44.78	-123.23
14194150	YAMMC 4061: South Yamhill River At Mcminnville	Yamhill	45.20	-123.17
14166000	WILHA 4053: Willamette River At Harrisburg	Upper W.	44.27	-123.17
14173500	CALAP 4038: Calapooia River At Albany	Upper W.	44.62	-123.13
14174000	WILAL 4055: Willamette River At Albany	Upper W.	44.63	-123.10
14191000	WILSA 4060: Willamette River At Salem	Middle W.	44.93	-123.03
14189000	SANJE 4040: Santiam River At Jefferson	North Santiam	44.71	-123.01
14155500	ROCOT 4050: Row River Near Cottage Grove	Coast Fork W.	43.78	-122.98
14197900	WILLA 4042: Willamette River At Newberg	Middle Will.	45.28	-122.96
14157500	WILGO 4051: Coast Fork Willamette River Near Goshen	Coast Fork W.	43.97	-122.95
14152000	WILMF 4034: Middle Fork Willamette River At Jasper	Middle Fork W.	44.00	-122.90
14154500	ROPIT 4035: Row River Above Pitcher Creek Near Dorena	Coast Fork W.	43.73	-122.87
14150000	WILDE 4049: Middle Fork Willamette River Near Dexter	Middle Fork W.	43.93	-122.83
14187500	SANWA 4059: South Santiam River At Waterloo	South Santiam	44.48	-122.82
14200000	MOLAL 4043: Molalla River Near Canby	MolallaPudding	45.24	-122.69
14187200	SANFO 4058: South Santiam River Near Foster	South Santiam	44.40	-122.68
14207500	TULIN 4062: Tualatin River At West Linn	Tualatin	45.35	-122.67

14211720	WILPO 4063: Willamette River At Portland	Lower W.	45.52	-122.67
14207740	WILFA 4064: Willamette River Above Falls At Oregon City	Middle W.	45.35	-122.62
14183000	SANME 4039: North Santiam River At Mehama	North Santiam	44.79	-122.62
14148000	WILNF 4048: Mf Willamette River Blw N Fork Nr Oakridge	Middle Fork	43.80	-122.55
14162500	MCKVI 4036: Mckenzie River Near Vida	McKenzie	44.13	-122.47
14145500	WILLS 4047: Mf Willamette River Abv Salt Crk Near Oakridge	Middle Fork	43.72	-122.43
14210000	RMILL 4046: Clackamas At River Mill Dam	Clackamas	45.30	-122.35
14181500	SANNI 4057: North Santiam River At Niagara	North Santiam	44.75	-122.28
14159500	MCKEN 4052: South Fork Mckenzie River Near Rainbow	McKenzie	44.13	-122.23
14209710	NFORK 4045: Clackamas River At North Fork Dam	Clackamas	45.17	-122.16
14178000	NOSAN 4056: No Santiam River Blw Boulder Crk Nr Detroit	North Santiam	44.70	-122.10
14209500	CLKTH 4044: Clackamas River Above Three Lynx Creek	Clackamas	45.13	-122.07
	Rogue River Basin			
14359000	Rogue River at Raygold Nr Central Point	Middle Rogue	42.44	-122.99
14357500	Bear Creek at Medford	Middle Rogue	42.33	-122.87
14362000	Applegate R near Copper	Applegate	42.06	-123.11
14366000	Applegate R near Applegate	Applegate	42.24	-123.14
14335500	South Fork Big Butte Creek Nr Butte Falls	Upper Rogue	42.54	-122.55
14339000	Rogue R at Dodge Bridge Nr Eagle Point	Upper Rogue	42.53	-122.84
14361500	Rogue R at Grants Pass	Middle Rogue	42.43	-123.32
14338000	Elk Ck Nr Trail	Upper Rogue	42.67	-122.74
14335200	S Fk Big Butte Creek ab Willow Cr Nr Butte Falls	Upper Rogue	42.52	-122.49
14343000	N Fk Little Butte Cr near Lakecreek	Upper Rogue	42.38	-122.36
14372500	E Fk Illinois R nr Takilma	Illinois	42.07	-123.63
14330000	Rogue R bl Prospect	Upper Rogue	42.73	-122.52

Historical Trend Analysis Methods

Monthly data of temperature, precipitation, and streamflow were aggregated for winter (DJF), spring (MAM), summer (JJA), fall (SON) and annually for the analysis. Annual and seasonal trends in maximum and minimum temperature and total precipitation for each station were estimated over the period 1901-2013. Trends in April 1 SWE were estimated over the period 1960-2014 for each station.

For temperature, precipitation, and April 1 SWE, standard least squares linear regression was used to estimate the linear trend (i.e., the slope) and calculate the 2.5%-97.5% confidence interval on the trend to determine statistical significance. A lack of statistical significance was reported if the confidence interval included a trend of zero.

Because these estimated confidence intervals assume the observed deviations from the linear trend (i.e., the residuals) are normally distributed, a test to confirm normality was performed. When the residuals were not normally distributed, the Mann-Kendall test, preferred in such cases, was used to assess significance in the trend. Strong autocorrelation in a time series can lead to overly narrow confidence intervals and therefore may lead to an improper conclusion of statistical significance when performing either standard linear regression or the Mann-Kendall test. Therefore, adjustments for autocorrelation were applied when strongly present.

Annual streamflow and volume hydrographs were generated using the historical data at each gage location for two 30-year periods representing past (1941-1970) and recent (1981-2010) conditions. Monthly 5th, 50th, and 95th percentile streamflow volumes were also calculated for each gage location.

Table 4 Summary of observed data used in this project

Dataset	Variables	#Stations	Time Range
USHCN	Maximum Temperature Minimum Temperature Precipitation	Willamette: 6 Rogue: 4	1901-2013
SNOTEL	April 1 SWE	Willamette: 10 Rogue: 13	1960-2014
USGS gages	Streamflow	Willamette: 25 Rogue: 12	70 years of data or more

Modeled Datasets & Methods

Global Climate Models

State-of-the-art global climate models (GCMs) from the Coupled Model Intercomparison Project phase 5 (CMIP5; Taylor et al., 2012) that were used in the latest fifth assessment report of the Intergovernmental Panel on Climate Change (IPCC), in addition to the previous generation of models, CMIP3 (Meehl et al., 2007) were used in this project. The GCMs from CMIP5 feature several scientific advances over CMIP3 including improved physics and finer spatial resolution, however, the range in the equilibrium response of CMIP5 models to a doubling of CO_2, or climate sensitivity, has not narrowed compared to CMIP3 (IPCC 2013). In addition, CMIP5 and CMIP3 models are comparable in their performance simulating 20th century observed climate evaluated over the Pacific Northwest (Rupp et al., 2013).

Both CMIP3 and CMIP5 GCMs are used for this project for two reasons (see Appendix A. Global Climate Models for a complete listing of all GCMs used in this study). The first is that the only dataset of routed streamflow projections for the Willamette Basin currently available for the timeline of this project is based on CMIP3. Secondly, CMIP5 represents state of the art and is widely used in current impacts assessments and hydrological modeling projects. In this project, the future projections of temperature, precipitation, snow water equivalent, wind, and cloud cover are based on CMIP5 where as streamflow projections are based on CMIP3 due to limitations in data availability. Future routed streamflow projections for the Willamette Basin based on CMIP5 are currently being created, but unfortunately were not available at the time of this project. New versions of 8 of the 10 CMIP3 models used in the streamflow projections are included in the ensemble of 20 CMIP5 climate projections (Appendix A. Global Climate Models).

Emissions Scenarios

A key difference between CMIP5 and CMIP3 is the set of driving scenarios for future climate simulations. The CMIP3 simulations of the 21st century were forced with emissions scenarios from the Special Report on Emissions Scenarios (SRES) based on future trajectories of population growth, economy, technology, energy use, and land use (Nakicenovic et al. 2000). In contrast, CMIP5 simulations of the 21st century were driven by "representative concentration pathways" (RCPs) that define concentrations of greenhouse gases, aerosols, and chemically active gases leading to set amount of radiative forcing, or extra energy trapped in the earth-atmosphere system, by the year 2100 without any assumptions regarding climate policy (van Vuuren et al., 2011).

Future routed streamflow projections from CMIP3 are available for SRES B1 and A1B and projections of other climate variables from CMIP5 are available for RCP4.5 and RCP8.5. B1

is characterized by low population growth, global economic development, and technological development of alternative resource-efficient energy systems and a decline in conventional oil and gas energy sources. A1B is also characterized by low population growth, but with rapid economic growth and a balanced energy portfolio between alternative and conventional energy sources with emissions leveling off by mid-century.

In the RCP4.5 scenario, emissions stabilize by mid-century reaching a peak of about 10 gigatonnes of carbon per year (GtC/yr) and then decline in the decades following. The trajectory of fossil fuel emissions and carbon dioxide concentrations for RCP4.5 is similar to B1, although warming for RCP4.5 tends to be somewhat larger than for B1. The RCP8.5 scenario represents a continuance of our current path of emissions throughout the 21st century that begins to stabilize toward the end of the century. Until about the 2030s and 2040s, RCP8.5 has a similar trajectory as A1B. After the 2040s, however, RCP8.5 emissions continue to grow whereas A1B emissions begin to stabilize peaking around 16 GtC/yr then declining. By the 2040s, the time frame for this project, RCP8.5 warming tends to be just slightly larger than A1B. Because of this, streamflow projections using A1B should be considered conservative when compared with climate projections using RCP8.5. Together, RCP4.5 and B1 represent realistic "low-end" scenarios and RCP8.5 and SRES A1B can be thought of as "business-as-usual" scenarios (Figure 3).

Results are presented from each of the scenarios described, that is, RCP4.5 and RCP8.5 for temperature, precipitation, snow water equivalent, wind, and cloud cover and A1B and B1 for streamflow. Our current trajectory is most consistent with the higher scenarios (RCP8.5/A1B) than the lower scenarios (RCP4.5/B1). However, the decisions made as a society today and in the future will determine future emissions and the likelihood of those decisions is an economic and social question, not a scientific question.

Figure 3 Fossil fuel emissions and carbon dioxide concentrations driving the four scenarios of future climate and hydrology projections used in this project. Data: live.magicc.org (Meinhauser et al., 2011)

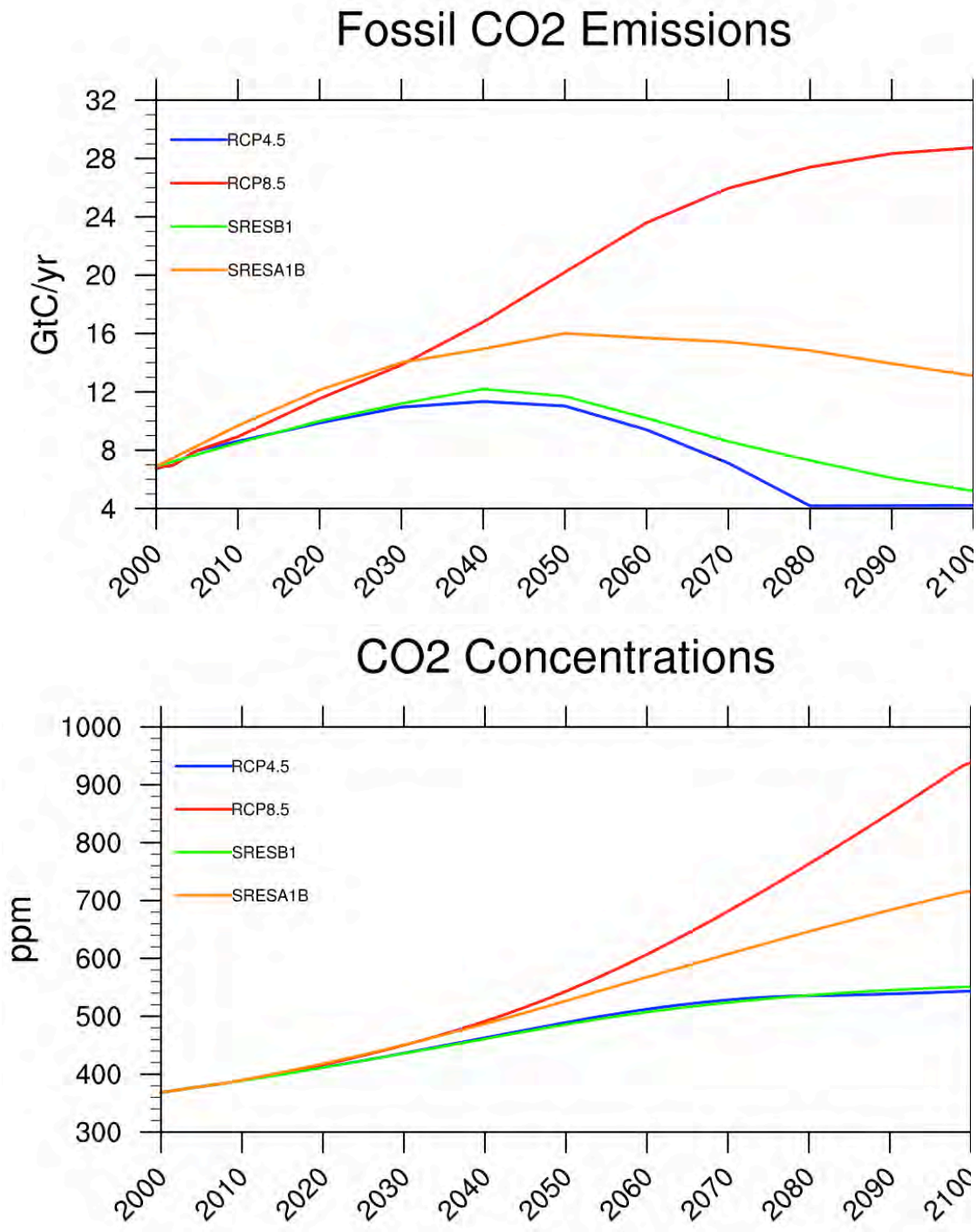

Climate & SWE Simulations

Statistically downscaled CMIP5 GCM output served as the basis for future projections of temperature, precipitation, snow water equivalent, wind, and cloud cover. The coarse resolution of GCMs output (100-300 km) was downscaled to a resolution of about 6km using the Multivariate Adaptive Constructed Analogs (MACA) method, which has demonstrated skill in complex topographic terrain (Abatzoglou and Brown, 2012). The MACA approach utilizes a gridded training observation dataset to accomplish the downscaling by applying bias-corrections and spatial pattern matching of observed large-scale to small-scale statistical relationships. (For a detailed description of the MACA method see: http://maca.northwestknowledge.net/MACAmethod.php.)

This downscaled gridded meteorological data (i.e., MACA data) is used as the climate inputs to an integrated climate-hydrology-vegetation modeling project called Integrated Scenarios of the Future Northwest Environment. Snow dynamics were simulated using the Variable-Infiltration Capacity hydrological model (VIC version 4.1.2.l; Liang et al. 1994 and updates) run on a 1/16º x 1/16º (6 km) grid.

Simulations of historical and future climate for the variables maximum temperature (*tasmax*), minimum temperature (*tasmin*), precipitation (*pr*), wind speed (*was*), and downward shortwave radiation at the surface (*rsds*) are available at the daily time step from 1950 to 2099 for 20 GCMs and 2 RCPs (i.e., RCP4.5 and RCP8.5). Simulations of snow water equivalent (*SWE*) are only available for the 10 GCMs used as input to VIC. Appendix A. Global Climate Models lists all 20 CMIP5 GCMs and indicates the subset of 10 used for SWE simulations. Data for all the models available was obtained for each variable from the Integrated Scenarios data archives in order to get the best uncertainty estimates.

All simulated climate data (temperature, precipitation, wind speed, downward short-wave radiation) and the streamflow data (see "Streamflow Simulations" section below) have been bias-corrected using quantile mapping techniques. Only SWE is presented without bias correction). Quantile mapping adjusts simulated values by creating a one-to-one mapping between the cumulative probability distribution of simulated values and the cumulative probability distribution of observed values. In practice, both the simulated and observed values of a variable (e.g., daily streamflow) over the some historical time period are separately sorted and ranked and the values are assigned their respective probabilities of exceedence. The bias corrected value of a given simulated value is assigned the observed value that has the same probability of exceedence as the simulated value. The historical bias in the simulations is assumed to stay constant into the future; therefore the same mapping relationship developed from the historical period was applied to the future scenarios. For MACA, a separate quantile mapping relationship was made for each non-

overlapping 15-day window in the calendar year. For streamflow, a separate quantile mapping relationship was made for each calendar month.

Climate Projections Methods

Daily *tasmax*, *tasmin*, *pr*, *was*, *rsds*, and *SWE* was aggregated using a weighted average of all grid boxes within each USGS HUC8 sub-basin in the Willamette and Rogue Basins. For *SWE*, the value on the first day of the month was averaged over sub-basins. The time series for each model and each scenario for each sub-basin was then aggregated to monthly, seasonal (i.e., DJF, MAM, JJA, SON), and annual time steps. Changes from historical (1970-1999) to future (2030-2059) were examined. For *SWE*, changes on the first day of each month divided by accumulated precipitation since the beginning of the water year (Oct. 1) were also examined.

To estimate cloud cover, daily *rsds* averaged over sub-basins was converted to daily percent of maximum *rsds* based on the maximum of a 21-day window centered on each day over the entire period of record. Then, each day was classified as one of four 'state of weather' codes irrespective of precipitation: clear, scattered clouds, broken clouds, or overcast as defined in Table 5 (Dalton et al., 2015). State of weather codes is one of the variables used by wildland fire managers to assess fire danger. The percent of days in each month, season, or year within each category was then computed.

Table 5 Definition of state of weather codes to define categories of cloud cover based on percent of maximum daily solar insolation (%$RSDS_{max}$).

Description	%$RSDS_{max}$
Clear	≥91
Scattered clouds	73≤%$RSDS_{max}$<91
Broken clouds	50≤%$RSDS_{max}$<73
Overcast	<50

Streamflow Simulations

The only routed streamflow projections currently available for the Willamette Basin are part of the Columbia Basin Climate Change Scenarios Project (CBCCSP) (Hamlet et al., 2010). This project developed hydrologic climate change scenarios for approximately 300 streamflow locations in the Columbia River basin to support climate change adaptation and long-range planning. The project produced routed streamflow projections for about 30 locations in the Willamette Basin (Table 3; Figure 4). Unfortunately, no routed streamflow projections are available in the Rogue River basin.

Bias-corrected simulations of historical and future streamflow at 11 locations within the Willamette Basin (Figure 4; also see highlighted sites in Table 3) were obtained from data archives of the CBCCSP. These 11 stations were chosen because they had complete data of historic and future simulated bias-corrected, naturalized routed streamflows. Unfortunately, some of the CBCCSP data was lost due to server failure at the University of Washington prior to this report (Guillaume Mauger, Climate Impacts Group, University of Washington, personal communication), which limited the number of sites with complete data available. The production of these streamflow simulations is described in detail in Hamlet et al. (2010; 2013). Their methods are summarized here.

Hydrology was simulated using the Variable-Infiltration Capacity hydrological model (VIC; Liang et al. 1994) run on a 1/16º x 1/16º (6 km) grid. To generate daily streamflow estimates, runoff from VIC grid cells was then routed to selected locations along the stream network using a daily-time-step routing model (Lohmann et al. 1998). Where records of naturalized flow were available, the daily streamflow estimates were then bias-corrected so that their statistical distributions matched those of the naturalized streamflows.

Figure 4 Location of Columbia Basin Climate Change Scenarios Project (CBCCSP) routed streamflow projections in the Willamette Basin. Labeled sites in red have complete datasets available.

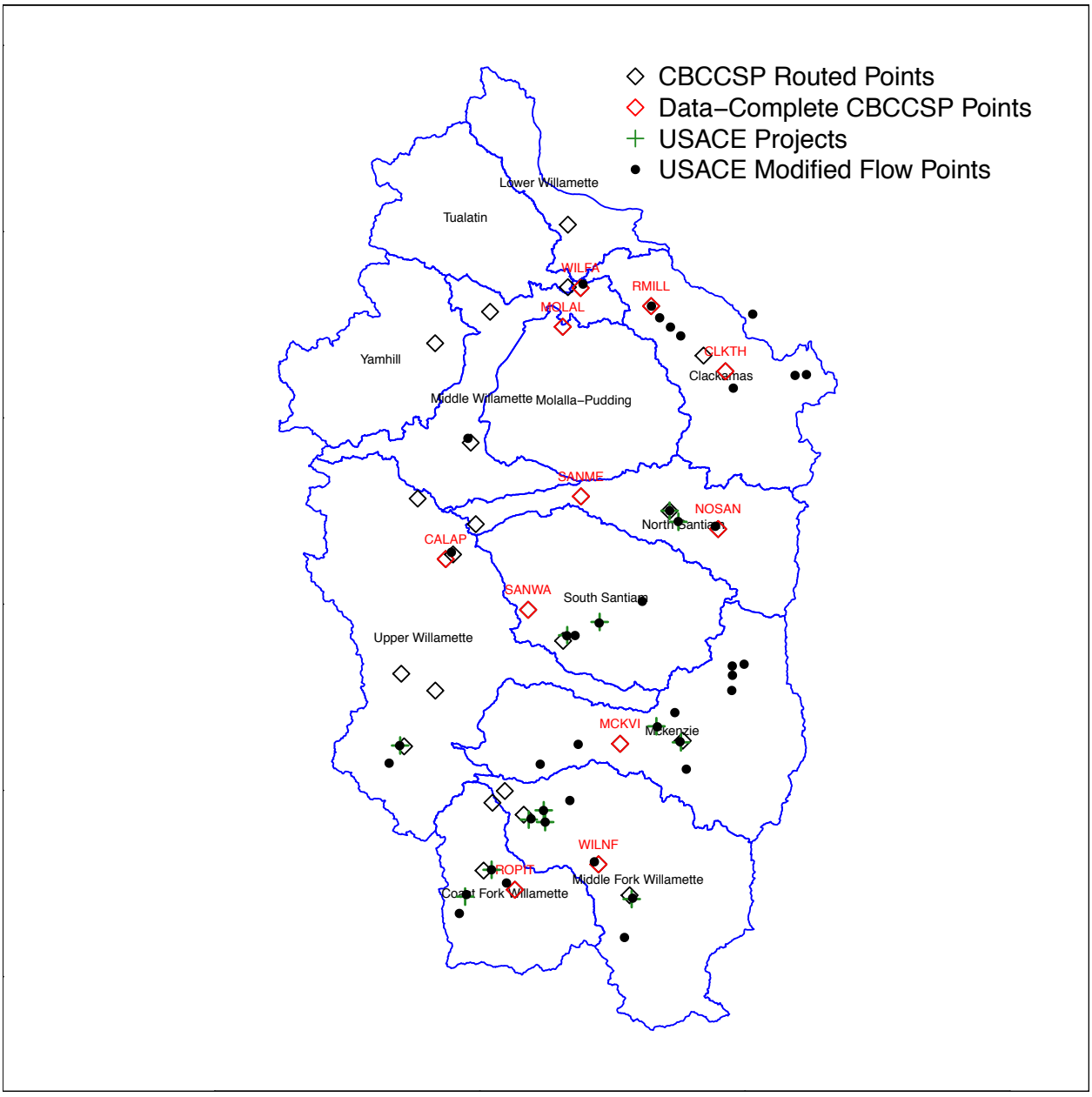

The VIC simulations used gridded daily temperature, precipitation, and wind speed as input variables while other meteorological variables were calculated internally by VIC. VIC was run using both historical meteorological data and projections of future meteorology. Gridded historical meteorological data for the period 1915-2006 were derived from interpolating station data, with adjustments made for topographic influence (Elsner at al., 2010; Hamlet et al., 2010). The future meteorological projections were generated using climate projections from 10 CMIP3 GCMs and two scenarios of future greenhouse gas

emissions: A1B and B1. The CBCCSP used three different methods to downscale climate projections to the resolution of the VIC simulations (see Hamlet et al., 2010, Chapter 4, for details on all three method). For this report, the method known as *hybrid-delta* was used because it was "was developed specifically to support the prediction of daily hydrologic extremes" (Hamlet et al. 2013).

The hybrid-delta method first statistically downscales the monthly output for 1950-2099 from each GCM using the Bias Correction and Spatial Downscaling (BCSD) method (Wood et al. 2002). The "training" data for the downscaling are the historical gridded data mentioned above. To achieve daily time series for each month, a technique involving random sampling from the observed daily records is applied. Lastly, a quantile-mapping technique is used to transform the observed historical meteorological record (1915-2006) so its statistical distribution, at the monthly scale, matches the statistical distribution of the BCSD data over the period 2030-2059. Hybrid-delta data are available for 10 GCMs for A1B and 9 GCMs for B1.

A key property of the hybrid-delta method is that it, through the final quantile-mapping step, "maintains realistic values by closely aligning the time series and spatial behavior of the future values with the gridded observations" (Hamlet et al., 2010). This is important because GCMs may simulate properties of time series (for example, interannual variability and persistence) that are different from observations, and the BCSD downscaling procedure itself does not correct for such discrepancies. Moreover, the daily BCSD procedure has been noted to generate unrealistic values, particularly of precipitation. The hybrid-delta method addresses both of these limitations of straight BCSD downscaling.

Where naturalized flows were available, an additional step was taken to bias-correct the simulated flows so that their statistical properties matched those of the naturalized flow records.

Streamflow Projections Methods

Changes in a variety of metrics/statistics of the simulated historical and future streamflow records were examined at the 11 locations for where there were bias-corrected flow simulations (Table 3, highlighted):

1. Annual streamflow hydrograph (mean climatological flow on each day of the calendar year and mean climatological for each month of the calendar year).
2. The 5th, 50th, and 95th percentiles of monthly streamflow.
3. Mean, 5th, 50th, and 95th percentiles of winter and summer streamflow. Winter was defined as December through February (DJF) and summer was defined as June through September (JJAS).

4. Flow-duration-frequency curves for annual maximum streamflow at 1-, 3-, 5-, 7-, and 15-day durations. Flow duration frequency curves were computed using a customized program written in R. The program emulates key features of the U.S. Army Corps of Engineers Statistical Software Package (HEC-SSP), but permitted greater flexibility in graphics and analysis.

Table 6 Summary of modeled data used in this project

Dataset	Variables	Scenarios	#GCMs	Time Range
Integrated Scenarios: Climate	Maximum Temperature Minimum Temperature Precipitation Wind Speed Downward Shortwave Radiation at the Surface	RCP4.5 RCP8.5	20 CMIP5	1970-1999 2030-2059
Integrated Scenarios: Hydrology	Snow Water Equivalent Precipitation	RCP4.5 RCP8.5	10 CMIP5	1970-1999 2030-2059
Columbia Basin Climate Change Scenarios Project (CBCCSP)	Streamflow	SRES B1 SRES A1B	10 CMIP3	1970-1999 2030-2059

Results

Temperature

Observed Changes

Annual averaged maximum and minimum temperature increased over the period 1901-2013 for nearly all stations in the Willamette and Rogue with warming rates ranging from 0.5°F to 3.9°F per century (Figure 5). The Pacific Northwest (PNW) warmed on average at a rate of about 1.0°F to 1.4°F per century depending on the start year 1901-1960 through 2012 (Abatzoglou et al., 2014). Annually, minimum temperature trends were greater than maximum temperature trends at 6 out of 10 stations in the Willamette and Rogue. For most stations in the PNW, this was also the case (Abatzoglou et al., 2014).

While the majority of locations have warmed, some locations (less than 15% of USHCN stations in the PNW) recorded significant cooling trends in minimum or maximum temperatures (Abatzoglou et al., 2014). Maximum temperature at Three Lynx in the Clackamas sub-basin and minimum temperature at Crater Lake in the Upper Rogue sub-basin decreased annually at a rate of 1.3°F and 1.4 °F per century, respectively; decreases were also noted for most seasons at these two locations (Table 7).

It is incorrect to assume that the cooling observed at Three Lynx and Crater Lake over the period 1901-2013 is indicative of future trends, but rather it simply indicates that at these few locations, natural variability (e.g., some years are colder, some years are warmer) producing temporary cooling trends overwhelmed the warming influence of rising greenhouse gases. Moreover, even at these few stations with cooling, the sign of change is sensitive to the choice of start and end year. Abatzoglou et al. (2014) investigated this question of 'attribution' in more detail. These observed changes are consistent with an expectation that temperature will generally increase under continuing greenhouse gas emissions, even if some locations exhibit cooling trends over shorter periods of time.

The PNW on average warmed during all seasons (Abatzoglou et al., 2014) for long enough periods of record. For those stations in the Willamette and Rogue that exhibited positive annual warming trends, warming also occurred in nearly all seasons with the exception of a few stations in winter and spring (Table 7). However, most negative seasonal temperature trends are not significant.

For maximum temperature, the largest warming occurred in the fall and the smallest warming occurred in the spring for most stations in the Willamette and Rogue (Table 7). For minimum temperature, the smallest increases occurred in the winter and spring and the largest increases were during summer and fall (Table 8). Averaged over the PNW, winter mean temperature warmed the most out of any season (Abatzoglou et al., 2014). This highlights the fact that temperature trend magnitudes vary by location and season.

The PNW-averaged trend in annual average temperature over the period 1901-2012 (i.e., the overall direction of change) was largely explained by rising greenhouse gases. The year-to-year fluctuations in temperature (i.e., some years being cooler or warmer than average) were explained by natural modes of variability (e.g., El Niño-Southern Oscillation and the Pacific North American pattern) and to a smaller degree by solar variability and volcanic forcings. These factors acted either to enhance or counteract the long-term anthropogenic warming trend at different times and in different seasons (Abatzoglou et al., 2014).

Table 7 Annual and seasonal trends in maximum temperature (°F/century) for 1901-2013. Statistically significant trends at the 95% level are denoted by an asterisk and shaded pink for positive trends or blue for negative trends.

Month	Annual	Winter	Spring	Summer	Fall
Corvallis	2.1*	2.6*	0.8	2.5*	2.5*
Cottage Grove	2.7*	2.7*	2.4*	2.5*	3.4*
McMinnville	0.5	0.2	0.4	0.2	1.3*
Forest Grove	1.1*	1.9*	0	0	2.6*
Three Lynx	-1.3*	-1.1	-2.2*	-1.6*	-0.4
McKenzie	0.7	-1.3	0.4	3.1*	0.7
Ashland	1.4*	1.2	0.3	1.7*	2.6*
Crater Lake	1.6*	1.8*	0.1	1.1	3.3*
Grants Pass	3.9*	4.2*	2.5*	4.3*	4.6*
Prospect	1.3*	1.6	-0.2	1.5*	2.5*

Table 8 Annual and seasonal trends in minimum temperature (°F/century). Statistically significant trends at the 95% level are denoted by an asterisk and shaded pink for positive trends or blue for negative trends.

Month	Annual	Winter	Spring	Summer	Fall
Corvallis	1.2*	1.1*	0.9	1.2*	1.8*
Cottage Grove	0.7*	-0.1	0	2.5*	0.6
McMinnville	2.5*	2.0*	1.7*	4.2*	2.1*
Forest Grove	3.3*	2.3*	2.7*	5.3*	2.9*
Three Lynx	0.5*	-0.1	0.2	0.5	1.5*
McKenzie	2.5*	2.5*	1.8*	3.5	2.4*
Ashland	2.6*	1.6*	2.7*	2.8*	3.4*
Crater Lake	-1.4*	-1.7*	-2.6*	-1.7*	0.3
Grants Pass	3.2*	3.5*	2.5*	4.5*	2.4*
Prospect	3.2*	3.2*	2.8*	4.3*	2.7*

Figure 5 Annual trends in maximum (left) and minimum (right) temperature for 10 USHCN stations in the Willamette and Rogue. Large circles denote statistically significant trends.

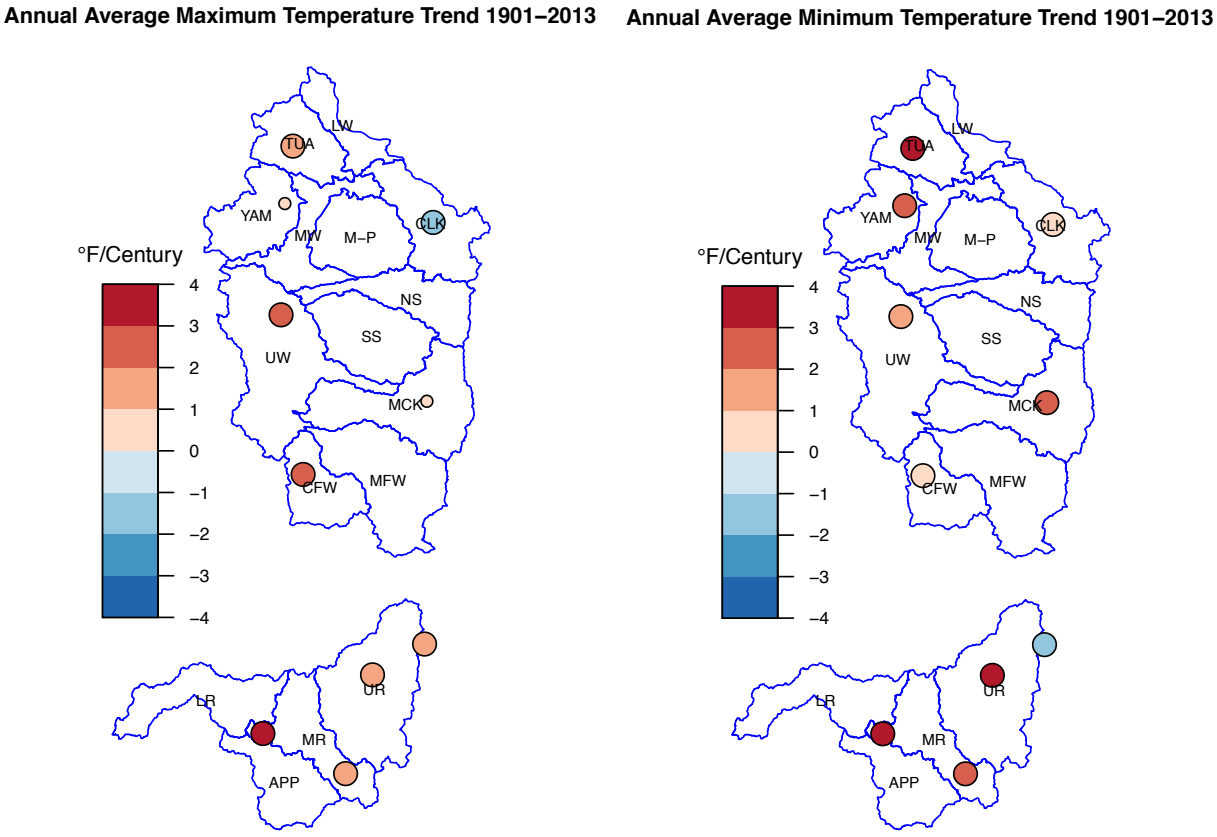

Future Projections

Not surprisingly, both maximum and minimum temperatures are projected to increase everywhere and in every month in the Willamette and Rogue basins for all models and all scenarios by mid-century (defined as 2030-2059 minus 1970-1999). The magnitude of projected warming is larger toward the east reflecting the declining maritime influence away from the coast (Figure 6). RCP8.5 shows more warming than RCP4.5, though the ranges of warming for the two future scenarios overlap. Not until later in the 21st century do the warming projections differ substantially.

Projected increases in maximum temperature tend to be greater than increases in minimum temperature annually and for summer and fall. The range across models, scenarios, and basins of projected increases in annual averaged minimum and maximum temperature is 0.8°F-5.3°F and 1.1°-5.5°F, respectively (Table 9). The largest warming is projected to occur in the summer and ranges from 0.7°F to 6.9°F for minimum temperature and 1.5°F to 7.8°F for maximum temperature (Table 9). (See Appendix C for graphs showing projections of minimum and maximum temperature for each sub-basin.)

Table 9 Mean and range across all models, scenarios, and sub-basins of projected changes in minimum and maximum temperature for the 2040s compared with simulated historical baseline (1970-1999).

Variable	Annual	Winter	Spring	Summer	Fall
Minimum Temperature (°F)	3.2 (0.8,5.3)	3.1 (0.8,5.4)	2.8 (1.0,4.5)	3.7 (0.7,6.9)	3.2 (0.1,5.7)
Maximum Temperature (°F)	3.6 (1.1,5.5)	3.1 (0.8,5.3)	3.1 (0.8,5.2)	4.5 (1.5,7.8)	3.5 (0.7,6.2)

It may seem inconsistent that a majority of stations across the PNW exhibited larger increases in minimum temperature than maximum temperature over the period 1901-2013 while future projections indicate that maximum temperature increases faster than minimum temperature in the Willamette and Rogue Basins. There are at least three explanations that reconcile these facts. First, while the majority of GCMs indicated maximum temperature to increase more than minimum temperature, a few GCMs indicated the opposite suggesting that either result is possible. Second, the manifestation of temperature changes at a point location is determined by local factors not simulated by GCMs. Finally, considerable analysis of the observed trends nationally and globally has noted that the more rapid increase in minimum temperatures happened mostly before 1960. The likeliest explanation for that observation is that before 1960s, both greenhouse gases and air pollution that reflects sunlight were increasing; as industrialized nations reduced air pollution and increased greenhouse gases, daytime highs rose faster relative to nighttime lows. The future emissions scenarios used in the project posit the continuation of these more recent trends, and consequently the GCMs universally conclude that temperatures, both minimum and maximum, will increase in the future under continued greenhouse gas emissions.

Figure 6 Annual and seasonal multi-model mean projections in maximum temperature for RCP4.5 and RCP8.5.

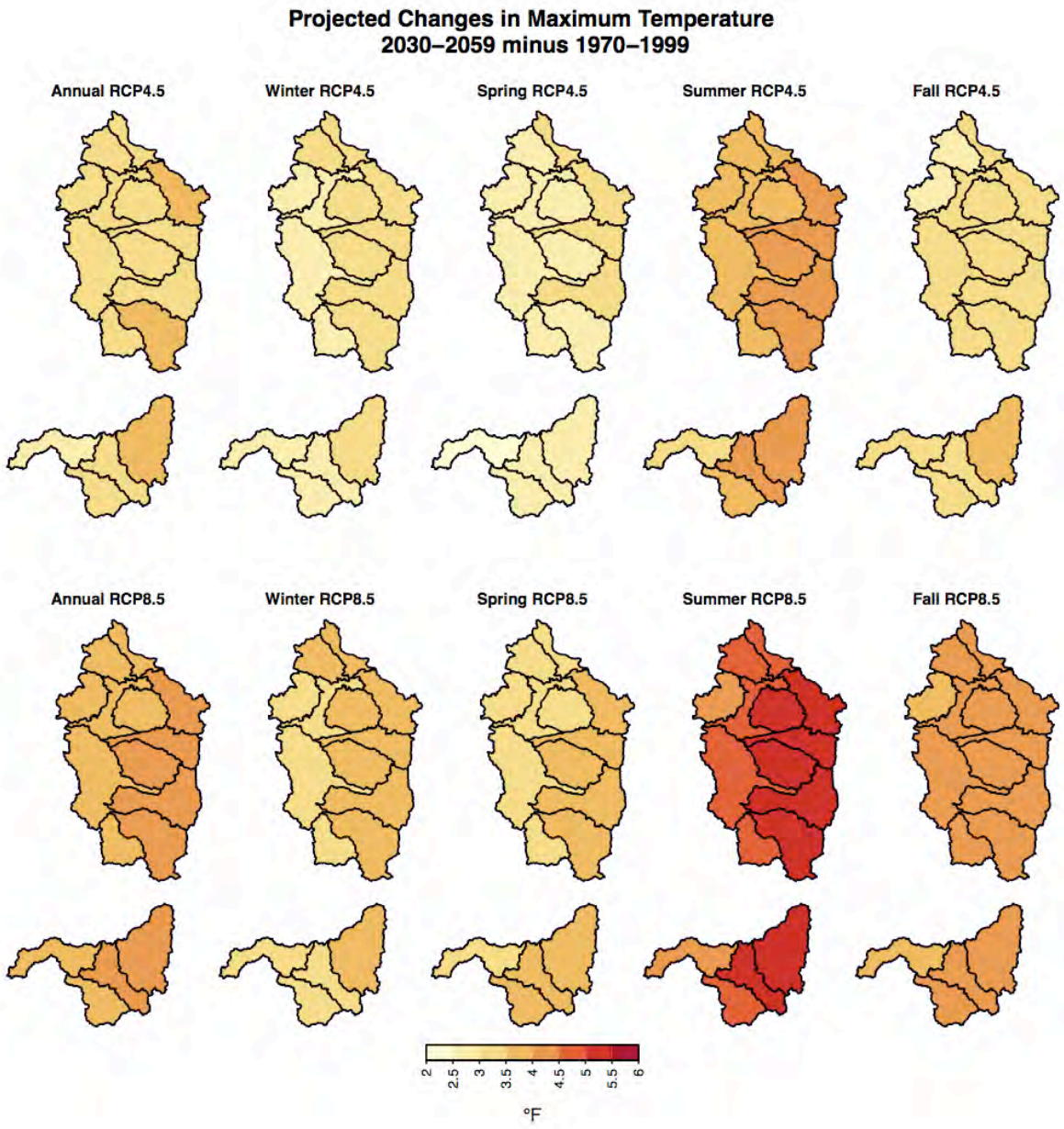

Precipitation

Observed Changes

Most annual and seasonal precipitation trends in the Willamette and Rogue are not significant. Significant positive water year precipitation trends of about 9 inches per century are noted for Three Lynx and Crater Lake and a significant negative trend of -6 inches per century is noted for McMinnville (Figure 7). At stations across the PNW, 28% of

stations had significant increases in water year precipitation from 1920-2012 while only 5% showed significant decreases (Abatzoglou et al., 2014).

Regional water year precipitation averaged over the PNW exhibits considerable variability from year to year and decade to decade with no significant trends from 1901-2012, but a significant positive trend was noted in spring (MAM) (Abatzoglou et al., 2014). There is large spatial variability and heterogeneity in seasonal precipitation trends across the PNW. Only in spring did many stations agree on a positive significant trend (Abatzoglou et al., 2014). For all stations in the Willamette and Rogue, except McMinnville, spring and summer precipitation increased, but the trend was significant for only a few stations (Table 10). Winter and fall precipitation decreased for half of stations in the Willamette and Rogue, but only the winter trend at McMinnville is significant (Table 10).

Unlike for temperature trends, increasing greenhouse gases did not contribute significantly to the observed PNW precipitation trends in any season, suggesting that natural variability is larger than any climate change signal over this period (Abatzoglou et al., 2014).

Table 10 Annual and seasonal precipitation trends (inches/century) over 1901-2013. Statistically significant trends are denoted by an asterisk and shaded pink for negative trends or blue for positive trends.

Month	Annual	Winter	Spring	Summer	Fall
Corvallis	3.9	0.1	2.3*	0.7*	0.8
Cottage Grove	2.5	-0.8	2	0.7*	0.7
McMinnville	-6.0*	-2.5*	-0.1	-0.2	-2.9
Forest Grove	-1.7	-1.3	1.1	0.3	-1.5
Three Lynx	9.1*	1.3	2.8	1.2	3.9
McKenzie	-6	-3.3	0.8	0.5	-4
Ashland	-0.9	-0.6	0.5	0.1	-0.9
Crater Lake	8.7*	1.2	3.9*	0.6	2.8
Grants Pass	1.6	0	1.3	0.4	0.1
Prospect	0.9	-0.8	1.7	0.5	-0.4

Figure 7 Annual precipitation trends from 10 USHCN stations in the Willamette and Rogue Basins. Large circles denote statistically significant trends.

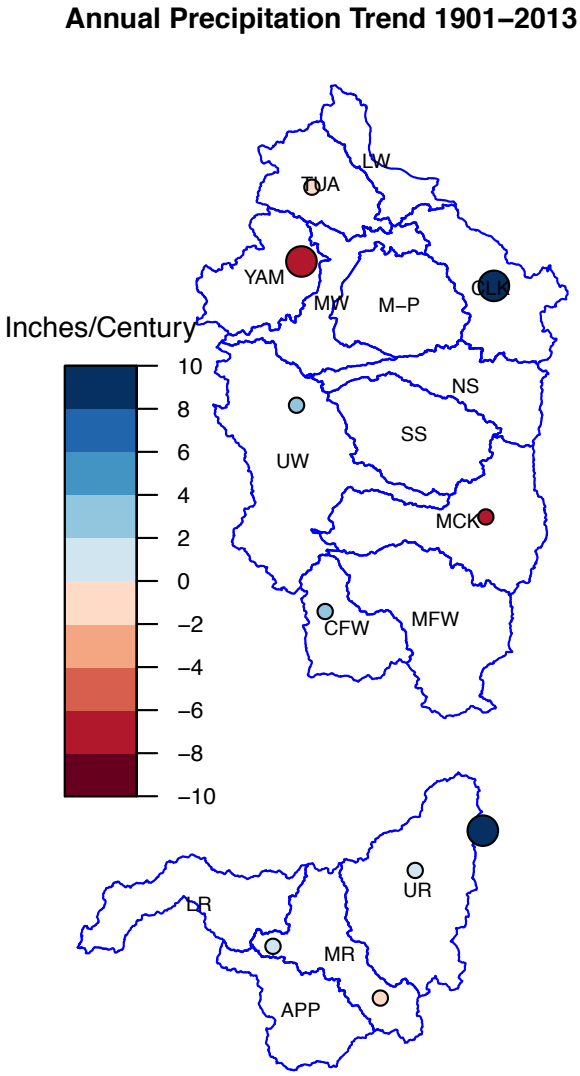

Future Projections

Annual precipitation is projected to change little. The range of model projections is not large, but includes both upward and downward changes in each season. Table 11 shows the mean and range of projected precipitation changes for each basin seasonally and annually. Annually, absolute changes in precipitation range from -6.7 inches to +8.2 inches across models, scenarios, and basins. The majority project decreases in summer precipitation and increases in winter precipitation by mid-century, but the multi-model mean change is quite small relative to natural variability in each season. The multi-model mean change in precipitation may not necessarily be the "best" estimate of future conditions so considering the range of plausible outcomes as represented by the range across models is recommended.

Table 11 Mean and range across all models, scenarios, and sub-basins of projected changes in precipitation for the 2040s compared with simulated historical baseline (1970-1999).

Variable	Annual	Winter	Spring	Summer	Fall
Precipitation (Inches)	0.8 (-6.7,8.2)	1.3 (-3.9, 6.9)	0.01(-2.6, 3.3)	-0.5 (-2.6, 1.3)	-0.1 (-4.6, 3.9)

The multi-model mean change in precipitation is negative in summer, positive in winter and annually for all basins under both future scenarios (Figure 8). Spring and fall precipitation changes are negative in some basins and positive in others. The apparent pattern of increasing precipitation to the north and decreasing precipitation to the south in the spring and fall is likely dependent on the climate models included in the average since using the smaller subset of 10 does not show this same relationship with latitude.

The multi-model mean and majority of models project decreases in summer precipitation which is opposite in sign of the observed summer precipitation trends. As mentioned before, changes in precipitation are dominated by factors other than rising greenhouse gases. In addition, the signal-to-noise ratio is low as indicated by the fact that few observed trends in precipitation are statistically significant, which is to say that a long-term trend could not be discerned amid the large year-to-year variability. Because natural variability in precipitation is particularly large, the sign of an observed trend depends on the choice of start and end year. Furthermore, future projections demonstrate a wide range of plausible futures, including a few models that project increases in summer precipitation. (See Appendix D for graphs comparing the simulated historic and future climatology of precipitation for each sub-basin.)

Figure 8 Annual and seasonal multi-model mean projected changes in precipitation for RCP4.5 and RCP8.5.

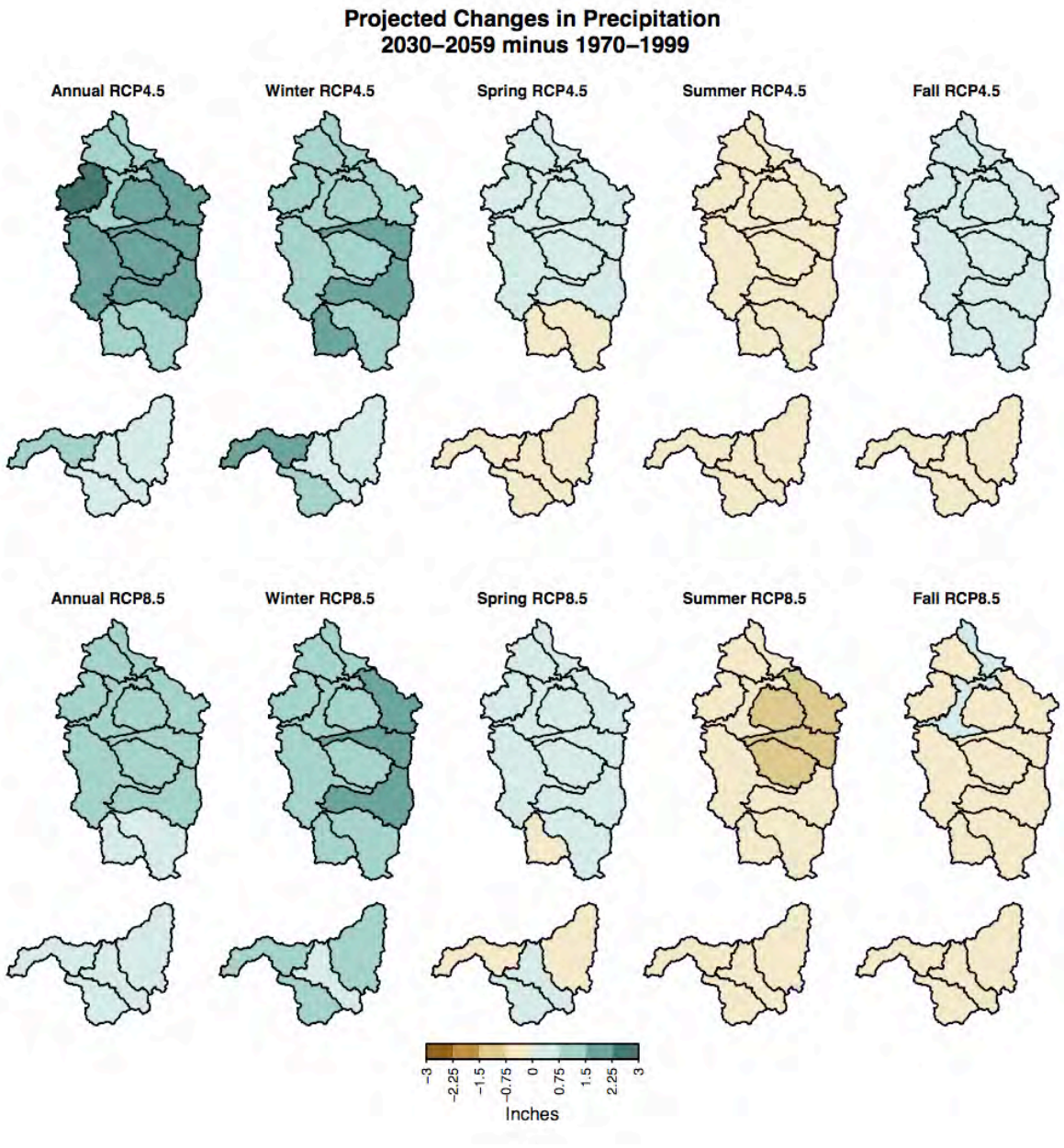

Snow Water Equivalent (SWE)

Observed Changes

Only two of the 23 stations in the Willamette and Rogue with data back to 1960 had significant trends in April 1 snow water equivalent (SWE) (Figure 9). At Hogg Pass, at about 4800 feet in the McKenzie sub-basin, and at Diamond Lake, at about 5300 feet in the Upper Rogue sub-basin, April 1 SWE declined by 34% and 59%, respectively, over the period 1960-2014. Trends at all other stations, except Siskiyou Summit in the Middle Rogue, were

negative ranging from a decrease of 3% to 60%. Siskiyou Summit had a positive, though not significant, trend in April 1 SWE amounting to a 100% increase over the period of record, however, the mean SWE is so small that the small absolute increase resulted in a large relative change.

Across the West, snowpack declined at about three-fourths of the more than 700 SNOTEL/Snow Course stations. The largest decreases in April 1 SWE occurred in Washington, Oregon, and the Northern Rockies, but the southern Sierra Nevada in California exhibited increases in snowpack. Averaged over all sites in the West, the average change in April 1 SWE over the period 1955-2013 was a 14% decline. About a quarter of all stations exhibited statistically significant trends in April 1 SWE, most being decreases (Mote and Sharp, 2014).

Stations in the Willamette and Rogue were grouped into the upper quartile (largest relative decrease), lower quartile (smallest relative decrease), and innerquartile of magnitude of relative decreases. Stations with the largest relative decreases had an average elevation of 4220 feet compared with 5637 feet as the average of stations with the smallest relative decreases. Snowpack decreased more at lower elevations where winter temperatures hover around freezing as reported by Mote et al. (2005) for the western US. In fact, it is these low elevation sites that are most “at-risk” for loss of snowpack under future climate change (Nolin and Daly, 2006).

Table 12 Trends in April 1 SWE from 1960-2014 ordered by largest to smallest relative decrease. Sites with statistically significant trends are denoted with an asterisk.

StationName	Elev(ft)	Trend%	TrendAbs(cm/yr)	MeanSWE(in)
Upper Quartile of Relative Decrease				
DeadwoodJunction_SC	4660	-60.0	-0.21	5.2
*DiamondLake_ST	5280	-58.5	-0.59	15.1
MarionForks_ST	2590	-44.5	-0.28	10.3
HowardPrairie_SC	4580	-38.9	-0.13	5.7
PeavineRidge_ST	3420	-34.5	-0.26	13.5
*HoggPass_ST	4790	-34.0	-0.68	36.2
Mean:	***4220***	***-45.1***	***-0.36***	***14.3***
Innerquartile Range of Relative Decrease				
FishLk._ST	4660	-32.9	-0.18	8.9
FourmileLake_ST	5970	-31.2	-0.54	28.7
BillieCreekDivide_ST	5280	-25.4	-0.31	21.0
JumpOffJoe_ST	3520	-24.7	-0.15	11.1
MarysPeak_SC	3580	-24.3	-0.11	8.5
SilverBurn_SC	3680	-20.4	-0.09	8.9
BeaverDamCreek_SC	5120	-20.3	-0.11	10.1
AnnieSprings_ST	6010	-19.7	-0.42	41.8
ColdSpringsCamp_ST	5940	-7.1	-0.09	27.2
SaltCreekFalls_ST	4220	-6.2	-0.06	18.9
Mean:	***4798***	***-21.2***	***-0.21***	***18.5***
Lower Quartile of Relative Decrease				
IrishTaylor_ST	5540	-5.5	-0.09	35.6
ParkH.q.Rev_SC	6570	-5.1	-0.14	58.7
SummitLake_ST	5610	-5.1	-0.10	38.5
CascadeSummit_ST	5100	-3.9	-0.06	31.6
RoaringRiver_ST	4950	-3.8	-0.05	29.0
BigRedMountain_ST	6050	-2.6	-0.03	27.4
Mean:	***5637***	***-4.3***	***-0.08***	***36.8***
Relative Increase				
SiskiyouSummit_SC	4560	100.8	0.12	4.0

Figure 9 April 1 SWE trends (cm/year) from 1960-2014 at SNOTEL/Snow Course sites in the Willamette and Rogue. Large circles denote statistically significant trends.

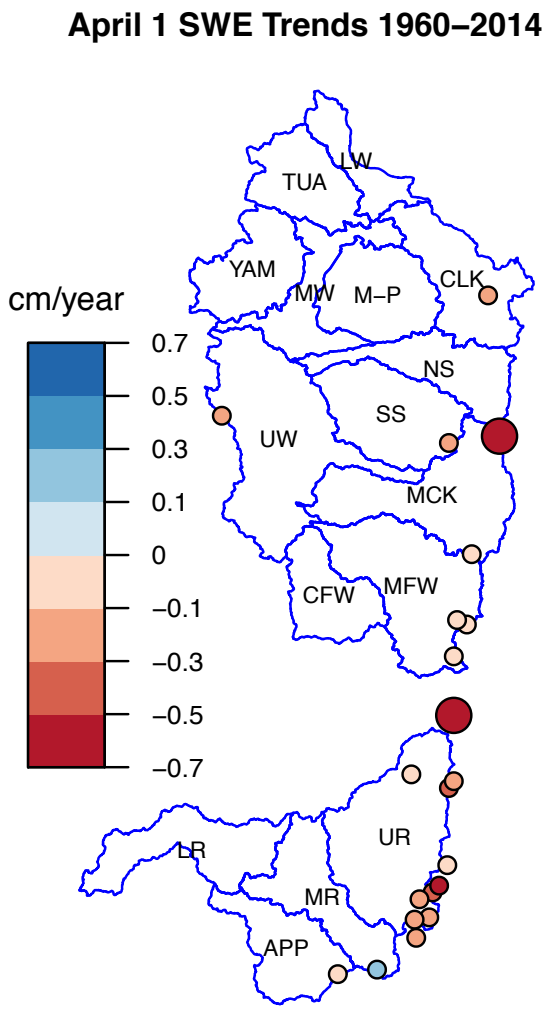

Future Projections

Projected changes in snow water equivalent (SWE) of the snowpack is presented as a fraction of accumulated water-year precipitation (P) because it removes the confounding influence of projected changes in precipitation (snow + rain) on changes in SWE. Consistent with previous CMIP3-based scenarios of future changes to SWE/P in the region (e.g. Hamlet et al. 2013), the CMIP5-VIC simulations show large reductions in SWE/P for those sub-basins in the Willamette and Rogue Basins that receive the most snow. For example, for the North Santiam Basin (17090005), a higher elevation basin on the windward side of the Cascades, April 1 SWE/P is projected to decrease from 35% historically to 17% for RCP4.5 and 15% for RCP8.5 (see Figure 10, upper panel). When considered as a relative change,

winter declines in SWE/P for the North Santiam average 47% and 56% for RCP4.5 and RCP8.5, respectively, with slightly greater relative reductions in spring (Figure 11).

Figure 10 Simulated historic and future basin-averaged, 30-year mean snow water equivalent (SWE) on the first day of the month as a percentage of accumulated water year precipitation for the North Santiam basin (17090005; upper panel) and Middle Willamette basin (17090007; lower panel). The solid line and shading give the mean and 5th to 95th percentile range, respectively, of simulations from 10 GCMs.

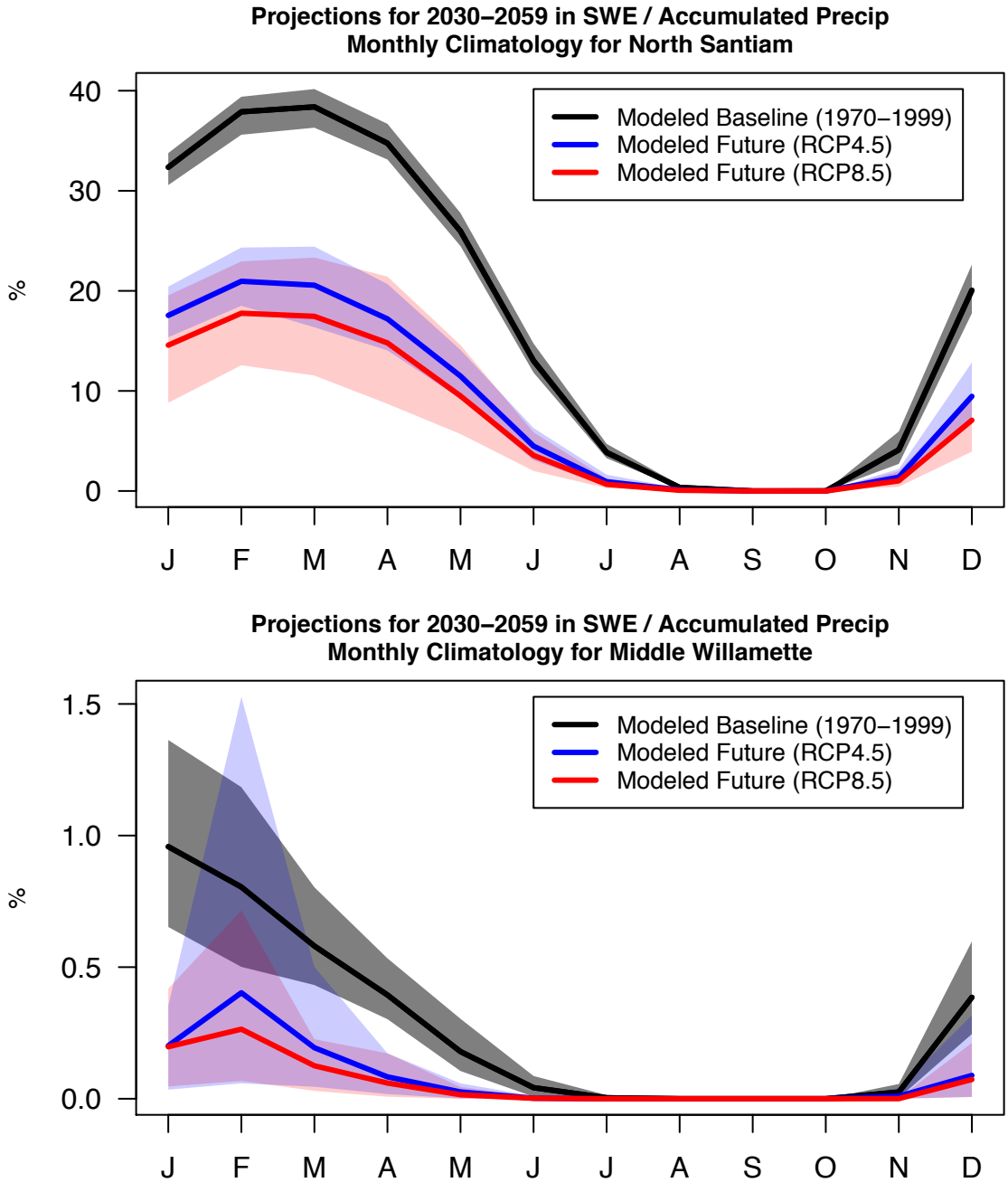

Those basins with historically small snow storage are projected to have negligible SWE/P in the future, as demonstrated by Middle Willamette Basin (17090007) April 1 SWE/P changing from 0.4% to < 0.1% (see Figure 10, lower panel). The other sub-basins in the Willamette and Rogue lie along a spectrum of changes bounded by these two examples. Historical and future SWE/P, and relative changes in SWE/P, for each of the 16 HUC8 basins are summarized in Table 13.

While higher elevation sub-basins in the eastern Willamette and Rogue basin show the largest absolute decreases in SWE/P, the more rain-dominated western sub-basins of the Willamette and Rogue Basin tend to show the larger relative declines in SWE/P (Figure 12). Though these relative declines in rain-dominated sub-basins exceed 80%, in, for example, winter for RCP8.5, the absolute drop in SWE/P is low. (See Appendix E for graphs showing projections of SWE/P for each sub-basin.)

Figure 11 "Box and whisker" plots showing changes in SWE/P. For each season, the figures indicate the distribution of projections from different GCMs of basin-averaged, 30-year mean snow water equivalent (SWE) on the first day of the month as a percentage of accumulated water year precipitation for the North Santiam basin (17090005). Individual GCM projections are given by the circles, and the box and whiskers show the median, inner quartile range, and 5th and 95th percentiles.

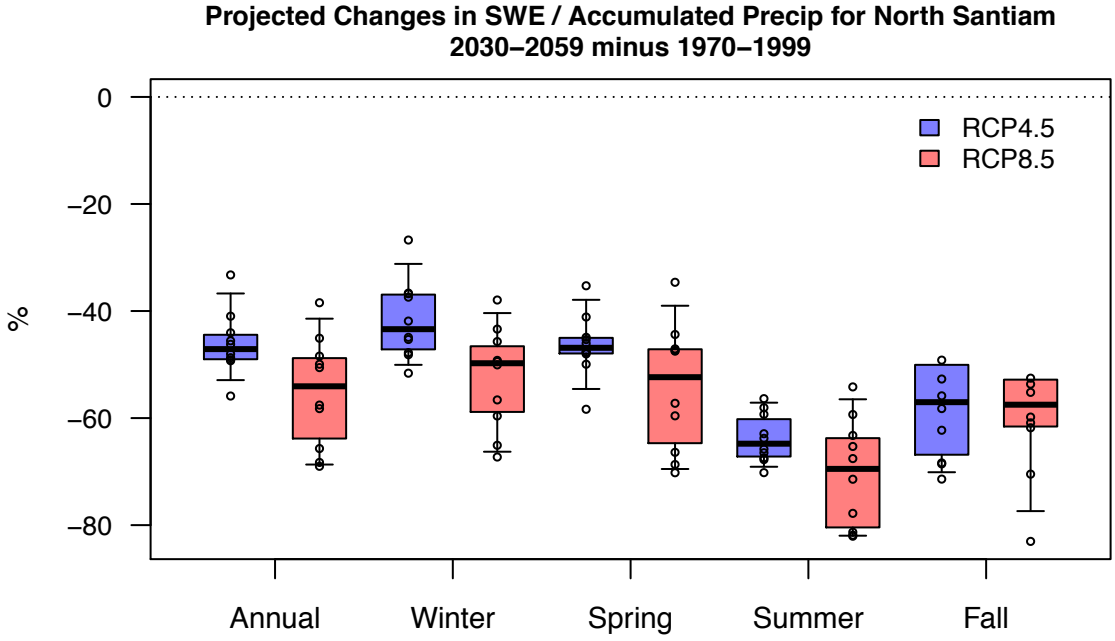

Table 13 Range across all models and scenarios of projected sub-basin averaged seasonal changes in snow water equivalent on the first day of the month as a percentage of accumulated water year precipitation (SWE/P). Rogue River sub-basins are shaded. Changes are given as relative differences (%). Asterisk denotes basins/seasons with little snow accumulation (at least one simulation of historical period with mean SWE/P < 1%).

HUC8 ID	Sub-Basin	Ann	Win	Spr	Sum	Fal
17090001	Middle Fork Willamette	-67, -30	-66, -24	-67, -32	-87, -58	*
17090002	Coast Fork Willamette	-81, -38	-79, -29	-85, -46	*	*
17090003	Upper Willamette	*	-88, -32	*	*	*
17090004	McKenzie	-62, -29	-60, -23	-63, -30	-78, -52	-74, -33
17090005	North Santiam	-69, -33	-67, -27	-70, -35	-82, -54	*
17090006	South Santiam	-82, -42	-79, -34	-86, -45	-98, -79	*
17090007	Middle Willamette	*	*	*	*	*
17090008	Yamhill	*	*	*	*	*
17090009	Molalla-Pudding	-89, -48	-84, -40	-94, -53	*	*
17090010	Tualatin	*	-93, -29	*	*	*
17090011	Clackamas	-76, -39	-73, -31	-78, -39	-94, -71	*
17090012	Lower Willamette	*	*	*	*	*
17100307	Upper Rogue	-70, -31	-68, -26	-69, -35	-90, -58	*
17100308	Middle Rogue	-71, -32	-70, -26	-71, -39	*	*
17100309	Applegate	-65, -27	-62, -21	-65, -32	-90, -60	*
17100310	Lower Rogue	-88, -34	-85, -26	-91, -43	*	*

Figure 12 Seasonal mean change from simulated historical to future basin-averaged, 30-year mean snow water equivalent (SWE) on the first day of the month as a percentage of accumulated water year precipitation. Changes are averaged over simulations from 10 GCMS and are calculated as relative differences. Non-shaded basins have less than a 1% mean SWE/P over the baseline period.

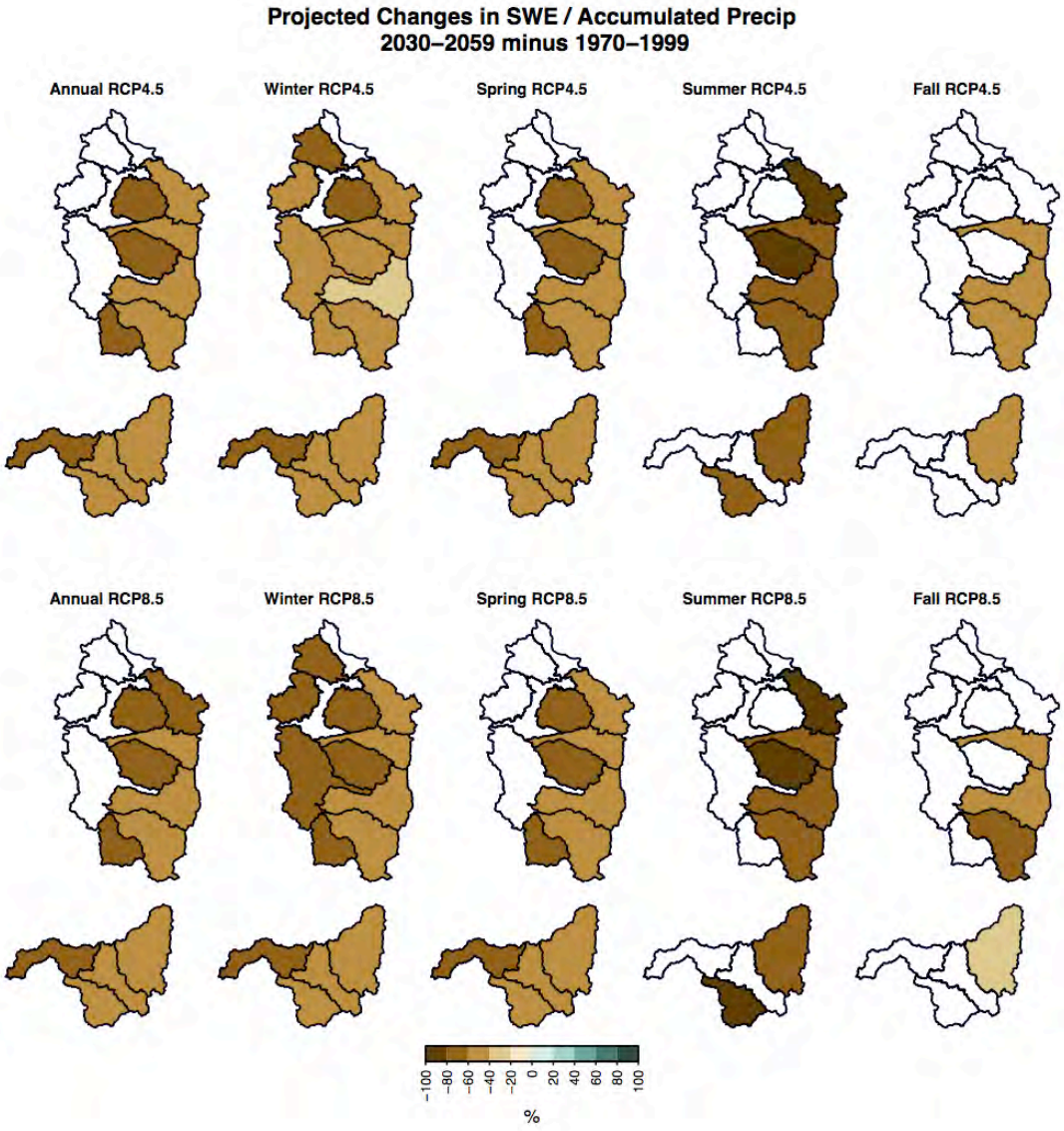

Wind Speed

The Corps requested projected changes in average wind speed to help discern future drought potential through wind-driven evaporation and negative water quality impacts through stratification.

Future Projections

In the Willamette and Rogue basins, simulated average wind speed is greatest in the winter with a smaller maximum in the summer (e.g., Figure 13). The local terrain influences the prevailing wind direction. In the Willamette Valley, for example, wind generally blows from the south in the winter and from the north in the summer following the orientation of the valley.

Figure 13 Average wind speed monthly climatology for simulated historic (1970-1999) and future (2030-2059) for the Lower Willamette basin (17090012). The solid line and shading give the mean and 5th to 95th percentile range, respectively, of simulations from 20 GCMs.

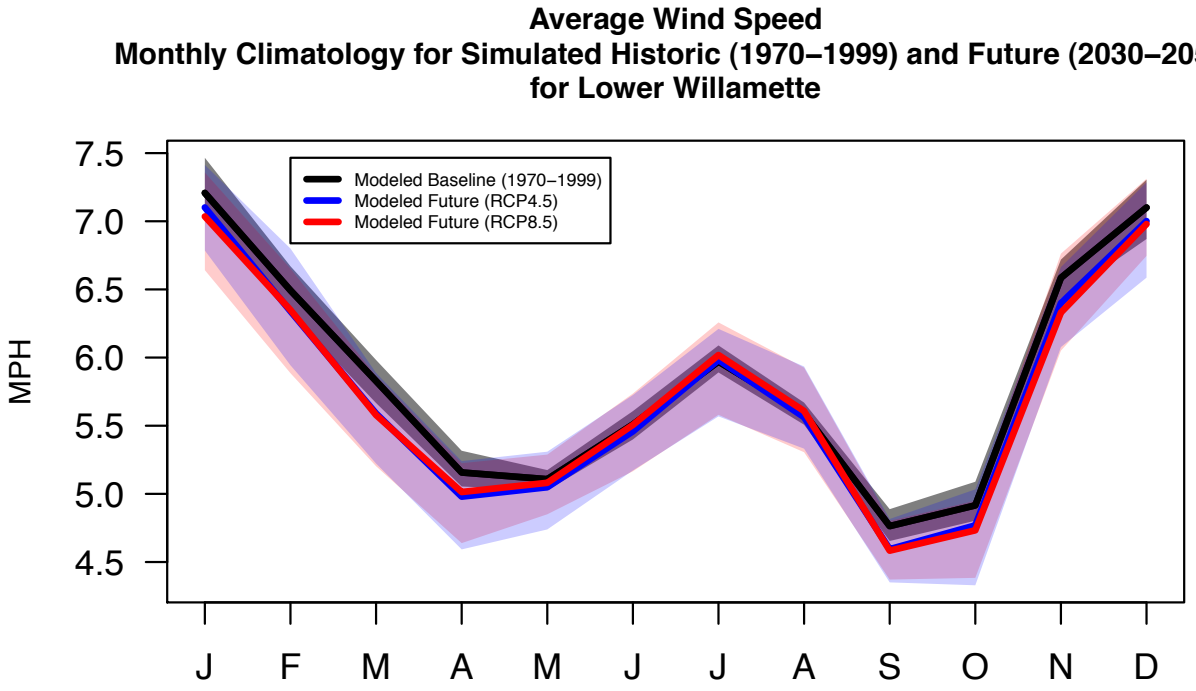

Wind speed in fall, winter, and spring and annually is projected to decrease for the multi-model mean by a few tenths of a mile per hour (Table 14). In the summer, wind speed is not projected to change. Some models projected increases and decreases in each season, but the majority of models projected decreases in fall, winter, and spring, whereas the models are roughly split between increases and decreases in summer.

Table 14 Mean and range across all models, scenarios, and sub-basins of projected changes in average wind speed for the 2040s compared with simulated historical baseline (1970-1999).

Variable	Annual	Winter	Spring	Summer	Fall
Wind Speed (mph)	-0.1(-0.5,0.2)	-0.1 (-0.8, 0.5)	-0.1 (-0.6, 0.2)	0.0 (-0.5, 0.6)	-0.2 (-0.5, 0.2)

Overall, the magnitude of changes is very small, less than one mile per hour. From the northern hemisphere sub-tropics to the pole, projected changes in wind speed at the surface are less than one standard deviation of the natural variability making a true climate change signal in surface wind speed difficult to detect even by the end of the 21st century (Collins et al., 2013). Furthermore, wind speed and direction is highly influenced by local topography.

Cloud Cover

Future Projections

Projections of changes in cloud cover were estimated by using downward shortwave radiation at the surface. Figure 14 presents historical and future climatologies of percent of days in each month in which cloud cover was considered clear, broken, scattered, or overcast based on the definitions in Table 5. Across all sub-basins, clear days are most common in the summer months, not surprisingly, and future projections indicated a higher percentage of clear summer days in the future (along with fewer days of broken clouds or overcast days). The percent of winter clear days is projected to remain the same (close to 0%). The typical overcast or mostly cloudy skies of winter will remain recognizable in the future, but projections suggest small increases in the percent of overcast days during winter months accompanied by small decreases in percent of days with broken clouds. These results reflect a strengthening of the seasonality of cloud cover with more sunny days in the summer and more cloudy days in the winter. It is important to note, however, that the previous statements are based on the multi-model mean change and that models do not unanimously agree on the sign of change in cloud cover for any category or month.

Figure 14 Projected changes by 2030-2059 in monthly cloud cover for Middle Fork Willamette (17090001). Percent of days in each month, in which skies are clear, scattered, broken, or overcast as defined in Table 5. Solid lines and shading denote the multi-model mean and 5th to 95th percentile range across 20 GCMs, respectively.

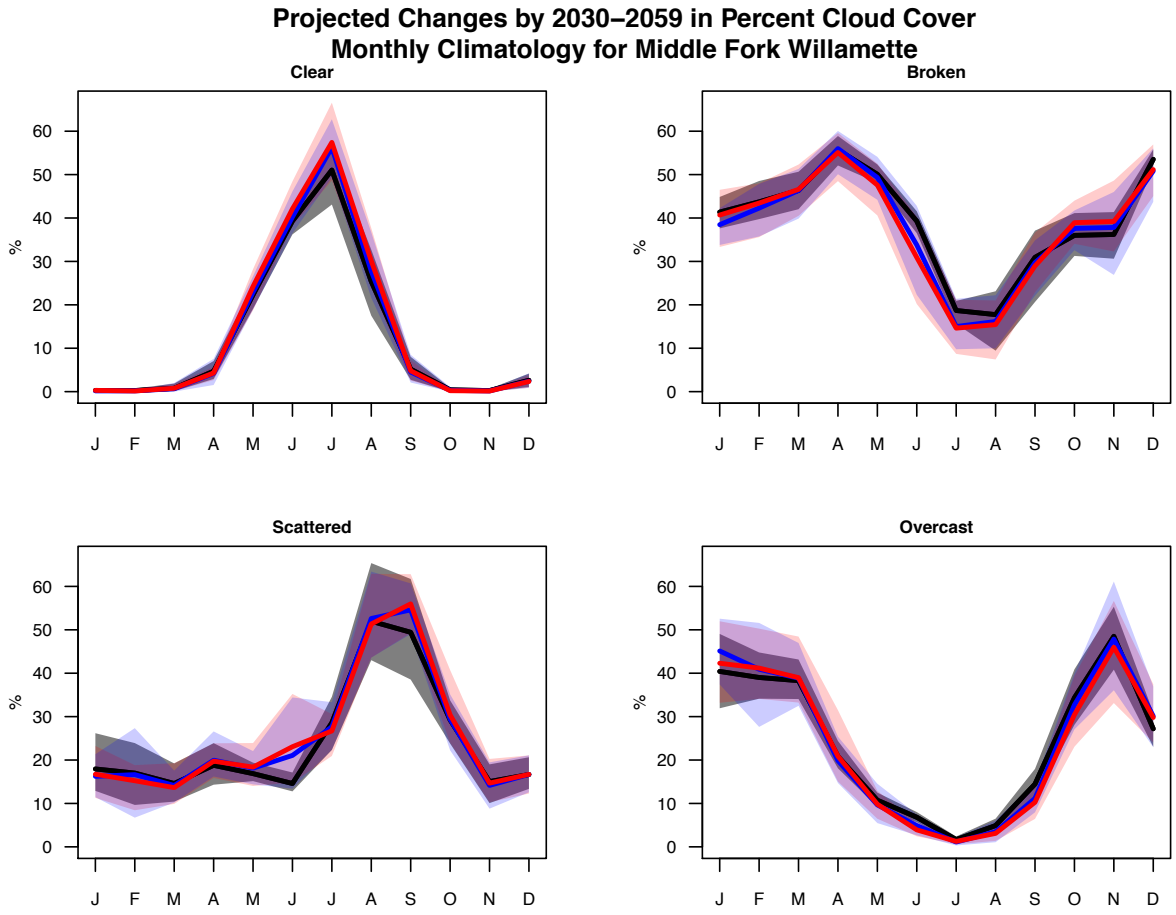

Streamflow Volumes

Observed Changes

Hydrographs are presented for two gages in the Willamette and one in the Rogue representing gages that show high and low sensitivity to snow. The North Santiam below Boulder Creek near Detroit (just above Detroit Dam, so there are no regulation effects) is an example of a high-sensitivity gage whereas the Willamette at Albany (substantial regulatory effect) and the Rogue River at Raygold near Central Point (also with regulation effects) are low-sensitivity gages. All of these gages were selected because they have a sufficiently long and complete historical record.

Hydrographs of the 95th (low flow), 50th, and 5th (high flow) percentile of monthly streamflow values were generated for the Rogue River at Raygold over the period 1905-2014 and the Willamette River at Albany over the period 1892-2014 (Figure 15). Both

gages see their peak highest flows in mid-winter and lowest flows in the late summer months. Both of these gages are below reservoirs, and are heavily influenced by regulation. Regulation upstream of Albany (multiple projects with varying construction years) began during the historical period (1941-1970) and Lost Creek dam was completed in 1977 between the two time periods examined (see Table 15).

Figure 15 5th, 50th, and 95th percentiles of monthly observed streamflow Willamette River at Albany (1892-2014; top) and Rogue River at Raygold (1905-2014; bottom).

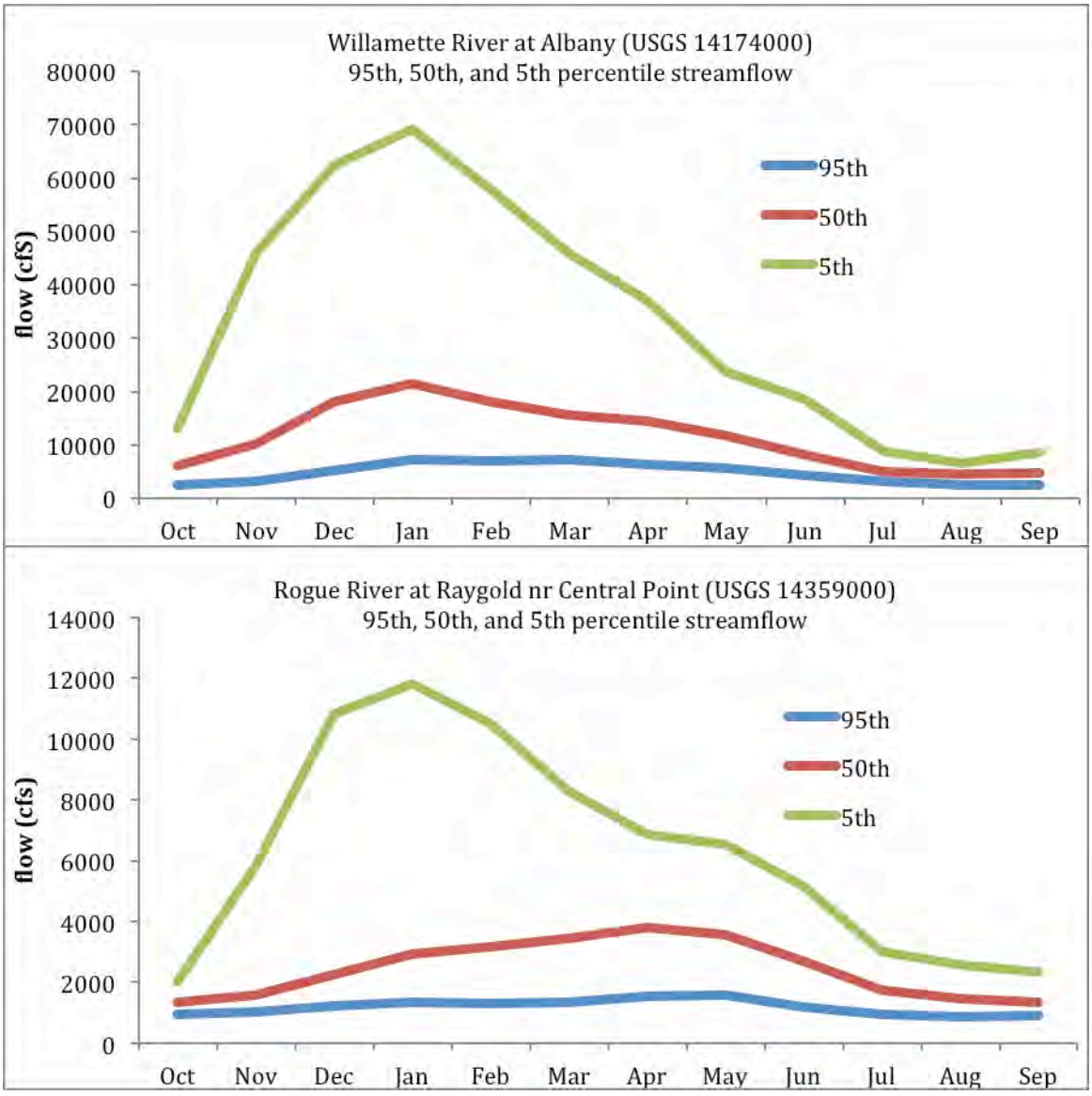

The North Santiam below Boulder Creek near Detroit (USGS 14178000) is above the reservoir, and therefore unregulated. The hydrograph at this gage has a bimodal pattern early in the record (1941-1970) with peaks in later winter and early summer. The 1981-2010 period shows nearly constant flows from December to May, with a decline starting in June and lower flows in the summer and fall (Figure 16, upper panel). Most of these changes are consistent with the pattern expected from warming: increased flows in spring and decreased flows in summer. Stewart et al. (2005) found such trends in streamflow throughout the West, in unregulated snowmelt-dominated basins. This finding is supported by trends in temperature and snow water equivalent.

In contrast to the North Santiam, the observed hydrographs from the two low-sensitivity gages reveal the opposite of what is expected with recent warming (Figure 16, center and lower panels). The plots in this study show higher summer flows and lower winter flows between the periods 1941-1970 and 1981-2010. This is consistent with regulation practices since the Willamette Basin is managed for flood control. Hatcher and Jones (2013) found that streamflow changed significantly at gages downstream of dams in the Willamette. They concluded that the significant trends were not due to climate change, but consistent with regulation practices. The hydrographs from the Willamette River at Albany and the Rogue River at Raygold near Central Point reflect the change in management between the two time periods to lower peak flows in the winter and supplement low flows in the dry season.

Figure 16 Historical streamflow for selected gages in the Willamette and Rogue River Basins reflecting conditions in the periods 1941-1970 and 1981-2010.

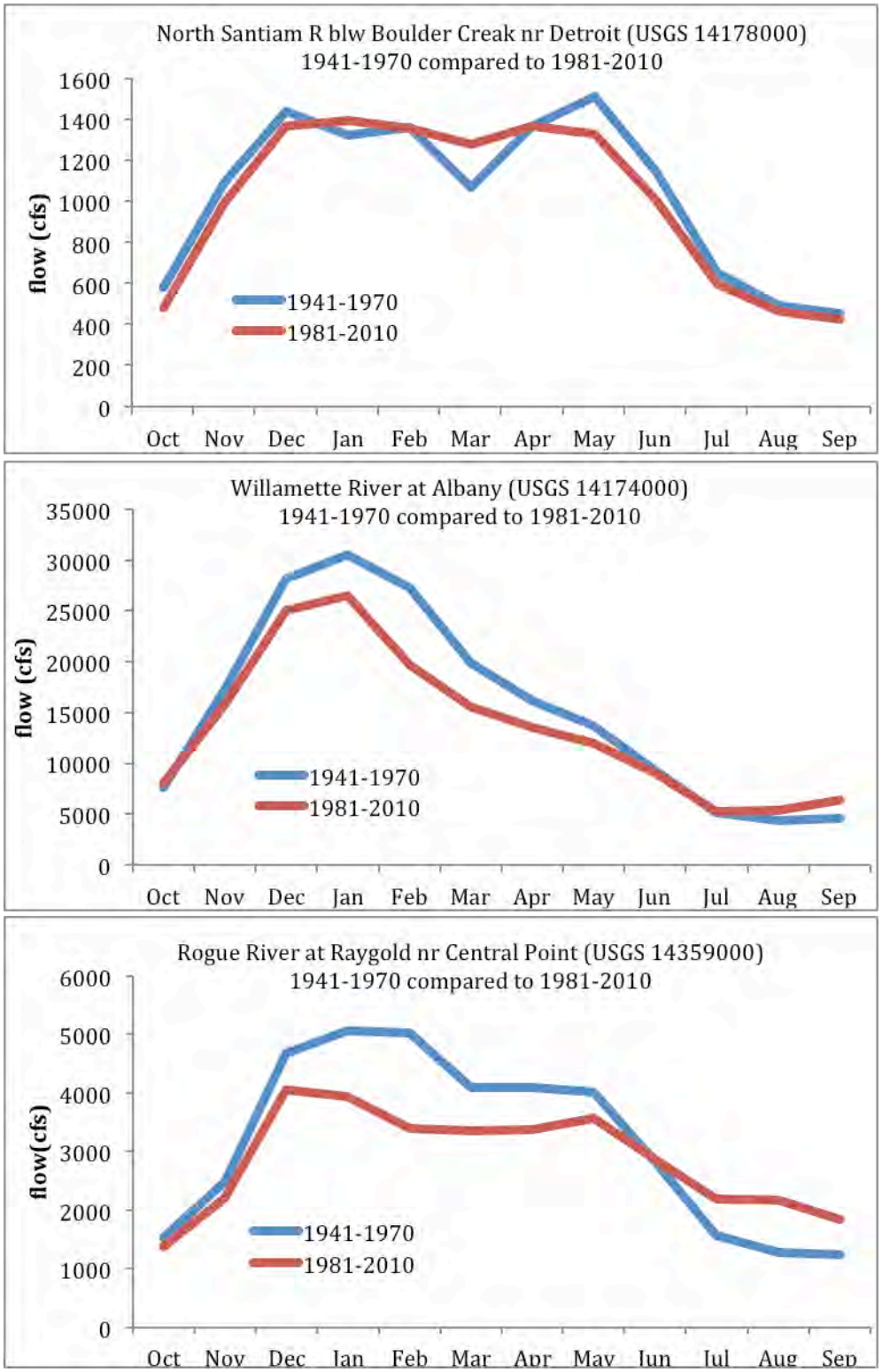

Future Projections

Because CBCCSP bias-corrected, naturalized streamflow projections are not available at each of the USACE Project sites, we instead associated a CBCCSP location with each Project. The association was based on an expected streamflow response to a changing climate.

Although precipitation is projected to increase in winter and decrease in summer over the region (see Figure 8), the variability across the Willamette sub-basins in terms of streamflow changes in response to projected climate change is driven primarily by changes in snow accumulation and melt. Therefore, the distribution of elevations above a Project is a primary control on projected streamflow changes. Other factors influencing variability in streamflow response from Project to Project are spatial differences in the magnitude of temperature and precipitation changes, and physical properties of the basins themselves, such as their deep groundwater contribution (Tague et al., 2008).

First, spatial proximity was considered when associating a CBCCSP to a Project, assuming physical basin properties and magnitude of climate change would be most similar in nearby locales. Then site elevation (as a proxy for upstream elevations) was used to alter the initial association when the elevation of the nearest CBCCSP site was very different from the Project elevation. In effect, this meant the one high-elevation CBCCSP site (at 1590 ft) was associated with all Projects above 1500 ft, even though the CBCSSP site was in a different sub-basin from the Project.

The 6 CBCCSP sites associated with the Projects are given in Table 15. Projected changes in streamflow are presented at each of these size sites. It is important to emphasize that the absolute magnitudes of projected streamflow changes from these associated CBCCSP sites will not be directly applicable to the Projects themselves because the gages measure discharge from upstream areas with different properties, of which total drained area is a principle, but not the only, meaningful property. (See Appendix F for graphs showing projections of streamflow for all 11 sites.)

Table 15 USACE Projects in the Willamette and Rogue Basins and associated CBCCSP locations with bias-corrected normalized streamflow projections

ID	Project Name (Year Completed)	Sub-Basin	Project elevation (NGVD, ft)	Associated CBCCSP gaging station	Gaging station elev. (ft)
Willamette River Basin					
HCR	Hills Creek (1961)	Middle Fork Willamette	1548	North Santiam R Blw Boulder Cr Nr Detroit (NOSAN)	1590
LOP	Lookout Point (1954)	Middle Fork Willamette	941	Middle Fork Willamatte R Blw N Fork Nr Oakridge (WILNF)	935
DEX	Dexter (1954)	Middle Fork Willamette	703	Middle Fork Willamatte R Blw N Fork Nr Oakridge (WILNF)	935
FAL	Fall Creek (1966)	Middle Fork Willamette	839	Middle Fork Willamatte R Blw N Fork Nr Oakridge (WILNF)	935
COT	Cottage Grove (1942)	Coast Fork Willamette	808	Row R above Pitcher Cr Nr Dorena (ROPIT)	856
DOR	Dorena (1949)	Coast Fork Willamette	866	Row R above Pitcher Cr Nr Dorena (ROPIT)	856
FRN	Fern Ridge (1941)	Upper Willamette	380	Row R above Pitcher Cr Nr Dorena (ROPIT)	856
CGR	Cougar (1963)	McKenzie	1700	North Santiam R Blw Boulder Cr Nr Detroit (NOSAN)	1590
BLU	Blue River (1969)	McKenzie	1362	McKenzie R Nr Vida (MCKVI)	856
GPR	Green Peter (1968)	South Santiam	941	South Santiam at Waterloo (SANWA)	370
FOS	Foster (1968)	South Santiam	703	South Santiam at Waterloo (SANWA)	370
DET	Detroit (1953)	North Santiam	1580	North Santiam R Blw Boulder Cr Nr Detroit (NOSAN)	1590
BCL	Big Cliff (1953)	North Santiam	1212	North Santiam R Blw Boulder Cr Nr Detroit (NOSAN)	1590
Rogue River Basin					
LOS	Lost Creek (1977)	Upper Rogue	1872	North Santiam R Blw Boulder Cr Nr Detroit (NOSAN)	1590
APP	Applegate (1980)	Applegate	1994	North Santiam R Blw Boulder Cr Nr Detroit (NOSAN)	1590

Hills Creek, Cougar, Detroit, and Big Cliff Projects – High streamflow sensitivity

The North Santiam below Boulder Creek near Detroit (*NOSAN 4056*) is used as an example of a *high-sensitivity* streamflow site, and associated it with the Hills Creek, Cougar, Detroit and Big Cliff Projects. Even though Hills Creek and Cougar are not located in the North Santiam, their high elevations place them into a category of high-sensitivity.

At *NOSAN*, historically, relatively high mean flows are sustained from December into June (Figure 17) because of the contribution from a melting snowpack, despite the reduction in precipitation from winter to summer. The A1B and B1 hybrid-delta climate scenarios lead to increases over historical flows in the winter months and lead to flow decreases from historical beginning in late April and continuing through the end of October. (Note: from the simulated streamflow data analyzed here, the timing of this shift from increasing to decreasing flow is imprecise due to step changes between months that are artifacts of the data. We ascribe these artifacts to the bias-correction of the normalized streamflow that is done independently for each calendar month, thus leading to some discontinuity from one month to the next.)

The projected increases in mean flow during the months of Dec.-Mar. occur in 18 of the 19 future climate scenarios while the projected decreases during the months of May-Sep. occur in all 19 scenarios (Figure 18). This agreement across simulations is remarkable given that the spread across the 19 projections arises not only from differences in GCMs and emissions scenarios (A1B vs. B1), but also from natural, or "internal", variability in temperature and particularly in precipitation that exists independent of increasing GHGs. Thus, one should expect to observe, with high certainty, the hydrological response "signal" to climate change to emerge from "noise" of natural variability by the 2040s *given* the hybrid-delta A1B or B1 scenarios.

Changes in the 5^{th}, 50^{th}, and 95^{th} percentiles of monthly flow generally follow the pattern of changes in the mean (Figure 19). Note also that although the year-to-year variability in monthly flow (as illustrated by 5^{th}-95^{th} percentile range) is large relative to the climate change response, the response is clearly evident: increased flows in the winter months, decreased flow in the summer months, and the response to A1B is larger than B1. Another clear trend is the reduction in year-to-year variability in May and June flow, with the reduction particularly strong in June. We credit this to the diminished impact of melting snow in May and June in the future scenarios (because there is so little snow in the future), whereas the variability in spring SWE and timing of melt historically contributed to greater streamflow variability.

Grouping months into winter (Dec.–Feb.) and summer (Jun.–Sep.) somewhat reduces noise arising from natural variability and permits easier side-by-side comparison across the flow

percentiles. All 10 A1B scenarios and 8 of 9 B1 scenarios show increasing winter flow volumes at the 5th, 50th, and 95th percentiles, and all 19 scenarios show decreasing summer flow in summer (Figure 20). Curiously, the increases in winter flows are larger for the 50th percentile than for the 95th percentile. Though there may be a physical mechanism behind this pattern, we have not ruled out it being an artifact of the multiple steps involved in the hybrid-delta methodology and bias correction of the normalized flows.

Figure 17 Mean annual hydrograph of daily simulated, bias-corrected, naturalized streamflow at North Santiam River below Boulder Creek near Detroit (NOSAN 4056, USGS 14178000) for the historical period and hybrid-delta A1B and B1 future scenarios. Thin lines show each of the 19 individual simulations.

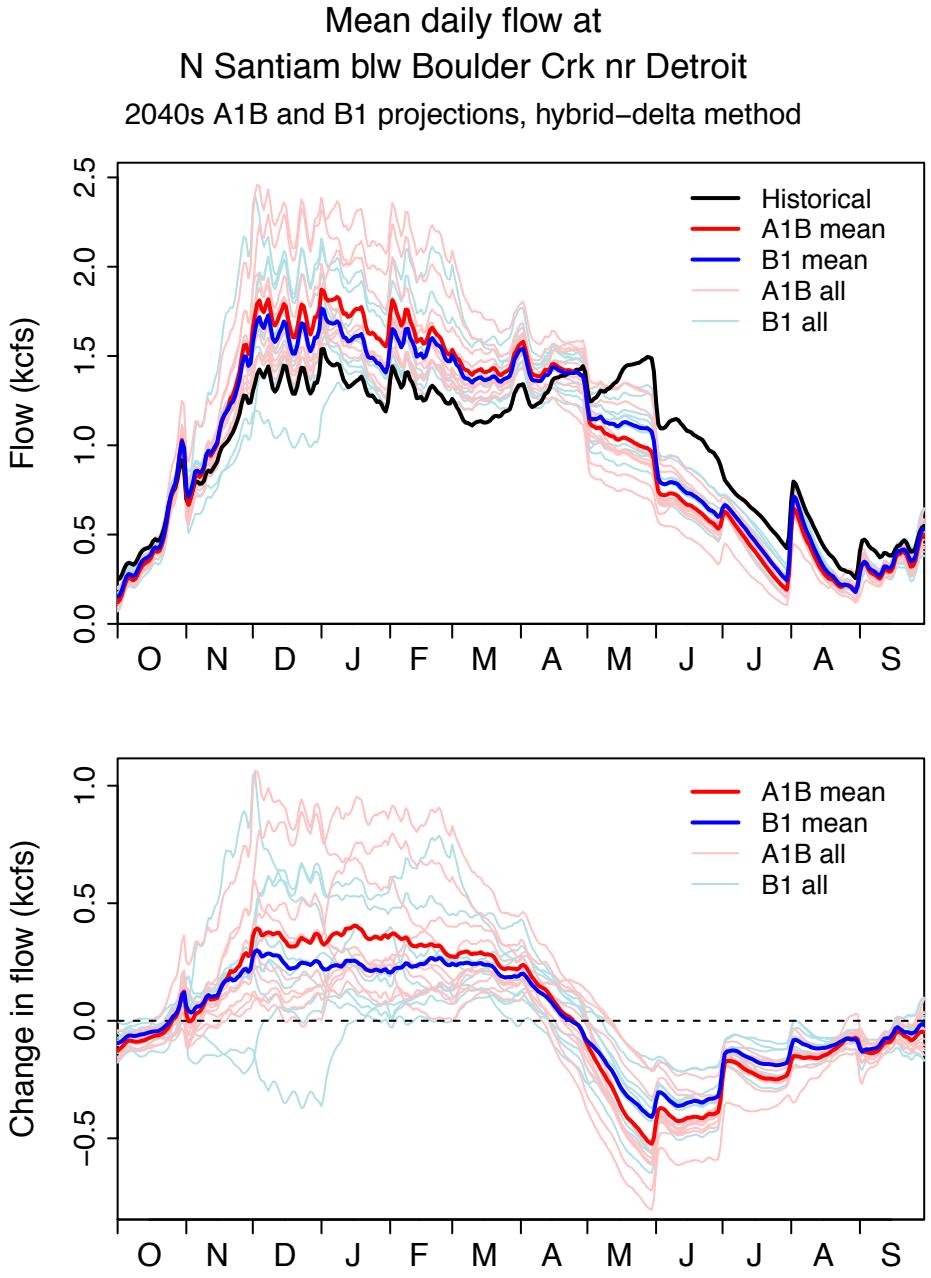

Figure 18 Mean annual hydrograph of monthly simulated, bias-corrected, naturalized streamflow at North Santiam River below Boulder Creek near Detroit (NOSAN 4056, USGS 14178000) for the historical period and hybrid-delta A1B and B1 future scenarios.

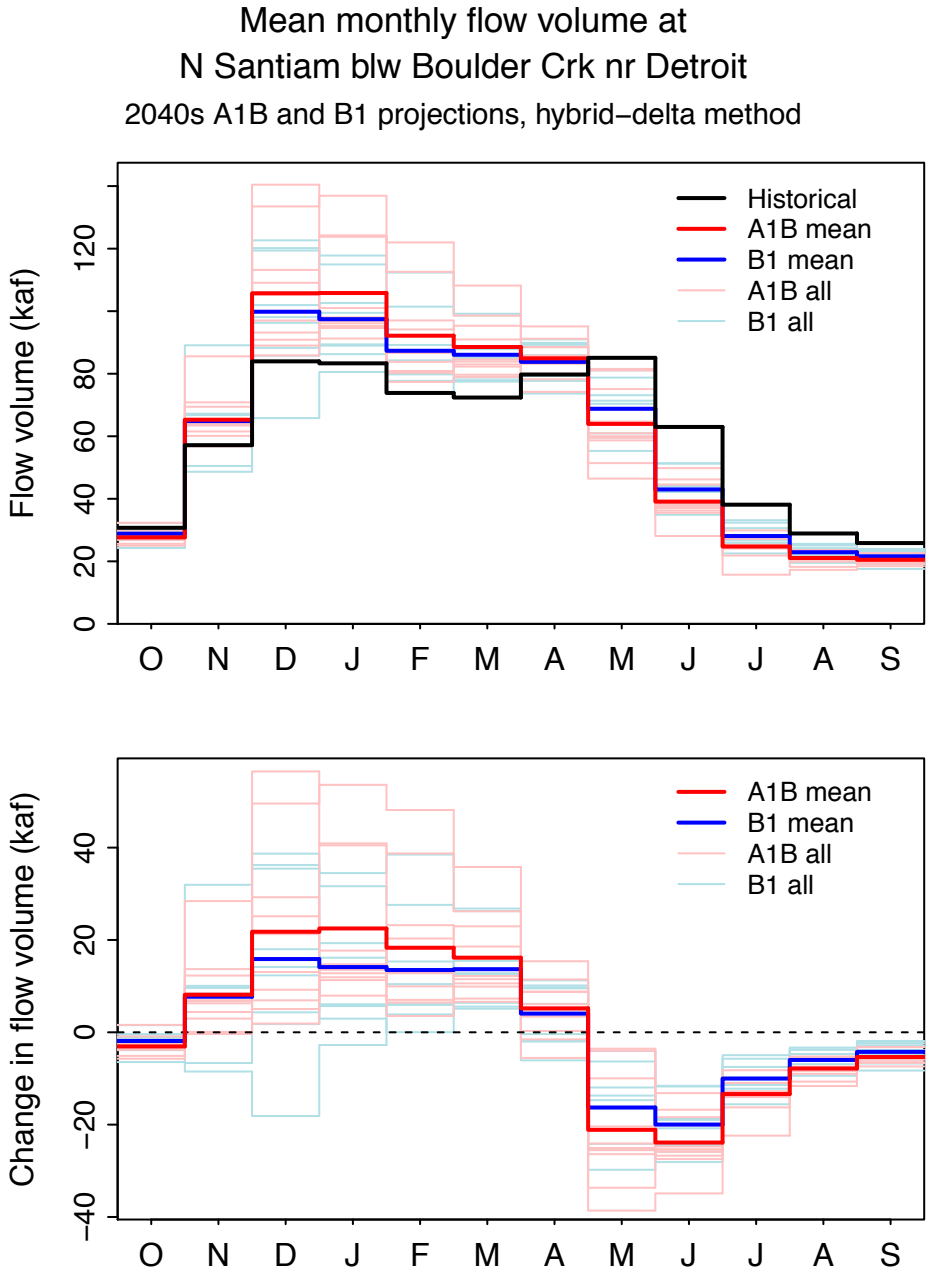

Figure 19 5th, 50th, and 95th percentiles of monthly simulated, bias-corrected, naturalized streamflow at North Santiam River below Boulder Creek near Detroit (NOSAN 4056, USGS 14178000) for the historical period and the A1B and B1 future scenarios.

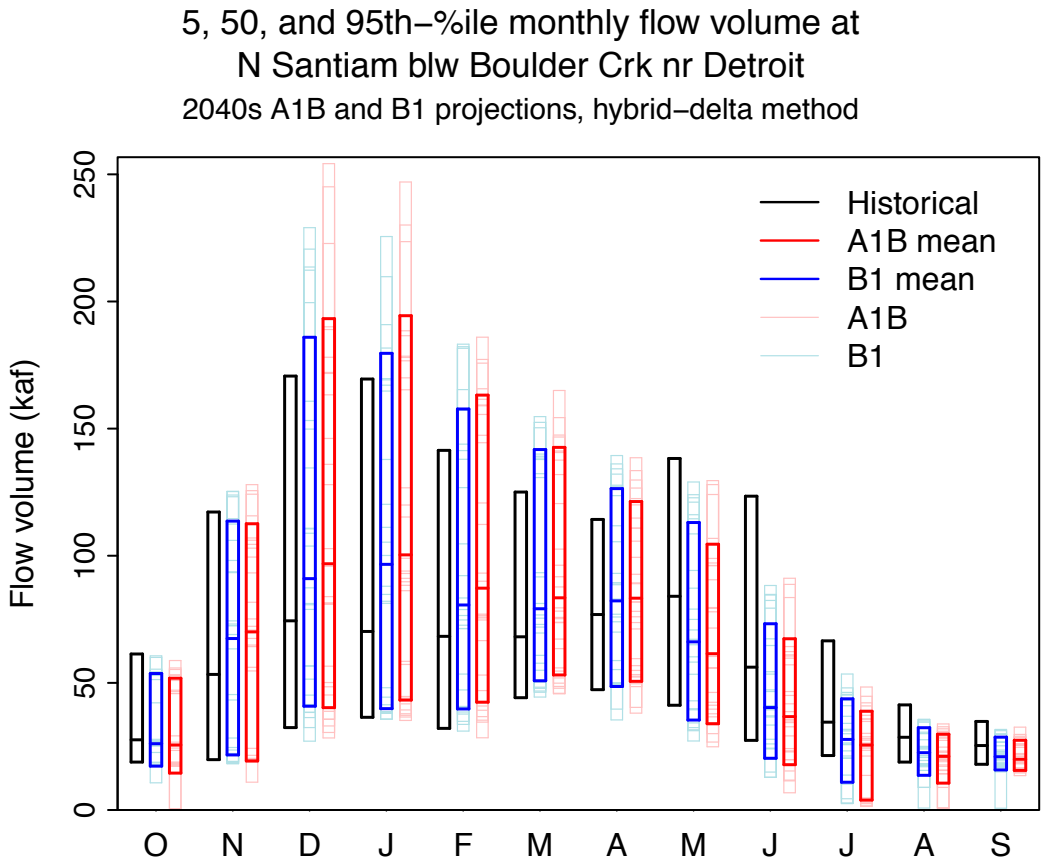

Figure 20 5th, 50th, and 95th percentiles of winter (DJF) and summer (JJAS) simulated, bias-corrected, naturalized streamflow at North Santiam River below Boulder Creek near Detroit (NOSAN 4056, USGS 14178000) for the historical period and hybrid-delta A1B and B1 future scenarios.

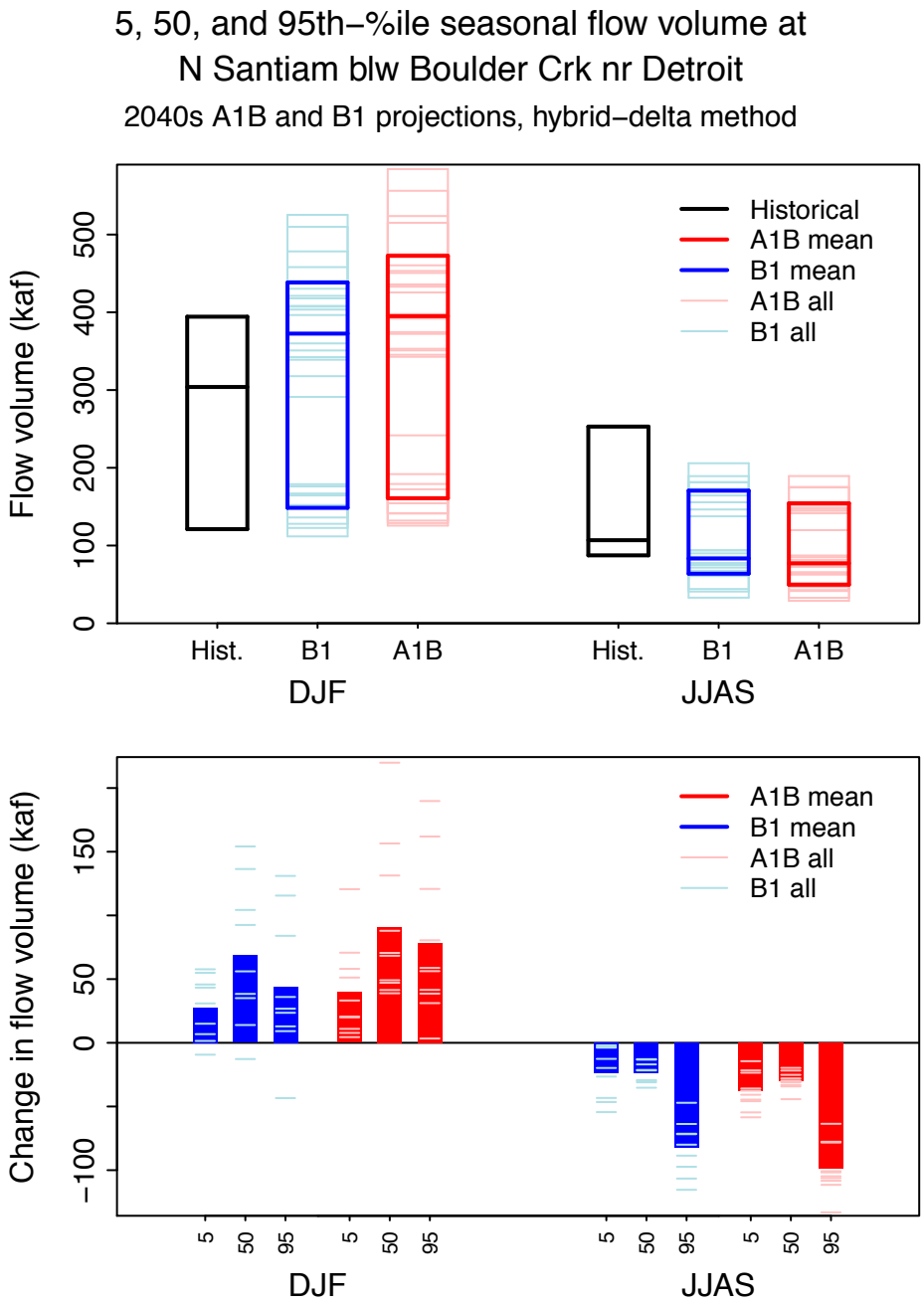

Cottage Grove, Dorena, and Fern Ridge Projects – Low streamflow sensitivity

The Row River above Pitcher Creek near Dorena (*ROPIT 4035*) is an example of a *low-sensitivity* site within the Willamette Basin. We associated *ROPIT* with the Cottage Grove and Dorena Projects in the Coast Fork of the Willamette River. We include Fern Ridge in this group, even though it drains an even more rain-dominated basin than *ROPIT* and may show the smallest changes of the USACE Projects.

At *ROPIT*, historically, mean flows peak in January and steadily decline through August (Figure 21), with snow accumulation and melt having a relatively small influence on the overall shape of the annual hydrograph.

The A1B and B1 hybrid-delta climate scenarios lead to small increases over historical flows during the months of November through January, with even smaller decreases in May and June; changes throughout the rest of the year are negligible in absolute terms (Figure 22). As with the high sensitivity basin, there is a trend towards increasing flow in winter transitioning towards a trend in decreasing flow, with the transition occurring in April, which is consistent with the climate projections showing slightly increased precipitation in winter and decreased precipitation in summer. However, the magnitude of this trend is very small with respect to the variability across the 19 simulations, especially when compared to high-sensitivity *NOSAN* site (compare Figure 18 and Figure 22). Moreover, for any given winter month, between 6 and 9 of the 19 simulations show decreasing streamflow from historical to future.

Trends in the 5th, 50th, and 95th percentiles of monthly flow from historical to future are small, but there is a general pattern of increased flow in winter months for both A1 and A1B (Figure 23). Grouping the months into season reveals that any sizeable absolute changes in seasonal flow volumes take place in winter (Figure 24). Curiously again (as with the high sensitivity *NOSAN* site), the increases in winter flows are larger for the 50th percentile than for the 95th percentile. Overall, the change in the 95th percentile is rather uncertain, with 6 of the 19 scenarios leading to a decrease in the 95th percentile of winter flow.

Figure 21 Mean annual hydrograph of daily simulated, bias-corrected, naturalized streamflow at Row River above Pitcher Creek near Dorena (ROPIT 4035, USGS 14154500) for the historical (1970-1999) and A1B and B1 future scenarios (2030-2059).

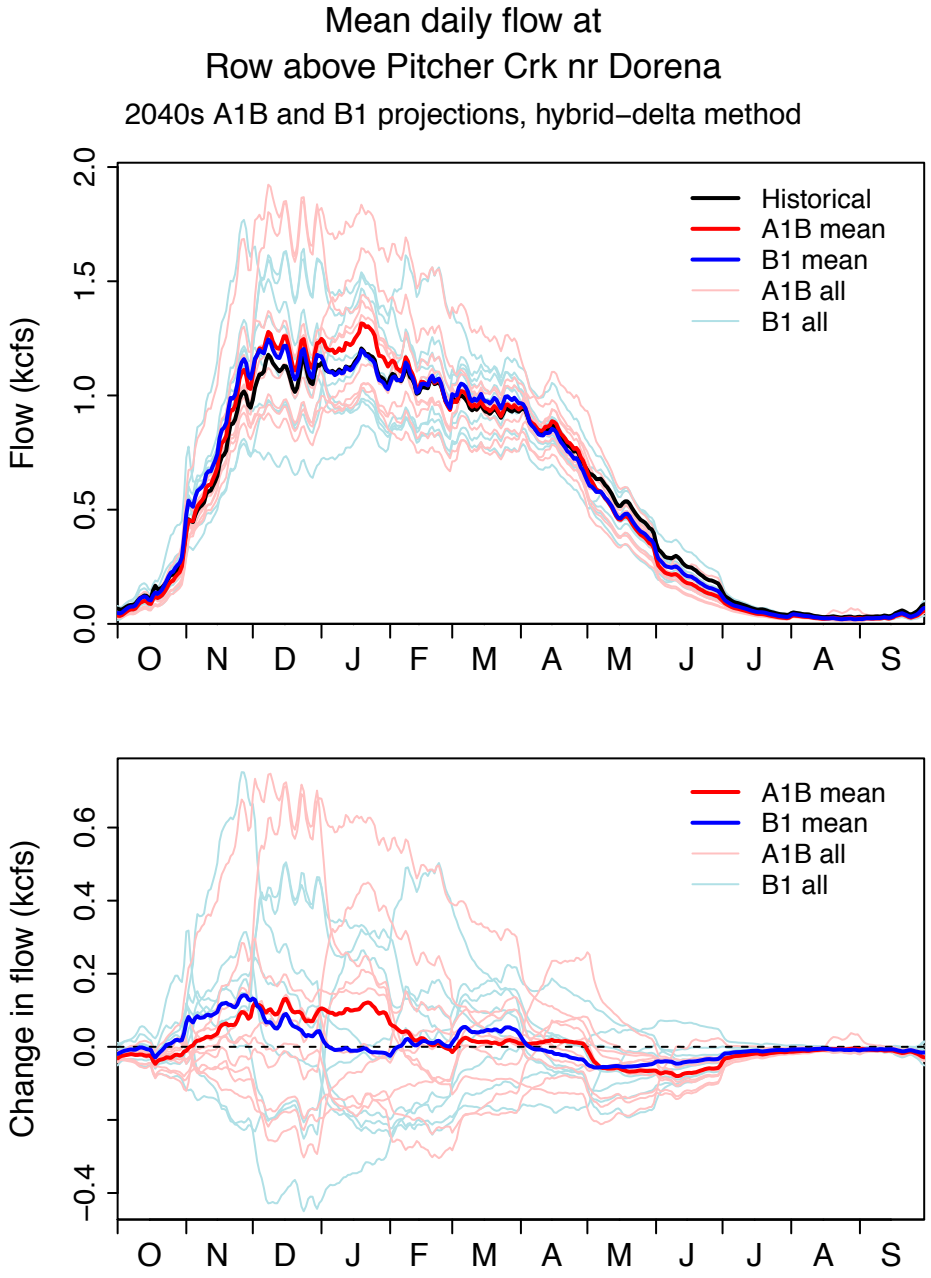

Figure 22 Mean annual hydrograph of monthly simulated, bias-corrected, naturalized streamflow at Row River above Pitcher Creek near Dorena (ROPIT 4035, USGS 14154500) for the historical (1970-1999) and A1B and B1 future scenarios (2030-2059).

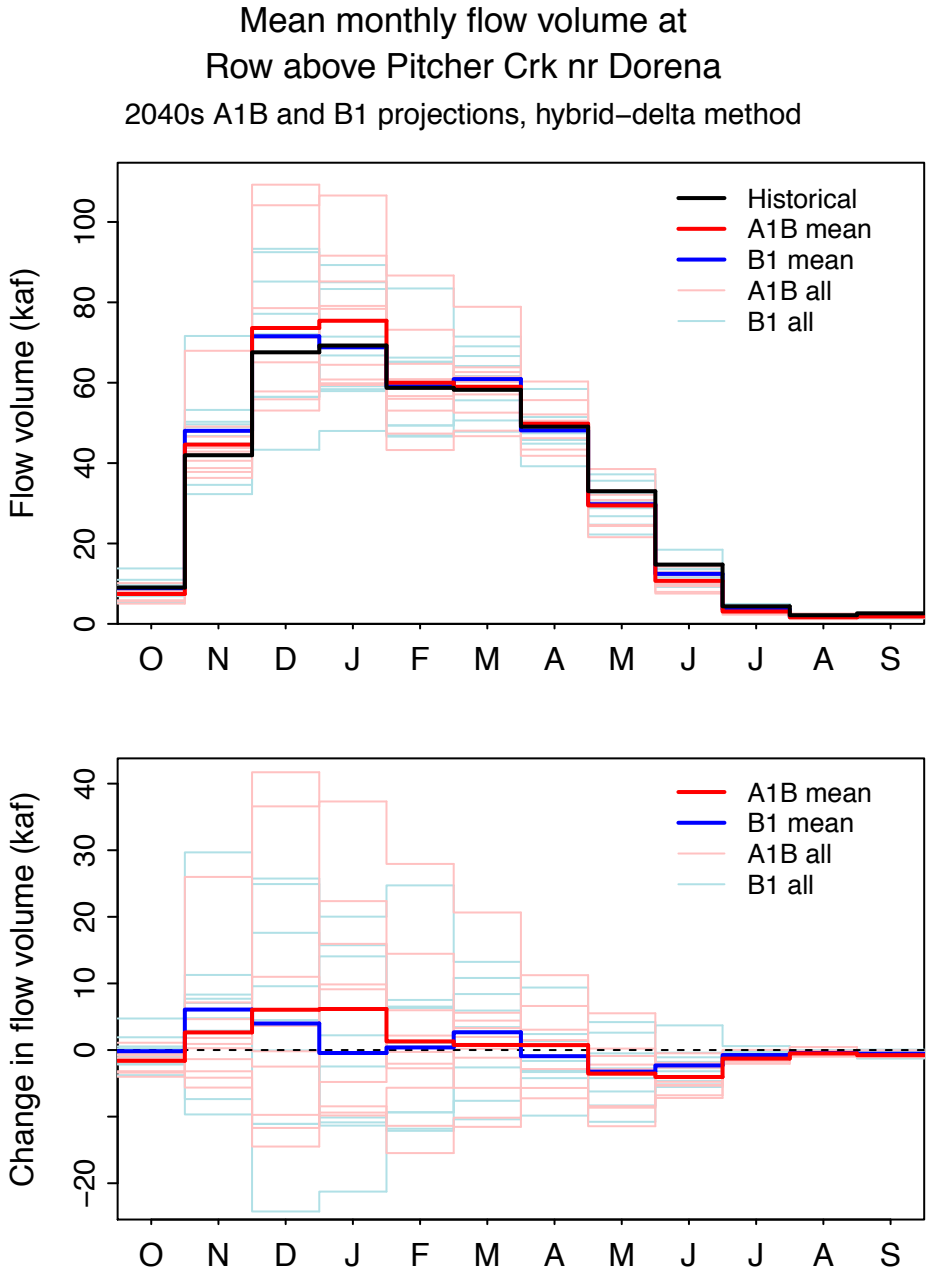

Figure 23 5th, 50th, and 95th percentiles of monthly simulated, bias-corrected, naturalized streamflow at Row River above Pitcher Creek near Dorena (ROPIT 4035, USGS 14154500) for the historical period and the A1B and B1 future scenarios.

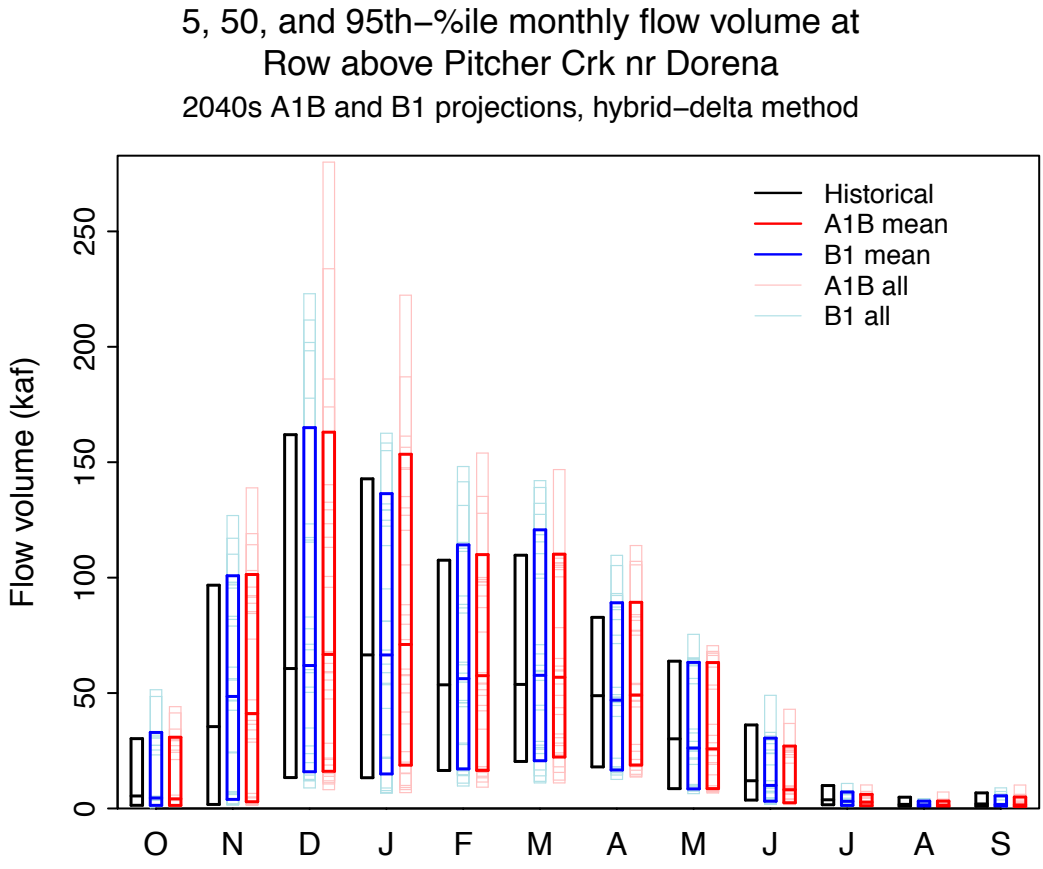

Figure 24 5th, 50th, and 95th percentile of winter (DJF) and summer (JJAS) simulated, bias-corrected, naturalized streamflow at Row River above Pitcher Creek near Dorena (ROPIT 4035, USGS 14154500) for the historical period and hybrid-delta A1B and B1 future scenarios.

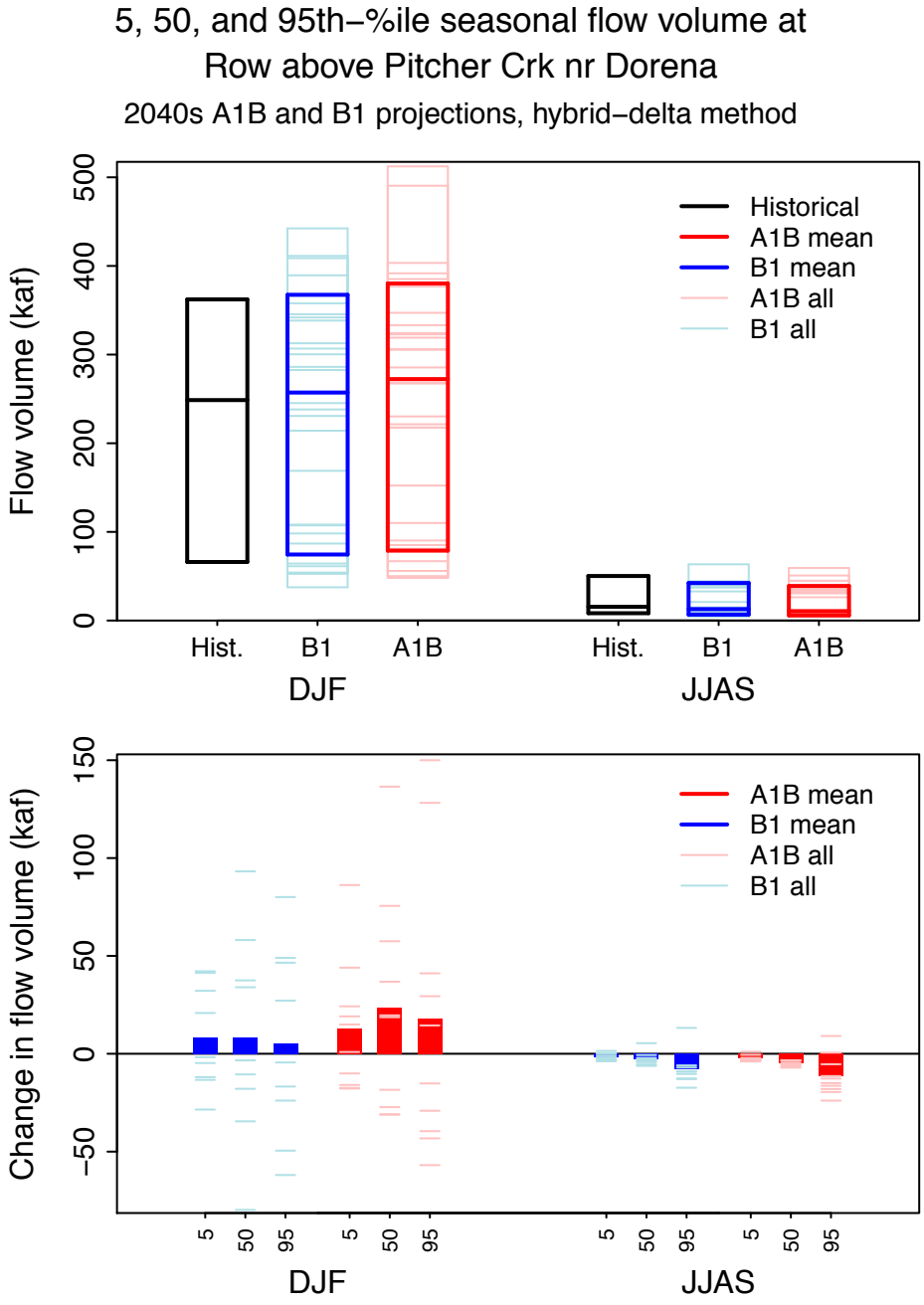

Lookout Point, Dexter and Fall Creek Projects – Moderate-to-high streamflow sensitivity

We associated the Middle Fork Willamette River below North Fork near Oakridge (*WILNF 4048*) with Lookout Point, Dexter and Fall Creek. In this case, the *WILNF* gage is located on the same river as all 3 Projects and is similar in elevation.

At *WILNF*, historically, relatively high mean flows are sustained into spring (Figure 25) because of the contribution from a melting snowpack. The A1B and B1 hybrid-delta climate scenarios lead to the familiar pattern of increases over historical flows in the winter months and decreases from historical beginning in late April and continuing through the end of the water year.

The difference between *WILNF* and the high-sensitivity *NOSAN* site is merely one of magnitude. With less snowpack per unit upstream area, the effect of increasing temperature on snowpack formation and ablation plays a reduced, but still substantial role, while variability in total precipitation plays a relatively larger role.

The projected increases in mean flow during the months of Dec.-Mar. occur in 13 to 17 (depending on month) of the 19 future climate scenarios while the projected decreases during the months of May-Aug. occur in all 19 scenarios (Figure 26).

Changes in the 5th, 50th, and 95th percentiles of monthly flow generally follow the pattern of changes in the mean (Figure 27). A notable difference from the high-sensitivity site (compare with Figure 19) is that the 95th percentile flow volume is lower for A1B than B1 during the months of February through April. This could be due to fewer years with very large snowpacks in the warmer A1B scenario than in the B1 scenario.

Seasonally, 8 of 10 A1B scenarios and at least 6 of 9 B1 scenarios show increasing winter flow volumes at the 5th, 50th, and 95th percentiles, and all 19 scenarios show decreasing summer flow in summer (Figure 28).

Figure 25 Mean annual hydrograph of daily simulated, bias-corrected, naturalized streamflow at Middle Fork Willamette River below North Fork near Oakridge (WILNF 4048, USGS 14148000) for the historical period and hybrid-delta A1B and B1 future scenarios. Thin lines show each of the 19 individual simulations.

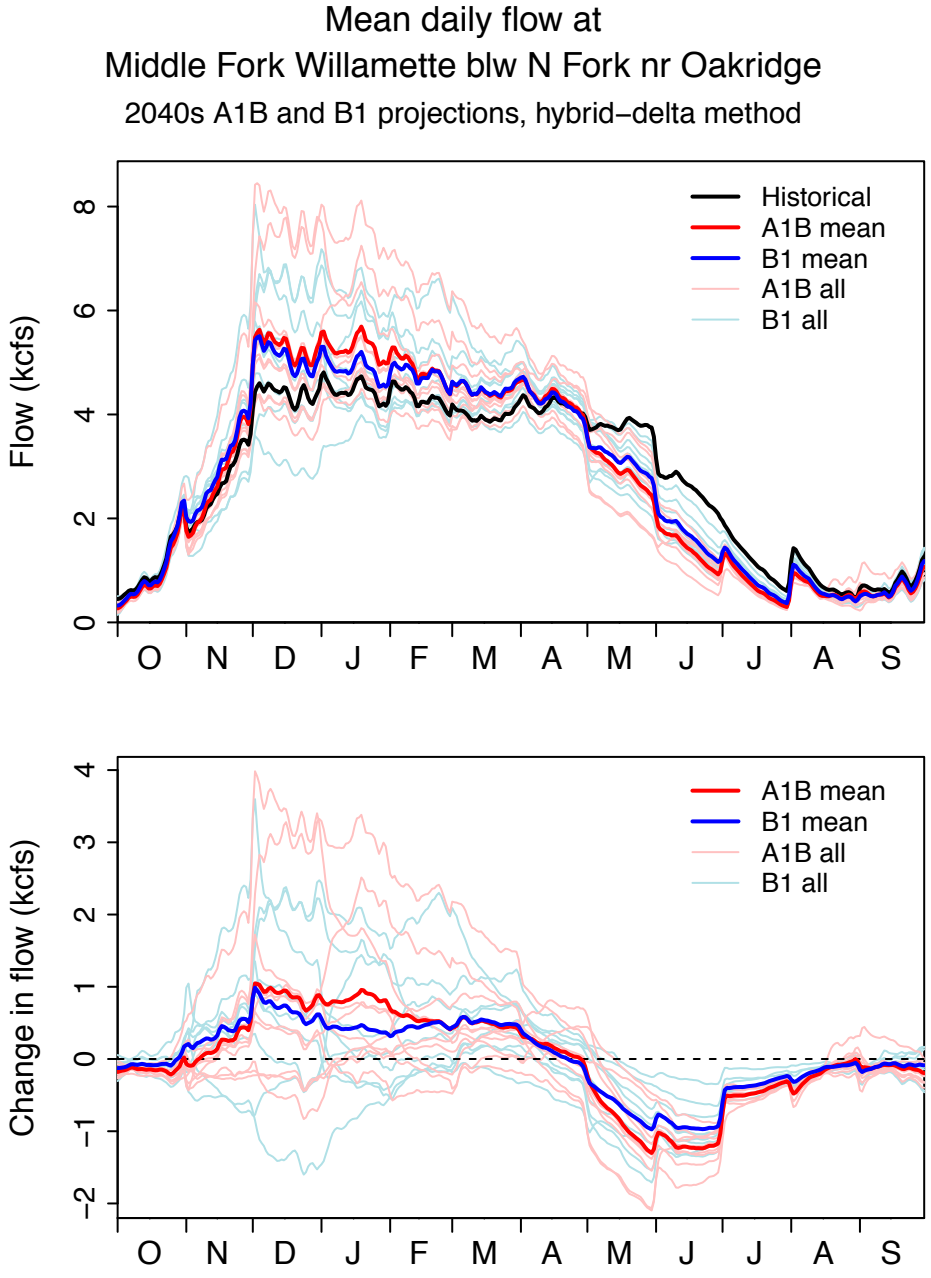

Figure 26 Mean annual hydrograph of monthly simulated, bias-corrected, naturalized streamflow at Middle Fork Willamette River below North Fork near Oakridge (WILNF 4048, USGS 14148000) for the historical (1970-1999) and A1B and B1 future scenarios (2030-2059).

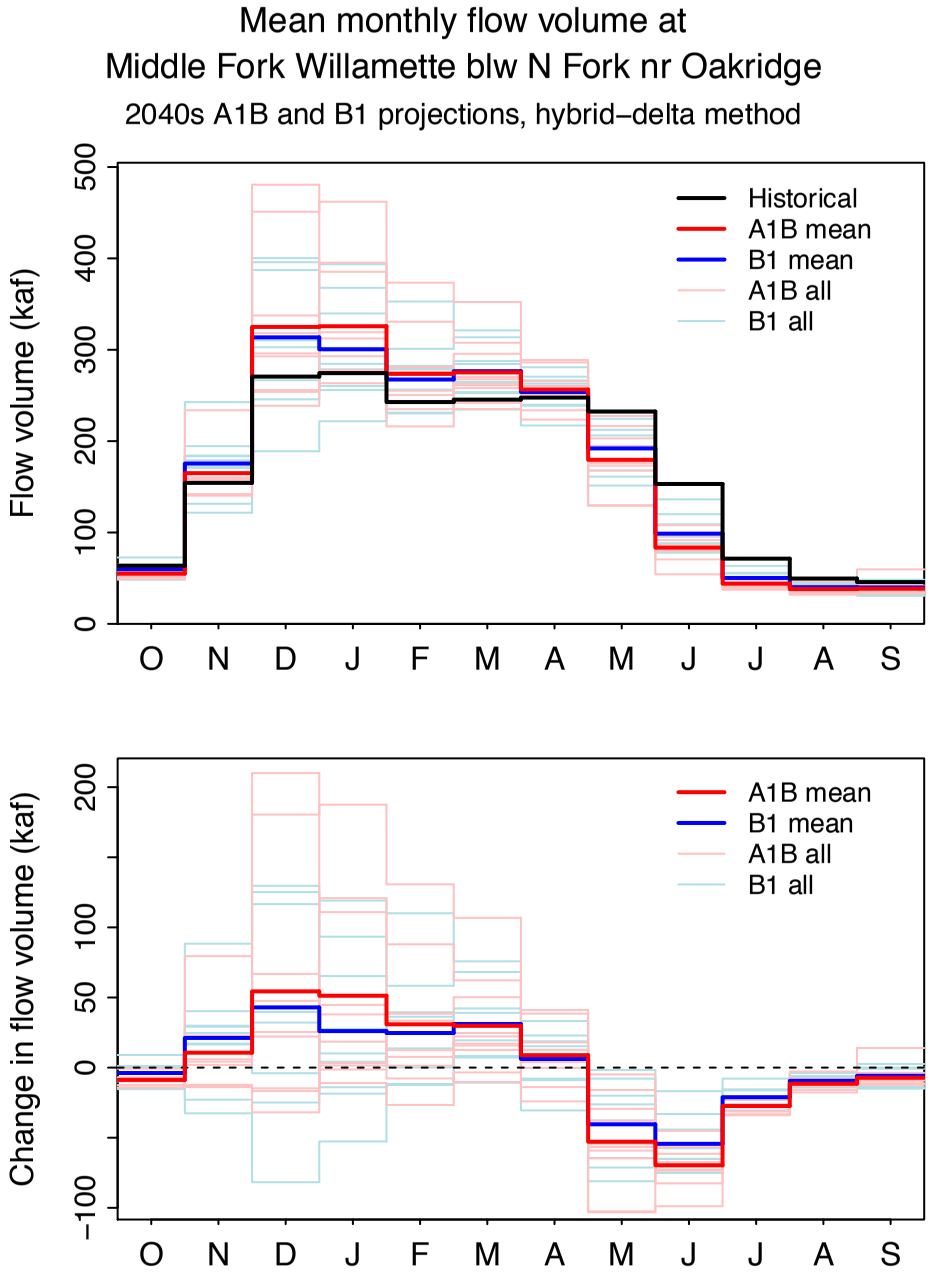

Figure 27 5th, 50th, and 95th percentiles of monthly simulated, bias-corrected, naturalized streamflow at Row River above Pitcher Creek near Dorena (ROPIT 4035, USGS 14154500) for the historical period and the A1B and B1 future scenarios.

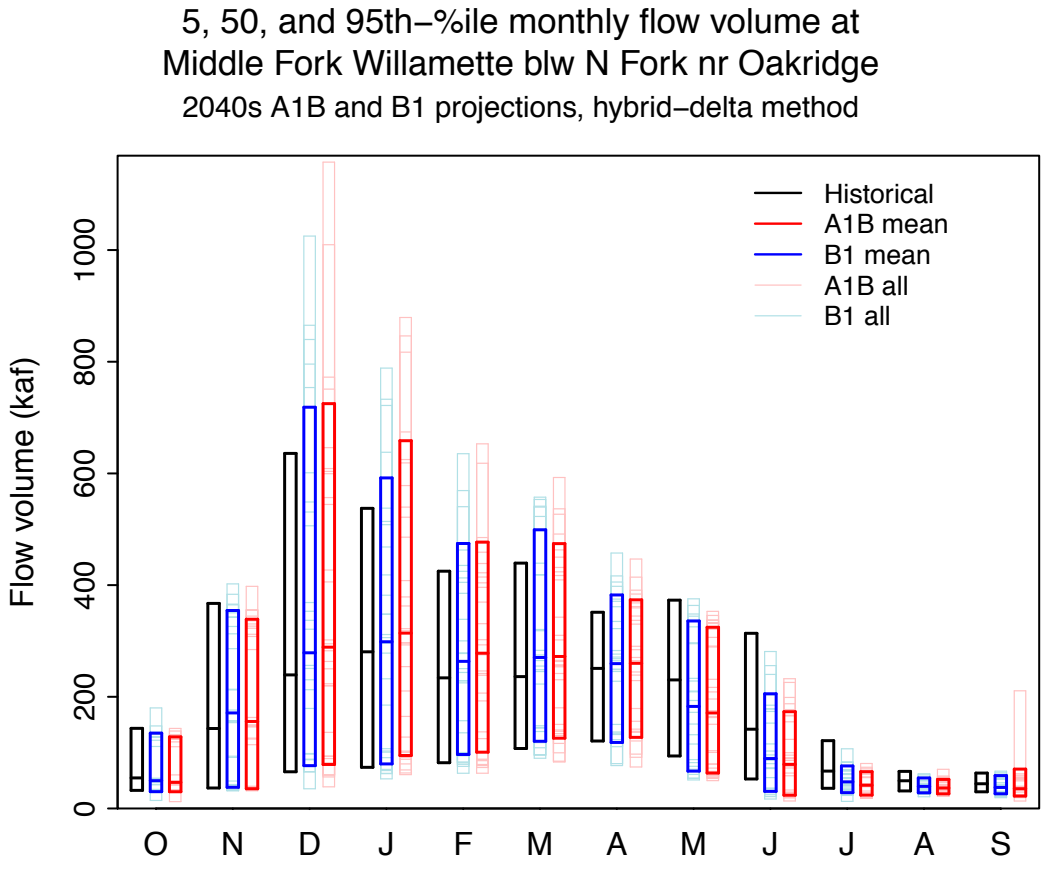

Figure 28 5th, 50th, and 95th percentile of winter (DJF) and summer (JJAS) simulated, bias-corrected, naturalized streamflow at Row River above Pitcher Creek near Dorena (ROPIT 4035, USGS 14154500) for the historical period and hybrid-delta A1B and B1 future scenarios.

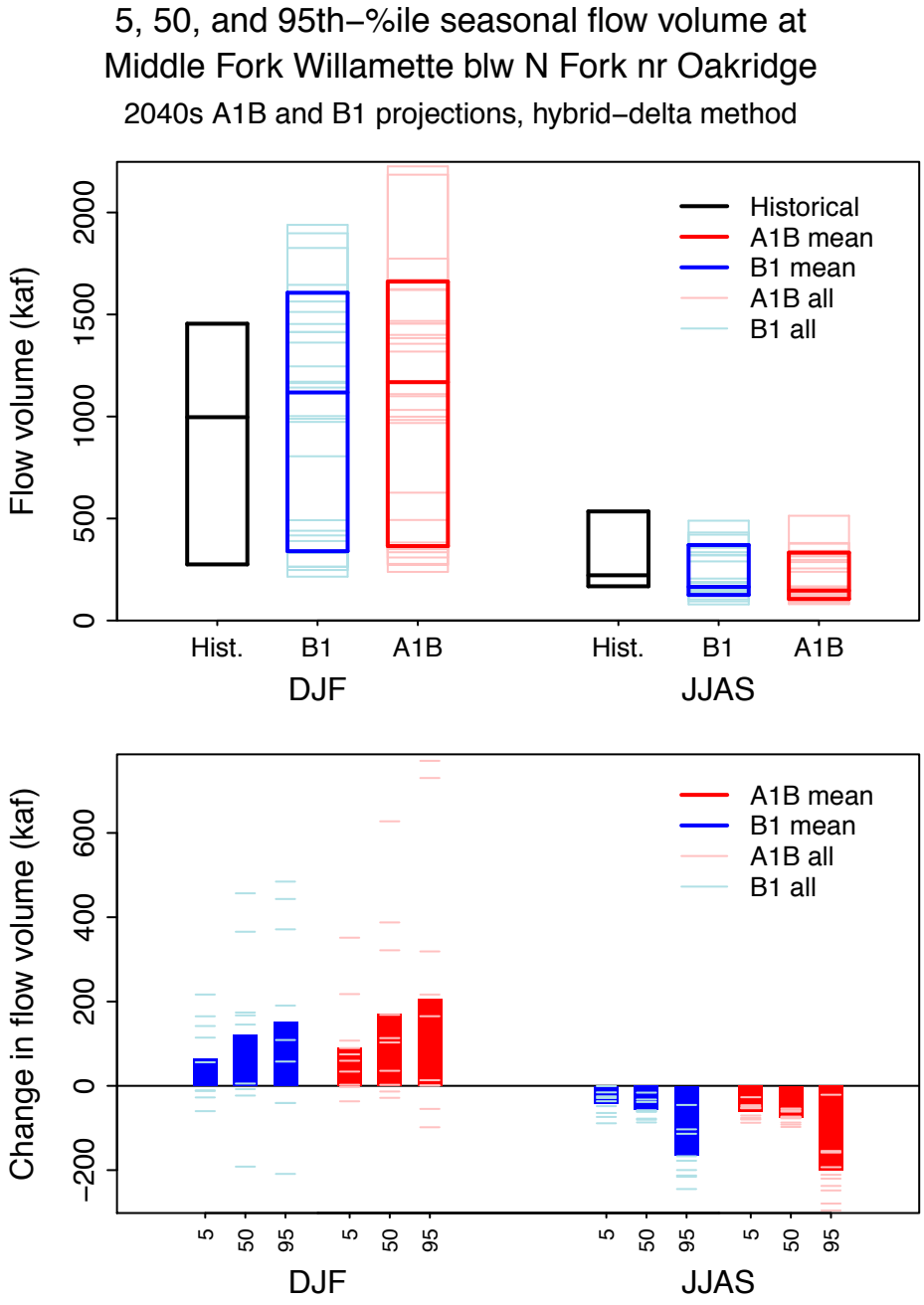

Blue River Project – Moderate-to-high streamflow sensitivity

We associated the McKenzie River at Vida (*MCKVI 4036*) the Blue River Project upstream.

The response of streamflow at *MCKVI* largely mirrors the moderate-to-high streamflow sensitivity *WILNF* site above: historically, relatively high mean flows are sustained into spring (Figure 29) because of the contribution from a melting snowpack. Again, the A1B and B1 hybrid-delta climate scenarios lead to similar increases over historical flows in the winter months and decreases from historical beginning in late April and continuing through the end of the water year.

The projected increases in mean flow during the months of Dec.-Mar. occur in 14 to 17 (depending on month) of the 19 future climate scenarios while the projected decreases during the months of May-Aug. occur in all 19 scenarios (Figure 30).

Changes in the 5th, 50th, and 95th percentiles of monthly flow generally follow the pattern of changes in the mean (Figure 31). However, as with *WILNF*, the 95th percentile flow volume is slightly lower for A1B than B1 during the months of February through April.

Seasonally, 9 of 10 A1B scenarios and at least 6 of 9 B1 scenarios show increasing winter flow volumes at the 5th, 50th, and 95th percentiles, and 18 of 19 scenarios show decreasing summer flow in summer at all 3 percentiles (Figure 32).

Figure 29 Mean annual hydrograph of daily simulated, bias-corrected, naturalized streamflow at McKenzie River near Vida (MCKVI 4036, USGS 14162500) for the historical period and hybrid-delta A1B and B1 future scenarios. Thin lines show each of the 19 individual simulations.

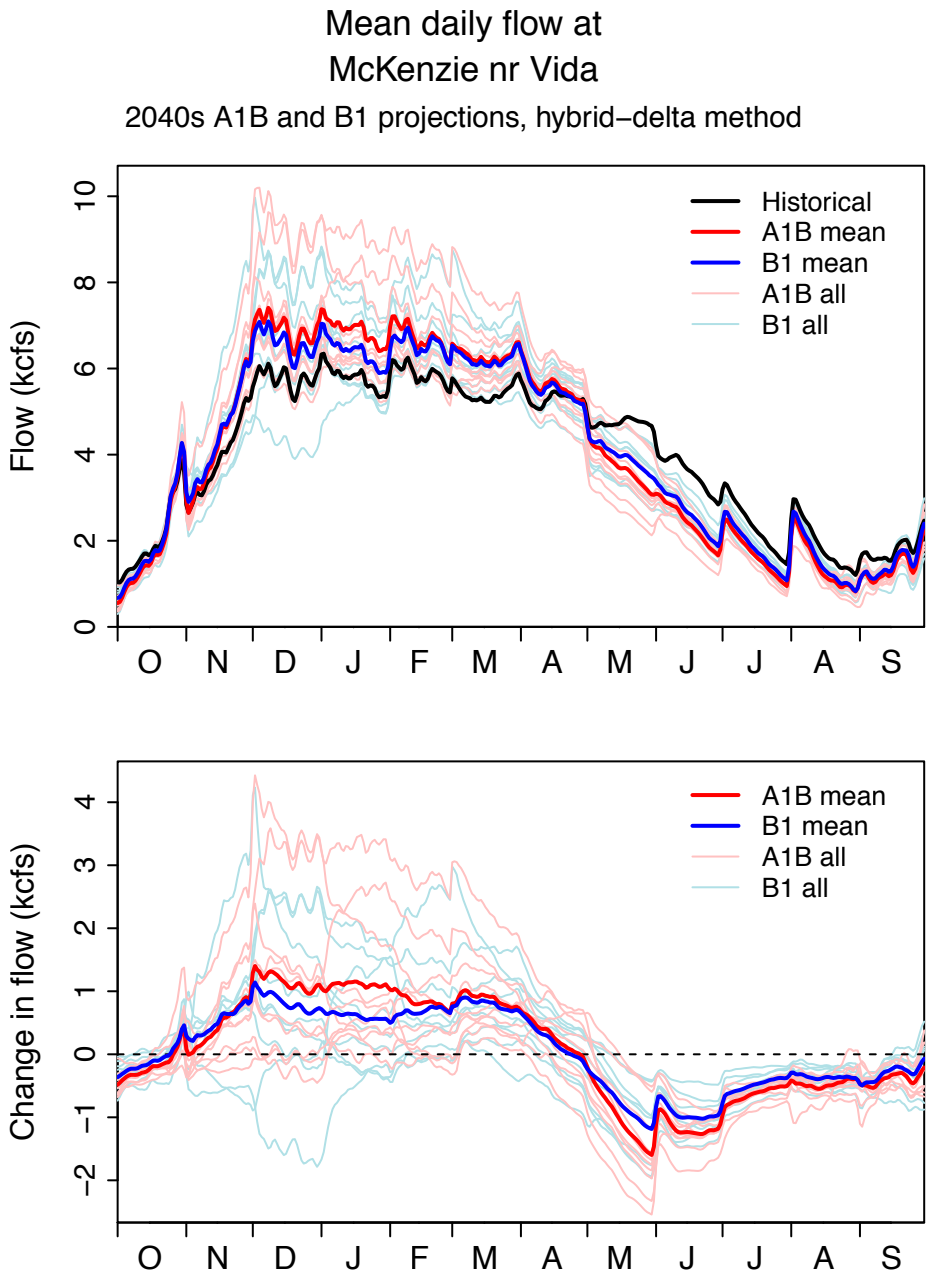

Figure 30 Mean annual hydrograph of monthly simulated, bias-corrected, naturalized streamflow at McKenzie River near Vida (MCKVI 4036, USGS 14162500) for the historical (1970-1999) and A1B and B1 future scenarios (2030-2059).

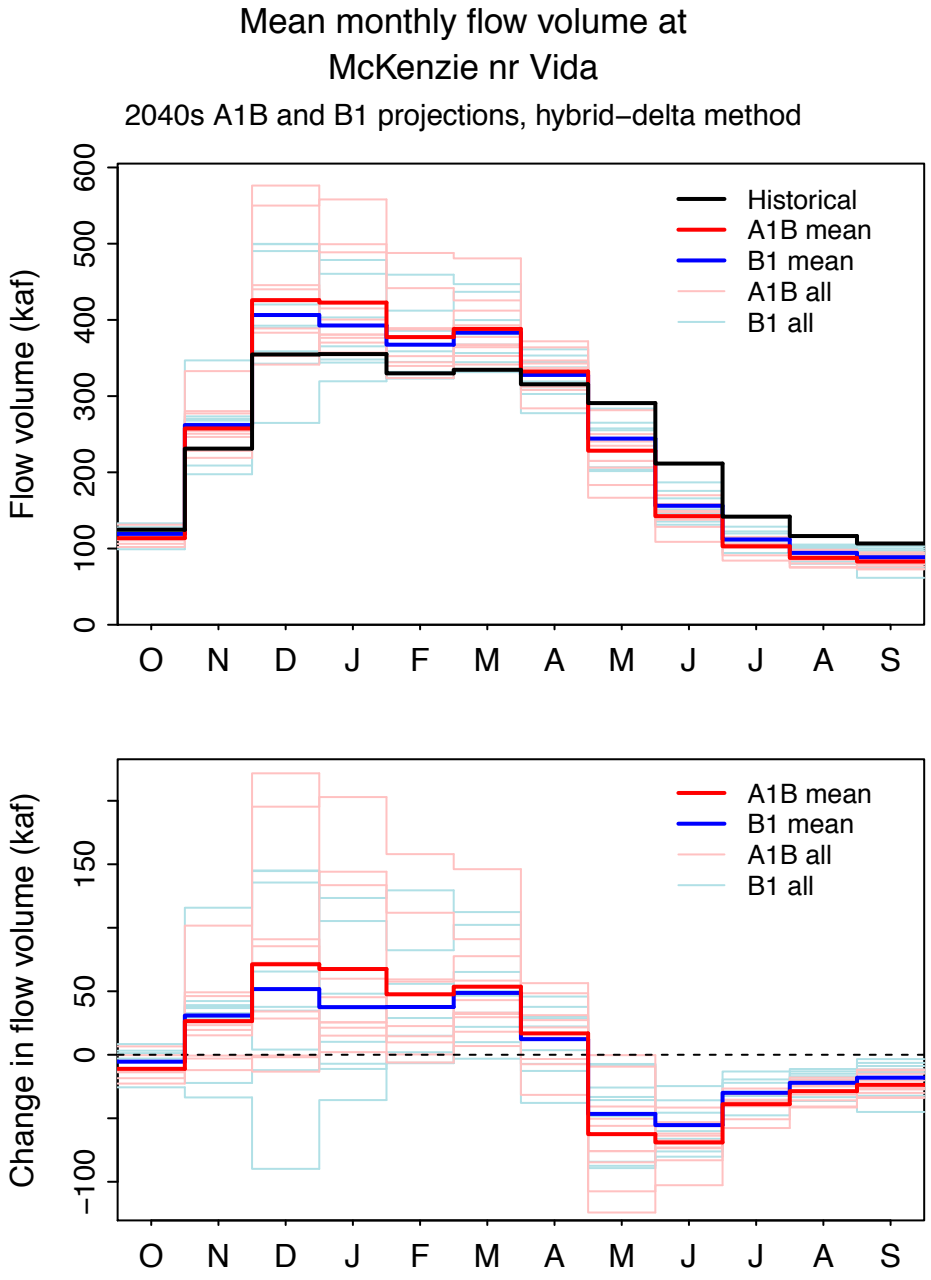

Figure 31 5th, 50th, and 95th percentiles of monthly simulated, bias-corrected, naturalized streamflow at McKenzie River near Vida (MCKVI 4036, USGS 14162500) for the historical period and the A1B and B1 future scenarios.

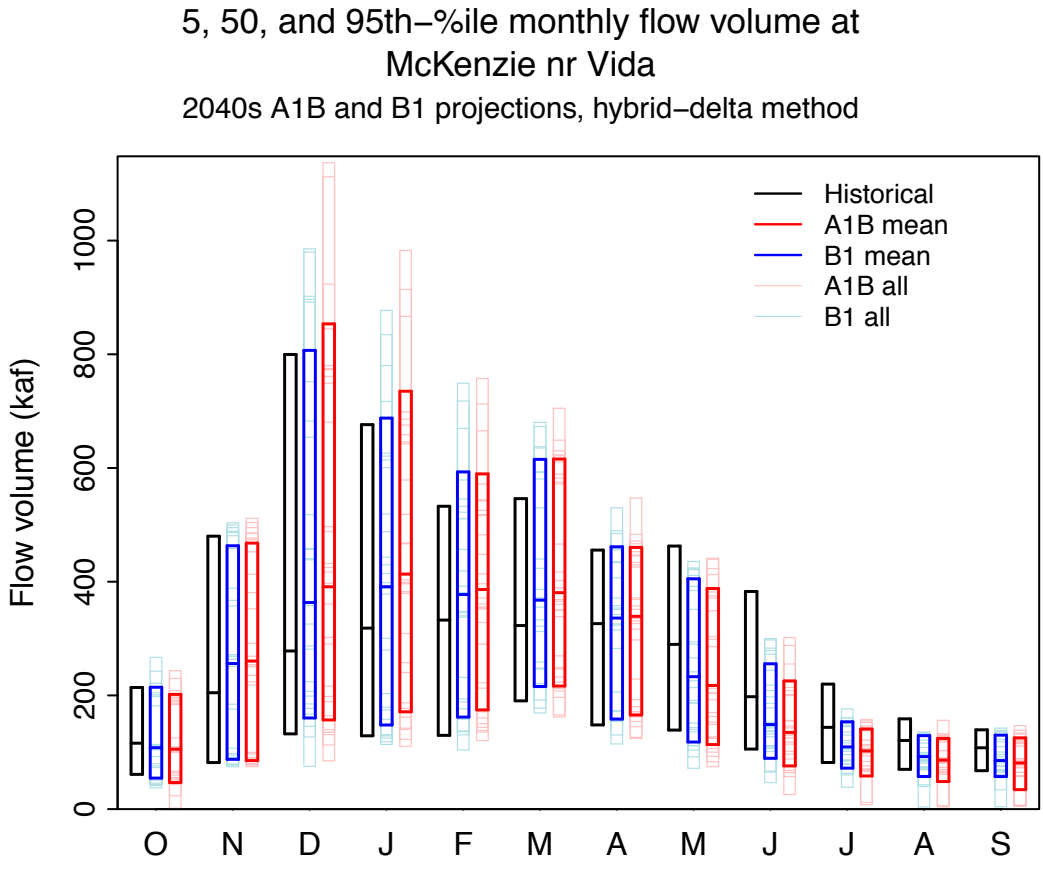

Figure 32 5th, 50th, and 95th percentile of winter (DJF) and summer (JJAS) simulated, bias-corrected, naturalized streamflow at McKenzie River near Vida (MCKVI 4036, USGS 14162500) for the historical period and hybrid-delta A1B and B1 future scenarios.

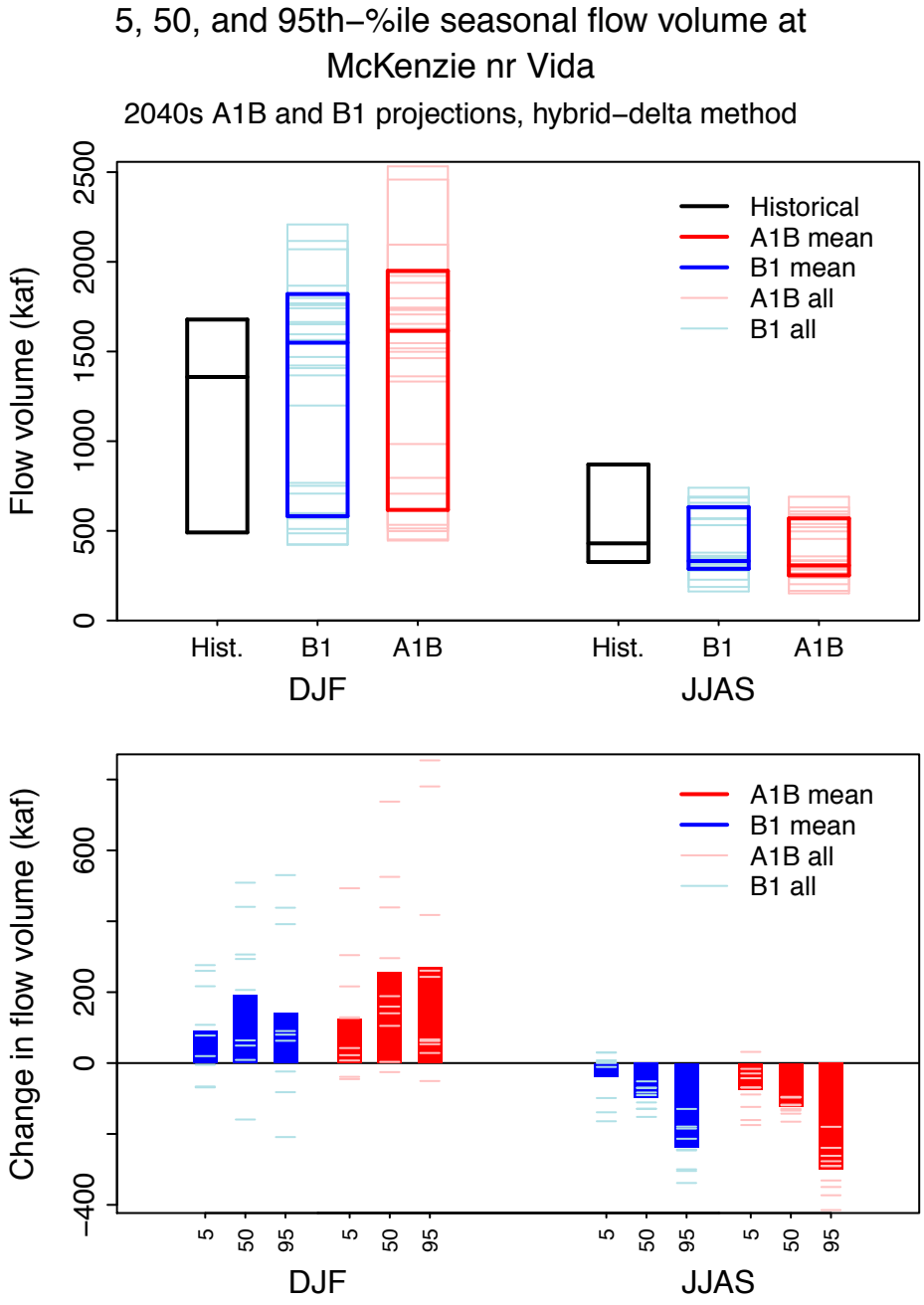

Green Peter and Foster Projects – Low-to-moderate streamflow sensitivity

We associate the South Santiam and Waterloo (*SANWA 4059*) with the Green Peter and Foster Projects. Given, however, that *SANWA* is located downstream and at a much lower elevation (370 ft), it may provide a conservative estimate of the changes expected at Green Peter and Foster.

At *SANWA*, the A1B and B1 hybrid-delta climate scenarios lead to small increases over historical flows during the months of November through March, with similarly smaller decreases in May and July (Figure 33 and Figure 34). This seasonal pattern in changing streamflow is slightly stronger than at *ROPIT*, therefore we categorized *SANWA* as having *low-to-moderate* streamflow sensitivity.

Trends in the 5th, 50th, and 95th percentiles of monthly flow from historical to future are small, but there is a general pattern of increased flow in winter months for both A1 and A1B (Figure 35).

Seasonally, 6 to 7 of the 10 A1B scenarios and 5 of 9 B1 scenarios show increasing winter flow volumes at the 5th, 50th, and 95th percentiles. In summer, all scenarios show decreasing summer flow at the 95th percentile (Figure 36). For 5th percentile summer flow volumes, 9 of 10 A1B scenarios and 6 of 9 B1 scenarios show decreasing flow.

Figure 33 Mean annual hydrograph of daily simulated, bias-corrected, naturalized streamflow at South Santiam at Waterloo (SANWA 4059, USGS 14187500) for the historical period and hybrid-delta A1B and B1 future scenarios. Thin lines show each of the 19 individual simulations.

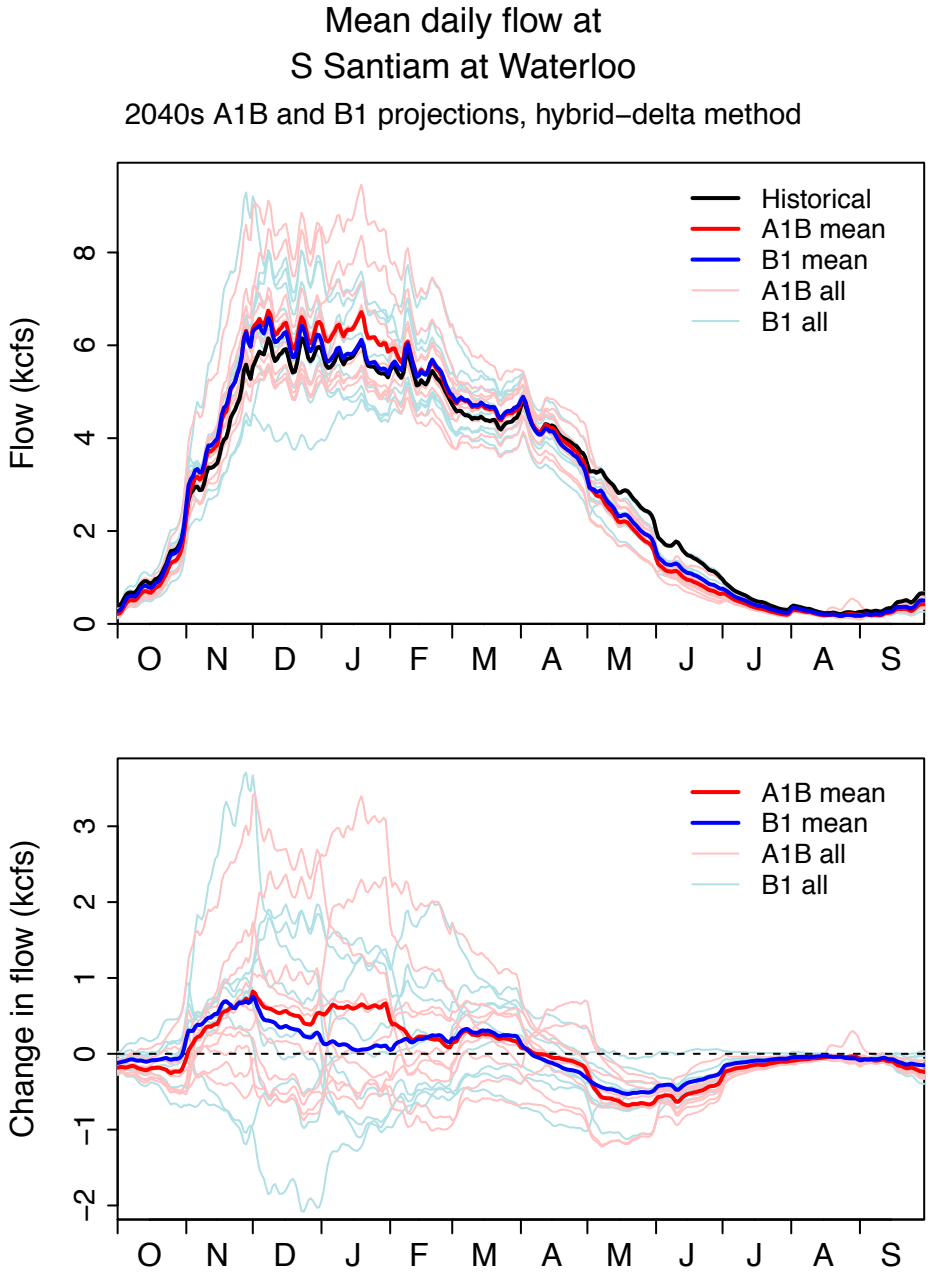

Figure 34 Mean annual hydrograph of monthly simulated, bias-corrected, naturalized streamflow at South Santiam at Waterloo (SANWA 4059, USGS 14187500) for the historical (1970-1999) and A1B and B1 future scenarios (2030-2059).

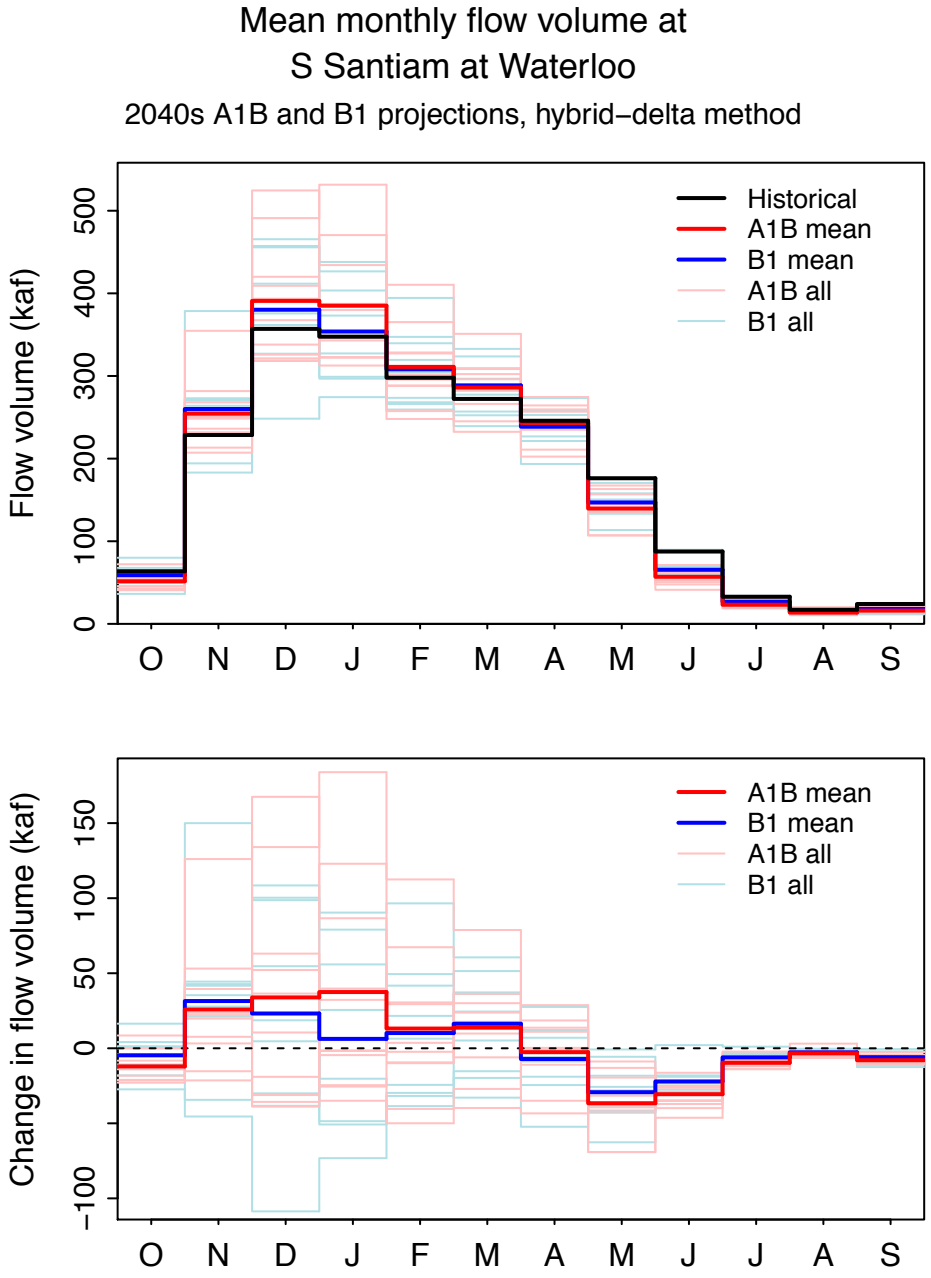

Figure 35 5th, 50th, and 95th percentiles of monthly simulated, bias-corrected, naturalized streamflow at South Santiam at Waterloo (SANWA 4059, USGS 14187500) for the historical period and the A1B and B1 future scenarios.

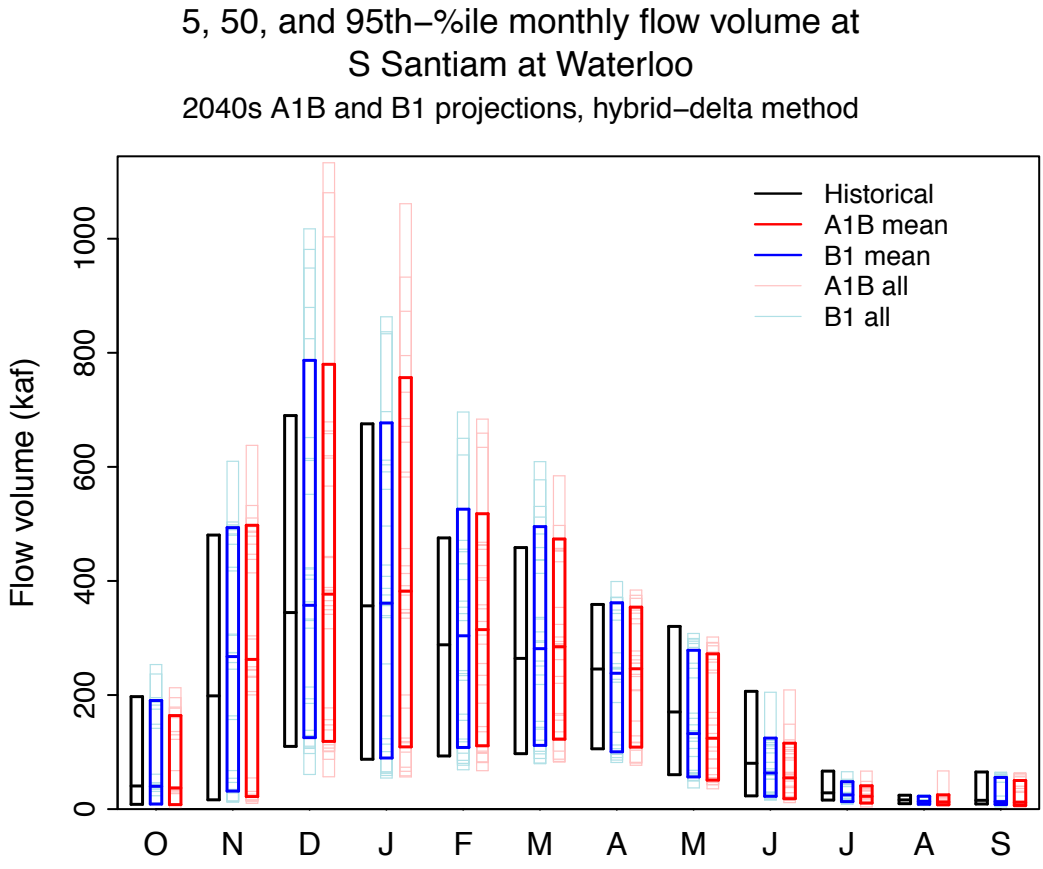

Figure 36 5th, 50th, and 95th percentile of winter (DJF) and summer (JJAS) simulated, bias-corrected, naturalized streamflow at South Santiam at Waterloo (SANWA 4059, USGS 14187500) for the historical period and hybrid-delta A1B and B1 future scenarios.

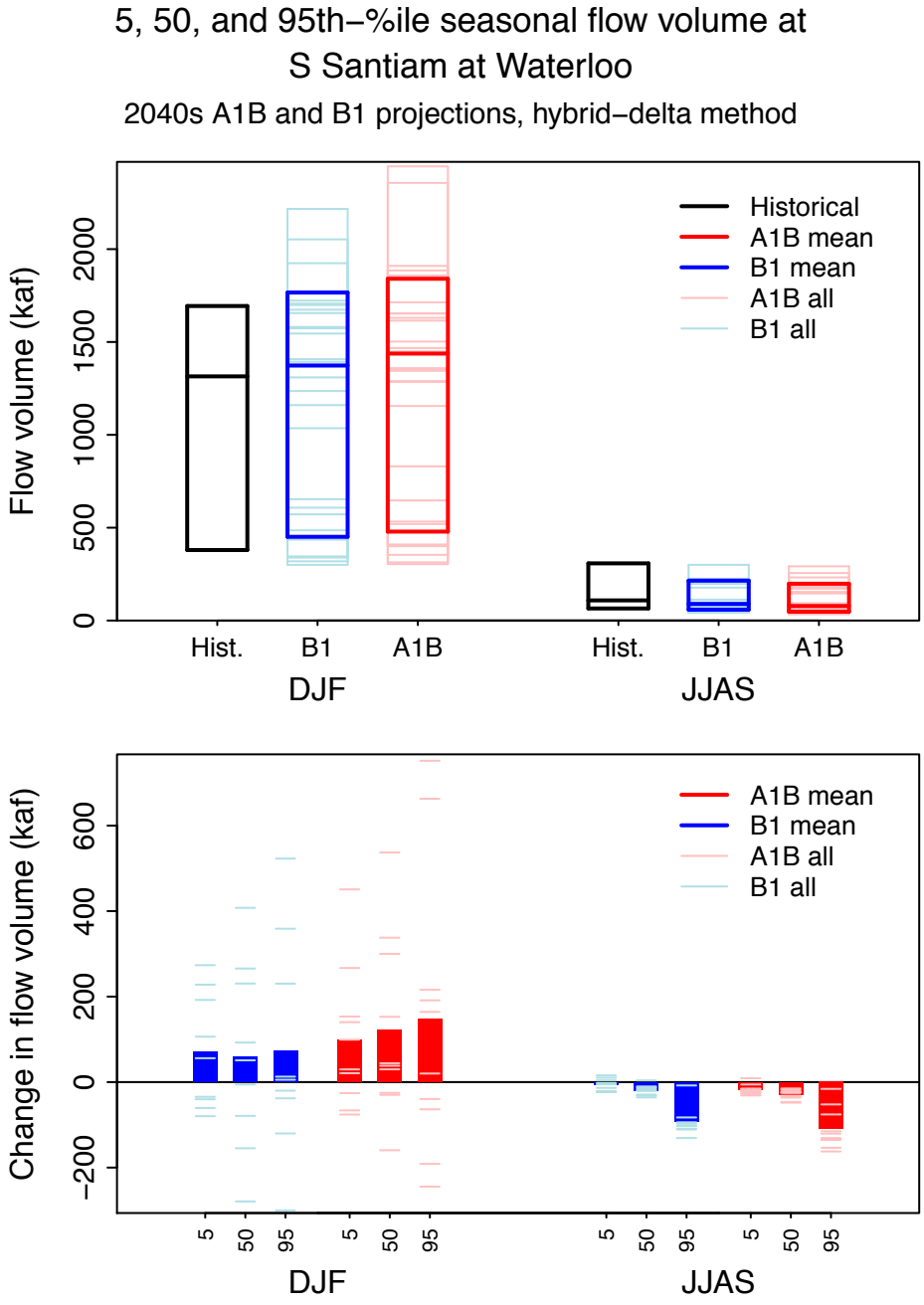

Lost Creek and Applegate Projects – High streamflow sensitivity

The 2 USACE Projects in the Rogue River basin do not have any clear analogs among the available CBSCCSP gages. Because of their high elevations, they may be most similar to the *NOSAN* gage used to represent changes in the other high elevation Projects (Hills Creek, Lookout Point, Dexter and Fall Creek), therefore changes at Lost Creek and Applegate may be similar to those illustrated in Figure 17 - Figure 20. Another possible surrogate is the *WILNF* gage (see Figure 25 - Figure 28) on the Middle Fork Willamette, which is the nearest gage geographically that is also at a moderately high elevation (935 ft), though still much lower than Lost Creek and Applegate.

All-basin summary

Projected changes in some streamflow properties from 6 gages are described above. Here changes across 11 gages in Willamette Basin are summarized (see also Table 16). Focusing on seasonal metrics, the projected increase in winter (DJF) mean flow ranges across the 11 basins from 2% to 18% for scenario B1 and 6% to 26% for scenario A1B (Figure 37). Relative changes in the 50th percentile generally follow changes in the mean. However, relative changes in the 5th percentile are nearly always higher than relative change in the mean, while changes in the 95th percentile are nearly always lower. This is unexpected, for at least 2 reasons. The first is that it is expected that the more extreme precipitation events will increase in intensity proportionally more with decreasing probability of exceedance (e.g. Dominguez et al., 2013). The second is the general property of basins that runoff ratios (the ratio of runoff to precipitation) increase with increasing precipitation (plus snowmelt) amount.

In summer (JJAS), the projected change in mean flow ranges from -15% to -29% for scenario B1 and -23% to -38% for scenario A1B (Figure 37). There is a tendency for those basins with higher relative increase in winter to show greater relative decreases in summer. This pattern is consistent with a loss of snow storage such that there is less snowmelt contribution to streamflow in the early, and even late, summer. However, the correlation is not perfect, as evident in Figure 37, which orders the sites by magnitude of winter streamflow change (low to high; A1B). Some locations with the largest decreases in winter flow do not show the largest relative decreases in summer flow: McKenzie River near Vida (MCKVI 4036), Clackamas At River Mill Dam (RMILL 4046), and Clackamas River above Three Lynx Creek (CLKTH 4044). These three locations show *relatively* large simulated sustained summer baseflows, implying a larger slow-release groundwater contribution from VIC, which serves to dampen the season variability in recharge. As a result, these basins are less sensitive to the loss of snowmelt with regards to summer flows than, in contrast, the basins gaged at Willamette River above Falls At Oregon City (WILFA 4064) and Willamette River below North Fork near Oakridge (WILNF 4048) with their proportionally lower simulated baseflow contribution. It is important to note, however,

that VIC may even be under-emphasizing these differences across basins because VIC uses a simple groundwater model that is known to under-predict summer flows in groundwater-dominated basins and over-predict summer flow in runoff-dominated basins in the Pacific Northwest US (Safeeq et al., 2014).

Relative changes in the 50th percentile summer flow generally follow changes in the mean. Relative decreases in the 5th percentile are typically smaller than the change in the mean, while relative decreases in the 95th percentile are typical larger than the change in the mean.

Table 16 Relative differences in mean seasonal streamflow volume between the historical (1970-1999) and A1B and B1 future scenarios (2030-2059) for selected CBCCSP locations

CBCCSP site	Associated Projects	Streamflow volume changes (%)			
		Winter (Dec.-Feb.)		Summer (May-Aug.)	
		A1B	B1	A1B	B1
Calapooia at Albany (CALAP)	None	6	2	-23	-15
Clackamas above Three Lynx Creek (CLKTH)	None	23	16	-27	-22
McKenzie near Vida (MCKVI)	Blue River	18	12	-28	-22
Molalla near Canby (MOLAL)	None	9	4	-32	-21
North Santiam below Boulder Creek near Detroit (NOSAN)	Hills Creek, Cougar, Detroit, Big Cliff, Lost Creek, Applegate	26	18	-32	-26
Clackamas at River Mill Dam (RMILL)	None	19	13	-26	-22
Row above Pitcher Creek near Dorena (ROPIT)	Cottage Grove, Dorena, Fern Ridge	7	2	-28	-17
North Santiam at Mahema (SANME)	None	17	11	-35	-27
South Santiam at Waterloo (SANWA)	Green Peter, Foster	8	4	-32	-23
Willamette above Falls at Oregon City (WILFA)	None	10	5	-38	-28
Middle Fork Willamette below North Fork near Oakridge (WILNF)	Lookout Point, Dexter, Fall Creek	17	12	-36	-28

Figure 37 Change from historical to future (A1B and B1) in the mean and 5th, 50th, and 95th percentiles of seasonal, simulated, bias-corrected, naturalized streamflow at 11 locations in the Willamette Basin. Sites are ordered by magnitude of change (low to high; A1B) in winter (Dec-Feb) streamflow.

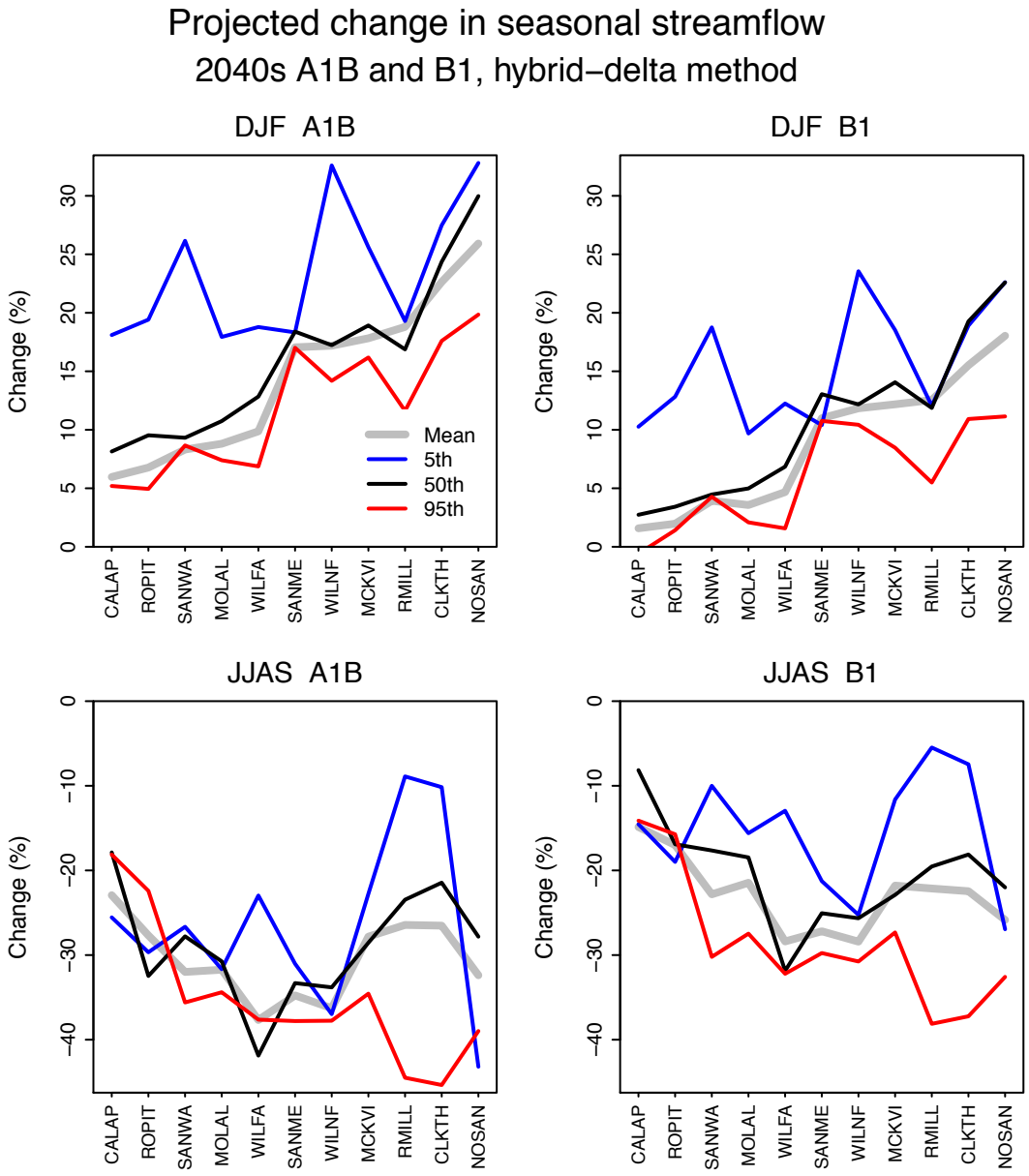

Flow-Duration-Frequency

Future Projections

Here changes in flow-duration-frequency (FDF) curves of annual maxima from the hybrid-delta simulations are discussed for two contrasting gages in a higher- and a lower-sensitivity basin, followed by a summary of changes over all 11 gages. Note that as above, bias-corrected, naturalized flows from the VIC hydrological model were used. (See Appendix G for graphs showing projections of flow-duration-frequency curves for all 11 sites.)

High sensitivity basin

We again used the North Santiam below Boulder Creek near Detroit (*NOSAN 4056*) as an example of a high-sensitivity site. In NOSAN, there is a strong tendency towards greater annual maxima flow in the future across most exceedance probabilities (Figure 38). Only 1 of the 19 hybrid-delta scenarios results in consistently lower annual maxima. This pattern is consistent across flow durations ranging from 1 to 15 days. However, for the more rare events (i.e., return periods greater than approximately 10 years) there is less agreement among the individual A1B and B1 simulations, and by the 50-year return interval, there is no detectable change on the annual maximum.

Differences between the historical and future FDF curves can be highlighted by plotting the relative differences in their flow, as shown in Figure 39. Increases in annual maxima flow average about 20% (decreasing slightly with increasing flow duration). However, the hybrid-delta simulations show a statistically significant trend towards smaller relative increases in flow with greater return period.

Low sensitivity basin

We used the Row River above Pitcher Creek near Dorena (*ROPIT 4035*) to represent a low-sensitivity site. At *ROPIT* there is a tendency towards greater annual maximum flow in the future when the changes in flow are averaged over all simulations. However, not all the individual simulations show increases in annual maximal; about one-quarter to one-third of the simulations have lower annual maxima, depending on the return period and duration (Figure 40). This disagreement in the sign of the change is consistent with internal variability in precipitation driving much of the variability among scenarios.

Increases in the annual maxima are roughly 10% depending on emissions scenario and flow duration. In contrast to the high-sensitivity site, *ROPIT* shows no clear trend in relative flow change with increases return period; only for the 1-day duration maxima is there a statistically, albeit marginally, significant trend towards greater relative increases in streamflow with longer return period.

All-basin summary

To summarize the changes in peak discharge across basins, the relative changes in the median of the annual maxima (i.e., the 2-year return period flows) are shown in Figure 42. The low-sensitivity basin shows increases in the 1-day duration maxima of 9% for B1 and 11% for A1B. In contrast, the high-sensitivity basin shows increases of 18% for B1 and 24% for A1B. The magnitudes of the relative change decrease consistently with increasing flow duration. For the 15-day duration maxima, the low-sensitivity basin shows increases of 6% and 8% for B1 and A1B, respectively, while the highest-sensitivity basin shows increases of 14% and 19%, respectively.

In addition to projected increases in the magnitude of peak flows, the streamflow simulations also show shifts in the mean timing of peak flows. Annual maximum flows of 1- to 5-day durations are projected to occur 0-5 days earlier in the water year at the majority of gauges, and up to 2 weeks earlier at locations with larger snowmelt influence, such as the gage on the North Santiam River (*NOSAN 4056*). Figure G23 in Appendix G gives the projected change in timing of streamflow maxima at all 11 gages.

There is concern over potential changes in the frequency of large "back-to-back" flow events, which could result from 1) changes in the inter-arrival times of heavy precipitation, or changes in the snow regime that could lead to 2) changes in the frequency of heavy rain-only events, or 3) changes in the frequency of rain-on-snow events. A change in the frequency of back-to-back flow events could manifest as large increases in the 15-day duration maxima relative to increases in shorter duration maxima. Although the peak flows at the 15-day duration do show increases in the future scenarios, the increases are clearly smaller than those at shorter durations (see Figure 42). This suggests that increases in 15-day duration peak flow arise largely from higher volumes of flow overall in the winter and not from a greater frequency of back-to-back events. However, these results are presented with an important caveat: The hybrid-delta climate scenarios are not suited to detecting changes resulting in precipitation inter-arrival times because the scenarios maintain the statistical properties of the timing of historical precipitation. Any simulated changes in the frequency of large back-to-back flow events could only arise from the interaction of precipitation and processes affected by changes in temperature.

Figure 38 Flow-duration-frequency curves for annual maxima streamflow of 1-, 3-, 5-, 7-, and 15-day durations for the historical and future periods at North Santiam River below Boulder Creek near Detroit (NOSAN 4056, USGS 14178000).

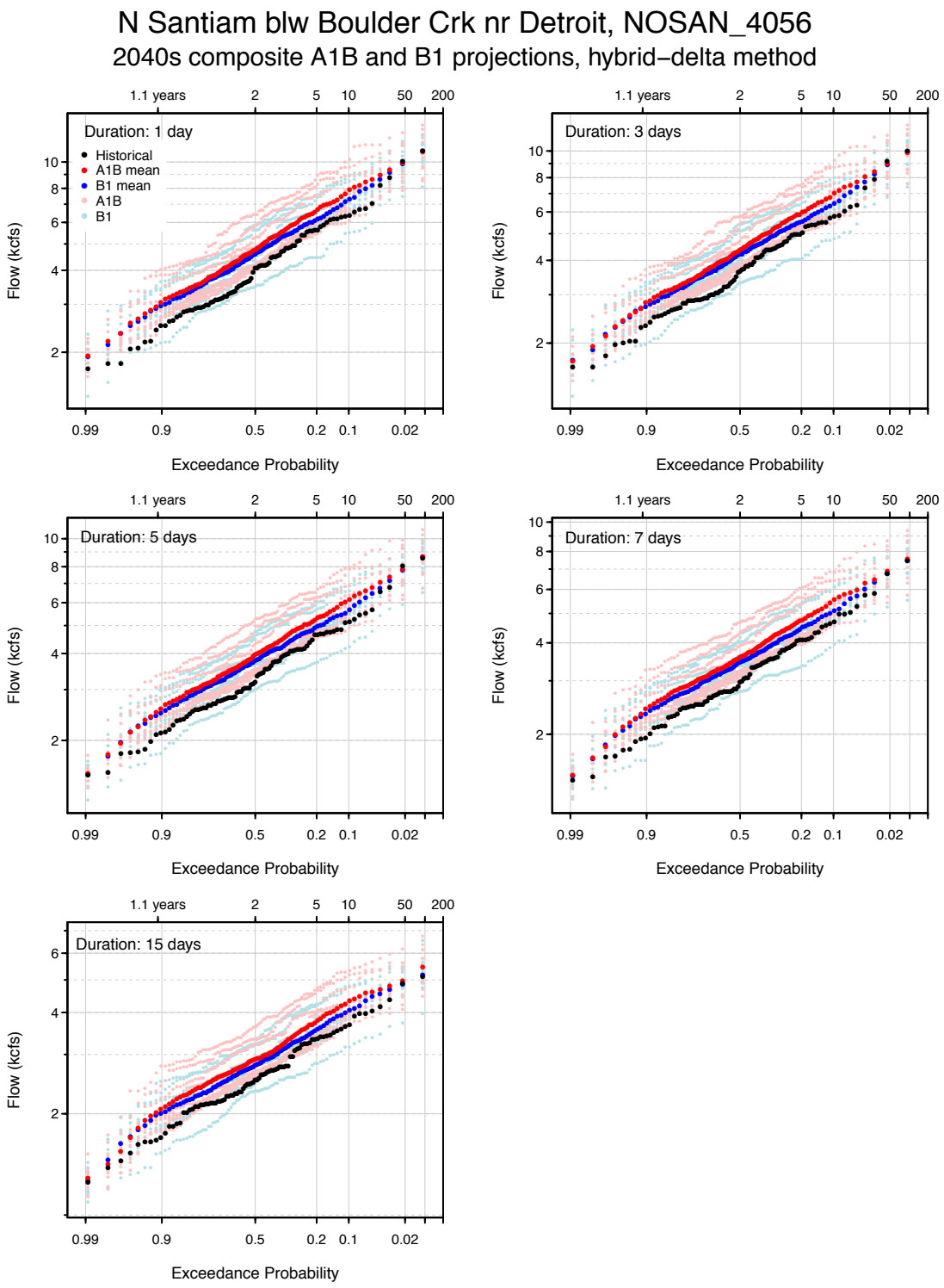

Figure 39 Relative change in flow in FDF curves of annual maximum from the historical to future periods at North Santiam River below Boulder Creek near Detroit (NOSAN 4056, USGS 14178000).

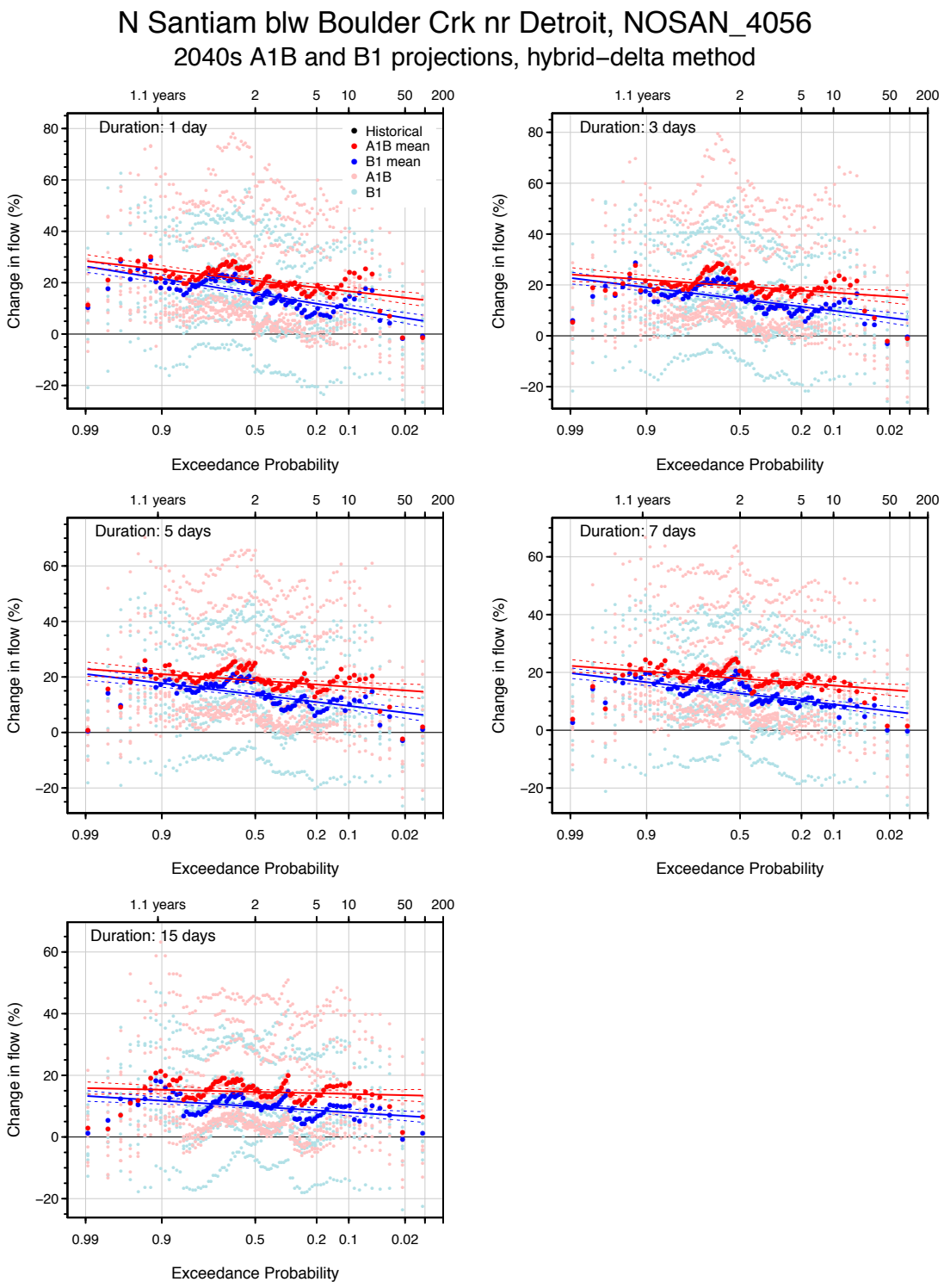

Figure 40 Flow-duration-frequency curves for annual maxima streamflow of 1-, 3-, 5-, 7-, and 15-day durations for the historical and future periods at Row River above Pitcher Creek near Dorena (ROPIT 4035, USGS 14154500).

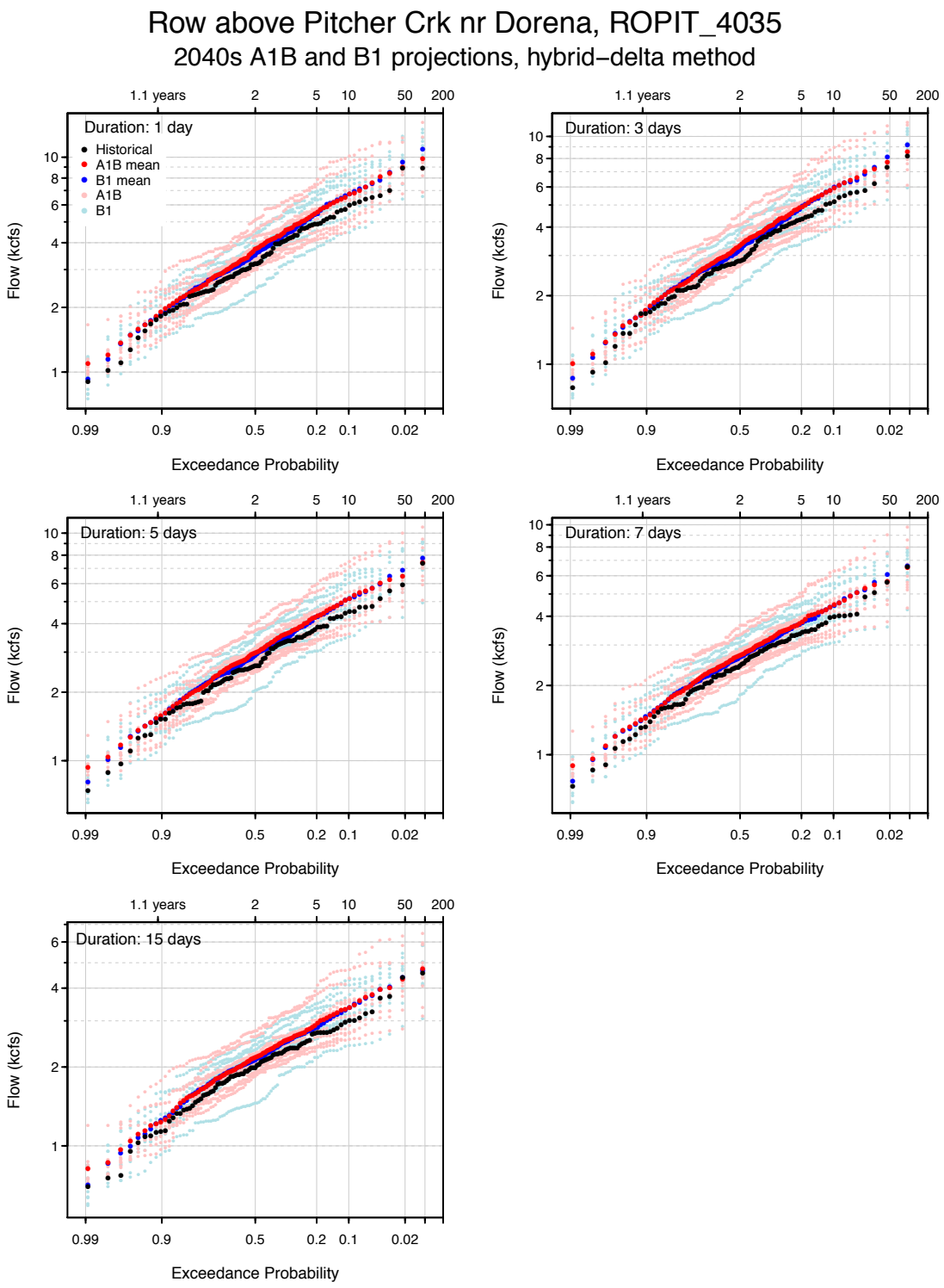

Figure 41 Relative change in flow in FDF curves of annual maximum from the historical to future periods at Row River above Pitcher Creek near Dorena (ROPIT 4035, USGS 14154500).

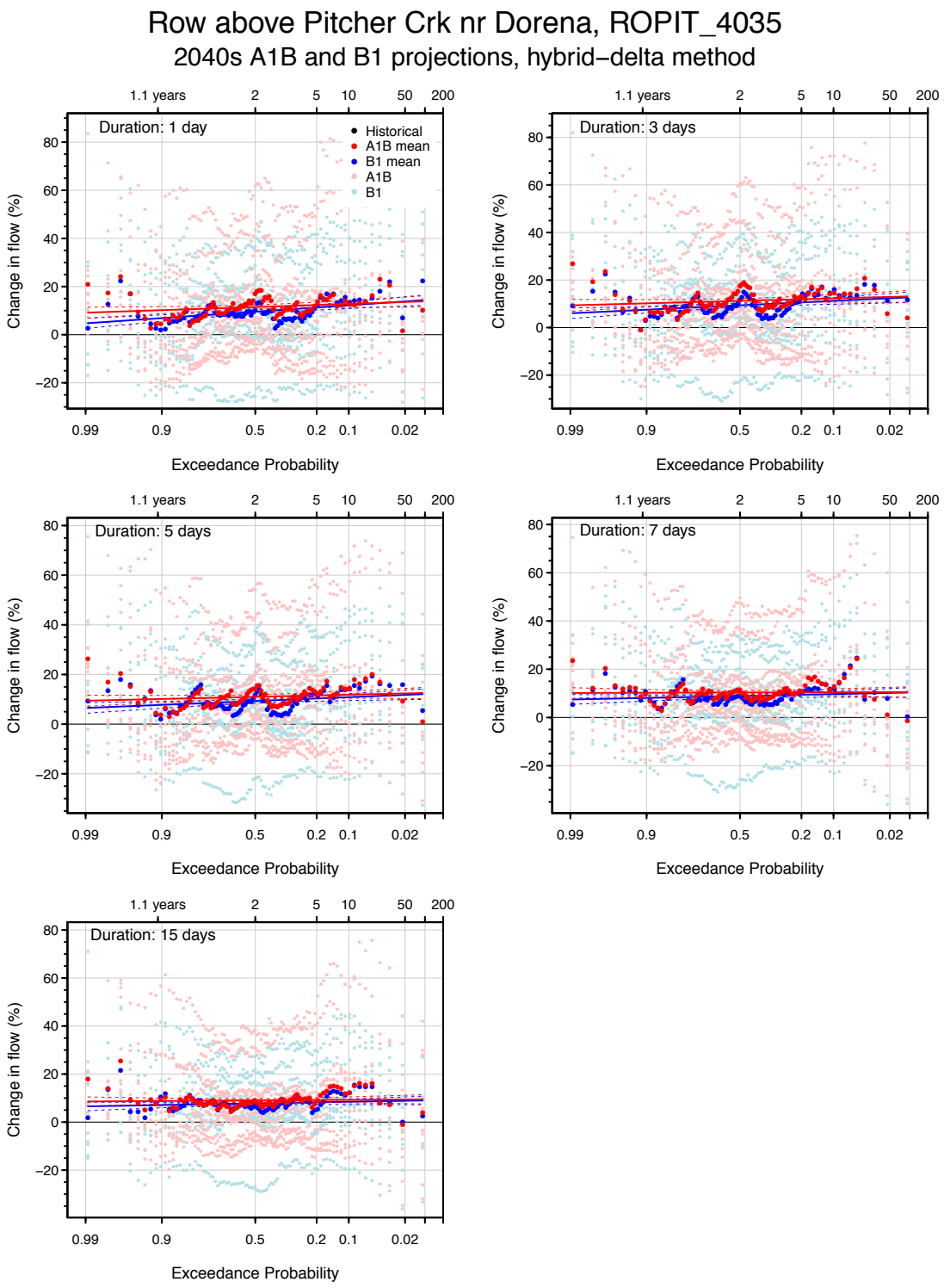

Figure 42 Relative change in the 2-year return period annual maximum flow from the historical to future periods.

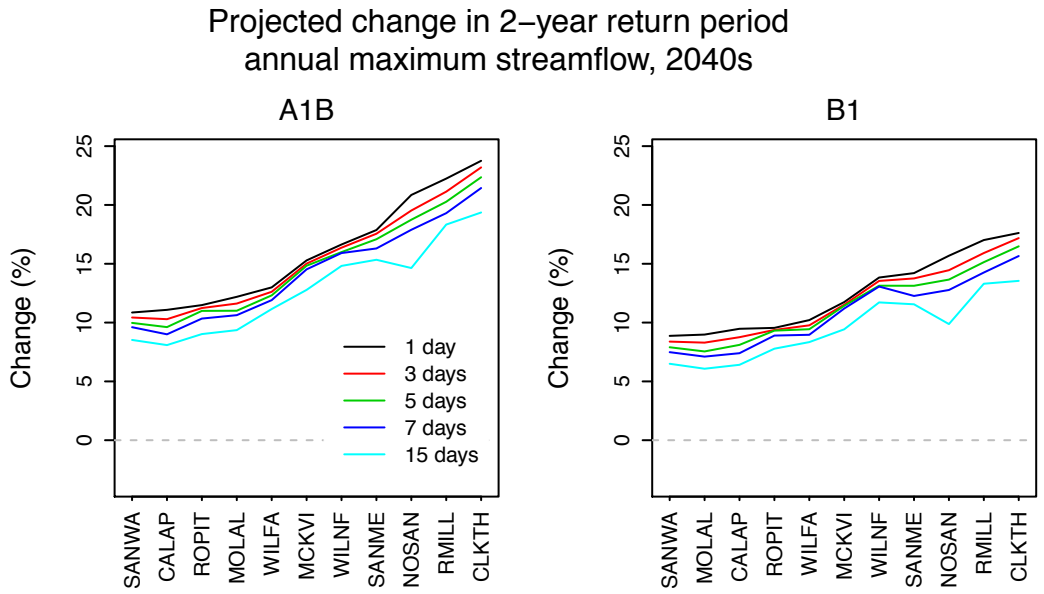

Conclusions

The Corps wants to understand better the potential implications of future climate change on water management operations in the Willamette and Rogue basins in the context of historical trends and variability in order to more effectively manage projects in the future. The Corps is concerned about potential climate change impacts on water management operations including changes in streamflow magnitude and timing, peak flow volumes, snowpack, temperature, precipitation, wind, and cloud cover. The metrics examined in this study included:

1. Annual streamflow hydrograph
2. The 5th, 50th, and 95th percentiles of monthly streamflow
3. Mean, 5th, 50th, and 95th percentiles of winter (DJF) and summer (JJAS) streamflow
4. Flow-duration-frequency curves for annual maximum streamflow at 1-, 3-, 5-, 7-, and 15-day durations
5. Monthly ratios of snow water equivalent (SWE) to accumulated precipitation
6. Seasonal temperature and precipitation
7. Monthly wind speed and cloud cover

Historical Observed Changes

Both maximum and minimum temperature increased annually from 1901-2013 for most stations in the Willamette and Rogue consistent with stations throughout the Northwest. Warming rates ranged from 0.5°F to 3.9°F per century with most trends statistically

different from zero. The greatest warming generally occurred in the summer and fall and the least warming occurred in the winter and spring. The observed warming is consistent with rising global greenhouse gas concentrations over this period. Spring and summer precipitation increased for most stations and precipitation increased annually and in winter and fall for about half of stations. Trends were statistically different from zero for only a few stations. Precipitation exhibits large natural variability from year to year such that detecting a climate change signal amidst the "noise" is difficult. Largely a consequence of warming temperature, snow water equivalent decreased at virtually all sites ranging from -3% to -60%, though trends were statistically different from zero at only a few locations. The largest decreases occurred at lower elevations that hover near freezing.

Streamflow hydrographs changed between the periods 1941-1970 to 1981-2010 in a way inconsistent with observed climate warming and reduction in snow water equivalent. At sites with low sensitivity to snowpack changes, winter streamflow decreased and summer streamflow increased reflecting current flood control management. In the basin with high sensitivity to snowpack changes, the streamflow hydrograph in which there were peaks in the hydrograph in both the winter and early summer in the period 1941-1970 became relatively stable throughout the wet season in the period 1981-2010. Observing a true climate change signal in the streamflow is difficult as most of the gages are located on stream reaches that are highly managed. As such, streamflow changes over the observed record are not representative of streamflow changes that can be expected in the future as the climate changes.

Future Climate Projections

Future climate projections indicate that annually-averaged daily minimum and maximum temperatures are projected to increase by 0.8°F-5.3°F and 1.1°-5.5°F, respectively, by the 2040s depending on the climate model, emissions scenario, and sub-basin. Summer minimum and maximum temperatures are expected to increase more by 0.7°F to 6.8°F and 1.5°F to 7.8°F, respectively. Increases and decreases in future precipitation are noted in each season, but the majority of models and the multi-model mean project precipitation increases in the winter and decrease in the summer. The Willamette and Rogue basins, as across the entire Northwest, can expect to experience warmer, wetter winters and warmer, drier summers in the future (Mote et al. 2014).

Some measures of extreme precipitation are projected to increase in the future, as the warmer atmosphere is able to accommodate larger amounts of water vapor. Over the Northwest, the magnitudes of the 20-year and 50-year precipitation events are projected to increase in the future (Dominguez et al., 2012) and in the Willamette Basin the 2-year and 25-year event also increase (Halmstad et al., 2013). Many of the flood-producing extreme precipitation events in the Northwest are associated with atmospheric river events, which

are projected to become stronger and more frequent along the Northwest coast (Warner et al., 2015). Rain-on-snow events that can lead to substantial flooding, such as the February 1996 event, have decreased in frequency in recent years. The strong negative correlation between temperature and frequency of rain-on-snow events suggests that as temperature continues to increase, the occurrence of rain-on-snow events is likely to decrease (McCabe et al., 2007).

Projected changes in wind speed are small (<1 mph) compared with the magnitude of the annual cycle. Some models project increases while others project decreases in every season, but the multi-model mean indicates decreases during all seasons except summer. Projected changes in cloud cover are also very small compared to the magnitude of the annual cycle and tend toward an enhancement of the annual cycle. That is, in the summer there is a slight shift away from scattered clouds toward clear skies and in the winter there is a slight shift away from broken clouds toward overcast skies.

Snowpack (SWE) as proportion of cumulative water year precipitation (P) is expected to decline markedly in the Willamette and Rogue basin, with decreases in SWE/P ranging from 21% to 93%, with lower elevation basins (e.g. Tualatin) typically showing the largest relative declines. Those sub-basins that historically receive the most snow such as North Santiam show projected winter declines of 27%-67% in SWE/P. Sub-basins with little snow currently, such as Middle Willamette, are projected to receive virtually no snow in the future. The small projected increases in total winter precipitation provide little offset to the decline in SWE/P due to the projected warming. The projections of warmer and drier summers and a declining snowpack point to an increased potential for drought conditions. The basins most at risk are those that partially rely on melting snowpack to provide dry season water supply.

Future Streamflow Projections

Winter (DJF) naturalized streamflow volumes at the USACE projects are projected to increase by 4% to 26% by the 2040s. In contrast, summer (JJAS) streamflow volumes are projected to decrease by -21% to -36%.

Two dimensions of projected regional climate change contribute to an increase in winter flow and a decrease in summer flow. The primary one is the increase in temperature leading to decreasing snow accumulation. Less precipitation stored in the snowpack in winter leads to increased streamflow during the snow accumulation period (winter and early spring), and subsequently less streamflow during the snow ablation period (spring into summer). This change in the snow regime explains most of the spatial variability in the anthropogenically forced response of streamflow across the Willamette Basins, with the

upper Cascade watersheds showing the largest changes while the historically rain-dominated watersheds are largely unaffected.

A secondary dimension is the seasonal variation in precipitation change, with winter showing precipitation increases and summer showing rainfall declines. The streamflow response is, as one would expect: more winter streamflow and decreased summer streamflow. However, this effect is smaller than the impact of the changing snow regime, as evidenced by the relatively small changes in the annual hydrograph in rain-dominated basins.

Spatial variability in precipitation changes attributable to climate change is not well understood within the Willamette and Rogue Basins, therefore its contribution to spatial variability in streamflow response is equally unknown. The spatial variability in mean seasonal precipitation changes reported here (Figure 8) is dominated by natural variability in space and time, even after averaging over 30 years and multiple downscaled GCM simulated. The precipitation change signal as given by the GCMs should therefore be considered to be spatially uniform. This is because the coarse-resolution GCMs are not able to accurately simulate precipitation changes that may arise from the interactions of changes in synoptic-scale weather patterns with local topography. Higher resolution modeling from RCMs has begun to shed light on such interactions (Salathé et al., 2010), but the science is young.

Additional basin-to-basin variability in streamflow response arises from heterogeneity in geology that leads to differing deep groundwater contributions between basins (Tague et al., 2008). Separating the effect of changing snow regime from geology on streamflow response in winter is complicated because the different primary geologies also occupy different snow regimes: High Cascades geology → Western Cascades geology → alluvium; snow-dominated → snow-rain mix → rain dominated [see, e.g., Figure 1 in Surfleet and Tullos (2013)]. In summer, however, when deep groundwater discharge is most pronounced and the snow pack is largely absent, the role of geology should be more apparent. In general, the sub-basins with a larger deep groundwater component of total flow show a smaller *relative* reduction in summer flow, other factors being similar. However, as pointed out by Tague et al. (2008) in their study of two sub-basins of the McKenzie River Basin, *absolute* declines can be greater, which may have more relevance depending on the particular impact of concern.

Changes in mean seasonal streamflow across sites given here are consistent with the spatial pattern, and the general magnitudes, of change across Willamette sub-basins calculated by Chang and Jung (2010) and Jung and Chang (2011). These two studies relied on the identical CMIP3 scenarios and downscaling method as in this report, but simulated

hydrologic processes using the Precipitation-Runoff Modeling System (PRMS). Additional studies have explored streamflow response to climate change to particular sub-basins of the Willamette: McKenzie Basin at/above Clear Leak and Lookout Creek Basin (Tague et al. 2008) and the Santiam Basin (Surfleet and Tullos, 2012; Surfleet et al., 2012). These sub-basin studies focused on the role of groundwater discharge, and expanded the number of hydrological models applied to the question (RHESSys: Tague et al., 2008; VIC, PRMS, PRMS-MODFLOW; Surfleet and Tullos, 2012; Surfleet et al., 2012). While there is indication that VIC overestimates the streamflow decline in summer in streams with high groundwater discharge (Surfleet et al., 2012), the overall patterns of change in mean flows are consistent across the studies.

Although all the studies combined still only provides a limited assessment of uncertainty due to choices made in hydrological modeling, it does suggest a relative *insensitivity* to hydrological model structure, with provides additional confidence that the *general* magnitudes of changes to *mean seasonal streamflow* are robust responses to the chosen climate change scenarios.

In addition to mean winter flow, the annual peak flows are projected to increase in the future. Increases range generally between 10% and 20% for 1-day duration peak flows, depending on the basin, when averaged over all the 19 scenarios. The larger relative increases in annual peak flows are in the more snow-affected basins, indicating again that in these sub-basins it is the change in the snow regime, and to a lesser extent the change in winter precipitation amount, that contributes to the increase in peak flows.

The potential for an increased frequency of large "back-to-back" flow events was examined by examining changes in the 15-day duration annual peak flows against peak flow of shorter durations. An increased frequency of these "back-to-back" events which could result from 1) changes in the inter-arrival times of heavy precipitation, or changes in the snow regime that could lead to 2) changes in the frequency of heavy rain-only events, or 3) changes in the frequency of rain-on-snow events. Although the peak flows at the 15-day duration do show increases in the future scenarios (+13%_averaged across basin), the increases are smaller than those at shorter durations (+15% for 1-day duration; see Figure 30), suggesting no potentially hazardous increase in the likelihood of back-to-back events by the 2040s. However, these results are presented with an important caveat: The hybrid-delta climate scenarios are not ideally suited to detecting changes resulting in precipitation inter-arrival times because the scenarios maintain the statistical properties of the timing of historical precipitation. Any simulated changes in the frequency of large back-to-back flow events could only arise from the interaction of precipitation and processes affected by changes in temperature.

An important result of the peak flow analysis is that the relative increases in peak flow do not always outpace the relative increases in the median winter flow. This may seem at odds with the expectation of what will occur with precipitation: the largest precipitation extremes are expected to increase proportionally more than the increase in the mean precipitation, as simulated in the region using both regional (Dominguez et al., 2012) and global (Rupp et al., 2014) climate models.

An explanation may stem from noting that this peak flow phenomenon is most pronounced for the snow-affected basins. Furthermore, there is a tendency for the peak flows with lower return periods (i.e. 2 years) to increase proportionally more than those with higher return periods. These apparent tendencies may be related to the interactions of rain and snow, if the larger peak flows occurred historically during rain-on-snow events. Surfleet and Tullos (2013) noted the same tendency in their study of the Santiam River Basin, even simulating a decrease in the peak flows with return periods greater than 10 years. They reported an increase in the frequency of rain-on-snow events in the future, but a decrease in SWE during these events, and concluded that the reduction in SWE could explain the decrease in the magnitudes of the largest peak flows.

Implications

The implications of climate change to future water resources management in the Willamette Basins were summarized by Change and Jung (2010) and Jung and Chang (2011) in their studies based on downscaled CMIP3 climate projections. The new generation of GCM simulations using different scenarios of future GHG emissions slightly amplify the projected warming, but the implications remain essentially the same: Winter flood risk and summer hydrological drought is projected to increase in the Willamette and Rogue Basins. These two changes are additional stressors to the management of the 13 dams in the Willamette Basin and 2 dams in the Rogue Basin operated by the USACE. The stressors are also competing, in the sense that attempting to ameliorate increased winter flow only further stresses the ability to manage for summer drought.

Jung and Chang (2011) propose investigating an earlier (e.g. one-month) reservoir filling to balance flood risk with summer water demand. Recent work by Moore (2015) in the Willamette Basin showed how a project's rule curve could be optimized to account for climate change impacts. In effect, the Corps could begin filling reservoirs earlier in the year but fill them at a slower rate. However, such changes should simultaneously consider the potential of increasing flood risk as the human population and development increases downstream of the dams. Chang and Jung (2010) also suggest some measures that would require new infrastructure, not only changes in operations: additional small-scale reservoirs, using aquifers for additional storage, and diverting and connecting runoff from High-Cascade basins to Western Cascade basins.

The apparent tendency for future peak flow magnitudes with large return periods to increase proportionally less (and in some cases even show no increase) than peak flows with shorter return periods is an important factor for determining the need for structural changes to infrastructure. It should be emphasized that the peak flow results presented here and those of others are based on the same set of downscaled climate projections provided by the CBCCSP (Hamlet et al., 2010) and may be sensitive to the downscaling methodology. Given the costly implications of these particular findings, it is recommended that this topic be a line of continued investigation.

Water management operations focused on environmental considerations are interested in how changes in temperature, cloud cover, and wind might affect stream temperatures and other in-stream measures of water quality. The projected changes in wind and cloud cover are small and uncertain and unlikely to have a discernible effect on water quality. However, projected increases in air temperature can result in higher in-stream temperatures (Isaak et al., 2010) and declines in dissolved oxygen threatening the health of endangered aquatic species (Raymondi et al., 2013). In addition, increased wildfire activity, related to increasing temperatures and drought conditions, can increase sediment and nutrient loads in streams (Cannon et al., 2010; Chang et al., 2010).

Uncertainties & Limitations

Inherent in global climate models projections is uncertainty due to emissions scenario, internal variability, and modeling physics and resolution. Given the same scenario of greenhouse gases, individual global climate models project different magnitudes of warming because the models' "climates" are either more or less sensitive to external radiative forcings (e.g., increasing greenhouse gases). Furthermore, the chaotic nature of the climate system means that even a single climate model, if identical simulations were started on a different day, yields a range of outcomes. A large source of uncertainty in climate sensitivity is the representation of clouds in the model atmosphere. Finer spatial resolution allows for more accurate topography leading to better simulation of regional climate, especially in the mountainous terrain of the West. However, at ~100 km horizontal resolutions, state-of-the-art climate models are still unable to resolve key topographical features that influence western US climate.

Temperature projections are the most certain whereas projections in variables related to the models' representation of clouds (e.g., precipitation, cloud cover) are least certain. Modeling accurate microphysical cloud processes requires resolutions much finer than current CMIP3 or CMIP5 GCMs can attain. In addition, precipitation exhibits high natural variability often masking any long-term change.

Downscaling GCM output to finer scales as done in this project, adds another layer of uncertainty. A limitation of all statistical downscaling methods is that historical relationships are held constant in the future and may unjustly constrain relationships in a changing climate; for example, local snow albedo feedbacks, which can influence local temperature changes, are not resolved in statistical downscaling. Furthermore, hydrologic modeling requires some assumptions, which adds yet another layer of uncertainty. For example, the groundwater component of VIC is simplistic and tends to over- or underestimate the groundwater component in certain sub-basins.

The hybrid-delta downscaled climate scenarios used as input to the hydrological modeling provide limited answers to some of the questions posed by the USACE. In particular, the question of whether there will be changes in the inter-arrival times between large events cannot be fully explored because the hybrid-delta scenarios retain the same temporal sequence of precipitation in both historical times series and the future time series (although the precipitation magnitudes differ). Addressing such questions using mutltiple downscaling methods would provide additional certainty in results.

Data Gaps

Updated routed streamflow projections based on CMIP5 are being generated by the Land Surface Hydrology Group at the University of Washington (UW) and are anticipated to become available in Fall 2016. These streamflow projections are being funded by the Bonneville Power Administration (BPA) for the River Management Joint Operating Committee II (RMJOCII). The new projections will consider uncertainty arising from using different climate model datasets, different downscaling methodologies, and different hydrological models. As part of this project, UW will apply the hybrid-delta downscaling method along with the VIC hydrological model as was done for the CBCCSP, so the opportunity will exist to compare the CMIP3-based and CMIP5-based streamflow projections using the same methodology. Furthermore, the new projections will include streamflow routing to 4 gage locations in the Rogue basin: (1) Gold Ray reservoir, (2) Grants Pass, (3) a gage about 10 miles upstream from Grants Pass, and (4) a point on tributary in Applegate, Oregon.

A better understanding is needed of how temperature and precipitation will change across the landscape when the interactions of local topography with larger-scale climate changes are considered. Advances can be made using dynamical downscaling with high-resolution regional climate models. Progress has been slow, but a concerted effort is being made at regional institutions to conduct coordinated experiments using regional climate models, in the spirit of CMIP.

References

Abatzoglou JT, Rupp DE, Mote PW (2014) Seasonal climate variability and change in the Pacific Northwest of the United States. *Journal of Climate* **27**, 2125-2142. DOI: 10.1175/JCLI-D-13-00218.1.

Abatzoglou JT, Brown TJ (2012) A comparison of statistical downscaling methods suited for wildfire applications. *Int. J. Climatology* **32**, 772-780, doi: 10.1002/joc.2312.

Cannon SH, Gartner JE, Rupert MG, Michael JA, Rea AH, Parrett C (2010) Predicting the probability and volume of post wildfire debris flows in the Intermountain Western United States. *Geological Society of America Bulletin* **122**, 127-144, doi: 10.1130/B26459.1.

Chang H, Jung I-W (2010) Spatial and temporal changes in runoff caused by climate change in a complex large river basin in Oregon. *J. Hydrol*. **388**, 186-207, doi:10.1016/j.jhydrol.2010.04.040.

Chang H, Jones J, Gannett M, Tullos D, Moradhkani H, Vache K, Parandvash H, Shandas V, Nolin A, Fountain A, Johnson S, Jung I-W, House-Peters L, Steele M, Copeland B (2010) Climate change and freshwater resources in Oregon. In *Oregon Climate Assessment Report*, edited by KD Dello and PW Mote, 69-149, Oregon Climate Change Research Institute, Oregon State University, Corvallis, Oregon.

Collins M, Knutti R, Arblaster J, Dufresne J-L, Fichefet T, Friedlingstein P, Gao X, Gutowski WJ, Johns T, Krinner G, Shongwe M, Tebaldi C, Weaver AJ, Wehner M (2013) Long-term climate change: projections, commitments and irreversibility. In *Climate Change 2013: The Physical Science Basis. Contribution of Working Group I to the Fifth Assessment Report of the Intergovernmental Panel on Climate Change*, edited by TF Stocker, D Qin, G-K Plattner, M Tignor, SK Allen, J Boschung, A Nauels, Y Xia, V Bex, and PM Midgley. Cambridge University Press, Cambridge, United Kingdom and New York, NY, USA.

Dalton MM, Mote PW, Snover AK, eds (2013) Climate change in the Northwest: Implications for our landscapes, waters, and communities. Island Press, Washington DC, 230 pp.

Dalton MM, Abatzoglou JT, Evers L, Hegewisch K (2015) Projected changes in the energy release component under climate change in Northwest Predictive Services Areas. A report to the Bureau of Land Management Oregon-Washington State Office. Prepared by the Oregon Climate Change Research Institute.

Dominguez F, Rivera E, Lettenmaier DP, Castro CL (2012) Changes in winter precipitation extremes for the western United States under a warmer climate as simulated by regional climate models. *Geophys. Res. Lett.*, **39**, L05803, doi:10.1029/2011GL050762.

Elsner MM, Cuo L, Voisin N, Deems JS, Hamlet AF, Vano J A, Lettenmaier DP (2010). Implications of 21st century climate change for the hydrology of Washington State. *Climatic Change* **102**, 225–260. doi: 10.1007/s10584-010-9855.

Halmstad A, Najafi MR, Moradkhani H (2013) Analysis of precipitation extremes with the assessment of regional climate models over the Willamette River Basin, USA. *Hydrol. Process*. **27**, 2579-2590. Doi: 10.1002/hyp.9376.

Hamlet AF, Carrasco P, Deems J, Elsner MM, Kamstra T, Lee C, Lee S-Y, Mauger G, Salathe EP, Tohver I, Whitely Binder L (2010) Final Project Report for the Columbia Basin Climate Change Scenarios Project, http://warm.atmos.washington.edu/2860/report/

Hamlet AF, Elsner MM, Mauger GS, Lee S-Y, Tohver I, Norheim RA (2013) An overview of the Columbia Basin climate change scenarios project: Approach, methods, and summary of key results. *Atmos.–Ocean* **51**, 392–415, doi: 10.1080/07055900.2013.819555.

Hatcher KL, Jones JA (2013) Climate and streamflow trends in the Columbia River basin: Evidence for ecological and engineering resilience to climate change. *Atmosphere-Ocean*, **51**(4), 436-455.

Isaak JF, Luce CH, Rieman BE, Nagel DE, Peterson EE, Horan DL, Parkes S, Chandler GL (2010) Effects of climate change and wildfire on stream temperature and salmonid thermal habitat in a mountain river network. *Ecological Applications* **20**, 1350-1371, doi: 10.1890/09-0822.1.

IPCC (2013) Climate Change 2013: The Physical Science Basis. Contribution of Working Group I to the Fifth Assessment Report of the Intergovernmental Panel on Climate Change [Stocker TF, Qin D, Plattner G-K, Tignor M, Allen SK, Boschung J, Nauels A, Xia Y, Bex V, Midgley RM (eds.)]. Cambridge University Press, Cambridge, United Kingdom and New York, NY, USA, 1535 pp. DOI: 10.1017/CBO9781107415324.

Jung I-W, Chang H (2011) Assessment of future runoff trends under multiple climate change scenarios in the Willamette River Basin, Oregon, USA. *Hydrol. Process*. **25**, 258–277. doi: 10.1002/hyp.7842.

Liang X, Lettenmaier DP, Wood EF, Burges SJ (1994) A simple hydrologically based model of land surface water and energy fluxes for general circulation models. *J. Geophys. Res.* **99**, 14415–14428, doi: 10.1029/94JD00483.

Lohmann D, Raschke E, Nijssen B, Lettenmaier, DP (1998) Regional scale hydrology: I. Formulation of the VIC-2L model coupled to a routingmodel. *Hydrological Sciences Journal* **43**, 131–141.

Mateus C, Tullos D, Surfleet CG (2015) Hydrologic sensitivity to climate and land use changes in the Santiam River Basin, Oregon. *J. Am. Water. Resour. Assoc*. **51**, 400-420. doi:10.1111/jawr.12256.

McCabe GJ, Clark MP, Hay LE (2007) Rain-on-snow events in the western United States. *Bulletin of the American Meteorological Society*, March, 319-328, doi: 10.1175/BAMS-88-3-319.

Meehl GA, Covey C, Delworth T, Latif M, McAvaney B, Mitchell JFB, Stouffer RJ, Taylor KE (2007) The WCRP CMIP3 Multimodel Dataset: A New Era in Climate Change Research. *Bulletin of the American Meteorological Society* **88**, 1383-1394. doi: 10.1175/BAMS-88-9-1383.

Meinshausen M, Raper SCB, Wigley TML (2011) Emulating coupled atmosphere-ocean and carbon cycle models with a simpler model, MAGICC6: Part I—Model Description and Calibration. *Atmospheric Chemistry and Physics* **11**, 1417-1456. Doi: 10.5194/acp-11-1417-2011.

Menne MJ, Williams CN, Vose RS (2009) The United States Historical Climatology Network Monthly Temperature Data - Version 2. *Bulletin of the American Meteorological Society*, **90**, 993-1107.

Moore K (2015) Optimizing reservoir operations to adapt to 21st century expectations of climate and social change in the Willamette River Basin, Oregon. Ph.D. Dissertation, College of Earth, Ocean, and Atmospheric Sciences, Oregon State University.

Mote P, Snover AK, Capalbo S, Eigenbrode SD, Glick P, Littell J, Raymondi R, Reeder S. (2014) Ch. 21: Northwest. Climate Change Impacts in the United States: The Third National Climate Assessment, edited by JM Melillo, TC Richmond, GW Yohe. US Global Change Research Program, 487-513, doi: 10.7930/J04Q7RWX.

Mote PW, Hamlet AF, Clark MP, Lettenmaier DP (2005) Declining mountain snowpack in Western North America. *Bulletin of the American Meteorological Society* **86**, 39-49. Doi: 10.1175/BAMS-86-1-39.

Mote PW, Sharp D (2014) Update to data originally published in: Mote PW, Hamlet AF, Clark MP, Lettenmaier DP (2005). Declining mountain snowpack in Western North America. *Bulletin of the American Meteorological Society* **86**, 39-49.

Nakićenović N, Davidson O, Davis G, Grübler A, Kram T, Lebre La Rovere E, Metz B, Morita T, Pepper W, Pitcher H, Sankovshi A, Shukla P, Swart R, Watson R, Dadi Z (2000) Special Report on Emissions Scenarios: A Special Report of Working Group III of the Intergovernmental Panel on Climate Change, Cambridge University Press, Cambridge, United Kingdom. 599 pp. Available on line at: http://www.grida.no/climate/ipcc/emission/index.htm.

Nolin AW, Daly C (2006) Mapping "at-risk" snow in the Pacific Northwest. *Journal of Hydrometeorology* **7**, 1164-1171. DOI: 10.1175/JHM543.1.

Raymondi RR, Cuhaciyan JE, Glick P, Capalbo SM, Houston LL, Shafer SL, Grah O (2013) Water Resources: Implications of changes in temperature and precipitation. In *Climate Change in the Northwest: Implications for our landscapes, waters, and communities*, edited by MM Dalton, PW Mote and AK Snover, 41-66, Oregon Climate Change Research Institute, Oregon State University. Corvallis, Oregon.

Rupp DE, Abatzoglou JT, Hegewisch KC, Mote PW (2013) Evaluation of CMIP5 20th century climate simulations for the Pacific Northwest USA. *J. Geophys. Res. Atmos*. **118**, 10 884–10 906, doi:10.1002/jgrd.50843.

Rupp DE, Mote P, Abatzoglou J, Hegewisch K (2014) New views on future Northwest climate: How will extremes change in relationship to changes in means? 5th Annual Pacific Northwest Climate Science ConferenceSeptember 9-10, 2014.

Safeeq M, Mauger GS, Grant GE, Arismendi I, Hamlet AF, Lee S-Y (2014) Comparing large-scale hydrological model predictions with observed streamflow in the Pacific Northwest: Effects of climate and groundwater. *J. Hydrometeor*, **15**, 2501–2521, doi: 10.1175/JHM-D-13-0198.1.

Salathé EP, Leung LR, Qian Y, Zhang Y (2010) Regional climate model projections for the State of Washington. *Climatic Change* **102**, 51-75, doi:10.1007/s10584-010-9849-y.

Sproles EA, Nolin AW, Rittger K, Painter TH (2013) Climate change impacts on maritime mountain snowpack in the Oregon Cascades. *Hydrol. Earth Syst. Sci.* **17**, 2581-2597, doi:10.5194/hess-17-2581-2013, 2013.

Stewart IT, Cayan DR, Dettinger MD (2005) Changes toward earlier streamflow timing across western North America. *Journal of climate* **18**(8), 1136-1155.

Surfleet CG, Tullos D, Chang H, Jung I-W (2012) Selection of hydrologic modeling approaches for climate change assessment: A comparison of model scale and structures. *J. Hydrol.* **464-465**, 233–248, doi:10.1016/j.jhydrol.2012.07.012.

Surfleet CG, Tullos D (2013) Variability in effect of climate change on rain-on-snow peak flow events in a temperate climate. *J. Hydrol*. **479**, 24-34, doi:10.1016/j.jhydrol.2012.11.021.

Surfleet CG, Tullos D (2013) Uncertainty in hydrologic modelling for estimating hydrologic response due to climate change (Santiam River, Oregon). *Hydrol. Process.* **27**, 3560–3576, doi:10.1002/hyp.9485.

Tague C, Grant G, Farrell M, Choate J, Jefferson A (2008) Deep groundwater mediates streamflow response to climate warming in the Oregon Cascades. *Climatic Change* **86**, 189–210, doi:10.1007/s10584-007-9294-8.

van Vuuren DP, Edmonds J, Kainuma M, Riahi K, Thomson A, Hibbard K, Hurtt GC, Kram T, Krey V, Lamarque J-F, Masui T, Heinshausen M, Nakićenović N, Smith SJ, Rose SK (2011) The Representative Concentration Pathways: An Overview. *Climatic Change* **109**, 5-31, doi: 10.1007/s10584-011-0148-z.

Warner MD, Mass CF, Salathé EP (2015) Changes in winter atmospheric rivers along the North American West Coast in CMIP5 climate models. *Journal of Hydrometeorology*, **16**, 118-128, doi: 10.1175/JHM-D-14-0080.1.

Wood AW, Maurer EP, Kumar A, Lettenmaier DP (2002) Long range experimental hydrologic forecasting for the eastern U.S. *J. Geophys. Res.* **107** (D20): 4429.

Appendix A. Global Climate Models

The 20 CMIP5 and 10 CMIP3 GCMs used in this project. The subset of 10 CMIP5 GCMs used in the Integrated Scenarios: Hydrology dataset are noted with asterisks.

Model Name	Ensemble	Modeling Center
BCC-CSM1-1	CMIP5	Beijing Climate Center, China Meteorological Administration
BCC-CSM1-1-M*	CMIP5	
BNU-ESM[1]	CMIP5	College of Global Change and Earth System Science, Beijing Normal University, China
CanESM2*	CMIP5	Canadian Centre for Climate Modeling and Analysis
CCSM4*	CMIP5	National Center for Atmospheric Research, USA
CCSM3	*CMIP3*	
PCM	*CMIP3*	
CNRM-CM5*	CMIP5	National Centre of Meteorological Research, France
CNRM-CM3	*CMIP3*	
CSIRO-Mk3-6-0*	CMIP5	Commonwealth Scientific and Industrial Research Organization/Queensland Climate Change Centre of Excellence, Australia
ECHAM5/MPI-OM	*CMIP3*	
ECHO-G	*CMIP3*	
GFDL-ESM2G	CMIP5	NOAA Geophysical Fluid Dynamics Laboratory, USA
GFDL-ESM2M	CMIP5	
HadGEM2-CC*	CMIP5	Met Office Hadley Center, UK
HadGEM2-ES*	CMIP5	
HadCM3	*CMIP3*	
HadGEM1	*CMIP3*	
INMCM4	CMIP5	Institute for Numerical Mathematics, Russia
IPSL-CM5A-LR	CMIP5	Institut Pierre Simon Laplace, France
IPSL-CM5A-MR*	CMIP5	

[1] This modeling center has recalled its precipitation data because the daily and monthly precipitation fields were not consistent and were unable to verify which is correct.

IPSL-CM5B-LR	CMIP5	
IPSL-CM4	*CMIP3*	
MIROC5*	CMIP5	Japan Agency for Marine-Earth Science and Technology, Atmosphere and Ocean Research Institute (The University of Tokyo), and National Institute for Environmental Studies
MIROC-ESM	CMIP5	
MIROC-ESM-CHEM	CMIP5	
MIROC3.2(medres)	*CMIP3*	
MRI-CGCM3	CMIP5	Meteorological Research Institute, Japan
MRI-CGCM3.1(T47)	*CMIP3*	
NorESM1-M*	CMIP5	Norwegian Climate Center, Norway

Appendix B. Datasets

A list and description of all the datasets used in this report.

National Weather Service (NWS) Cooperative Observer Program (COOP)
http://www.ncdc.noaa.gov/data-access/land-based-station-data/land-based-datasets/cooperative-observer-network-coop
A network of over 10,000 volunteers who record daily weather observations across the US.

U.S. Historical Climatology Network (USHCN)
http://www.ncdc.noaa.gov/data-access/land-based-station-data/land-based-datasets/us-historical-climatology-network-ushcn
A designated subset of the NWS COOP network with sites selected according to their spatial coverage, record length, data completeness, and historical stability. This data is used to quantify national- and regional-scale temperature changes.

Carbon Dioxide Information Analysis Center (CDIAC)
http://cdiac.ornl.gov/epubs/ndp/ushcn/ushcn.html
The US Department of Energy's primary climate change data and information analysis center, which hosts recent versions of several climate change-related datasets including the USHCN dataset. The website has a simple interface for downloading data by site.

Natural Resources Conservation Service (NRCS) Snow Telemetry (SNOTEL) and Snow Course Data
http://www.wcc.nrcs.usda.gov/snow/

A network of high-elevation automated SNOTEL stations and manually-measured snow courses in the Western US that measures snowpack and related meteorological variables.

US Geological Survey (USGS) National Water Information System (NWIS)
http://waterdata.usgs.gov/or/nwis/rt
A web interface to access current water data for a network of stream gages.

Oregon Water Resources Department Historical Streamflow & Lake Level Data
http://apps.wrd.state.or.us/apps/sw/hydro_report/
A website that hosts the USGS streamflow and lake level data and provides a simple interface to download data by basin and station.

Integrated Scenarios of the Future Northwest Environment
http://climate.nkn.uidaho.edu/IntegratedScenarios/index.php
A project involving Oregon State University, University of Washington, and University of Idaho that produced a coordinated set of climate, hydrology, and vegetation future scenarios for the Northwest US based on the latest generation of global climate models.

Columbia Basin Climate Change Scenarios Project (CBCCSP)
http://warm.atmos.washington.edu/2860/
University of Washington project that developed hydrologic climate change scenarios for the Columbia River basin based on the previous generation of global climate models.

Appendix C. Temperature Projections

Figure C1. Annual and seasonal mean change from simulated historical (1970-1999) to future (2030-2059) basin-averaged, 30-year mean, maximum temperature for the Middle Fork Willamette (17090001). Box and whiskers display the 5th, 25th, mean, 75th, 95th percentiles.

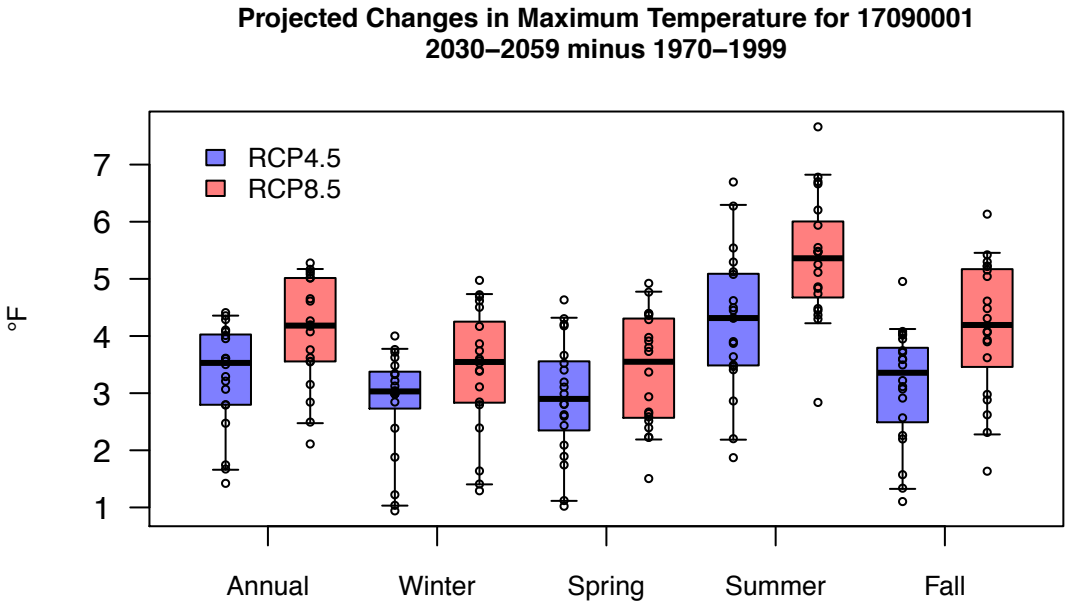

Figure C2. Annual and seasonal mean change from simulated historical (1970-1999) to future (2030-2059) basin-averaged, 30-year mean, minimum temperature for the Middle Fork Willamette (17090001). Box and whiskers display the 5th, 25th, mean, 75th, 95th percentiles.

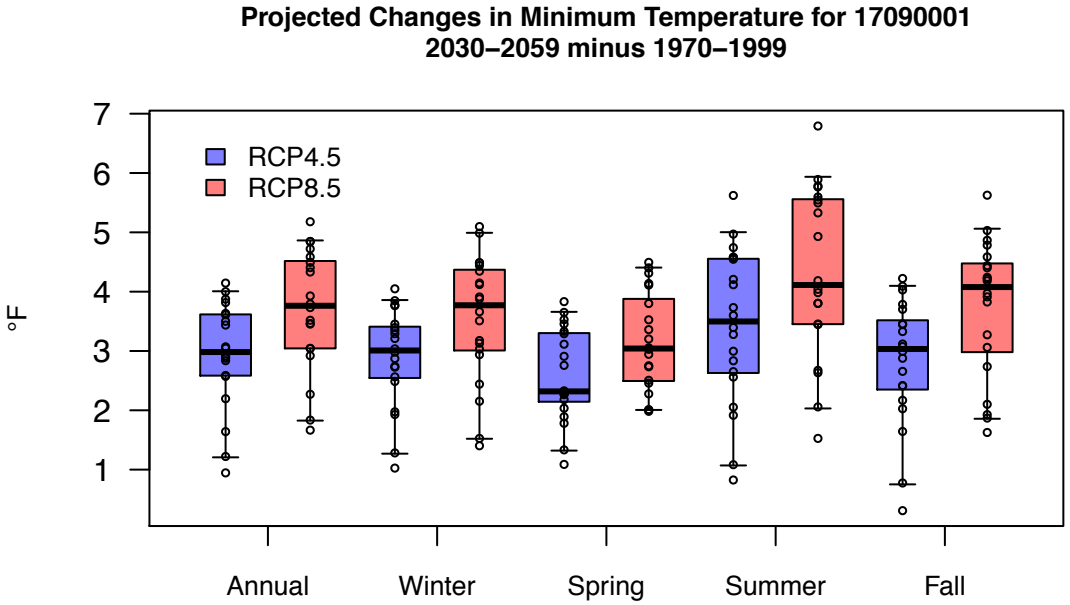

Figure C3. Annual and seasonal mean change from simulated historical (1970-1999) to future (2030-2059) basin-averaged, 30-year mean, maximum temperature for the Coast Fork Willamette (17090002). Box and whiskers display the 5th, 25th, mean, 75th, 95th percentiles.

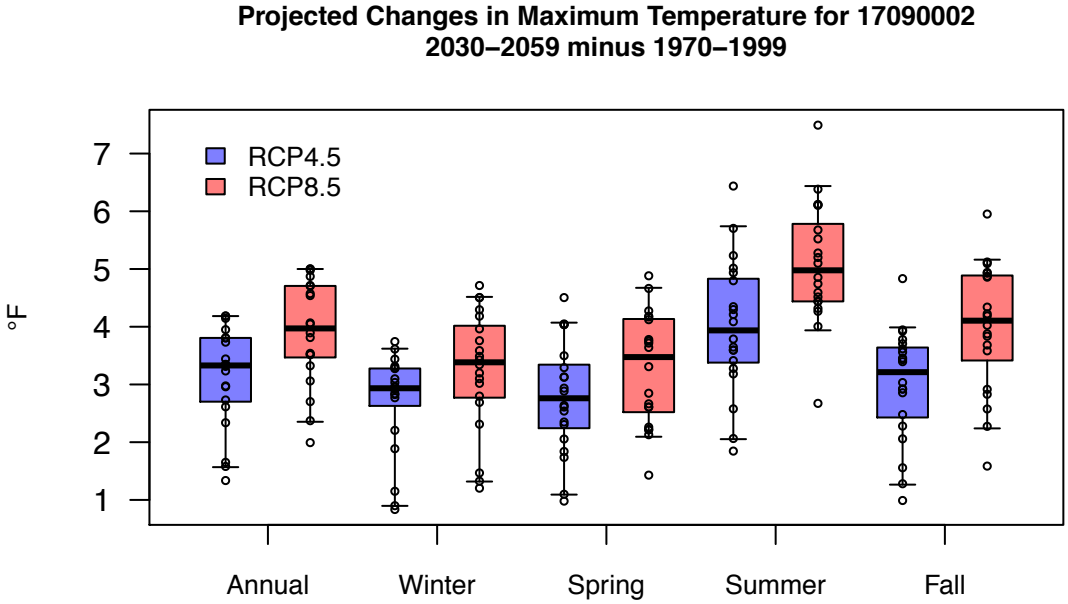

Figure C4. Annual and seasonal mean change from simulated historical (1970-1999) to future (2030-2059) basin-averaged, 30-year mean, minimum temperature for the Coast Fork Willamette (17090002). Box and whiskers display the 5th, 25th, mean, 75th, 95th percentiles.

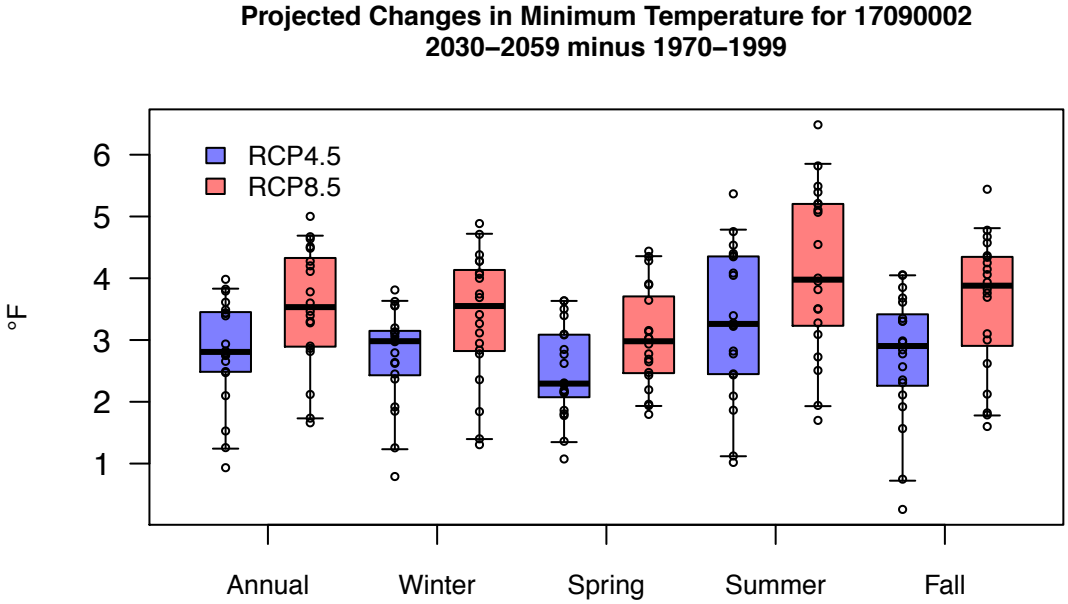

Figure C5. Annual and seasonal mean change from simulated historical (1970-1999) to future (2030-2059) basin-averaged, 30-year mean, maximum temperature for the Upper Willamette (17090003). Box and whiskers display the 5th, 25th, mean, 75th, 95th percentiles.

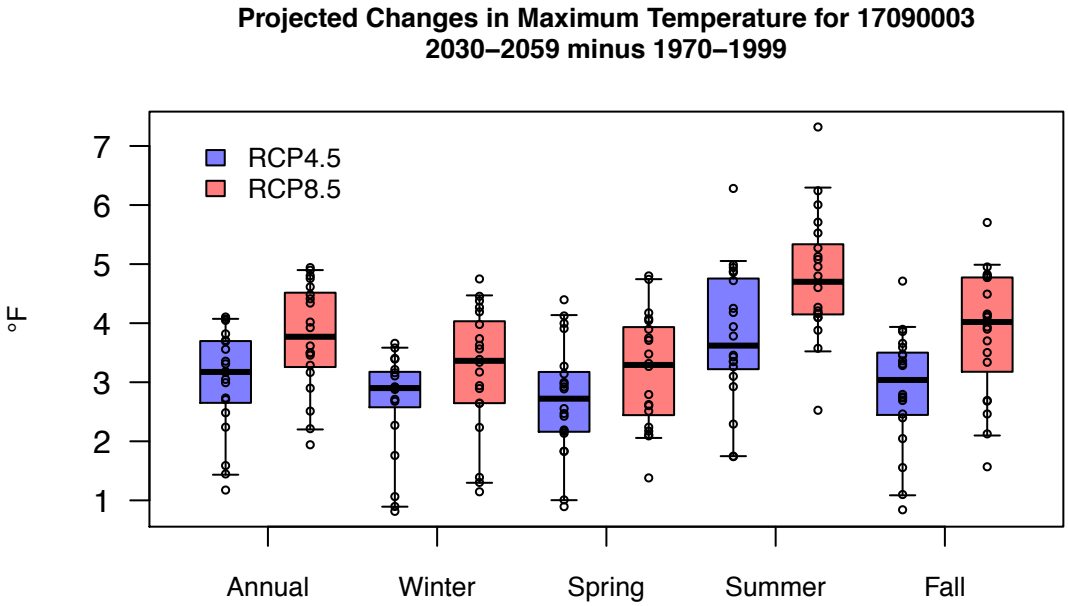

Figure C6. Annual and seasonal mean change from simulated historical (1970-1999) to future (2030-2059) basin-averaged, 30-year mean, minimum temperature for the Upper Willamette (17090003). Box and whiskers display the 5th, 25th, mean, 75th, 95th percentiles.

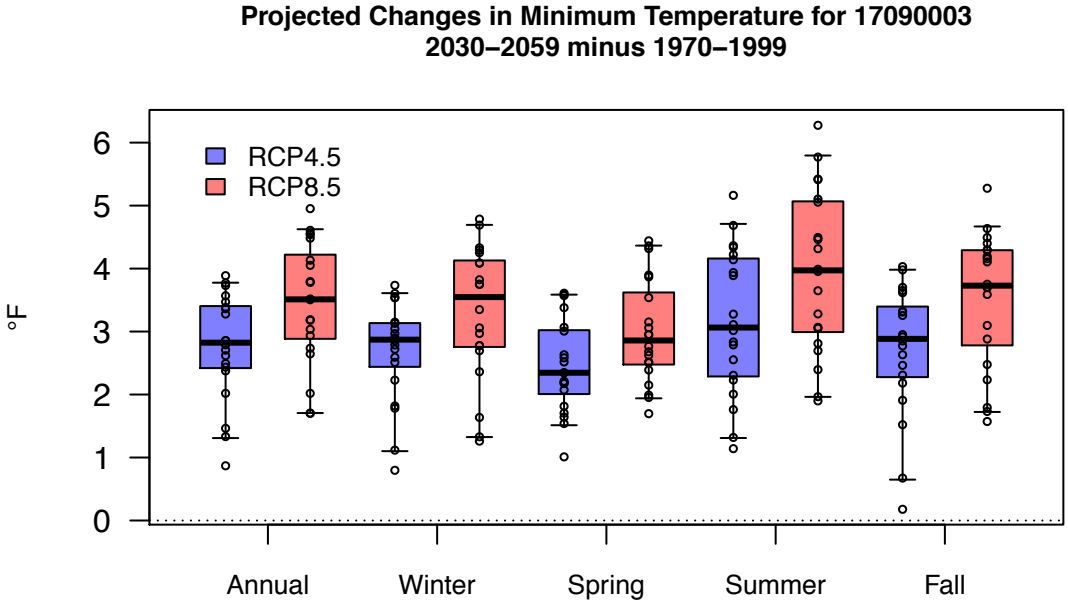

Figure C7. Annual and seasonal mean change from simulated historical (1970-1999) to future (2030-2059) basin-averaged, 30-year mean, maximum temperature for the McKenzie (17090004). Box and whiskers display the 5th, 25th, mean, 75th, 95th percentiles.

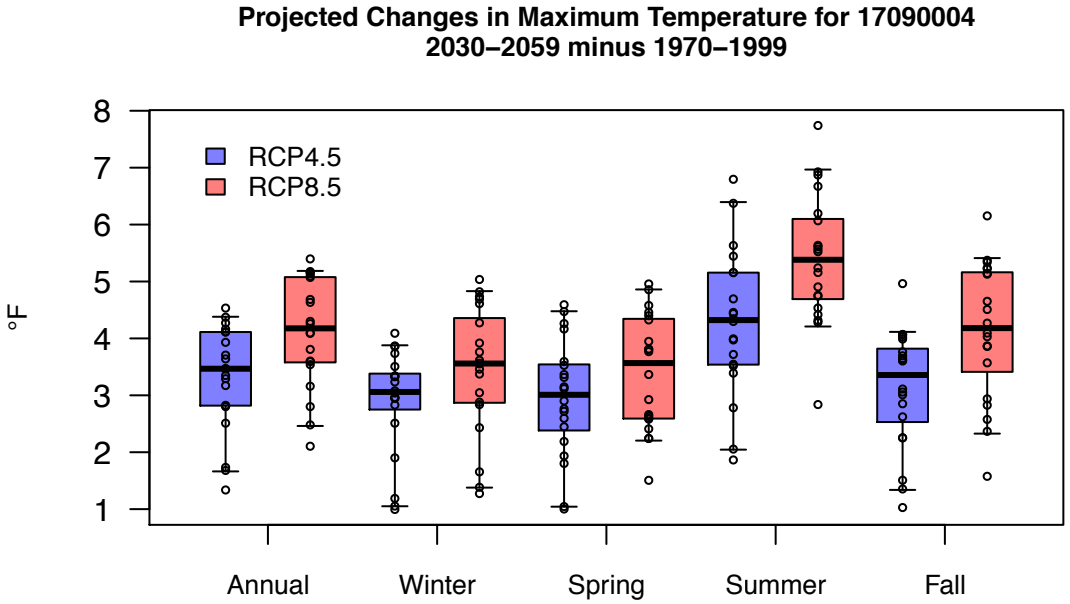

Figure C8. Annual and seasonal mean change from simulated historical (1970-1999) to future (2030-2059) basin-averaged, 30-year mean, minimum temperature for the McKenzie (17090004). Box and whiskers display the 5th, 25th, mean, 75th, 95th percentiles.

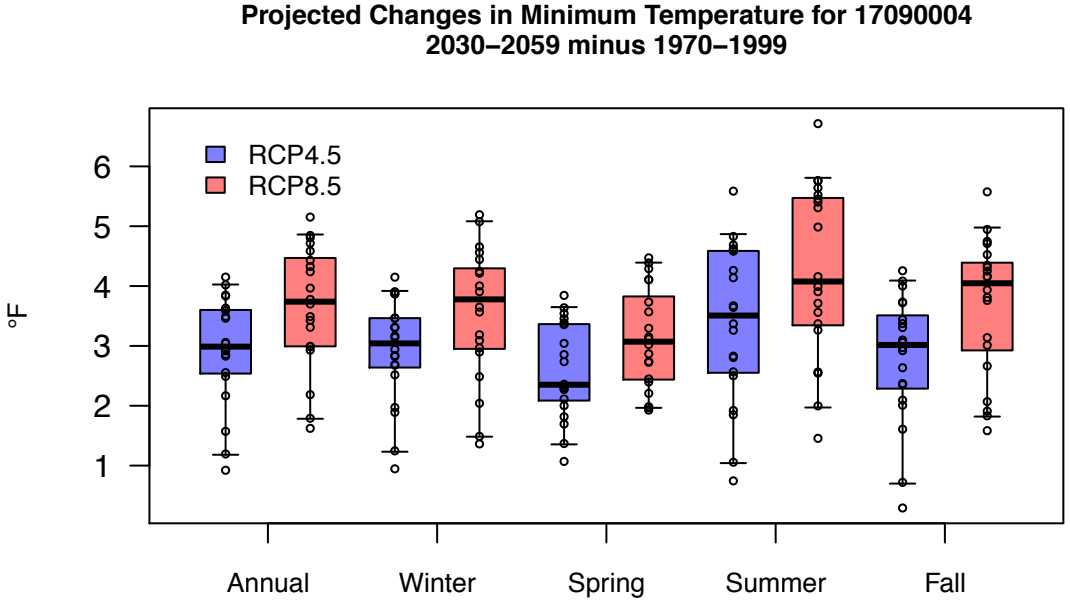

Figure C9. Annual and seasonal mean change from simulated historical (1970-1999) to future (2030-2059) basin-averaged, 30-year mean, maximum temperature for the North Santiam (17090005). Box and whiskers display the 5th, 25th, mean, 75th, 95th percentiles.

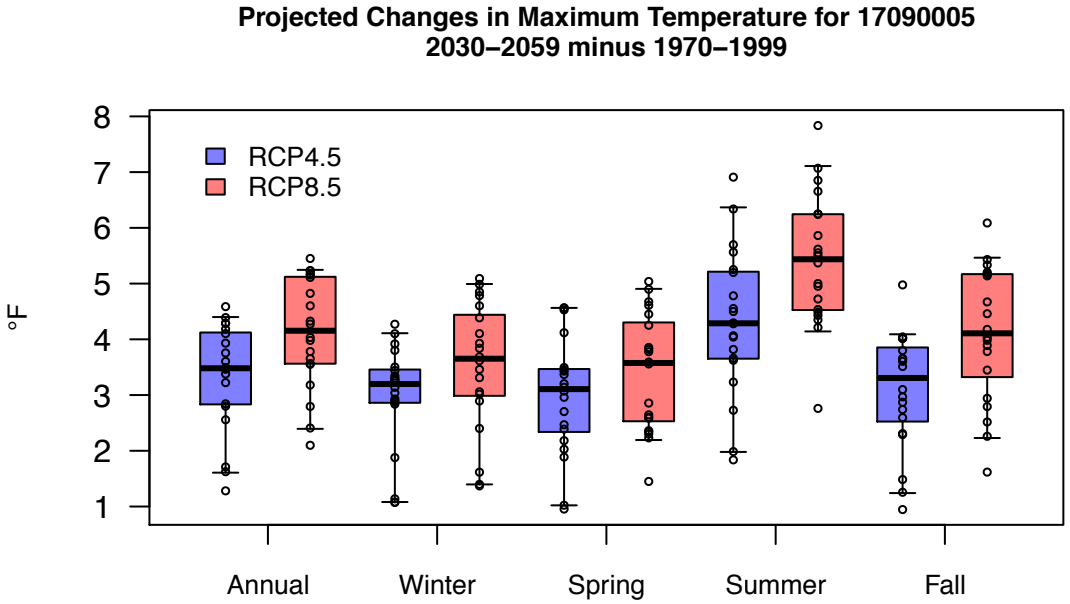

Figure C10. Annual and seasonal mean change from simulated historical (1970-1999) to future (2030-2059) basin-averaged, 30-year mean, minimum temperature for the North Santiam (17090005). Box and whiskers display the 5th, 25th, mean, 75th, 95th percentiles.

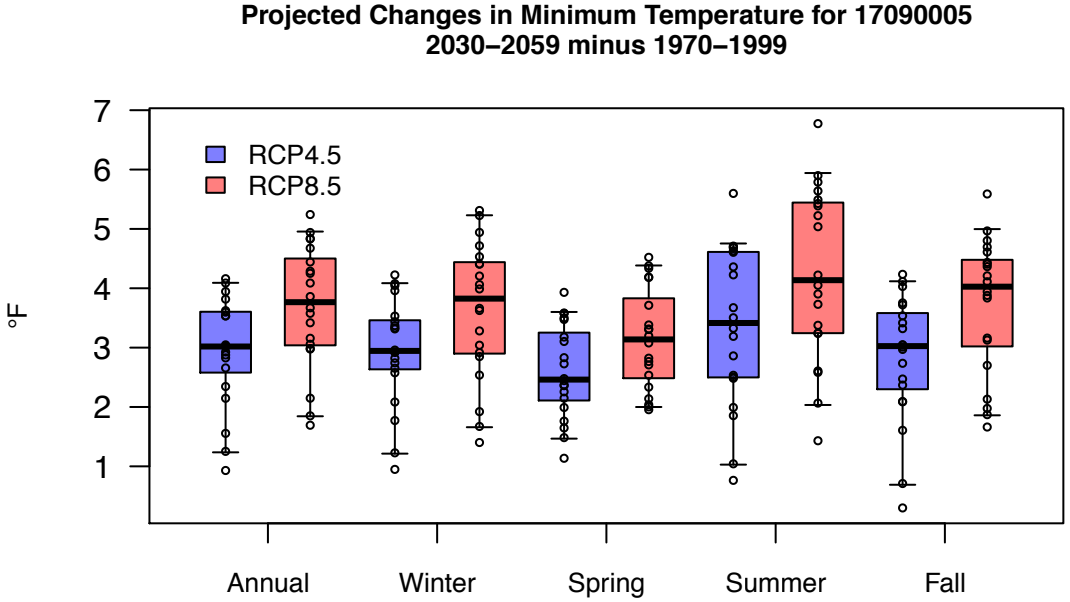

Figure C11. Annual and seasonal mean change from simulated historical (1970-1999) to future (2030-2059) basin-averaged, 30-year mean, maximum temperature for the South Santiam (17090006). Box and whiskers display the 5th, 25th, mean, 75th, 95th percentiles.

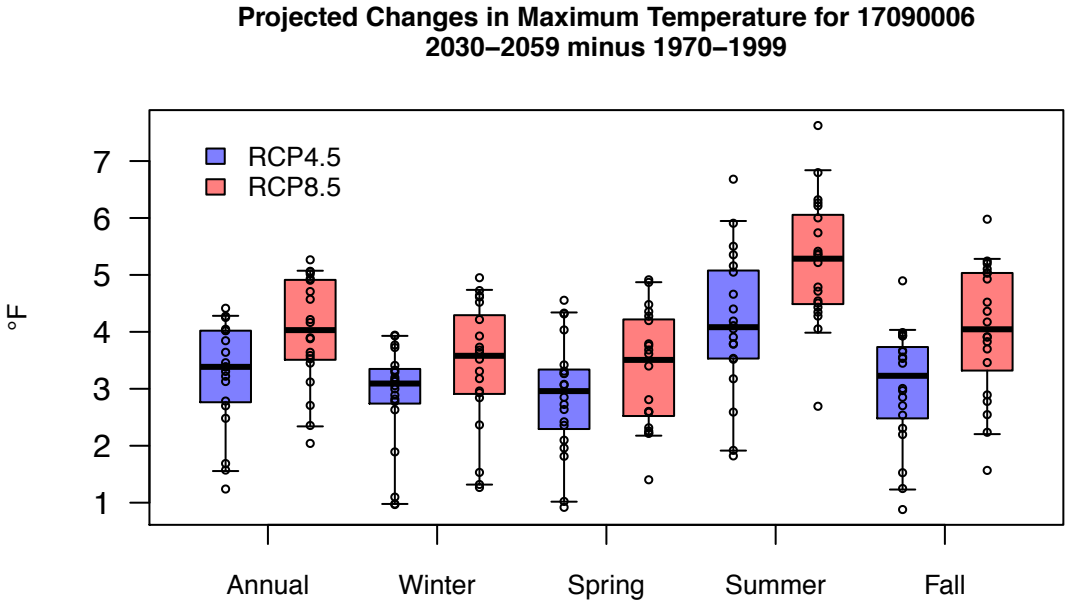

Figure C12. Annual and seasonal mean change from simulated historical (1970-1999) to future (2030-2059) basin-averaged, 30-year mean, minimum temperature for the South Santiam (17090006). Box and whiskers display the 5th, 25th, mean, 75th, 95th percentiles.

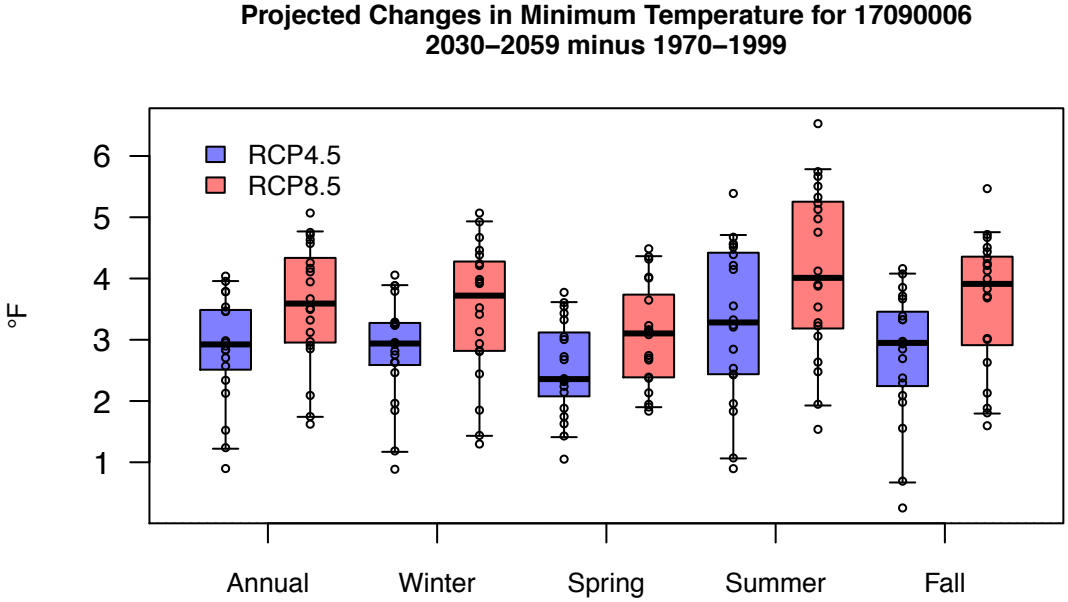

Figure C13. Annual and seasonal mean change from simulated historical (1970-1999) to future (2030-2059) basin-averaged, 30-year mean, maximum temperature for the Middle Willamette (17090007). Box and whiskers display the 5th, 25th, mean, 75th, 95th percentiles.

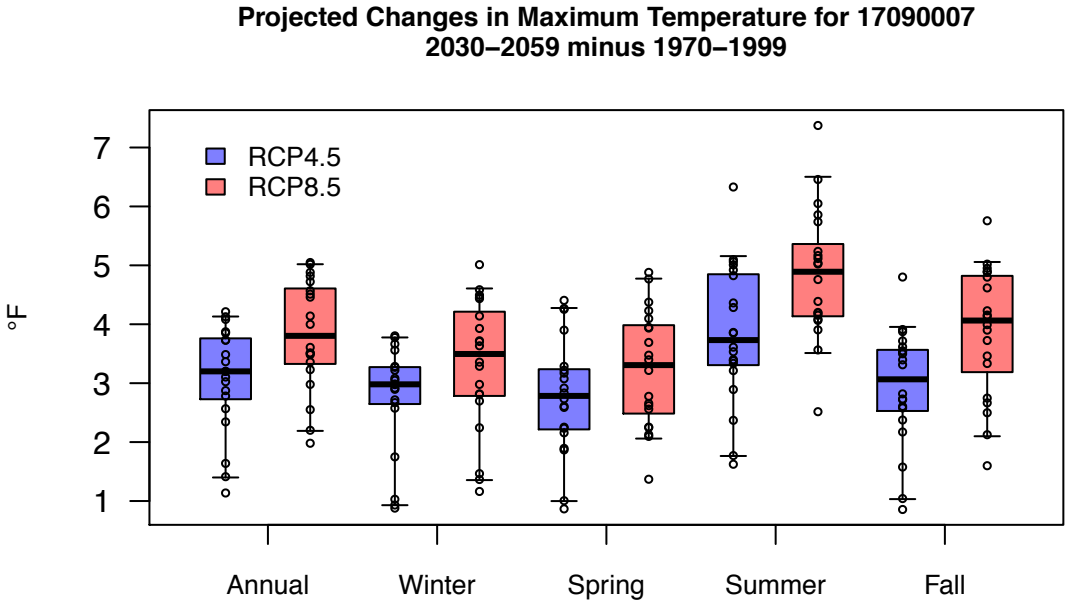

Figure C14. Annual and seasonal mean change from simulated historical (1970-1999) to future (2030-2059) basin-averaged, 30-year mean, minimum temperature for the Middle Willamette (17090007). Box and whiskers display the 5th, 25th, mean, 75th, 95th percentiles.

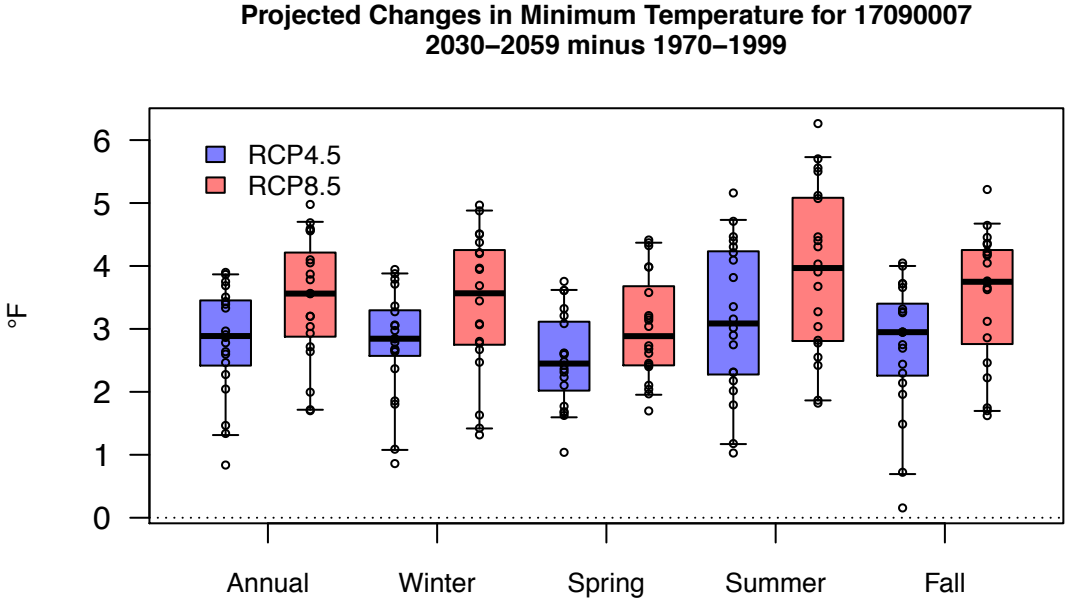

Figure C15. Annual and seasonal mean change from simulated historical (1970-1999) to future (2030-2059) basin-averaged, 30-year mean, maximum temperature for the Yamhill (17090008). Box and whiskers display the 5th, 25th, mean, 75th, 95th percentiles.

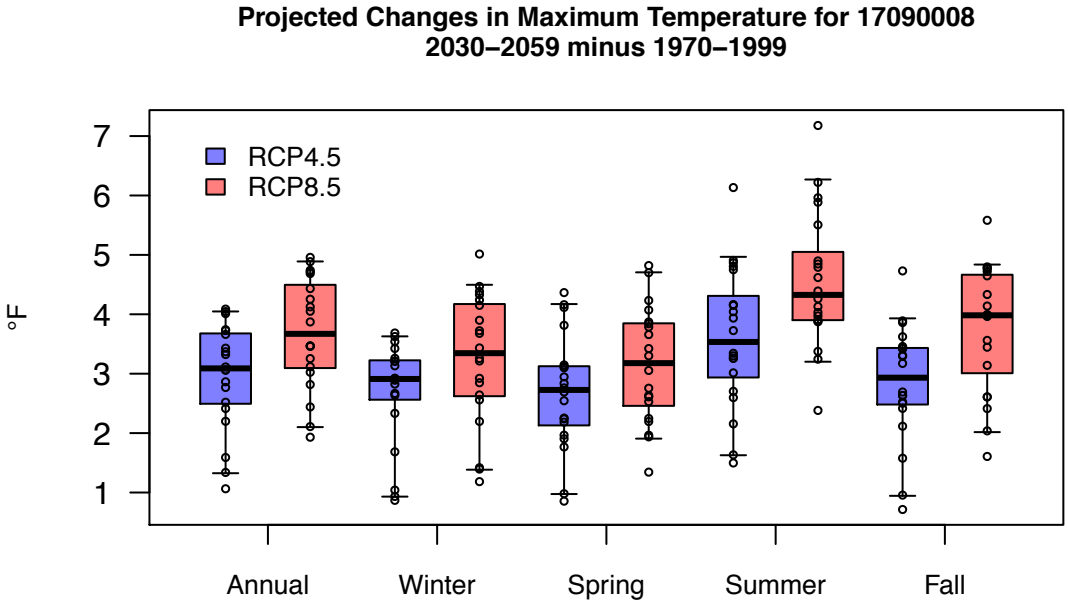

Figure C16. Annual and seasonal mean change from simulated historical (1970-1999) to future (2030-2059) basin-averaged, 30-year mean, minimum temperature for the Yamhill (17090008). Box and whiskers display the 5th, 25th, mean, 75th, 95th percentiles.

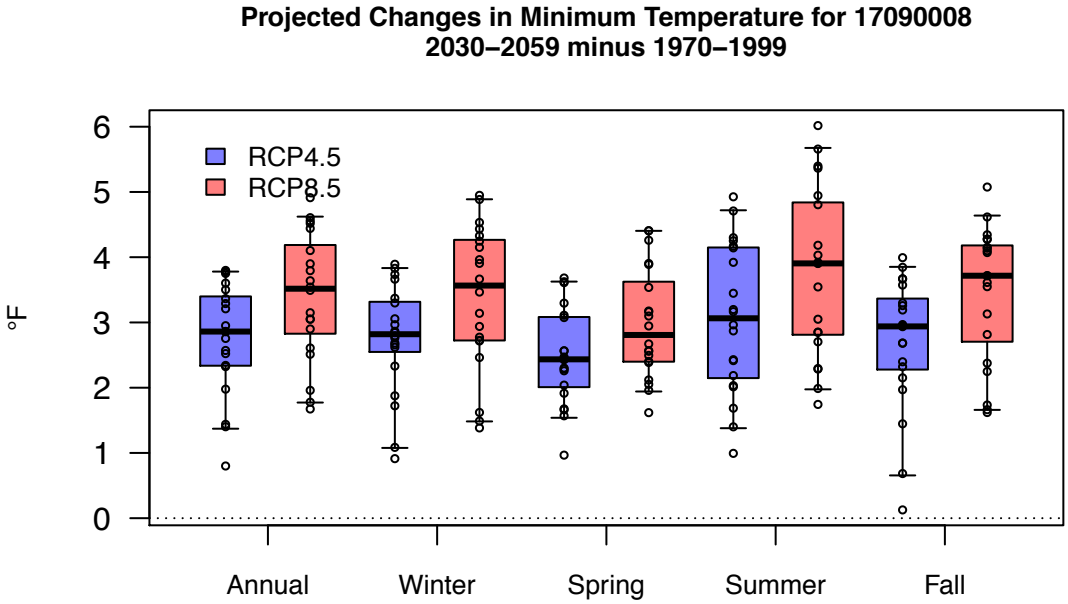

Figure C17. Annual and seasonal mean change from simulated historical (1970-1999) to future (2030-2059) basin-averaged, 30-year mean, maximum temperature for the Molalla-Pudding (17090009). Box and whiskers display the 5th, 25th, mean, 75th, 95th percentiles.

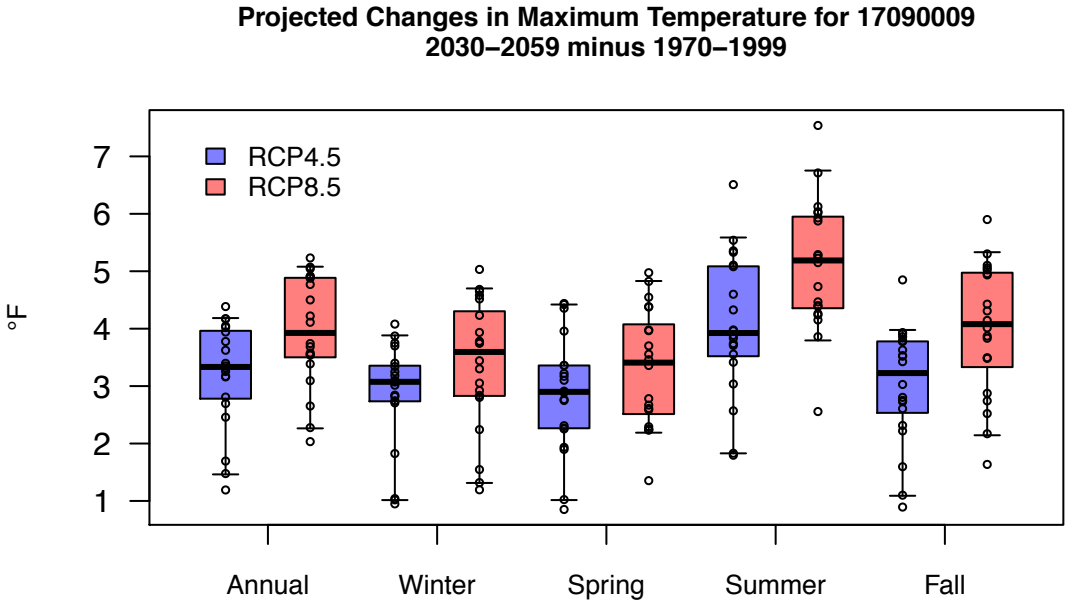

Figure C18. Annual and seasonal mean change from simulated historical (1970-1999) to future (2030-2059) basin-averaged, 30-year mean, minimum temperature for the Molalla-Pudding (17090009). Box and whiskers display the 5th, 25th, mean, 75th, 95th percentiles.

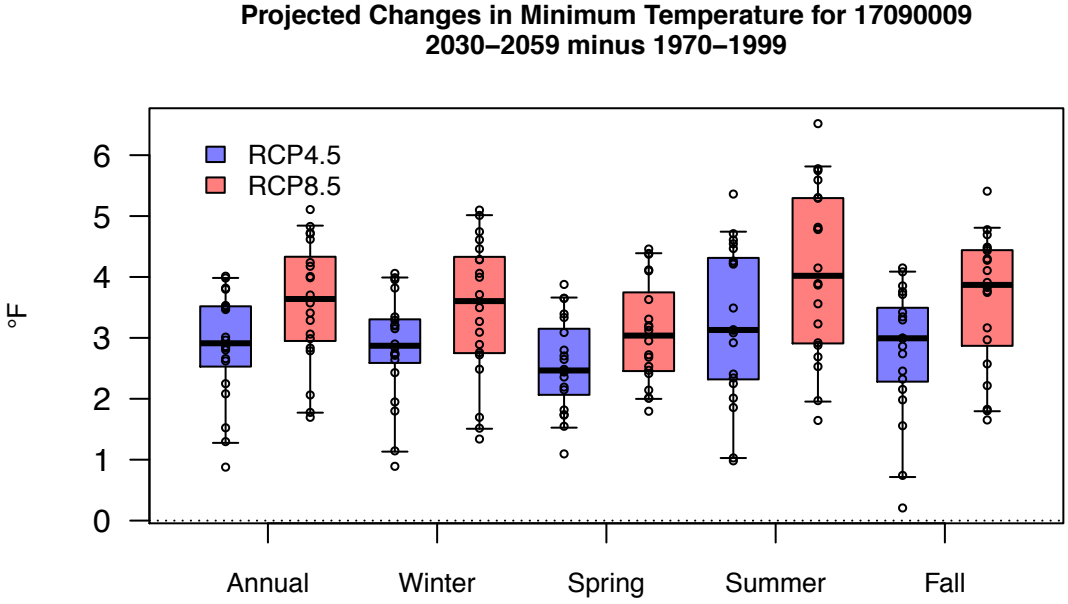

Figure C19. Annual and seasonal mean change from simulated historical (1970-1999) to future (2030-2059) basin-averaged, 30-year mean, maximum temperature for the Tualatin (17090010). Box and whiskers display the 5th, 25th, mean, 75th, 95th percentiles.

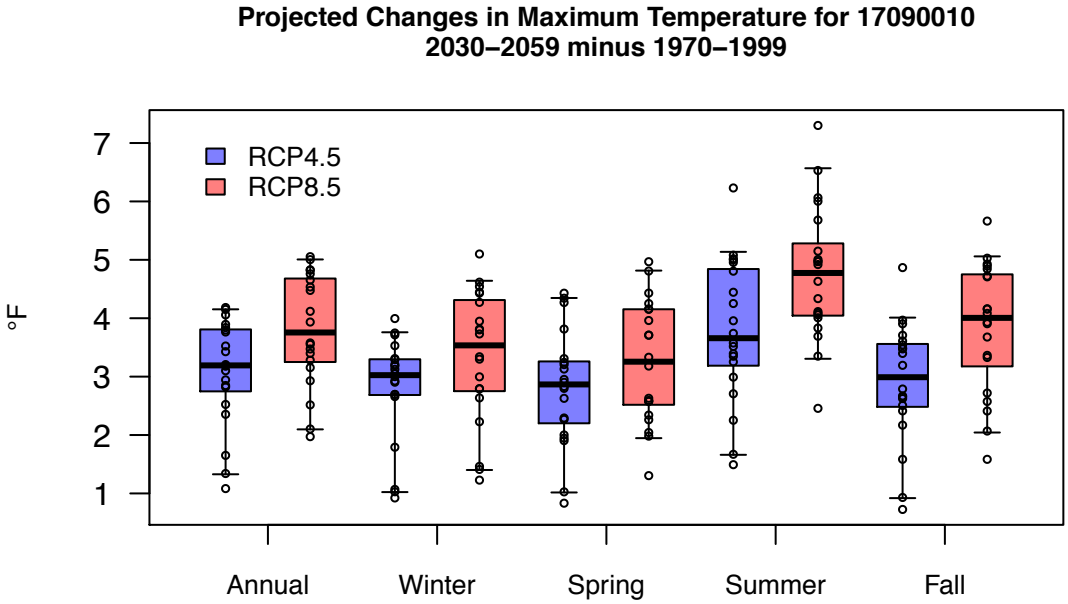

Figure C20. Annual and seasonal mean change from simulated historical (1970-1999) to future (2030-2059) basin-averaged, 30-year mean, minimum temperature for the Tualatin (17090010). Box and whiskers display the 5th, 25th, mean, 75th, 95th percentiles.

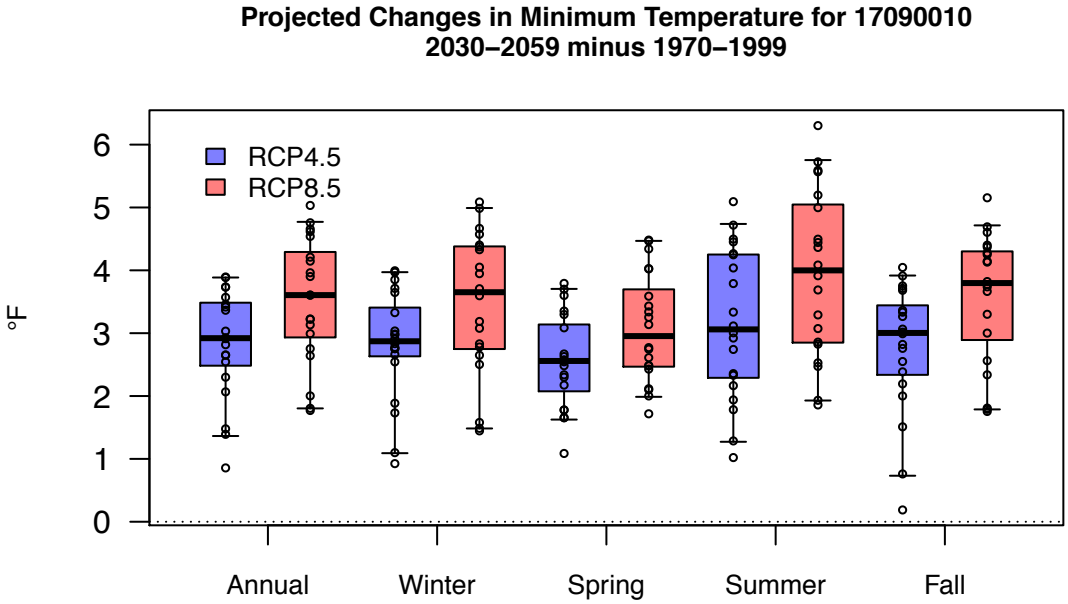

Figure C21. Annual and seasonal mean change from simulated historical (1970-1999) to future (2030-2059) basin-averaged, 30-year mean, maximum temperature for the Clackamas (17090011). Box and whiskers display the 5th, 25th, mean, 75th, 95th percentiles.

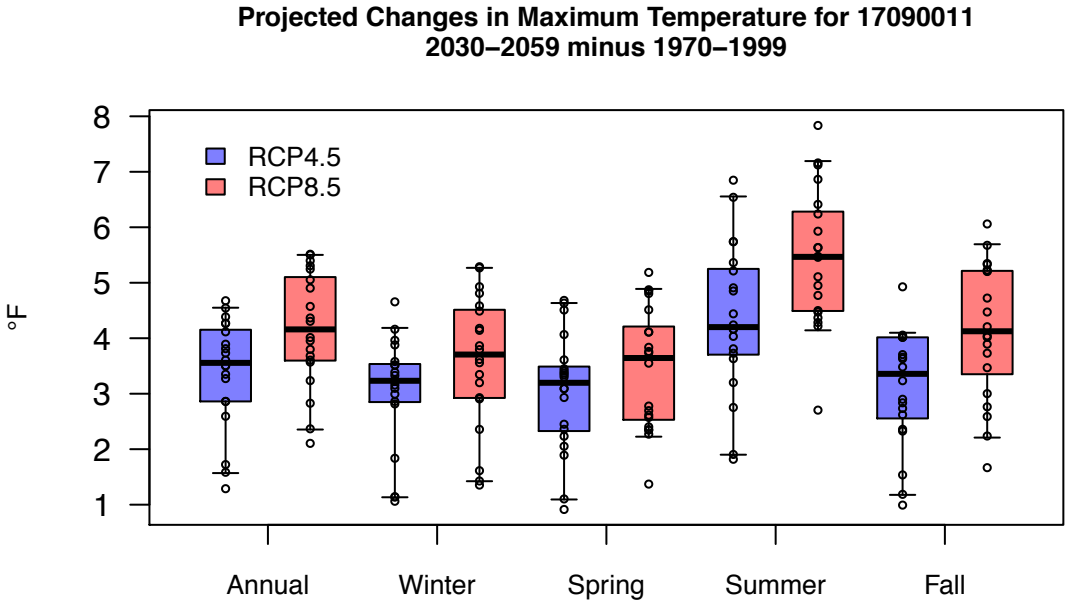

Figure C22. Annual and seasonal mean change from simulated historical (1970-1999) to future (2030-2059) basin-averaged, 30-year mean, minimum temperature for the Clackamas (17090011). Box and whiskers display the 5th, 25th, mean, 75th, 95th percentiles.

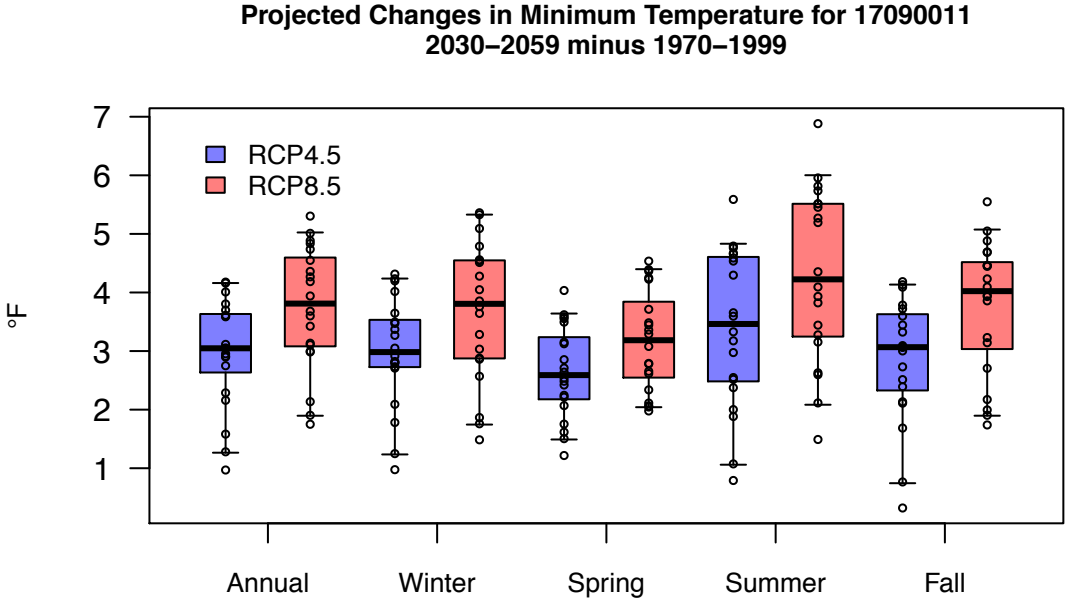

Figure C23. Annual and seasonal mean change from simulated historical (1970-1999) to future (2030-2059) basin-averaged, 30-year mean, maximum temperature for the Lower Willamette (17090012). Box and whiskers display the 5th, 25th, mean, 75th, 95th percentiles.

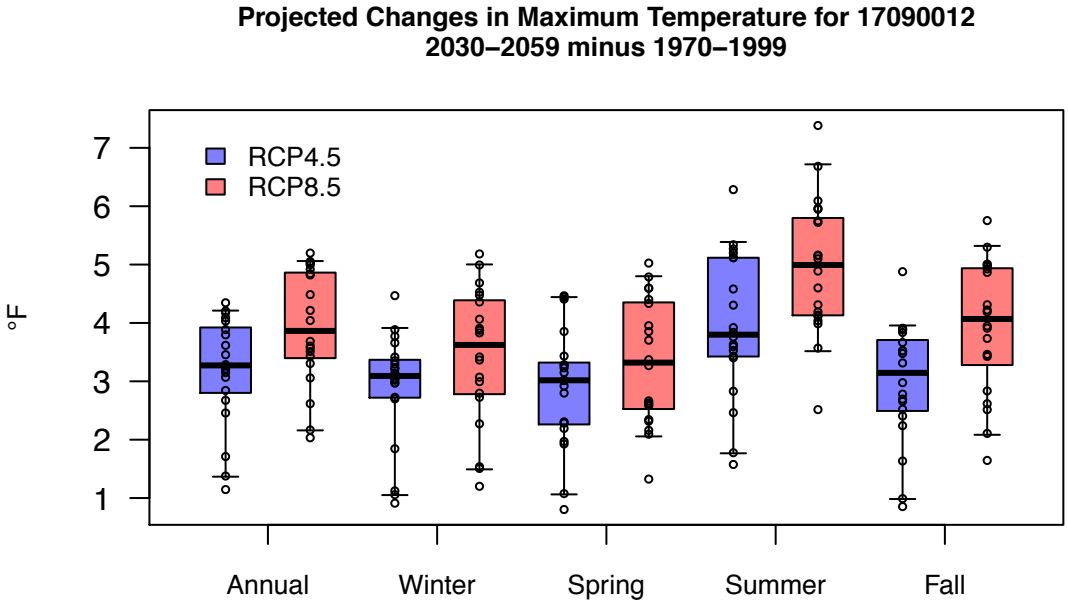

Figure C24. Annual and seasonal mean change from simulated historical (1970-1999) to future (2030-2059) basin-averaged, 30-year mean, minimum temperature for the Lower Willamette (17090012). Box and whiskers display the 5th, 25th, mean, 75th, 95th percentiles.

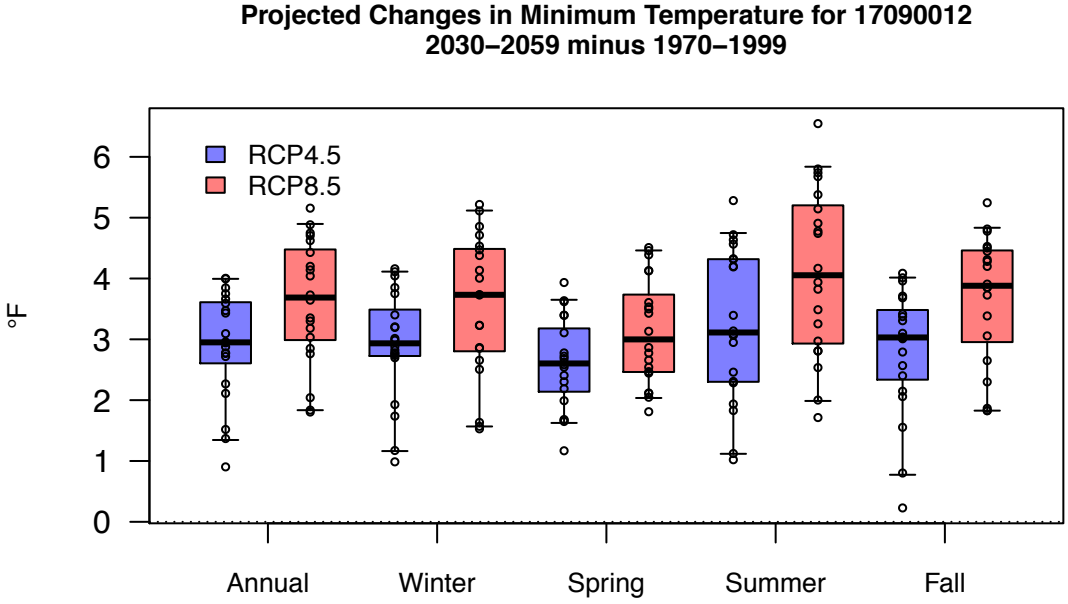

Figure C25. Annual and seasonal mean change from simulated historical (1970-1999) to future (2030-2059) basin-averaged, 30-year mean, maximum temperature for the Upper Rogue (17100307). Box and whiskers display the 5th, 25th, mean, 75th, 95th percentiles.

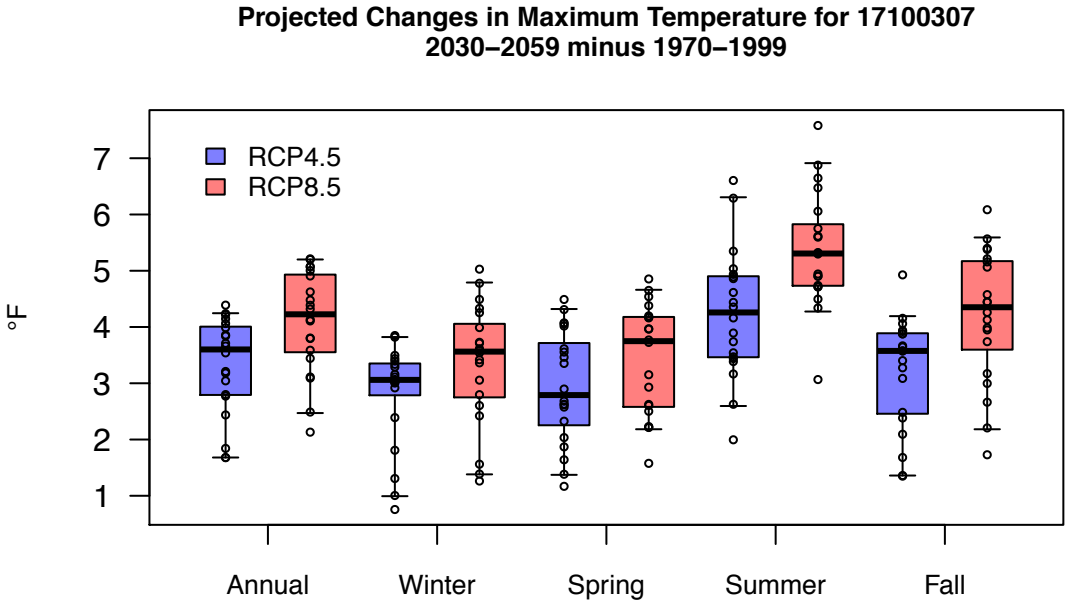

Figure C26. Annual and seasonal mean change from simulated historical (1970-1999) to future (2030-2059) basin-averaged, 30-year mean, minimum temperature for the Upper Rogue (17100307). Box and whiskers display the 5th, 25th, mean, 75th, 95th percentiles.

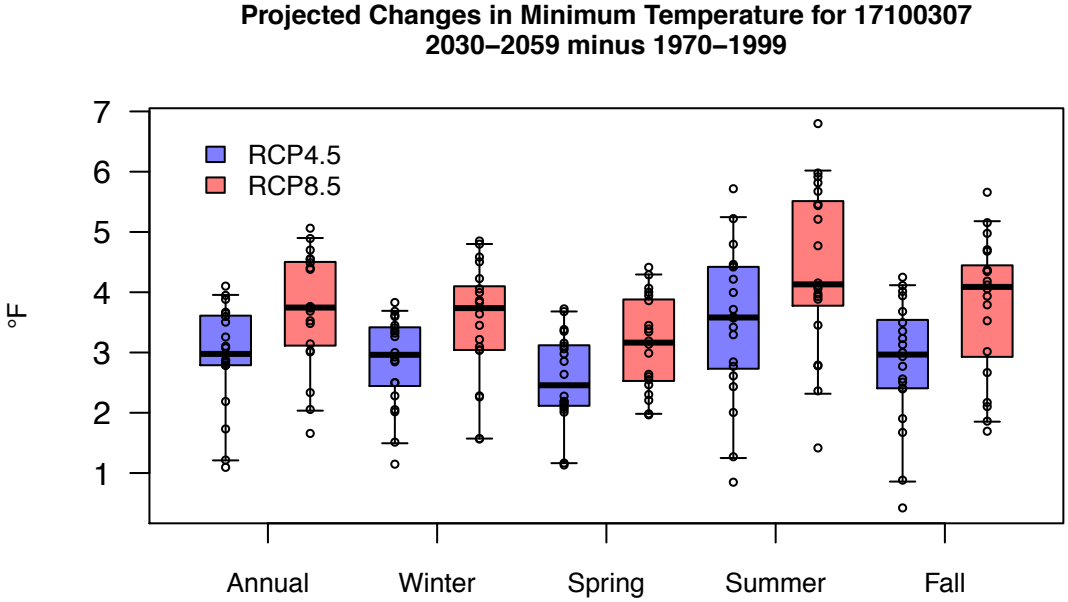

Figure C27. Annual and seasonal mean change from simulated historical (1970-1999) to future (2030-2059) basin-averaged, 30-year mean, maximum temperature for the Middle Rogue (17100308). Box and whiskers display the 5th, 25th, mean, 75th, 95th percentiles.

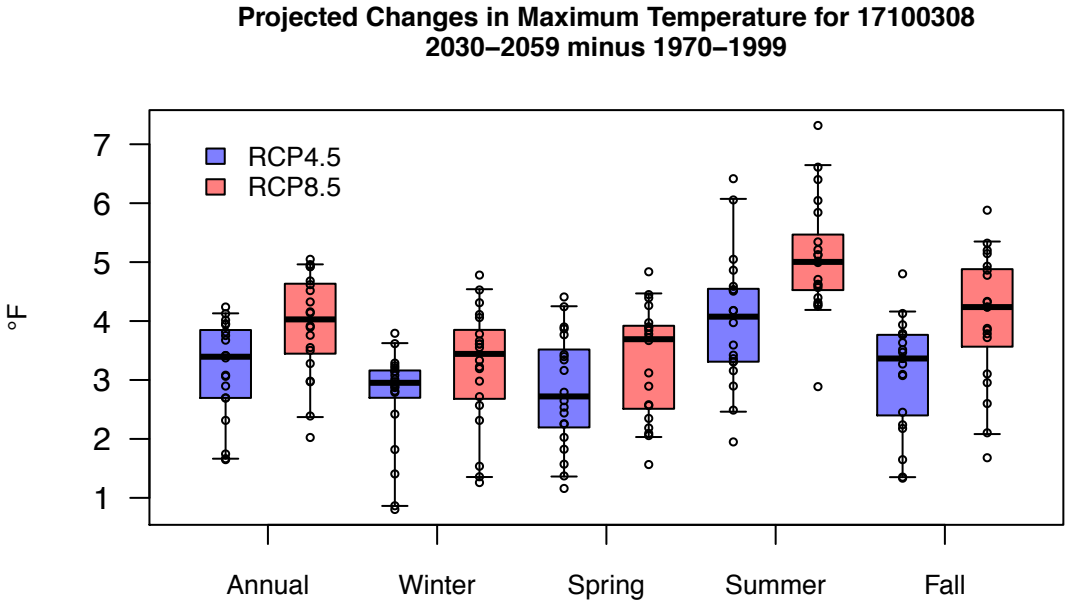

Figure C28. Annual and seasonal mean change from simulated historical (1970-1999) to future (2030-2059) basin-averaged, 30-year mean, minimum temperature for the Middle Rogue (17100308). Box and whiskers display the 5th, 25th, mean, 75th, 95th percentiles.

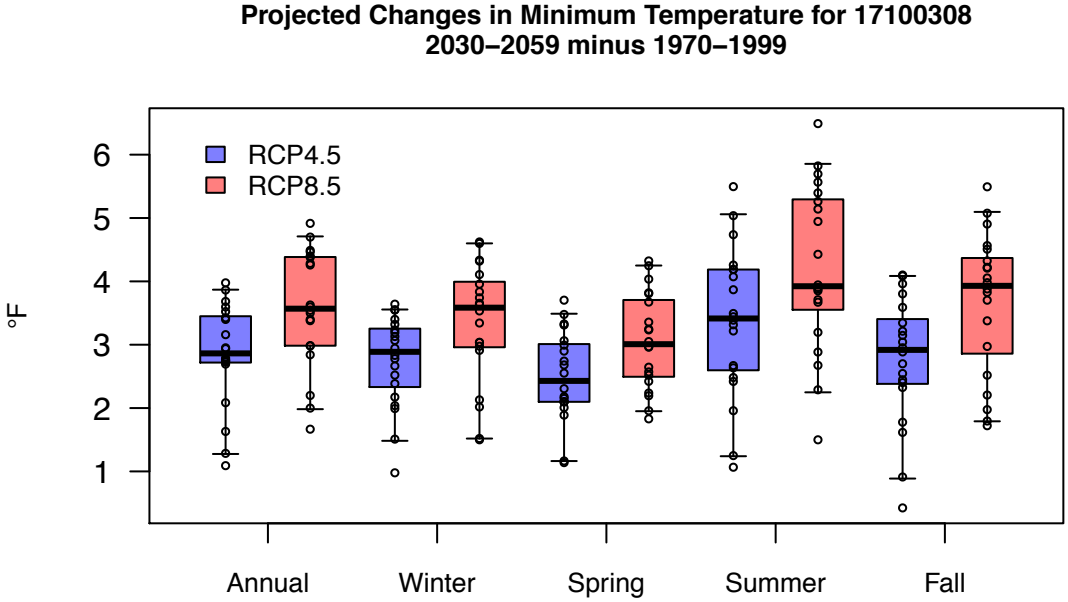

Figure C29. Annual and seasonal mean change from simulated historical (1970-1999) to future (2030-2059) basin-averaged, 30-year mean, maximum temperature for the Applegate (17100309). Box and whiskers display the 5th, 25th, mean, 75th, 95th percentiles.

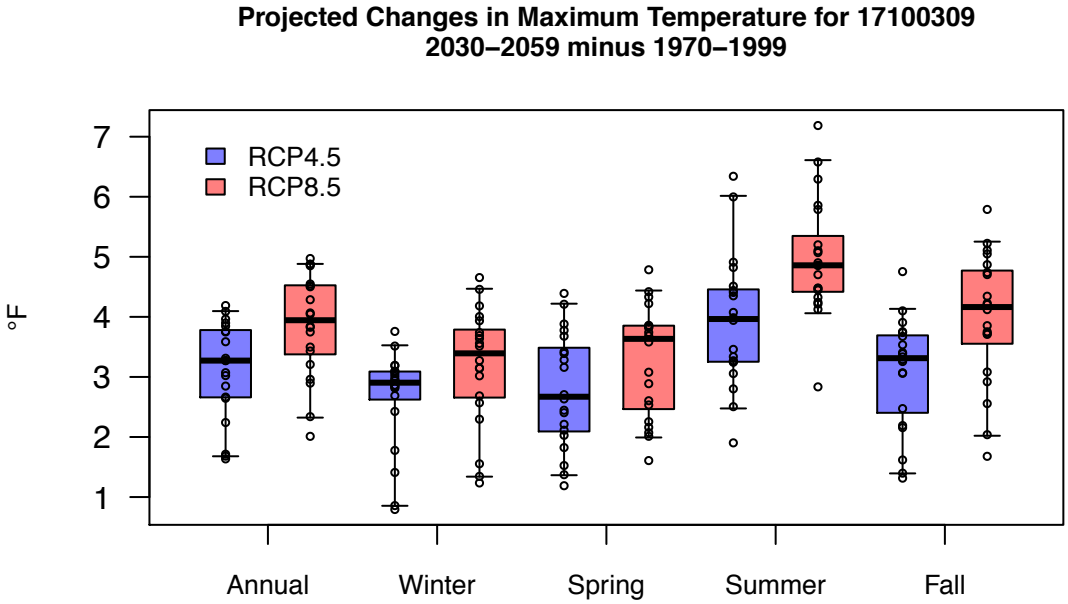

Figure C30. Annual and seasonal mean change from simulated historical (1970-1999) to future (2030-2059) basin-averaged, 30-year mean, minimum temperature for the Applegate (17100309). Box and whiskers display the 5th, 25th, mean, 75th, 95th percentiles.

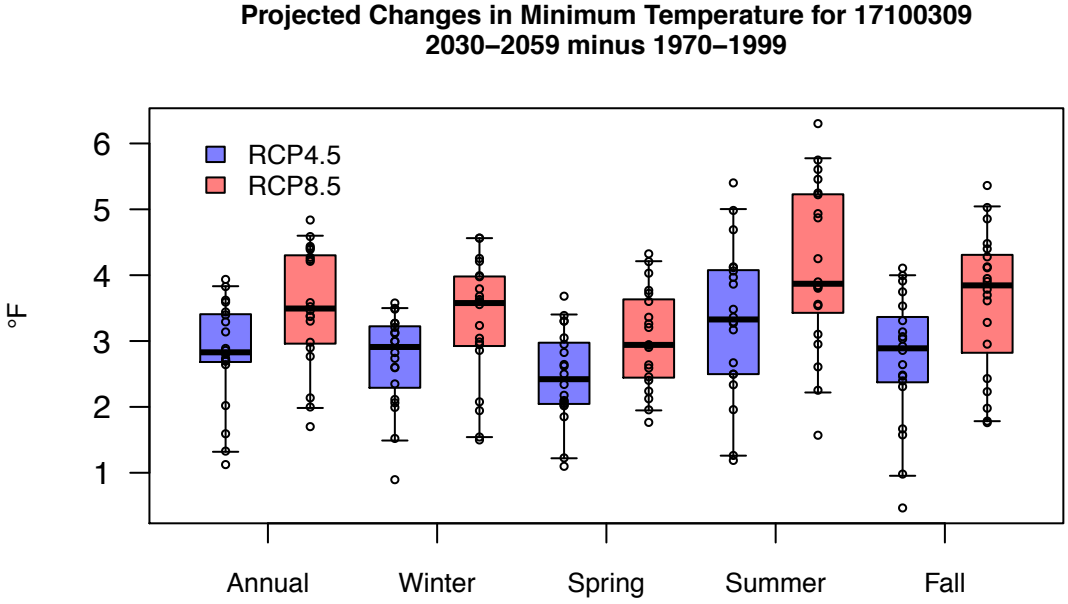

Figure C31. Annual and seasonal mean change from simulated historical (1970-1999) to future (2030-2059) basin-averaged, 30-year mean, maximum temperature for the Lower Rogue (17100310). Box and whiskers display the 5th, 25th, mean, 75th, 95th percentiles.

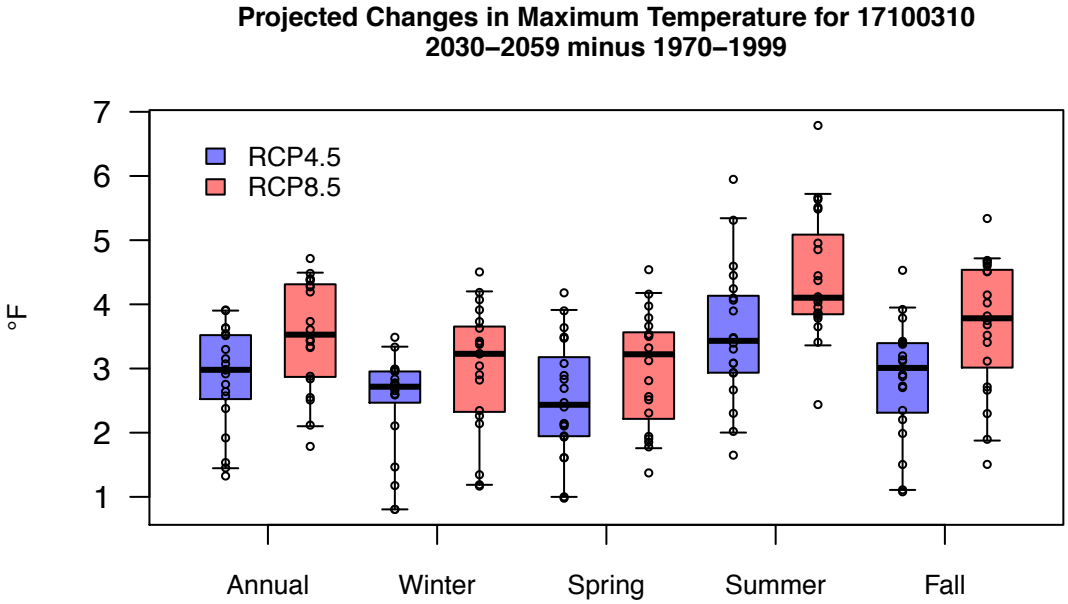

Figure C32. Annual and seasonal mean change from simulated historical (1970-1999) to future (2030-2059) basin-averaged, 30-year mean, minimum temperature for the Lower Rogue (17100310). Box and whiskers display the 5th, 25th, mean, 75th, 95th percentiles.

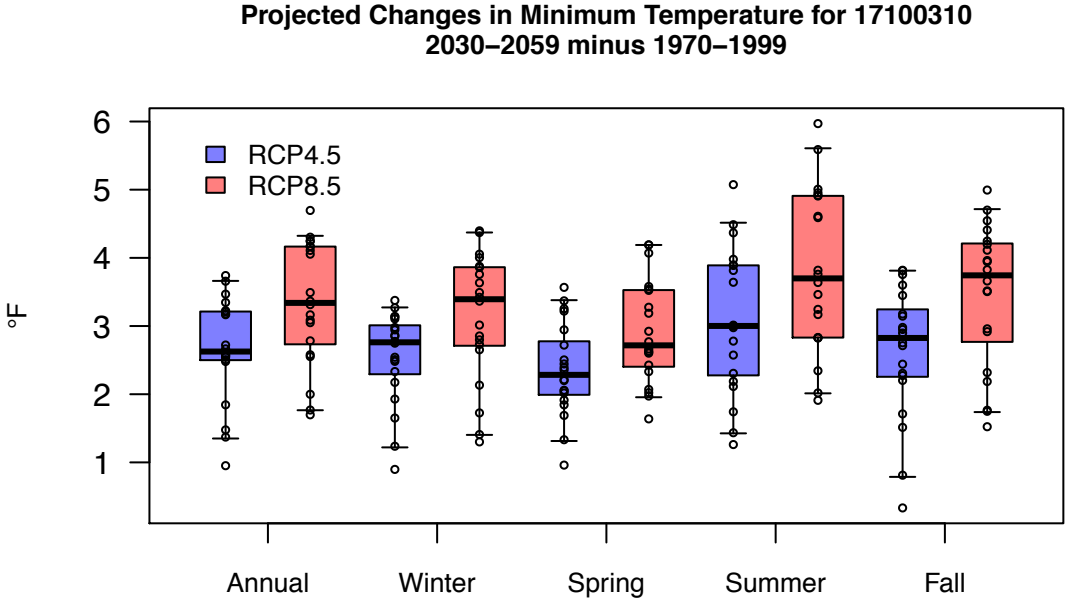

Appendix D. Precipitation Projections

Figure D1. Simulated historic (1970-1999) and future (2030-2059) basin-averaged, 30-year mean, monthly precipitation for the Middle Fork Willamette (17090001). The solid line and shading give the mean and 5th to 95th percentile range, respectively, of simulations from 20 GCMs.

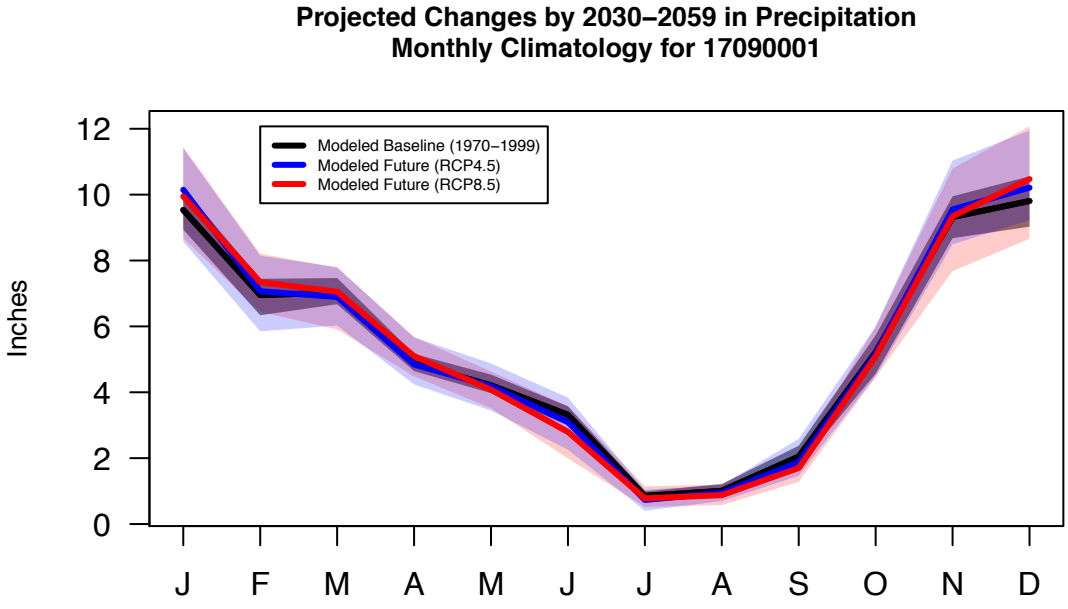

Figure D2. Simulated historic (1970-1999) and future (2030-2059) basin-averaged, 30-year mean, monthly precipitation for the Coast Fork Willamette (17090002). The solid line and shading give the mean and 5th to 95th percentile range, respectively, of simulations from 20 GCMs.

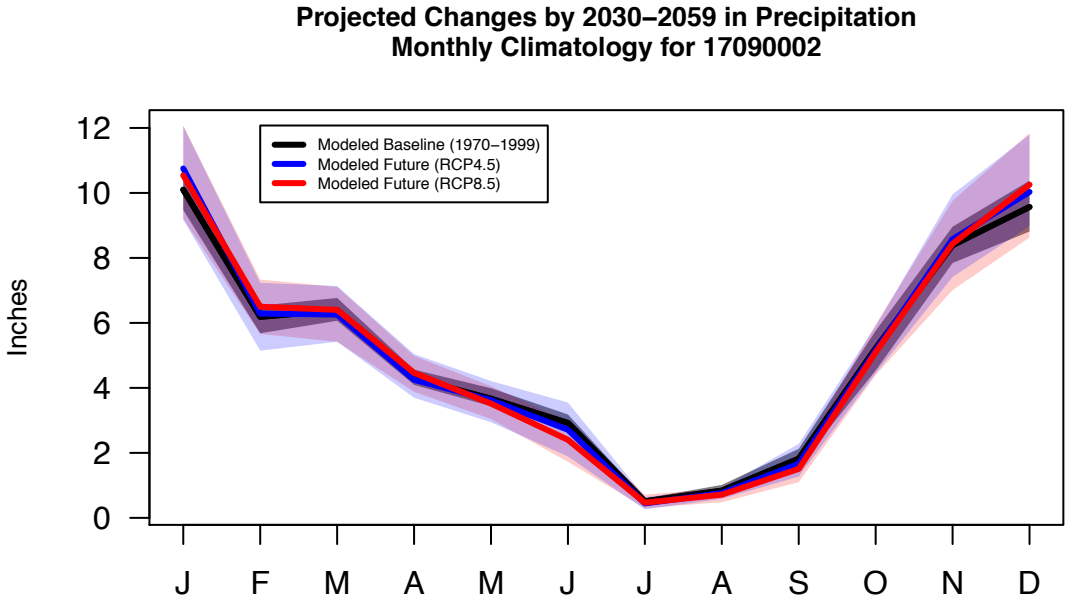

Figure D3. Simulated historic (1970-1999) and future (2030-2059) basin-averaged, 30-year mean, monthly precipitation for the Upper Willamette (17090003). The solid line and shading give the mean and 5th to 95th percentile range, respectively, of simulations from 20 GCMs.

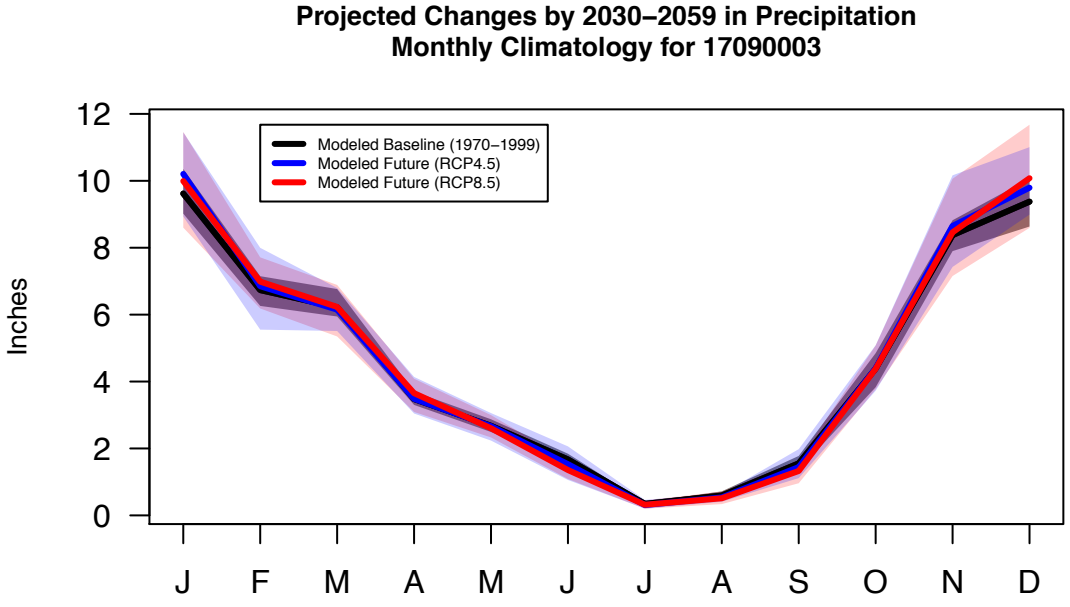

Figure D4. Simulated historic (1970-1999) and future (2030-2059) basin-averaged, 30-year mean, monthly precipitation for the McKenzie (17090004). The solid line and shading give the mean and 5th to 95th percentile range, respectively, of simulations from 20 GCMs.

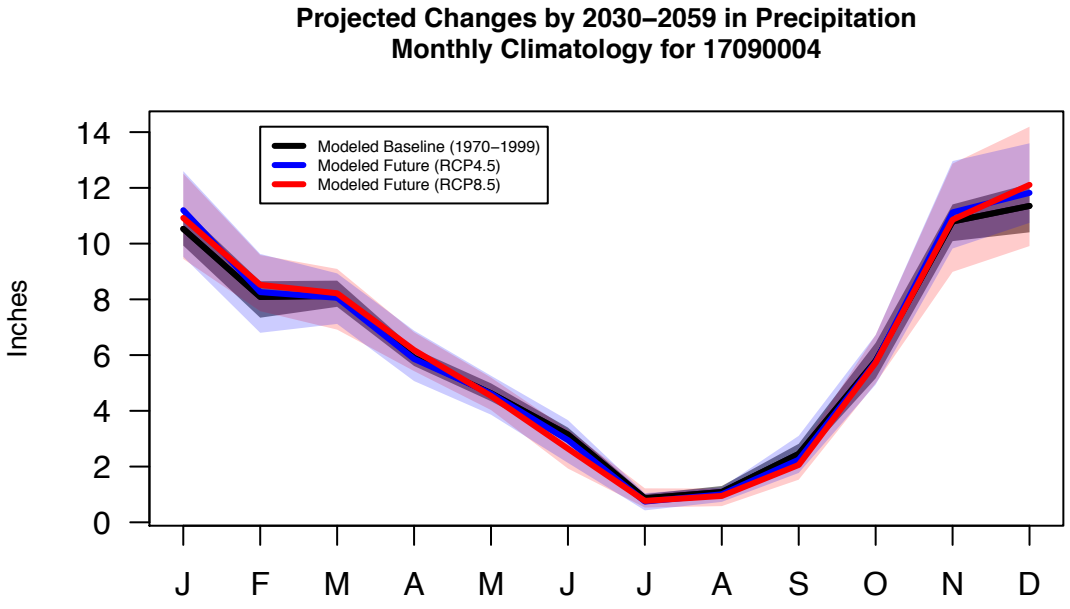

Figure D5. Simulated historic (1970-1999) and future (2030-2059) basin-averaged, 30-year mean, monthly precipitation for the North Santiam (17090005). The solid line and shading give the mean and 5th to 95th percentile range, respectively, of simulations from 20 GCMs.

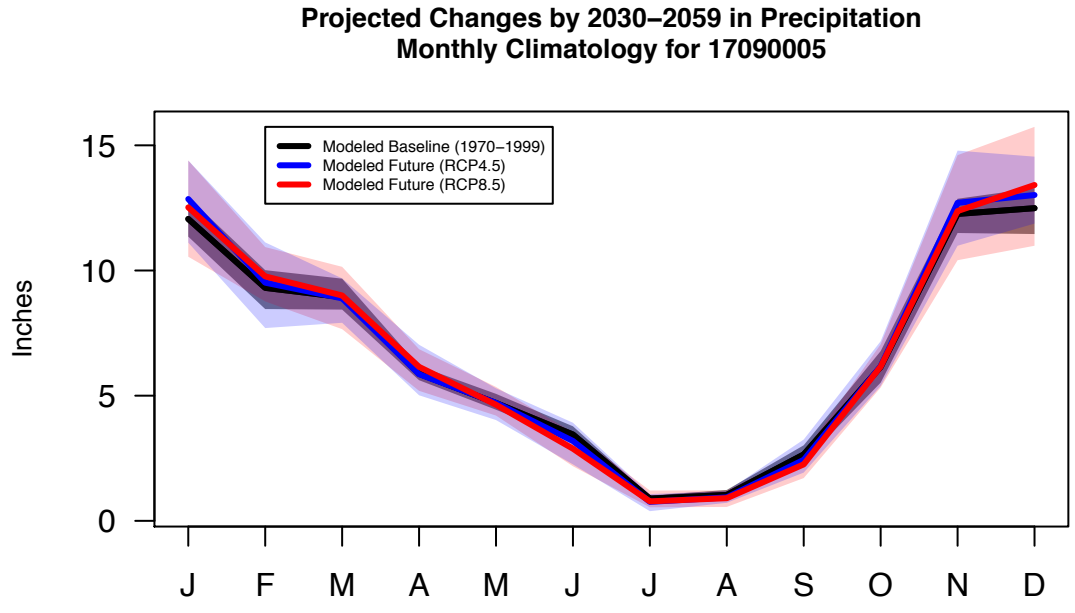

Figure D6. Simulated historic (1970-1999) and future (2030-2059) basin-averaged, 30-year mean, monthly precipitation for the South Santiam (17090006). The solid line and shading give the mean and 5th to 95th percentile range, respectively, of simulations from 20 GCMs.

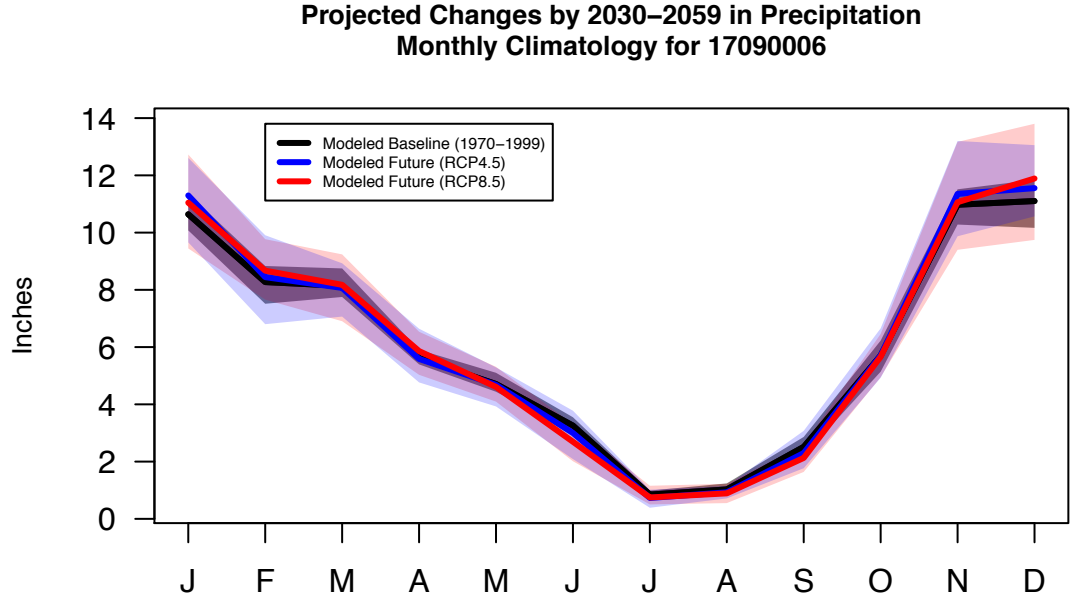

Figure D7. Simulated historic (1970-1999) and future (2030-2059) basin-averaged, 30-year mean, monthly precipitation for the Middle Willamette (17090007). The solid line and shading give the mean and 5th to 95th percentile range, respectively, of simulations from 20 GCMs.

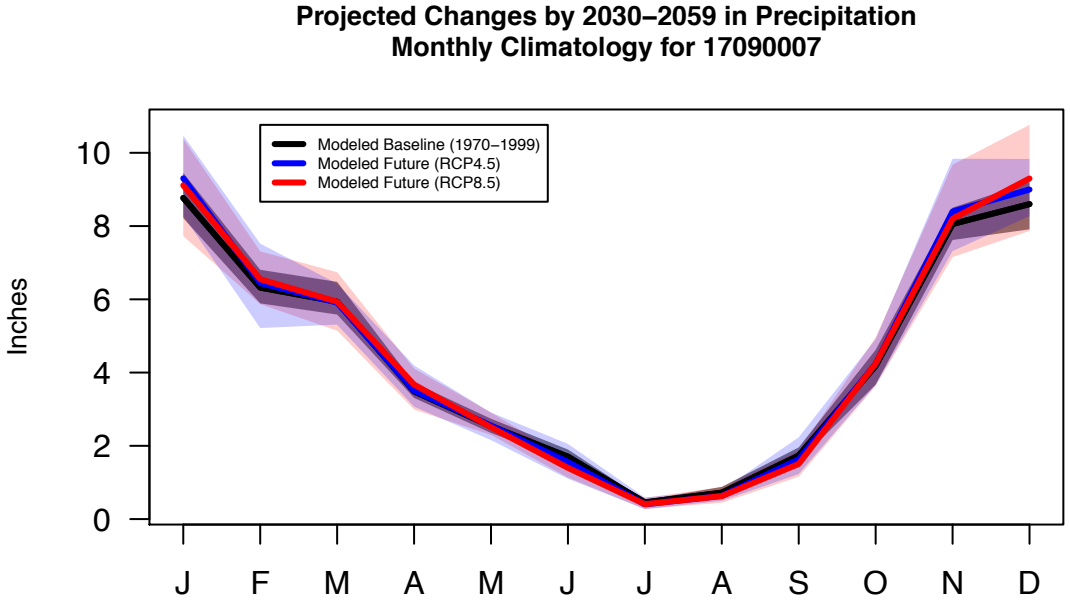

Figure D8. Simulated historic (1970-1999) and future (2030-2059) basin-averaged, 30-year mean, monthly precipitation for the Yamhill (17090008). The solid line and shading give the mean and 5th to 95th percentile range, respectively, of simulations from 20 GCMs.

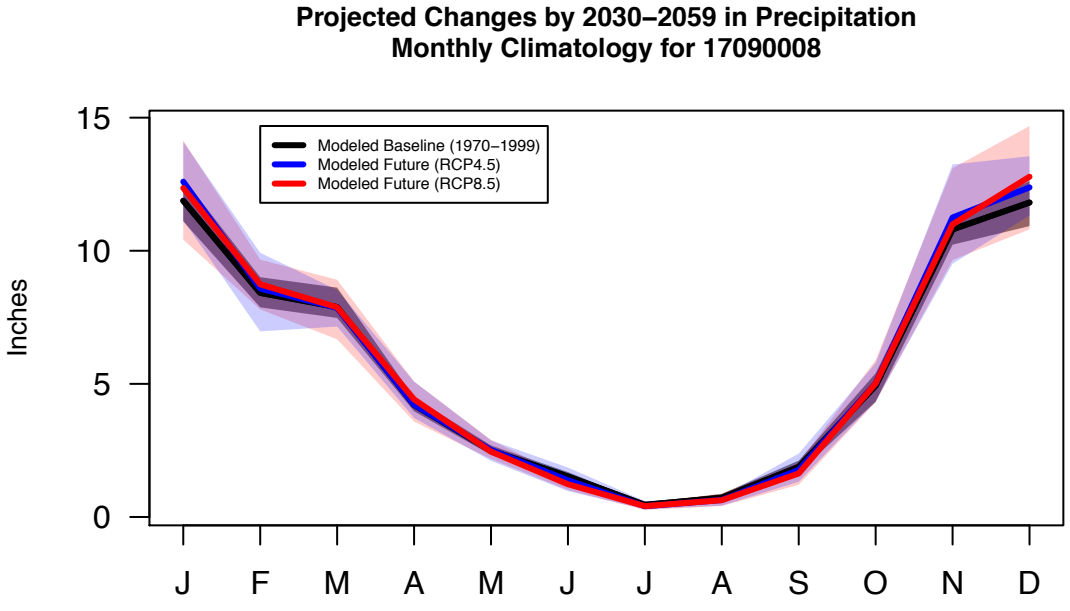

Figure D9. Simulated historic (1970-1999) and future (2030-2059) basin-averaged, 30-year mean, monthly precipitation for the Molalla-Pudding (17090009). The solid line and shading give the mean and 5th to 95th percentile range, respectively, of simulations from 20 GCMs.

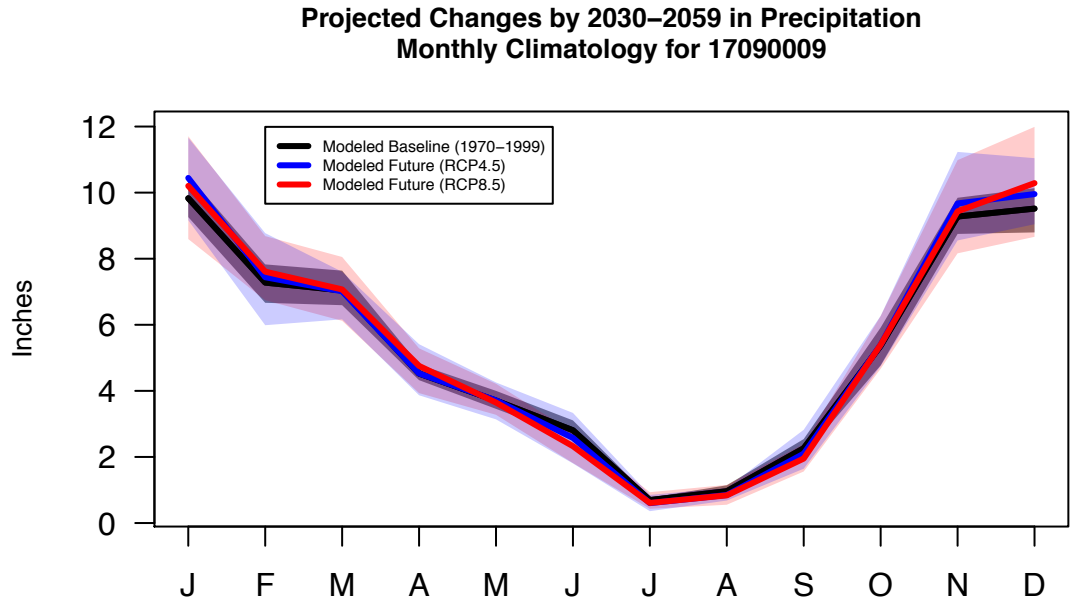

Figure D10. Simulated historic (1970-1999) and future (2030-2059) basin-averaged, 30-year mean, monthly precipitation for the Tualatin (17090010). The solid line and shading give the mean and 5th to 95th percentile range, respectively, of simulations from 20 GCMs.

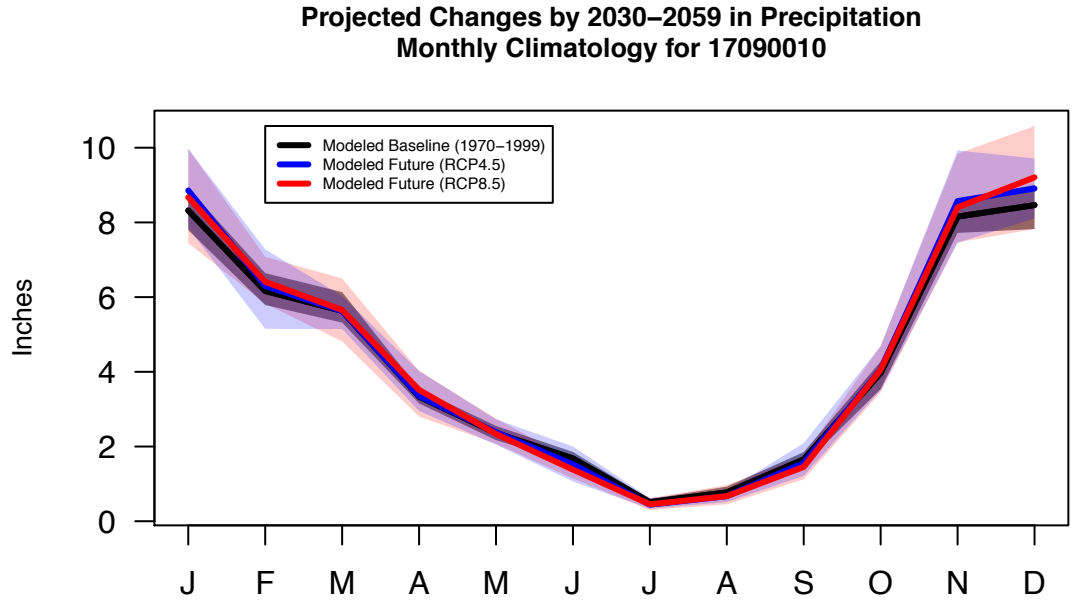

Figure D11. Simulated historic (1970-1999) and future (2030-2059) basin-averaged, 30-year mean, monthly precipitation for the Clackamas (17090011). The solid line and shading give the mean and 5th to 95th percentile range, respectively, of simulations from 20 GCMs.

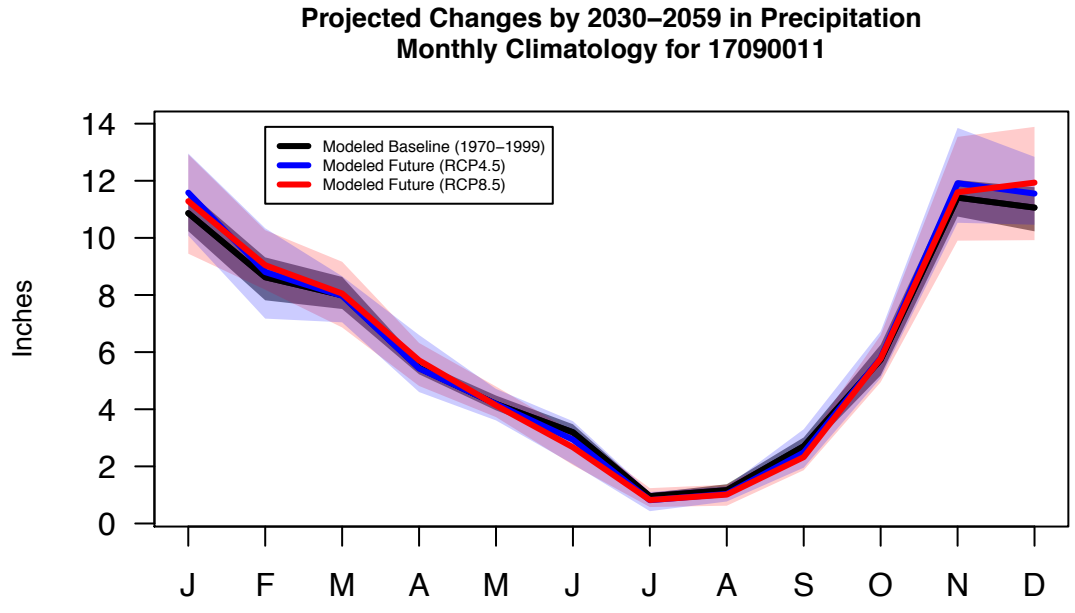

Figure D12. Simulated historic (1970-1999) and future (2030-2059) basin-averaged, 30-year mean, monthly precipitation for the Lower Willamette (17090012). The solid line and shading give the mean and 5th to 95th percentile range, respectively, of simulations from 20 GCMs.

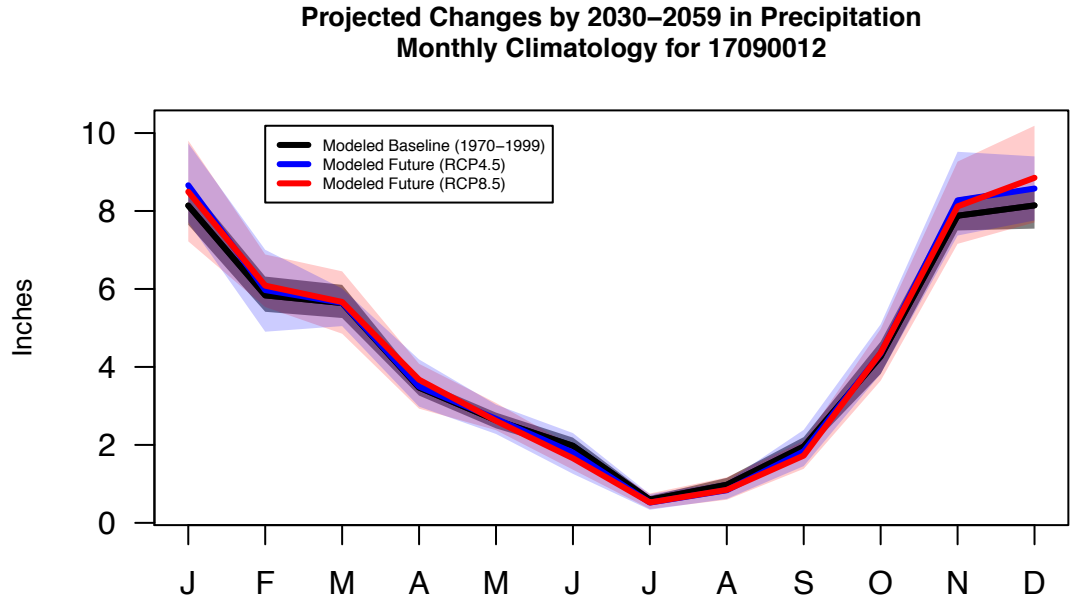

Figure D13. Simulated historic (1970-1999) and future (2030-2059) basin-averaged, 30-year mean, monthly precipitation for the Upper Rogue (17100307). The solid line and shading give the mean and 5th to 95th percentile range, respectively, of simulations from 20 GCMs.

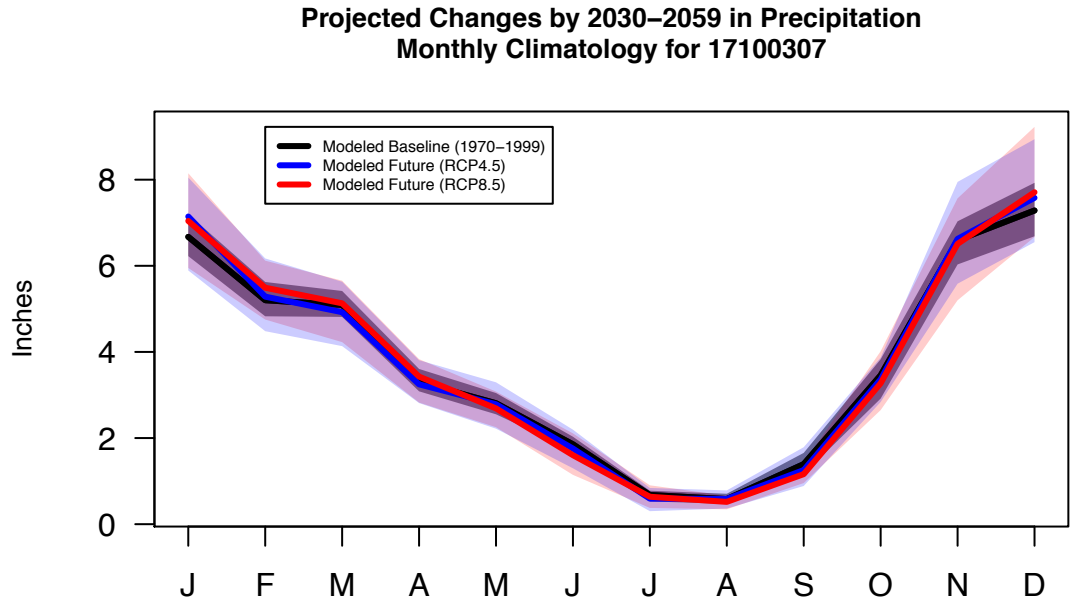

Figure D14. Simulated historic (1970-1999) and future (2030-2059) basin-averaged, 30-year mean, monthly precipitation for the Middle Rogue (17100308). The solid line and shading give the mean and 5th to 95th percentile range, respectively, of simulations from 20 GCMs.

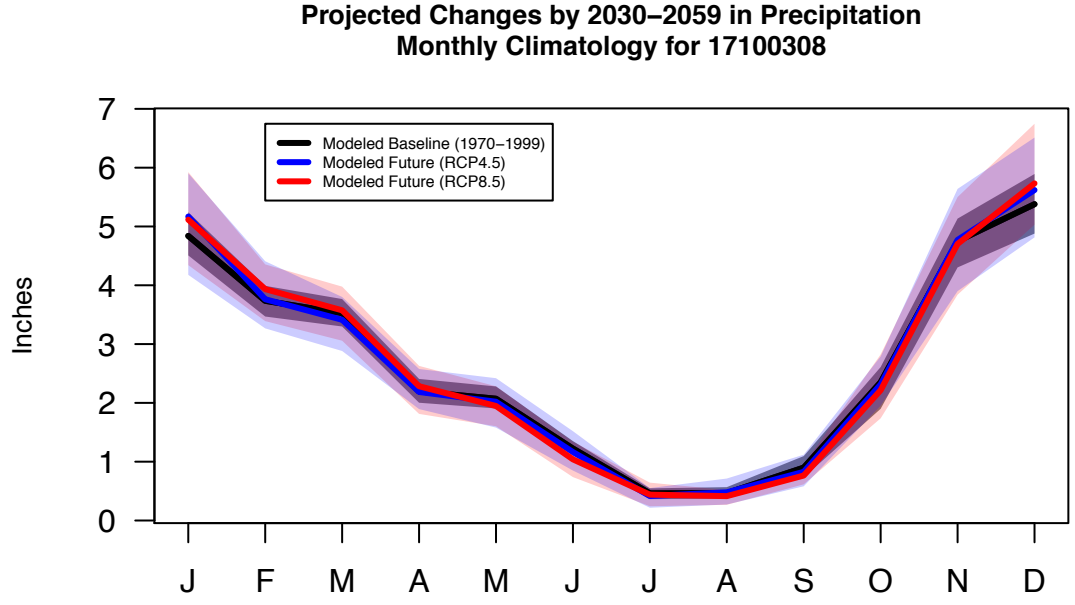

Figure D15. Simulated historic (1970-1999) and future (2030-2059) basin-averaged, 30-year mean, monthly precipitation for the Applegate (17100309). The solid line and shading give the mean and 5th to 95th percentile range, respectively, of simulations from 20 GCMs.

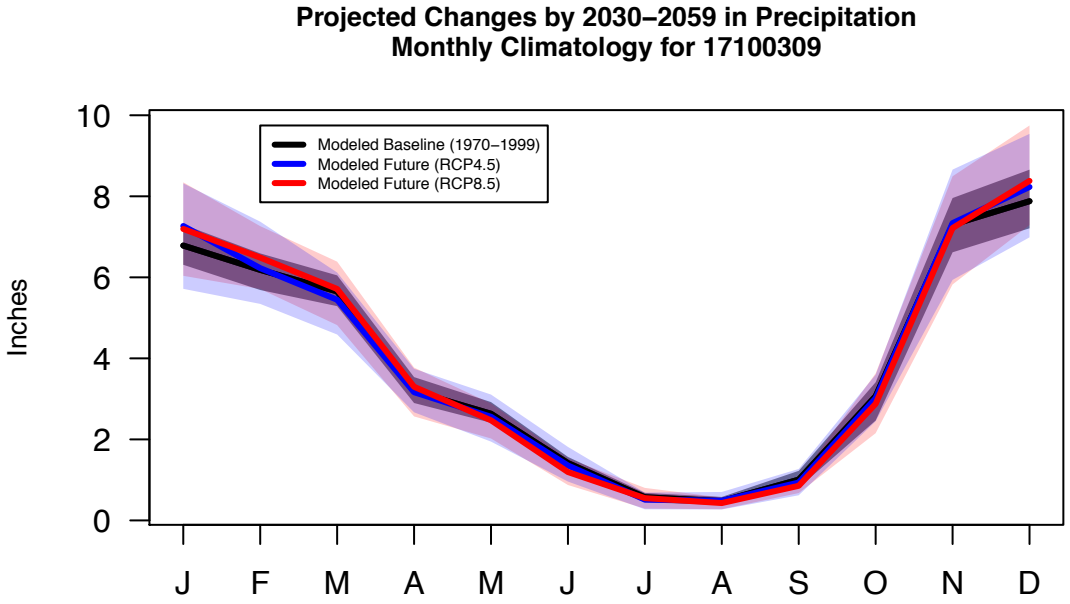

Figure D16. Simulated historic (1970-1999) and future (2030-2059) basin-averaged, 30-year mean, monthly precipitation for the Lower Rogue (17100310). The solid line and shading give the mean and 5th to 95th percentile range, respectively, of simulations from 20 GCMs.

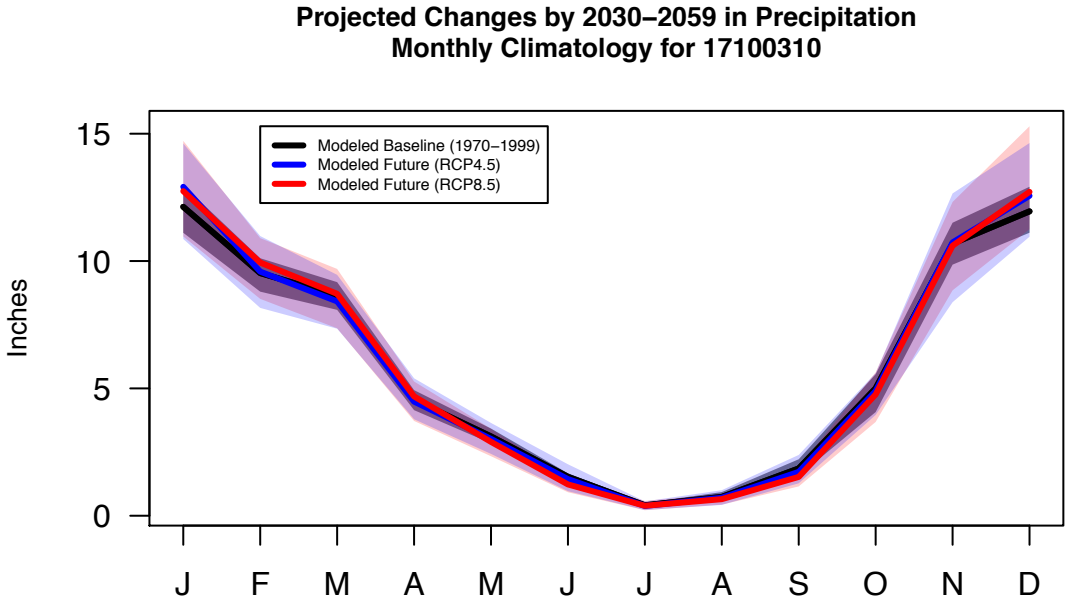

Appendix E. Snow Water Equivalent Projections

Figure E1. Simulated basin-averaged, 30-year mean, snow water equivalent (SWE) on the first day of the month as a percentage accumulated water year precipitation for the Middle Fork Willamette (17090001). The solid line and shading give the mean and range, respectively, of simulations from 10 GCMs.

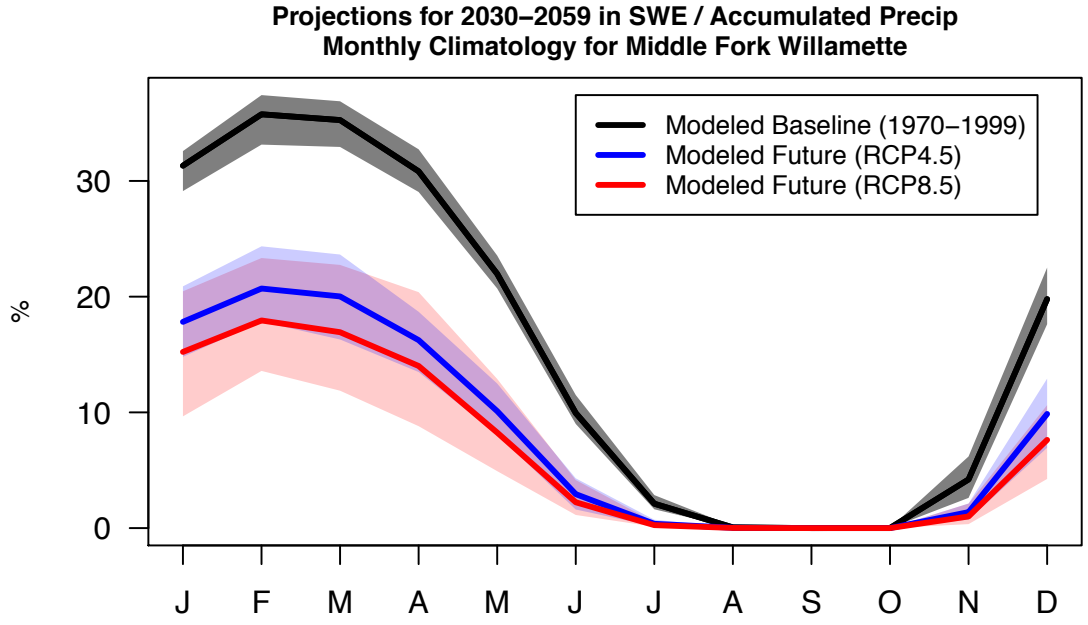

Figure E2. Relative seasonal mean change from simulated historical to future basin-averaged, 30-year mean, snow water equivalent (SWE) on the first day of the month as a percentage accumulated water year precipitation for the Middle Fork Willamette (17090001).

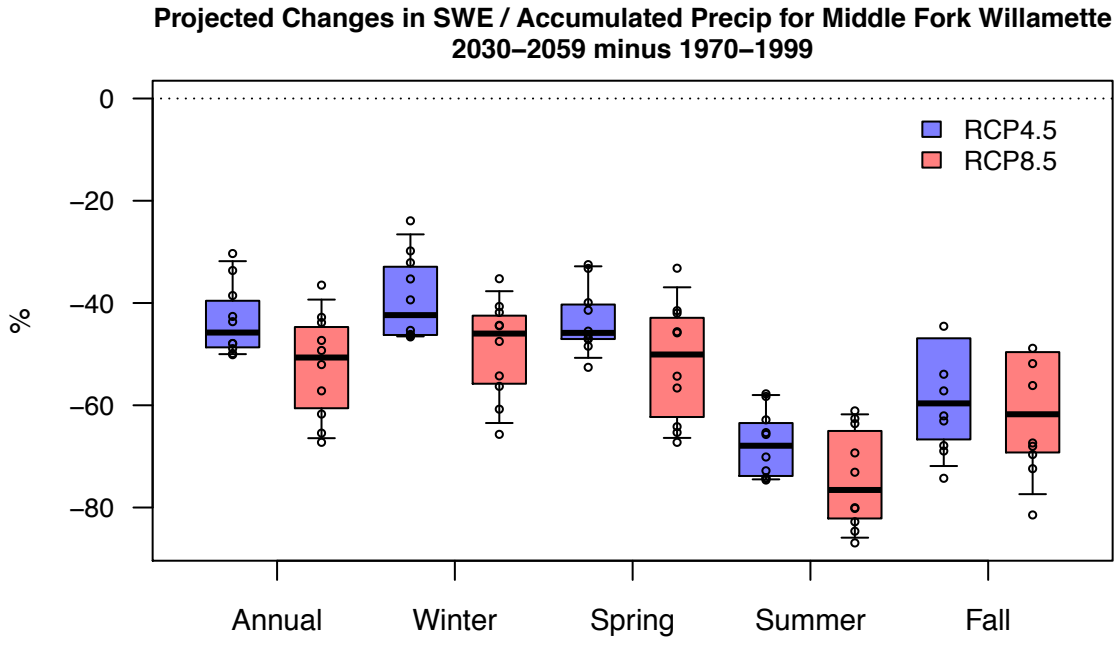

Figure E3. Simulated basin-averaged, 30-year mean, snow water equivalent (SWE) on the first day of the month as a percentage accumulated water year precipitation for the Coast Fork Willamette (17090002). The solid line and shading give the mean and range, respectively, of simulations from 10 GCMs.

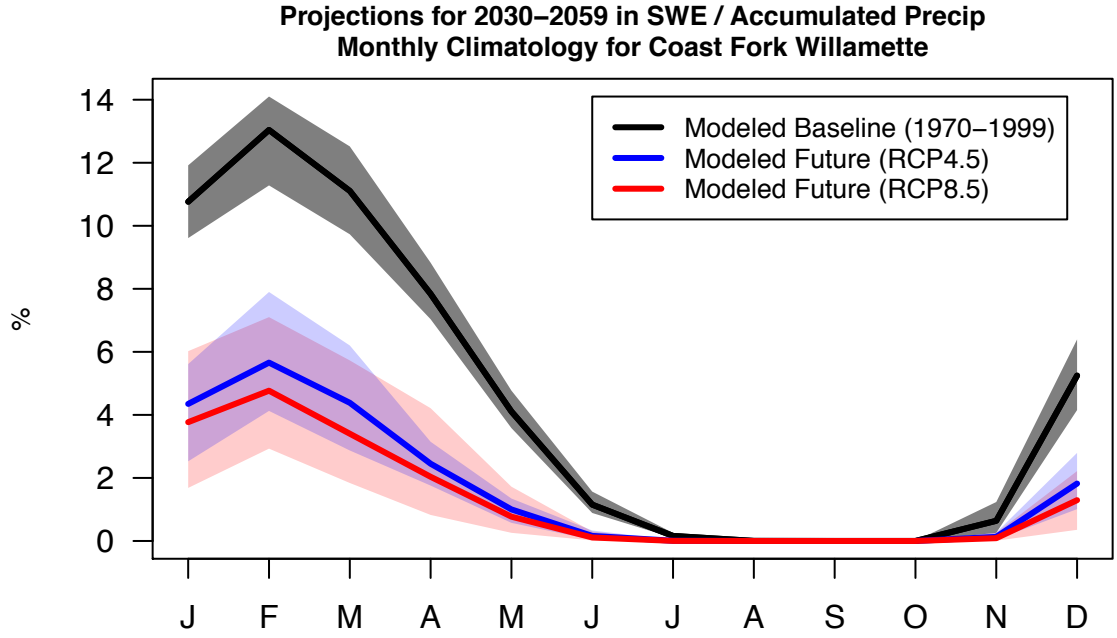

Figure E4. Relative seasonal mean change from simulated historical to future basin-averaged, 30-year mean, snow water equivalent (SWE) on the first day of the month as a percentage accumulated water year precipitation for the Coast Fork Willamette (17090002).

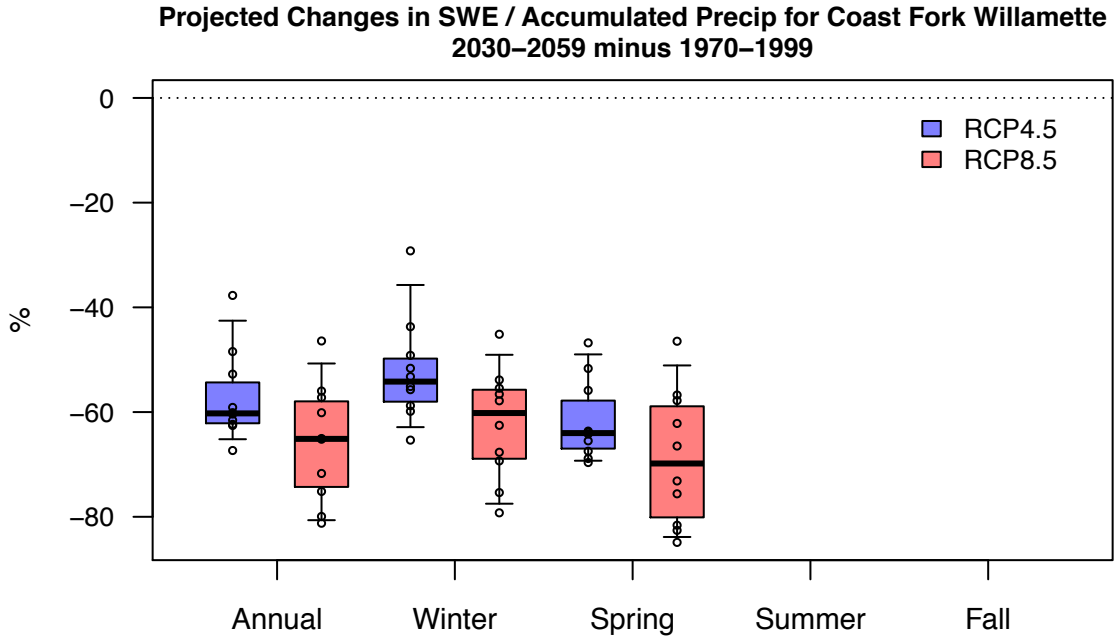

Figure E5. Simulated basin-averaged, 30-year mean, snow water equivalent (SWE) on the first day of the month as a percentage accumulated water year precipitation for the Upper Willamette (17090003). The solid line and shading give the mean and range, respectively, of simulations from 10 GCMs.

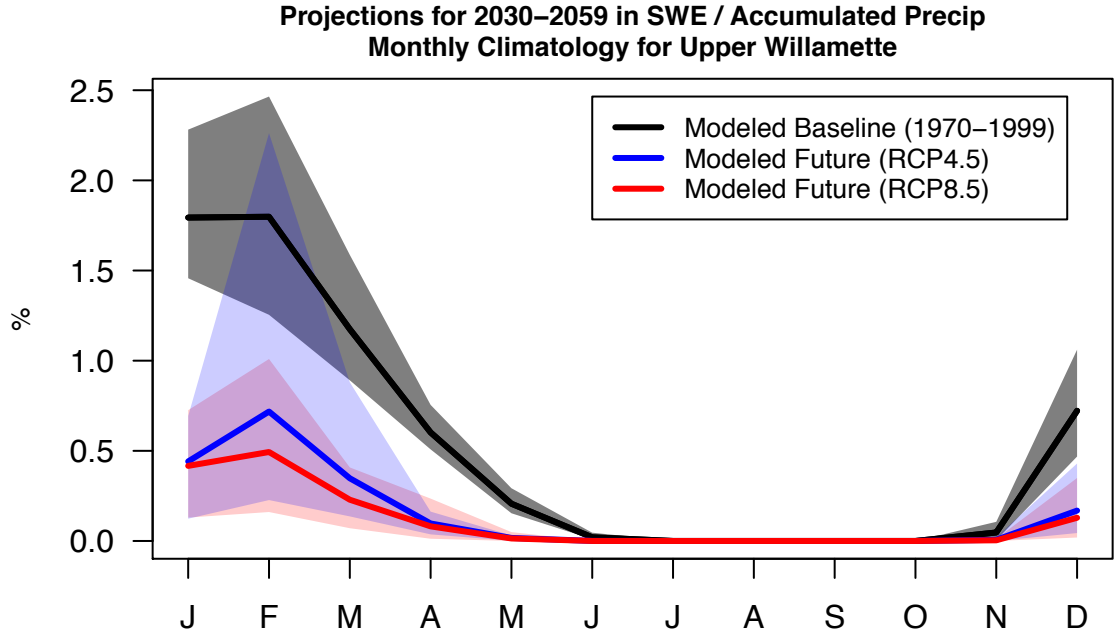

Figure E6. Relative seasonal mean change from simulated historical to future basin-averaged, 30-year mean, snow water equivalent (SWE) on the first day of the month as a percentage accumulated water year precipitation for the Upper Willamette (17090003).

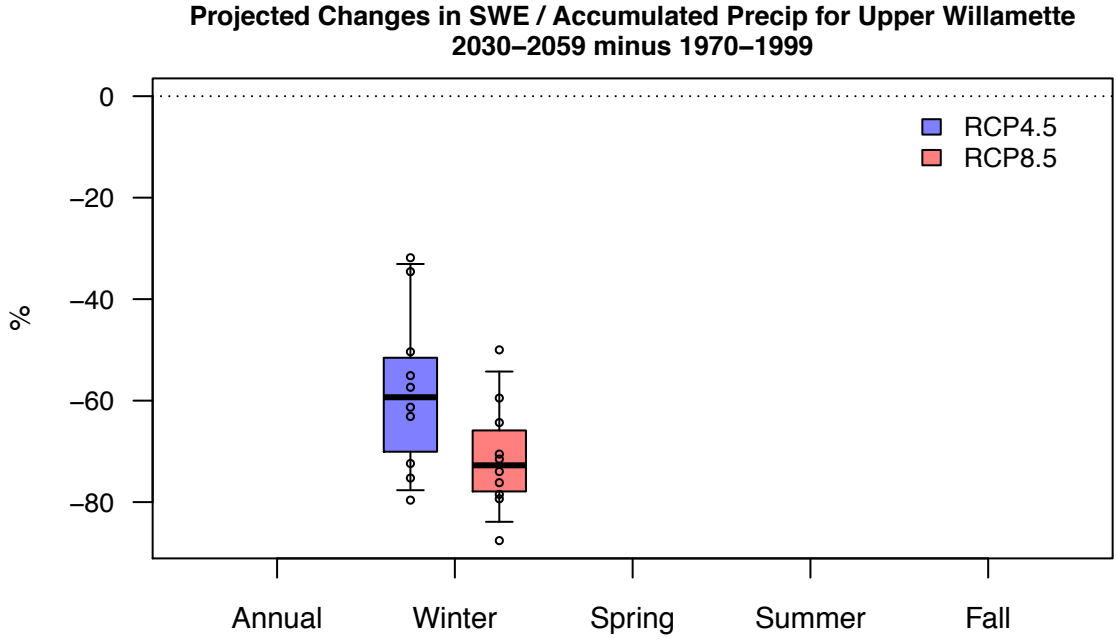

Figure E7. Simulated basin-averaged, 30-year mean, snow water equivalent (SWE) on the first day of the month as a percentage accumulated water year precipitation for the McKenzie (17090004). The solid line and shading give the mean and range, respectively, of simulations from 10 GCMs.

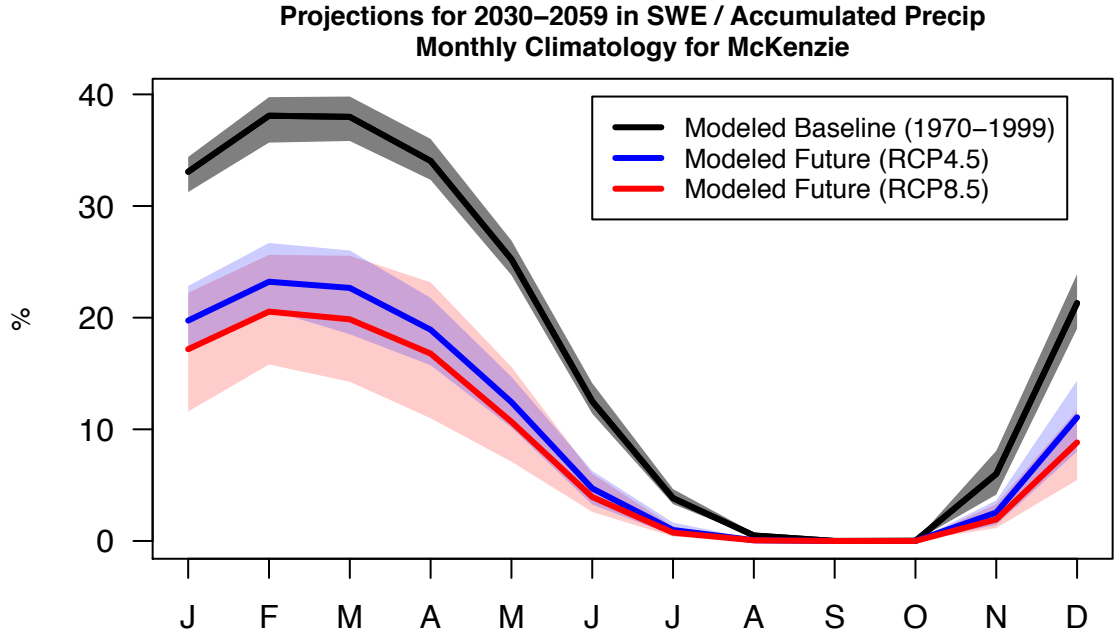

Figure E8. Relative seasonal mean change from simulated historical to future basin-averaged, 30-year mean, snow water equivalent (SWE) on the first day of the month as a percentage accumulated water year precipitation for the McKenzie (17090004).

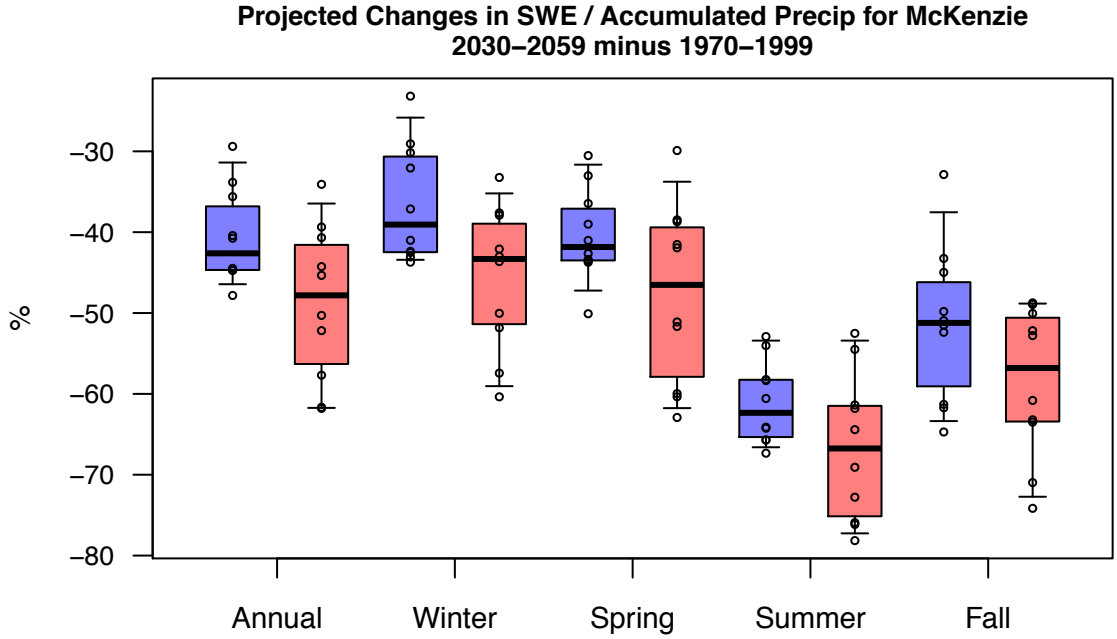

Figure E9. Simulated basin-averaged, 30-year mean, snow water equivalent (SWE) on the first day of the month as a percentage accumulated water year precipitation for the North Santiam (17090005). The solid line and shading give the mean and range, respectively, of simulations from 10 GCMs.

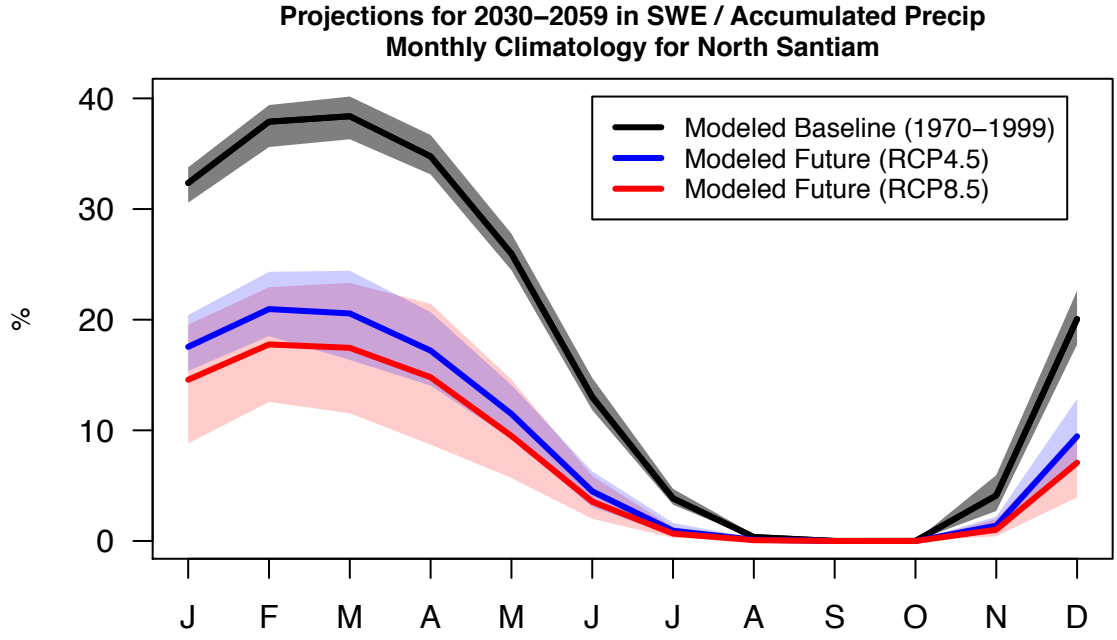

Figure E10. Relative seasonal mean change from simulated historical to future basin-averaged, 30-year mean, snow water equivalent (SWE) on the first day of the month as a percentage accumulated water year precipitation for the North Santiam (17090005).

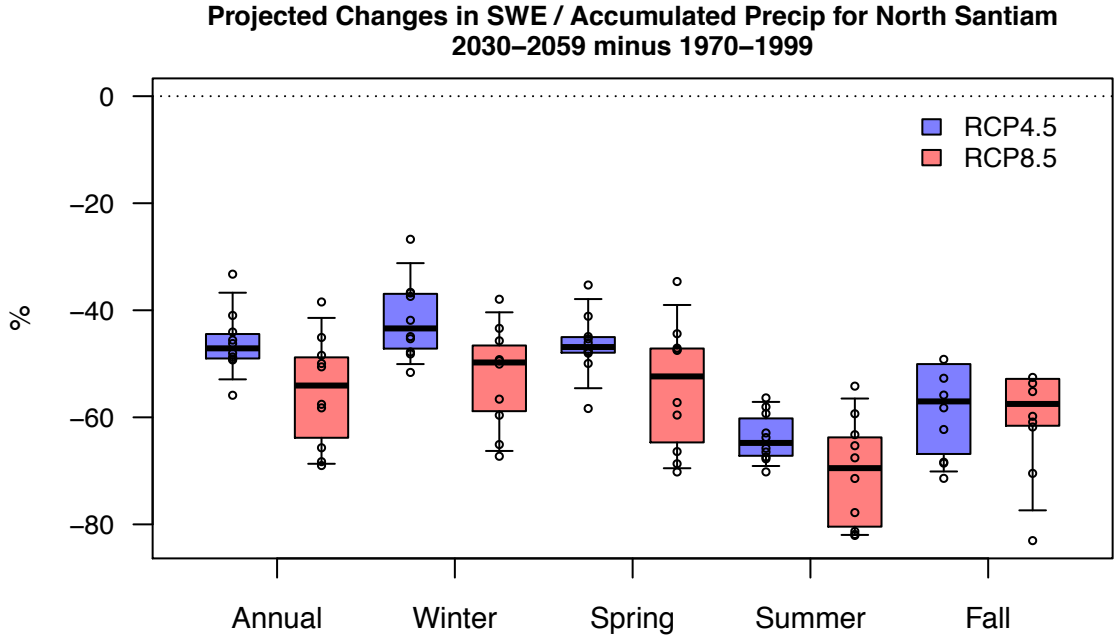

Figure E11. Simulated basin-averaged, 30-year mean, snow water equivalent (SWE) on the first day of the month as a percentage accumulated water year precipitation for the South Santiam (17090006). The solid line and shading give the mean and range, respectively, of simulations from 10 GCMs.

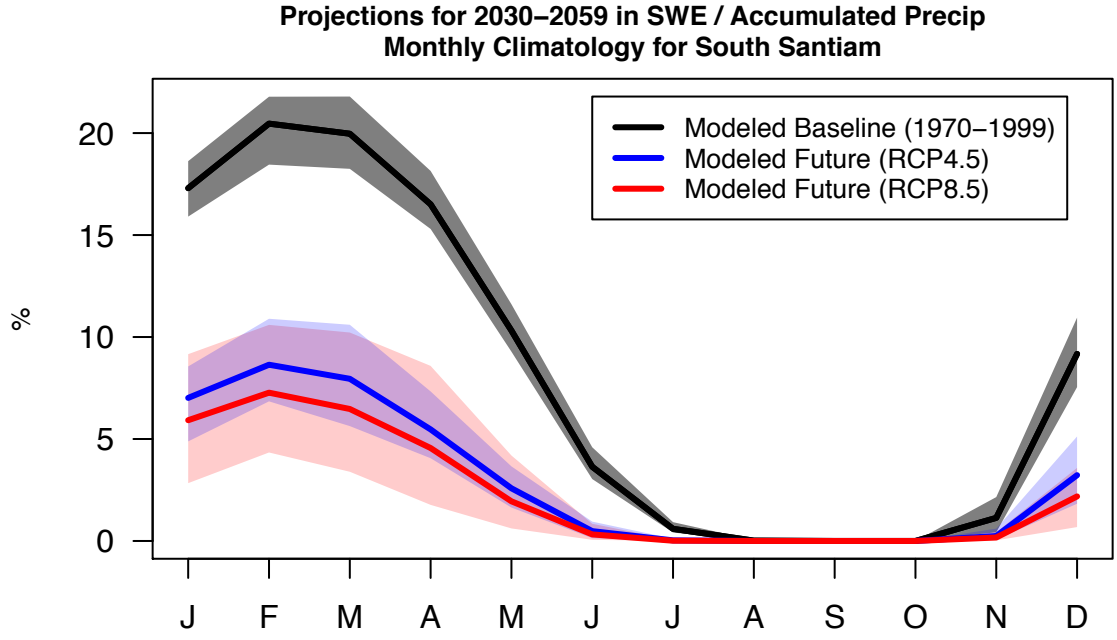

Figure E12. Relative seasonal mean change from simulated historical to future basin-averaged, 30-year mean, snow water equivalent (SWE) on the first day of the month as a percentage accumulated water year precipitation for the South Santiam (17090006).

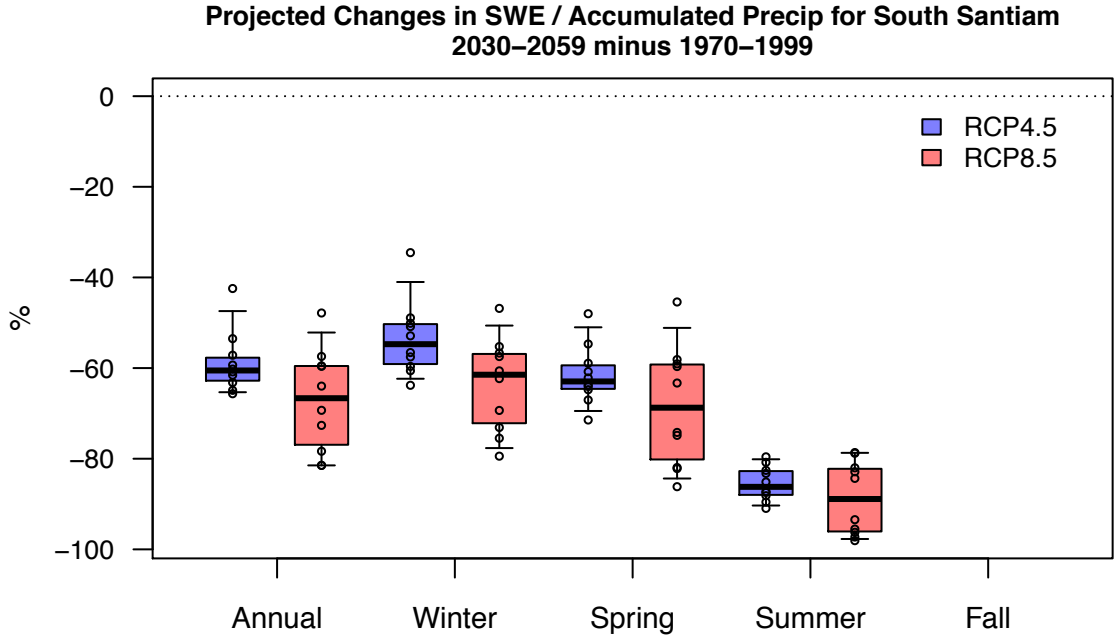

Figure E13. Simulated basin-averaged, 30-year mean, snow water equivalent (SWE) on the first day of the month as a percentage accumulated water year precipitation for the Middle Willamette (17090007). The solid line and shading give the mean and range, respectively, of simulations from 10 GCMs.

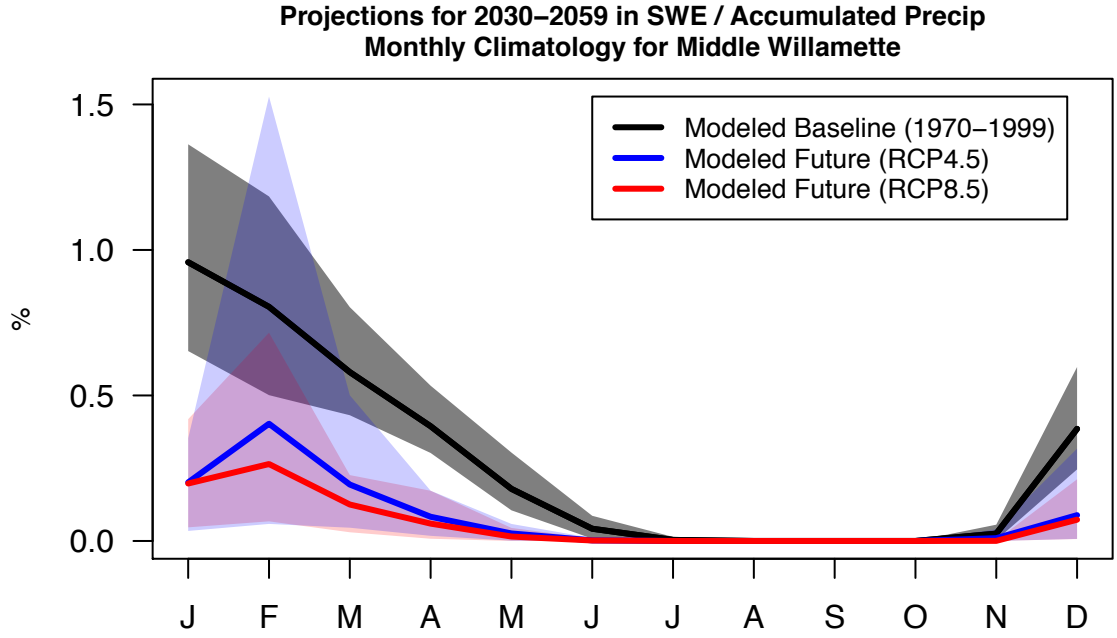

Figure E14. Relative seasonal mean change from simulated historical to future basin-averaged, 30-year mean, snow water equivalent (SWE) on the first day of the month as a percentage accumulated water year precipitation for the Middle Willamette (17090007).

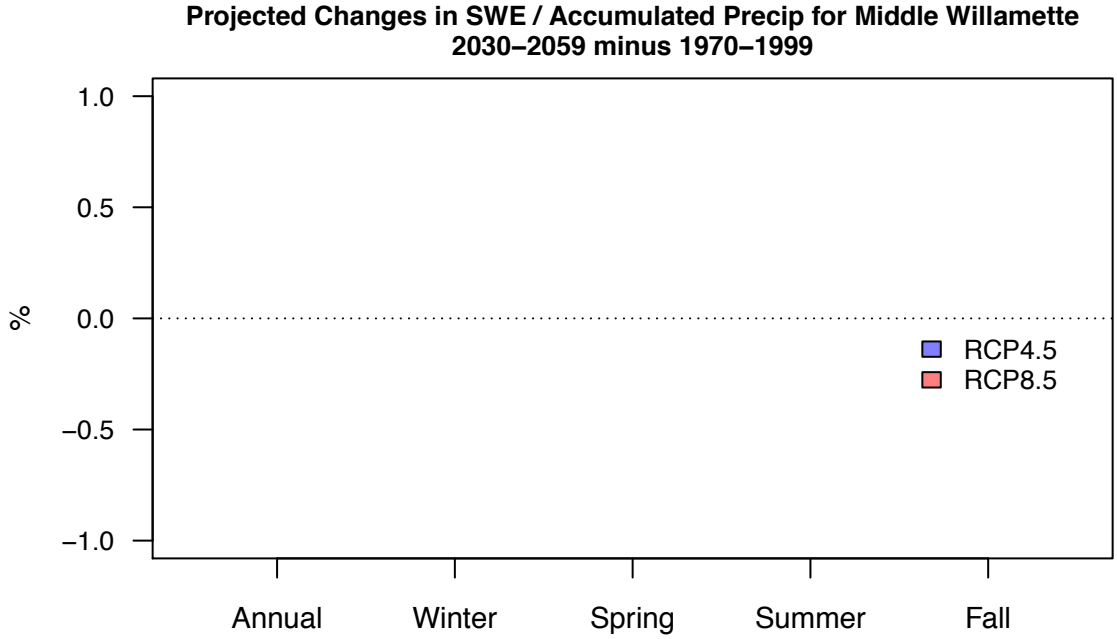

Figure E15. Simulated basin-averaged, 30-year mean, snow water equivalent (SWE) on the first day of the month as a percentage accumulated water year precipitation for the Yamhill (17090008). The solid line and shading give the mean and range, respectively, of simulations from 10 GCMs.

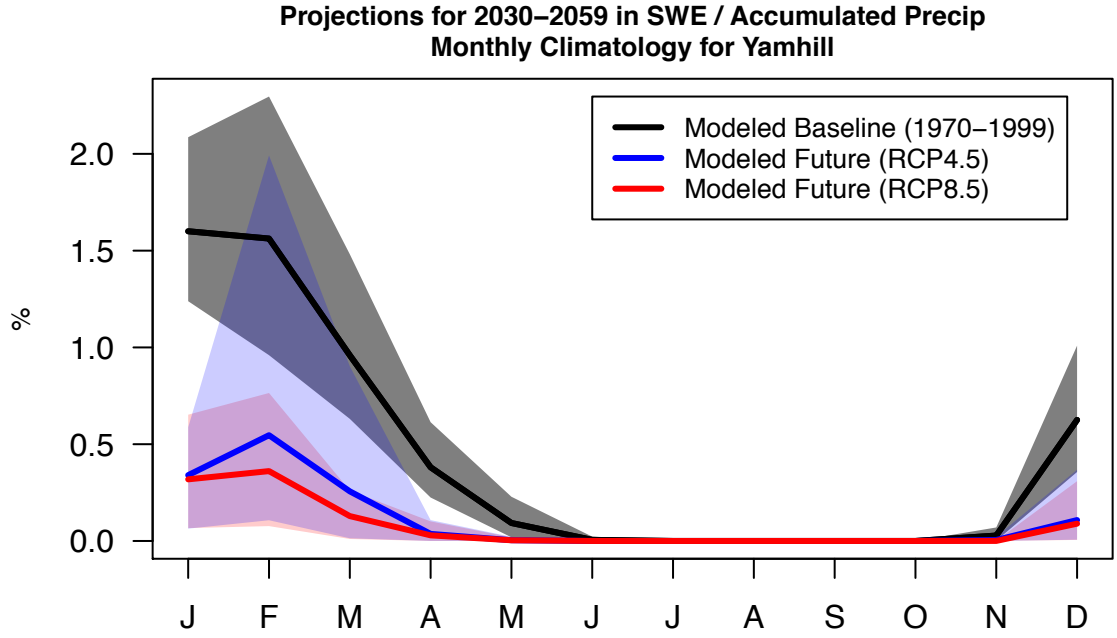

Figure E16. Relative seasonal mean change from simulated historical to future basin-averaged, 30-year mean, snow water equivalent (SWE) on the first day of the month as a percentage accumulated water year precipitation for the Yamhill (17090008).

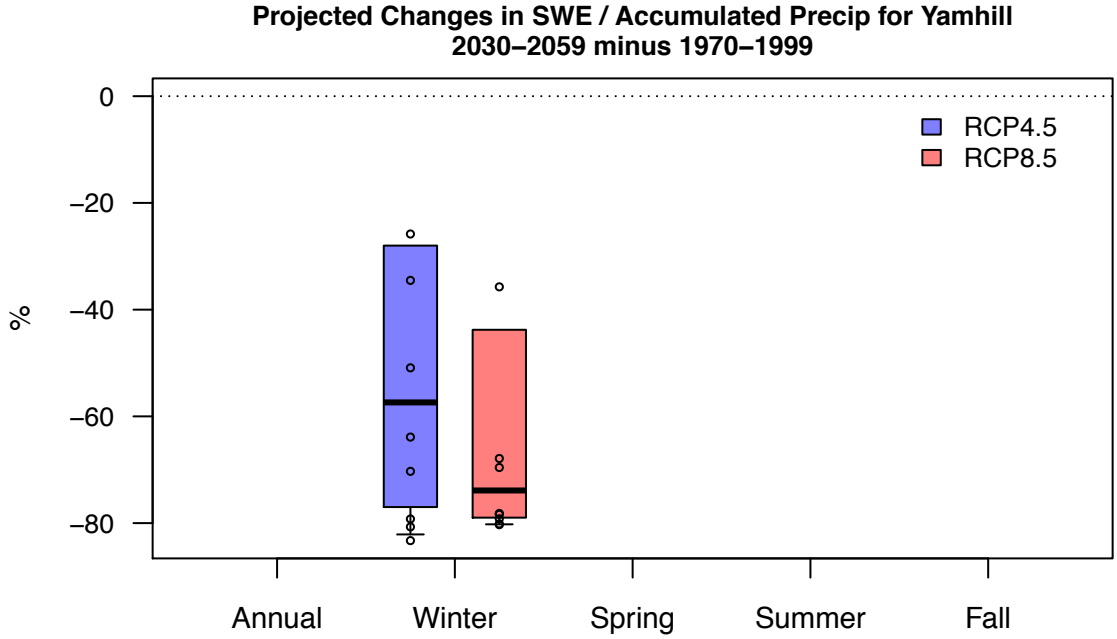

Figure E17. Simulated basin-averaged, 30-year mean, snow water equivalent (SWE) on the first day of the month as a percentage accumulated water year precipitation for the Molalla-Pudding (17090009). The solid line and shading give the mean and range, respectively, of simulations from 10 GCMs.

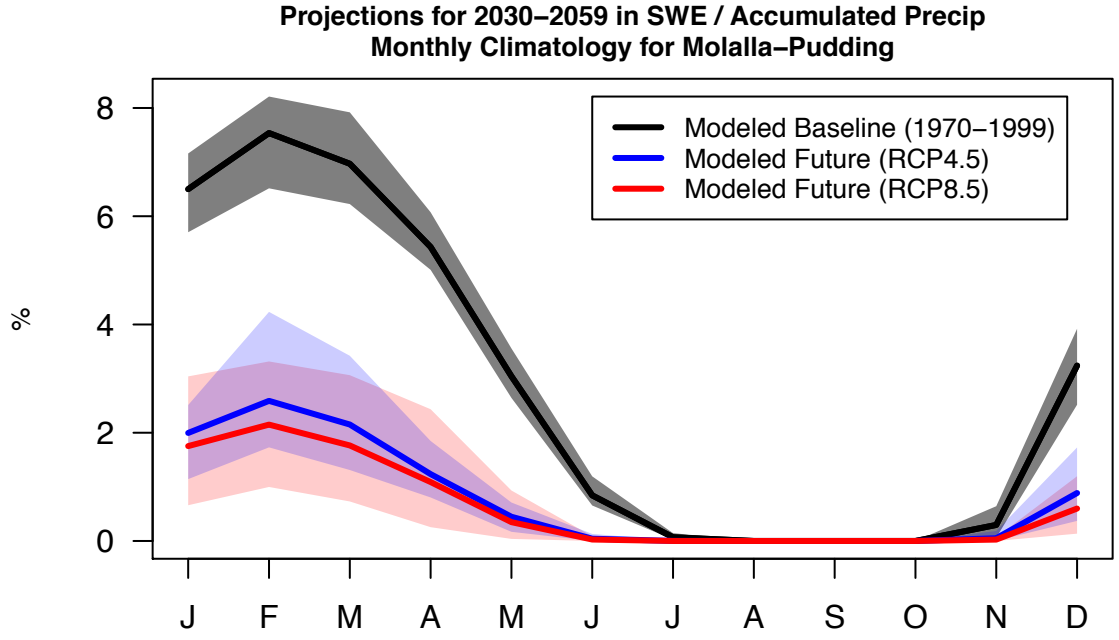

Figure E18. Relative seasonal mean change from simulated historical to future basin-averaged, 30-year mean, snow water equivalent (SWE) on the first day of the month as a percentage accumulated water year precipitation for the Molalla-Pudding (17090009).

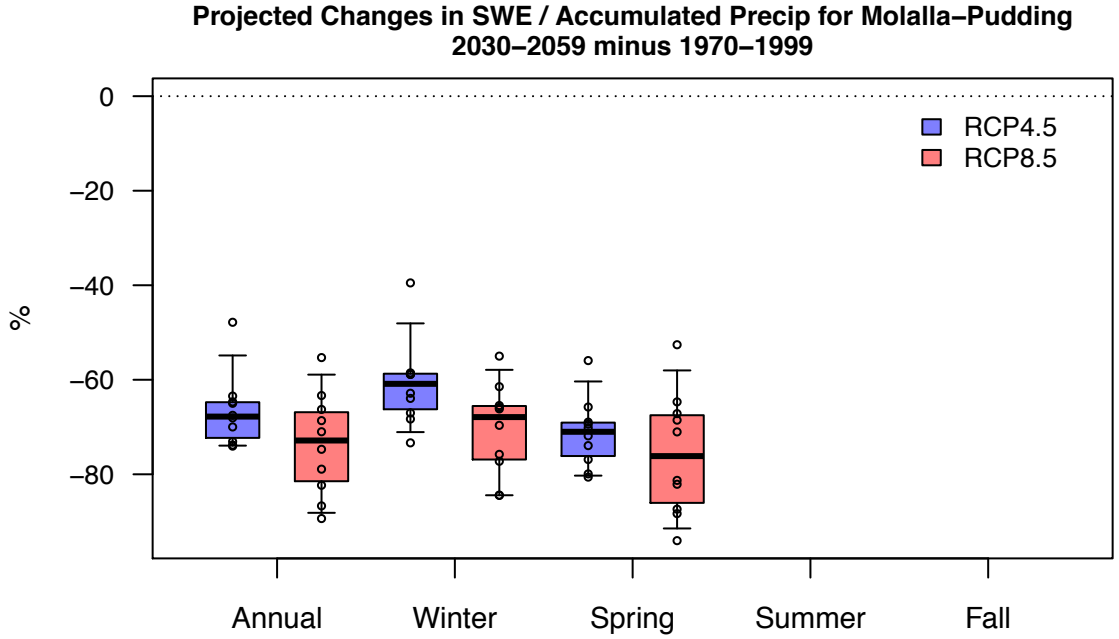

Figure E19. Simulated basin-averaged, 30-year mean, snow water equivalent (SWE) on the first day of the month as a percentage accumulated water year precipitation for the Tualatin (17090010). The solid line and shading give the mean and range, respectively, of simulations from 10 GCMs.

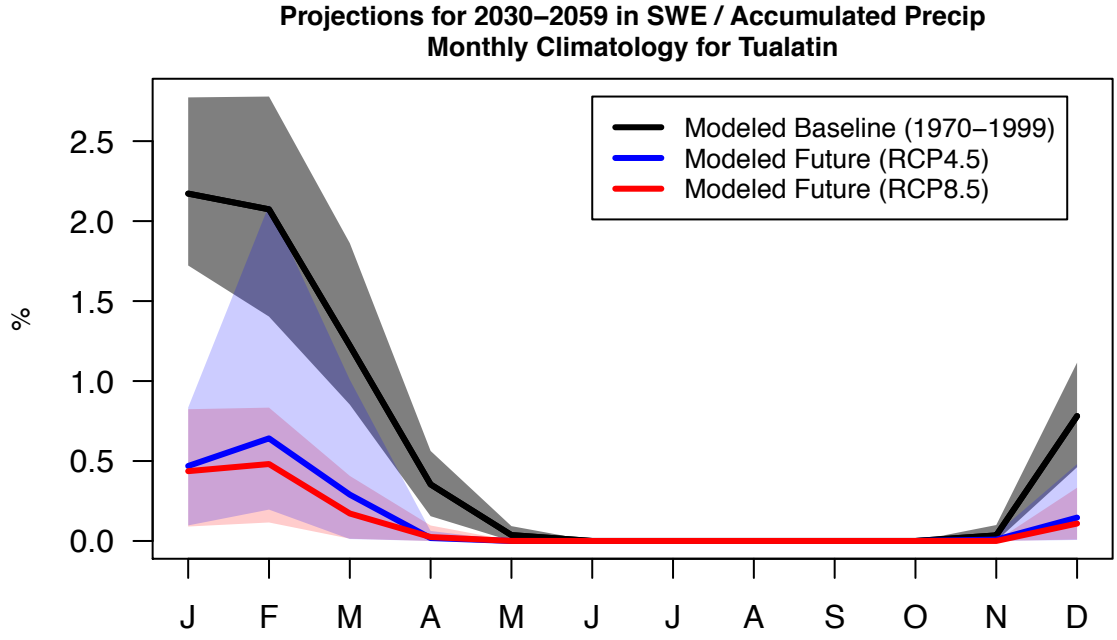

Figure E20. Relative seasonal mean change from simulated historical to future basin-averaged, 30-year mean, snow water equivalent (SWE) on the first day of the month as a percentage accumulated water year precipitation for the Tualatin (17090010).

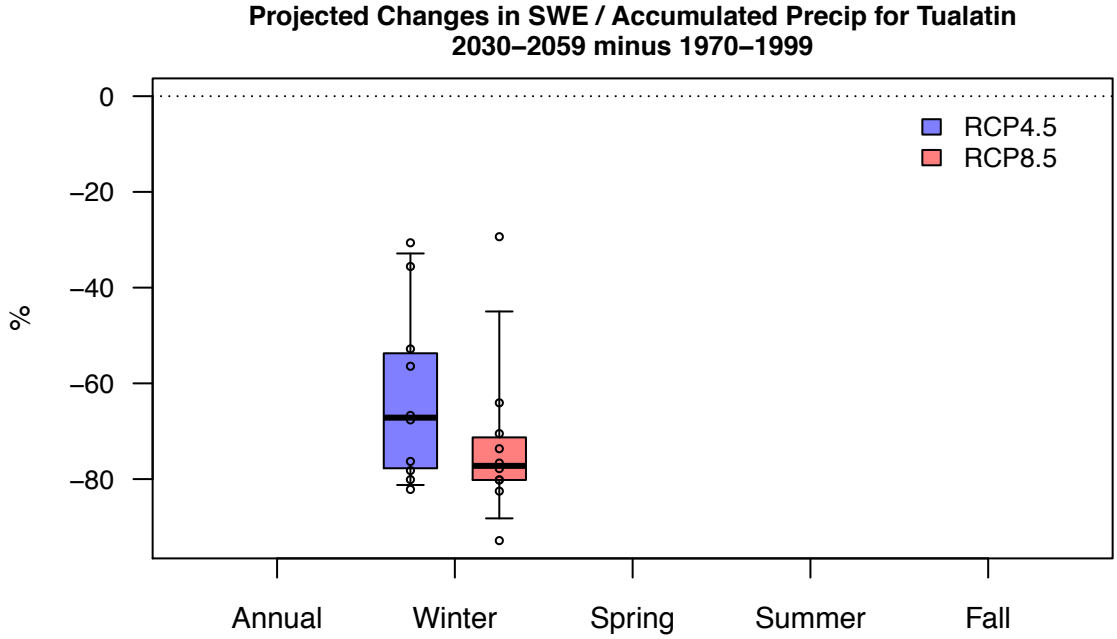

Figure E21. Simulated basin-averaged, 30-year mean, snow water equivalent (SWE) on the first day of the month as a percentage accumulated water year precipitation for the Clackamas (17090011). The solid line and shading give the mean and range, respectively, of simulations from 10 GCMs.

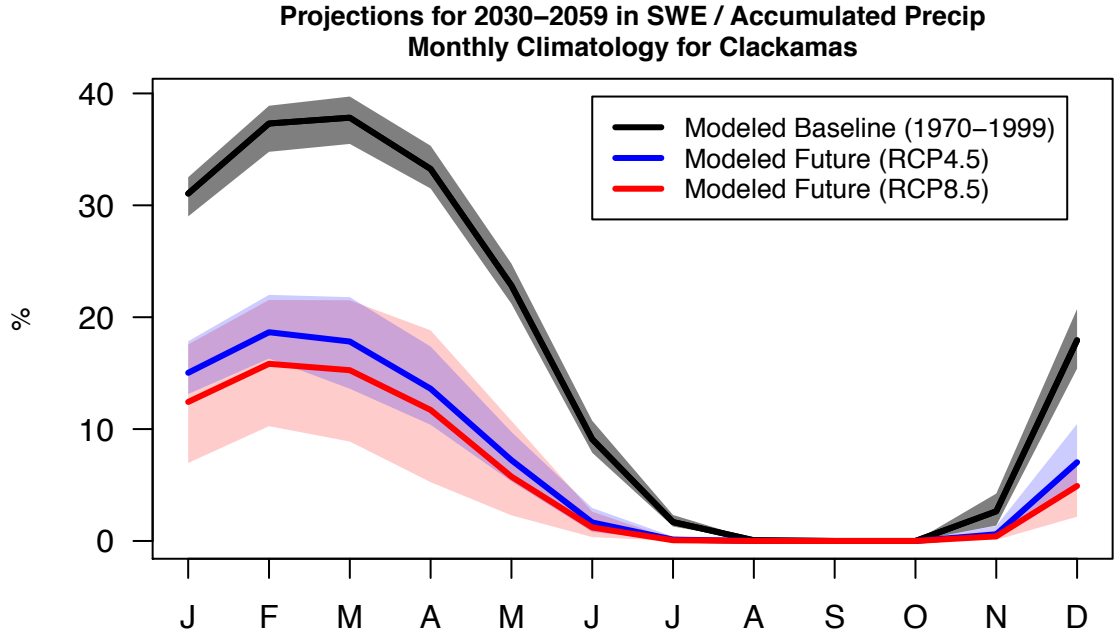

Figure E22. Relative seasonal mean change from simulated historical to future basin-averaged, 30-year mean, snow water equivalent (SWE) on the first day of the month as a percentage accumulated water year precipitation for the Clackamas (17090011).

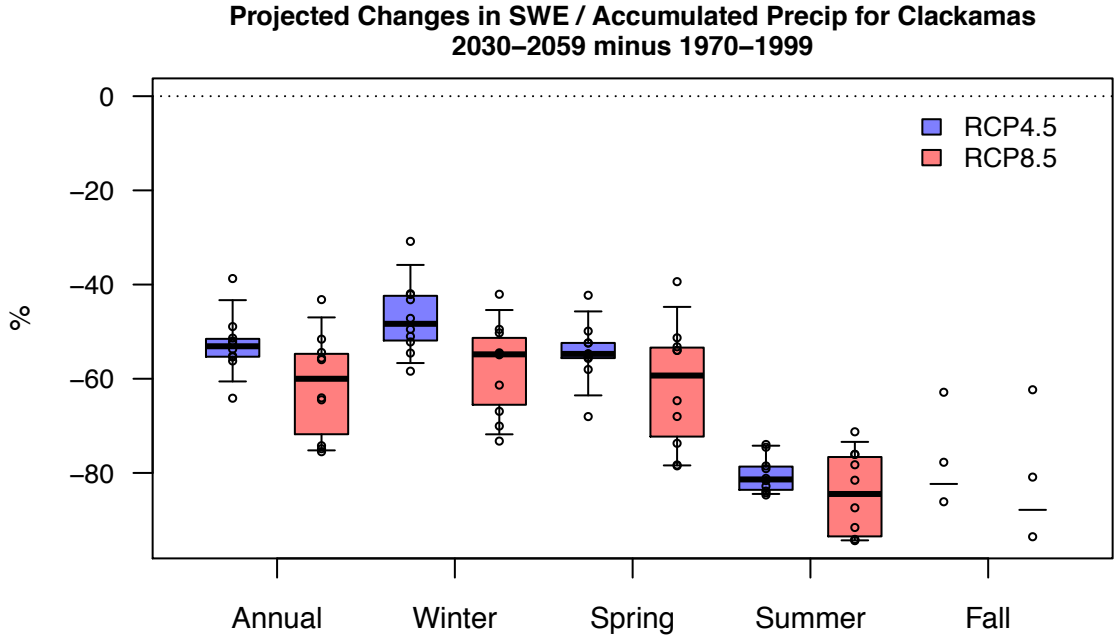

Figure E23. Simulated basin-averaged, 30-year mean, snow water equivalent (SWE) on the first day of the month as a percentage accumulated water year precipitation for the Lower Willamette (17090012). The solid line and shading give the mean and range, respectively, of simulations from 10 GCMs.

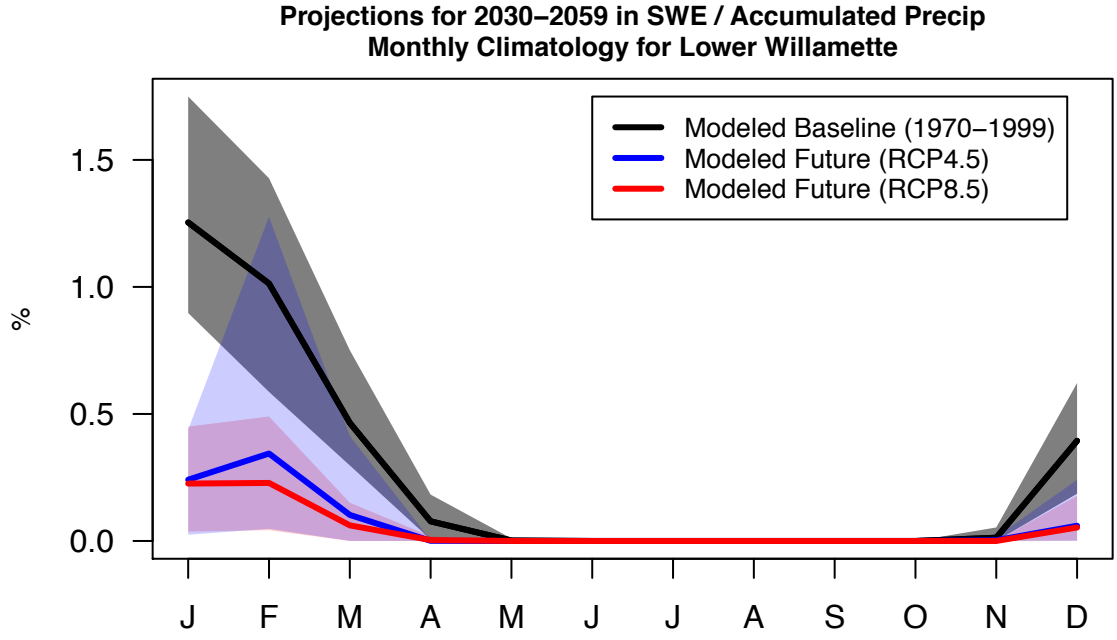

Figure E24. Relative seasonal mean change from simulated historical to future basin-averaged, 30-year mean, snow water equivalent (SWE) on the first day of the month as a percentage accumulated water year precipitation for the Lower Willamette (17090012).

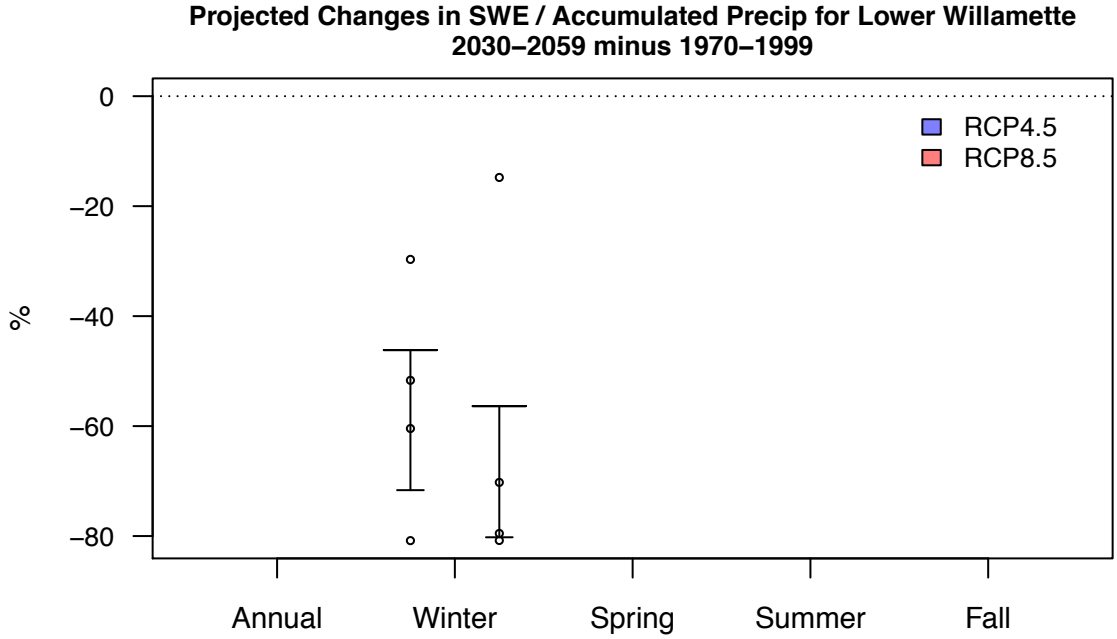

Figure E25. Simulated basin-averaged, 30-year mean, snow water equivalent (SWE) on the first day of the month as a percentage accumulated water year precipitation for the Upper Rogue (17100307). The solid line and shading give the mean and range, respectively, of simulations from 10 GCMs.

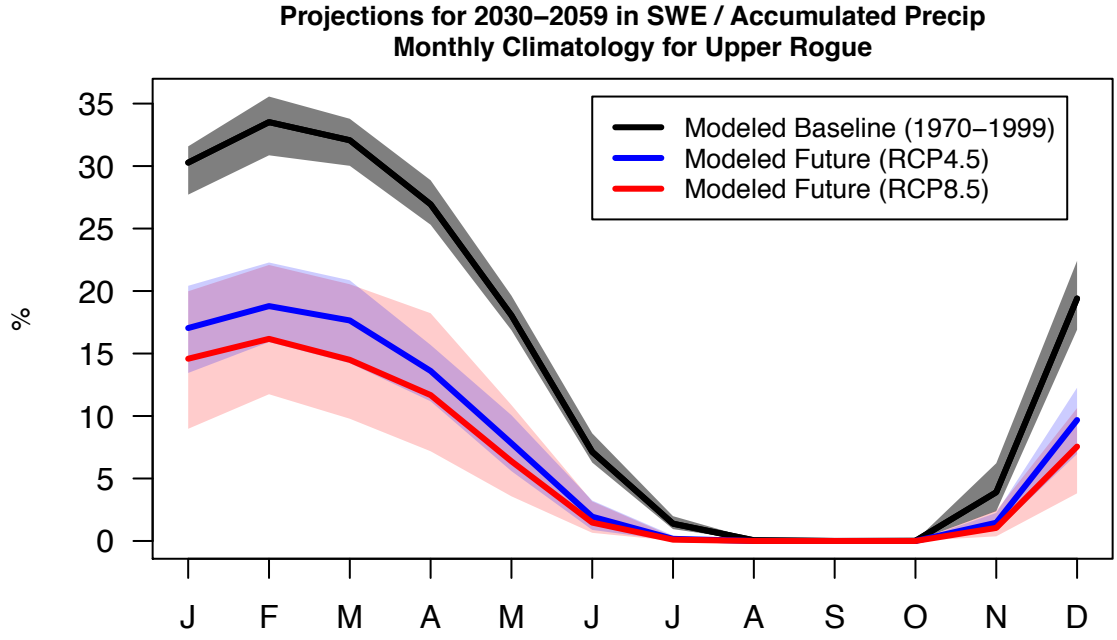

Figure E26. Relative seasonal mean change from simulated historical to future basin-averaged, 30-year mean, snow water equivalent (SWE) on the first day of the month as a percentage accumulated water year precipitation for the Upper Rogue (17100307).

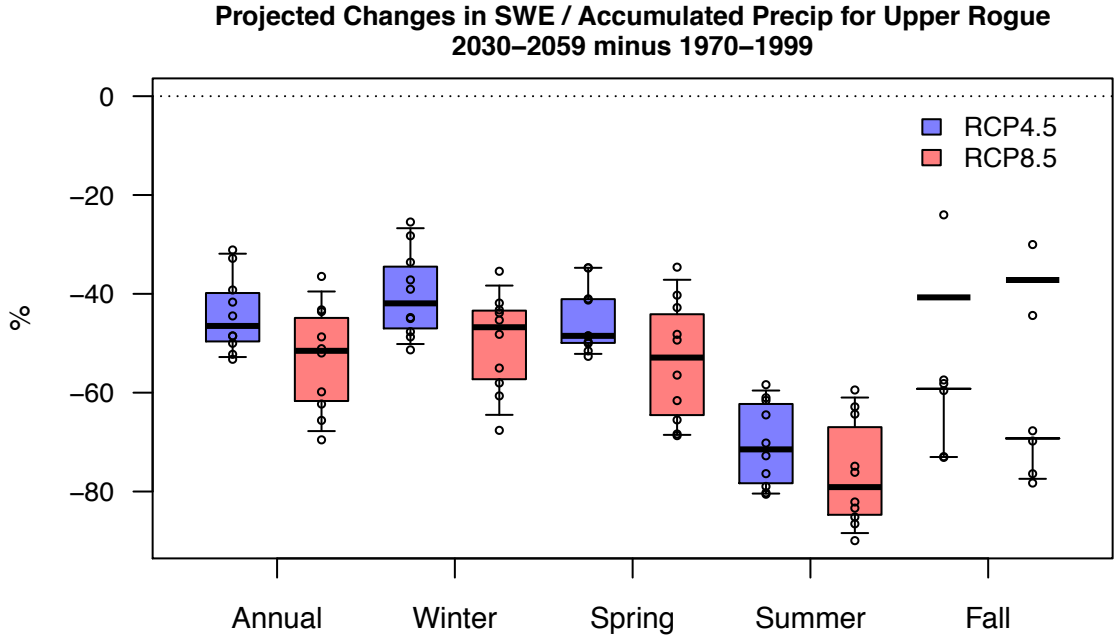

Figure E27. Simulated basin-averaged, 30-year mean, snow water equivalent (SWE) on the first day of the month as a percentage accumulated water year precipitation for the Middle Rogue (17100308). The solid line and shading give the mean and range, respectively, of simulations from 10 GCMs.

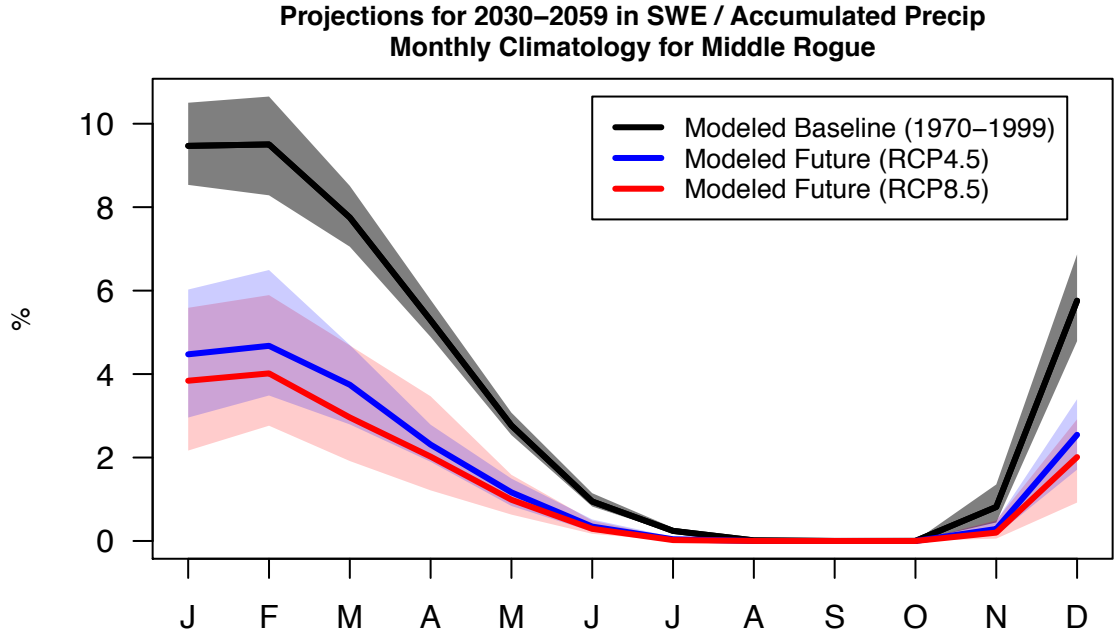

Figure E28. Relative seasonal mean change from simulated historical to future basin-averaged, 30-year mean, snow water equivalent (SWE) on the first day of the month as a percentage accumulated water year precipitation for the Middle Rogue (17100308).

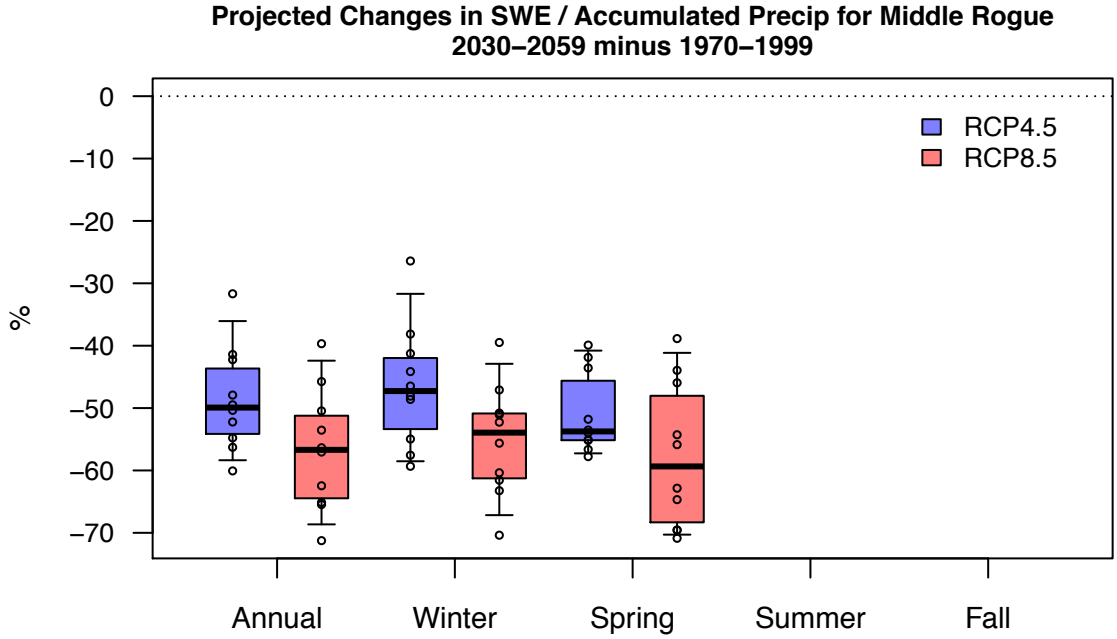

Figure E29. Simulated basin-averaged, 30-year mean, snow water equivalent (SWE) on the first day of the month as a percentage accumulated water year precipitation for the Applegate (17100309). The solid line and shading give the mean and range, respectively, of simulations from 10 GCMs.

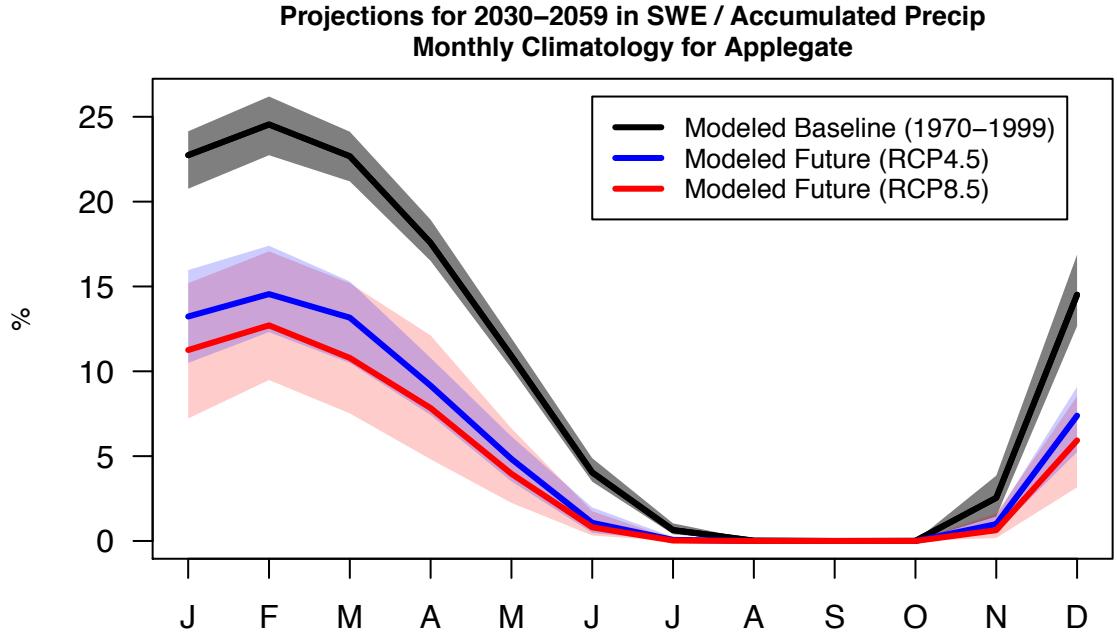

Figure E30. Relative seasonal mean change from simulated historical to future basin-averaged, 30-year mean, snow water equivalent (SWE) on the first day of the month as a percentage accumulated water year precipitation for the Applegate (17100309).

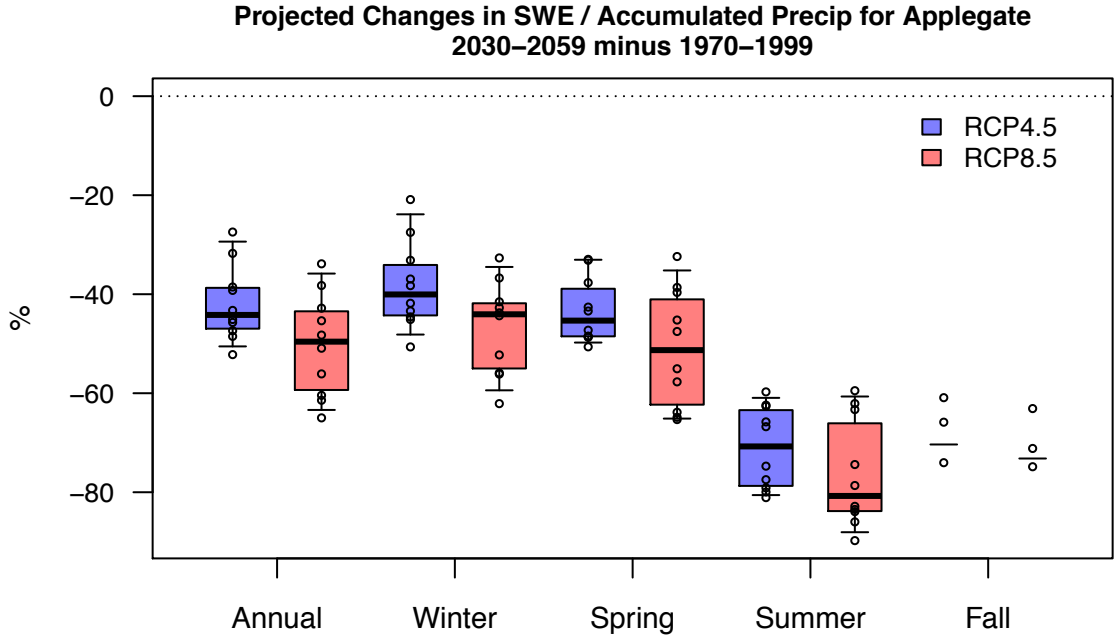

Figure E31. Simulated basin-averaged, 30-year mean, snow water equivalent (SWE) on the first day of the month as a percentage accumulated water year precipitation for the Lower Rogue (17100310). The solid line and shading give the mean and range, respectively, of simulations from 10 GCMs.

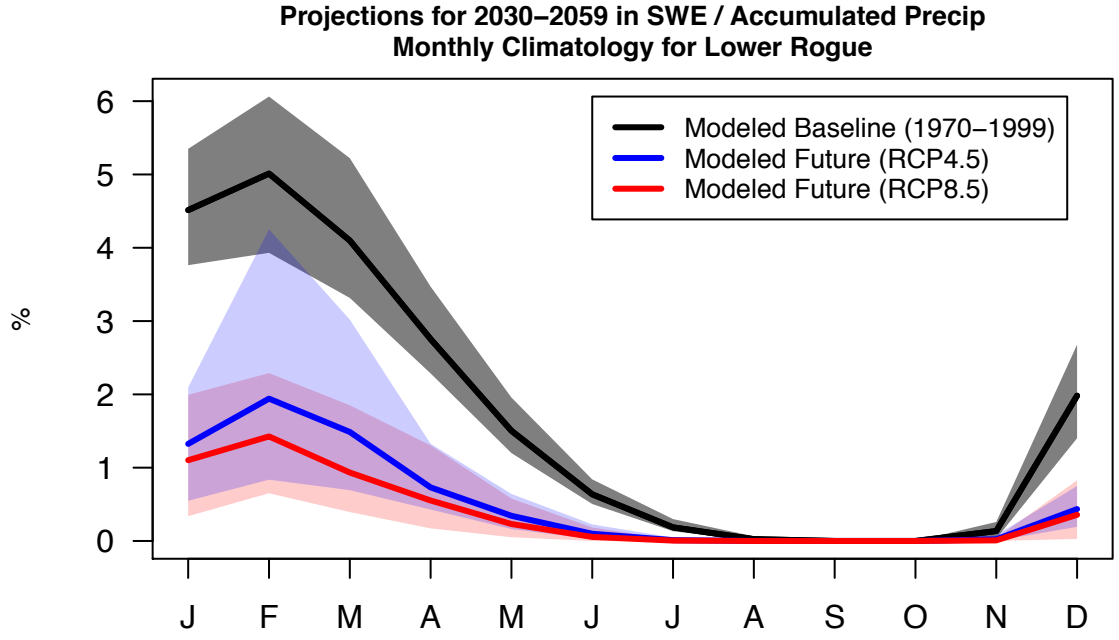

Figure E32. Relative seasonal mean change from simulated historical to future basin-averaged, 30-year mean, snow water equivalent (SWE) on the first day of the month as a percentage accumulated water year precipitation for the Lower Rogue (17100310).

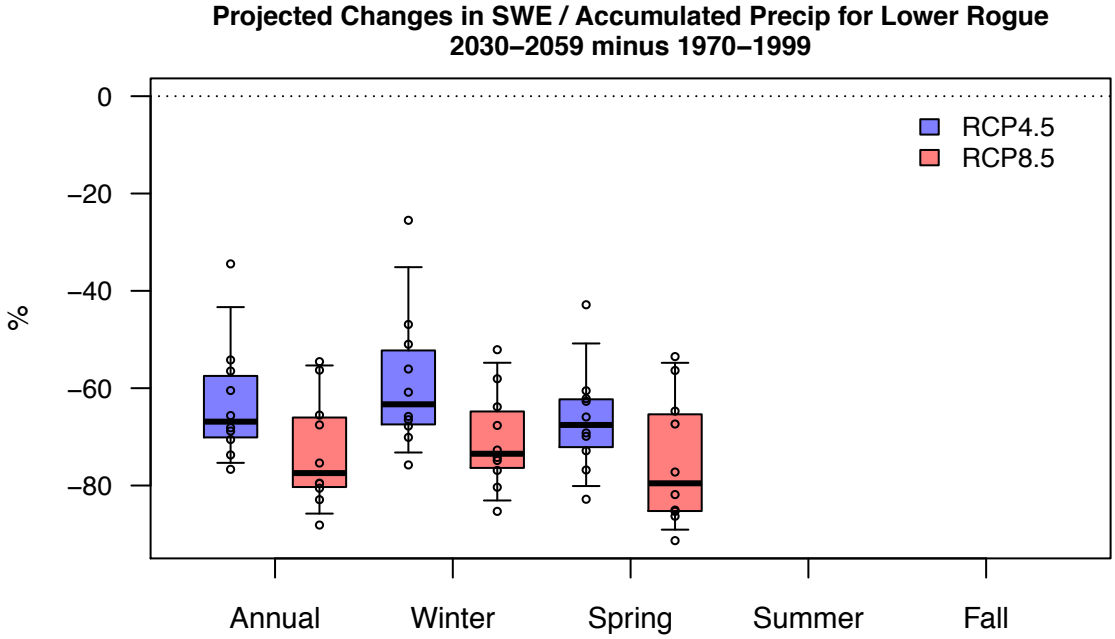

Appendix F. Projections of Future Streamflow

Figure F1. Mean annual hydrograph of daily simulated, bias-corrected, naturalized streamflow at Calapooia at Albany (CALAP 4038). for the historical period and hybrid-delta 2040s A1B and B1 future scenarios (upper panel) and change in flow from historical to future (lower panel).

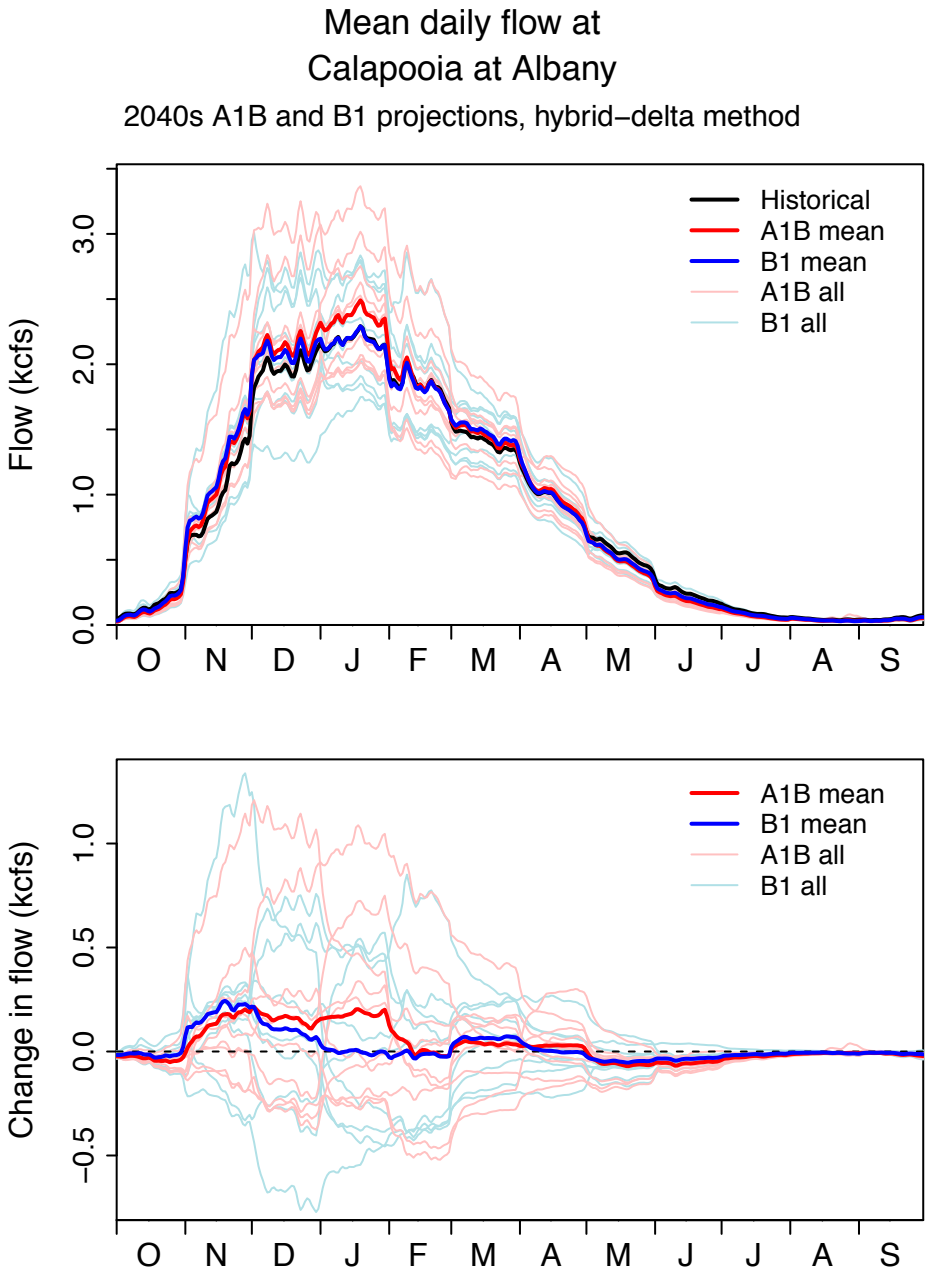

Figure F2. Mean annual hydrograph of monthly simulated, bias-corrected, naturalized streamflow at Calapooia at Albany (CALAP 4038) for the historical period and hybrid-delta 2040s A1B and B1 future scenarios (upper panel) and change in flow volume from historical to future (lower panel).

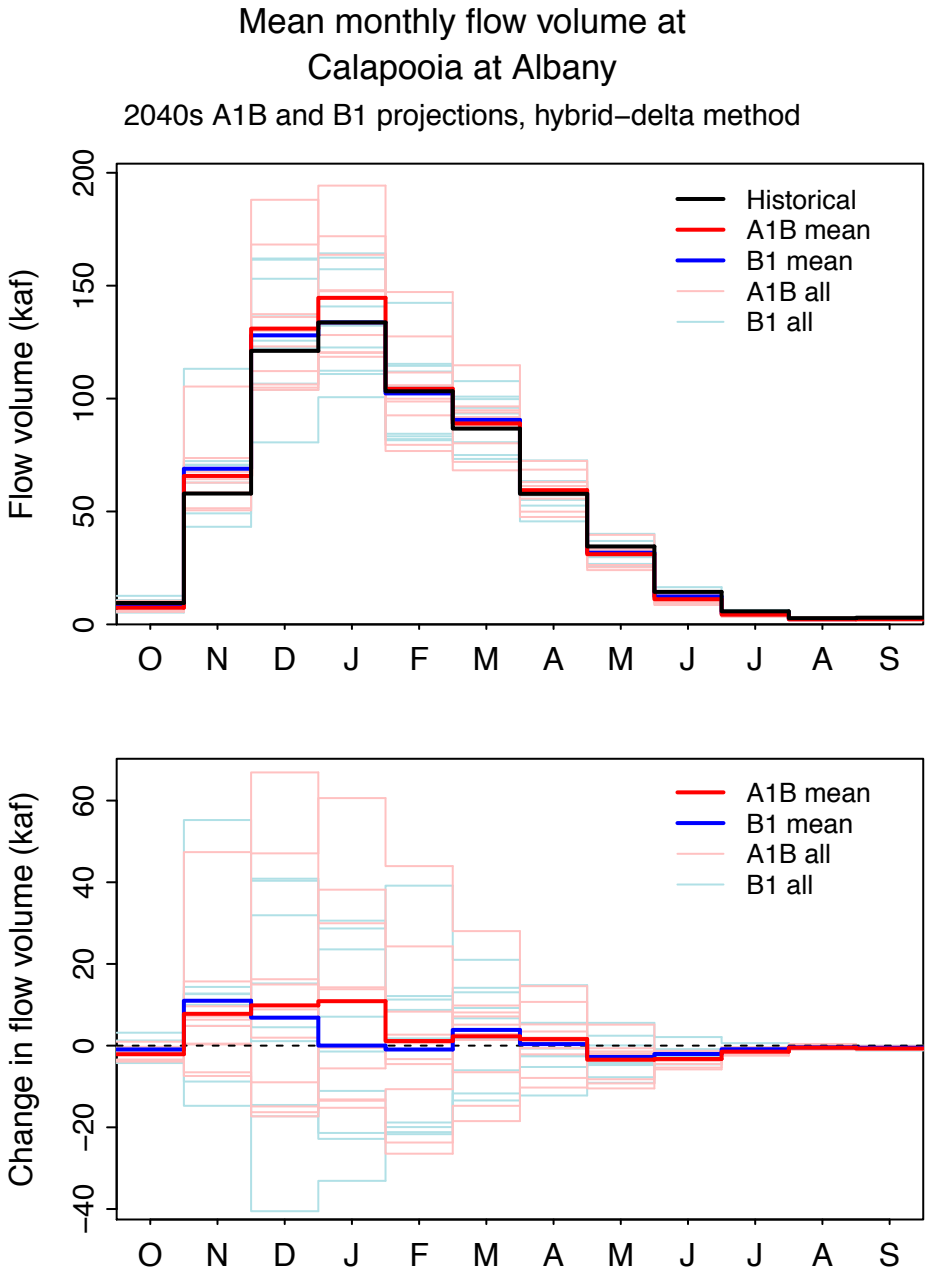

Figure F3. 5, 50, and 95th percentiles of monthly simulated, bias-corrected, naturalized streamflow at Calapooia at Albany (CALAP 4038) for the historical period and hybrid-delta 2040s A1B and B1 future scenarios.

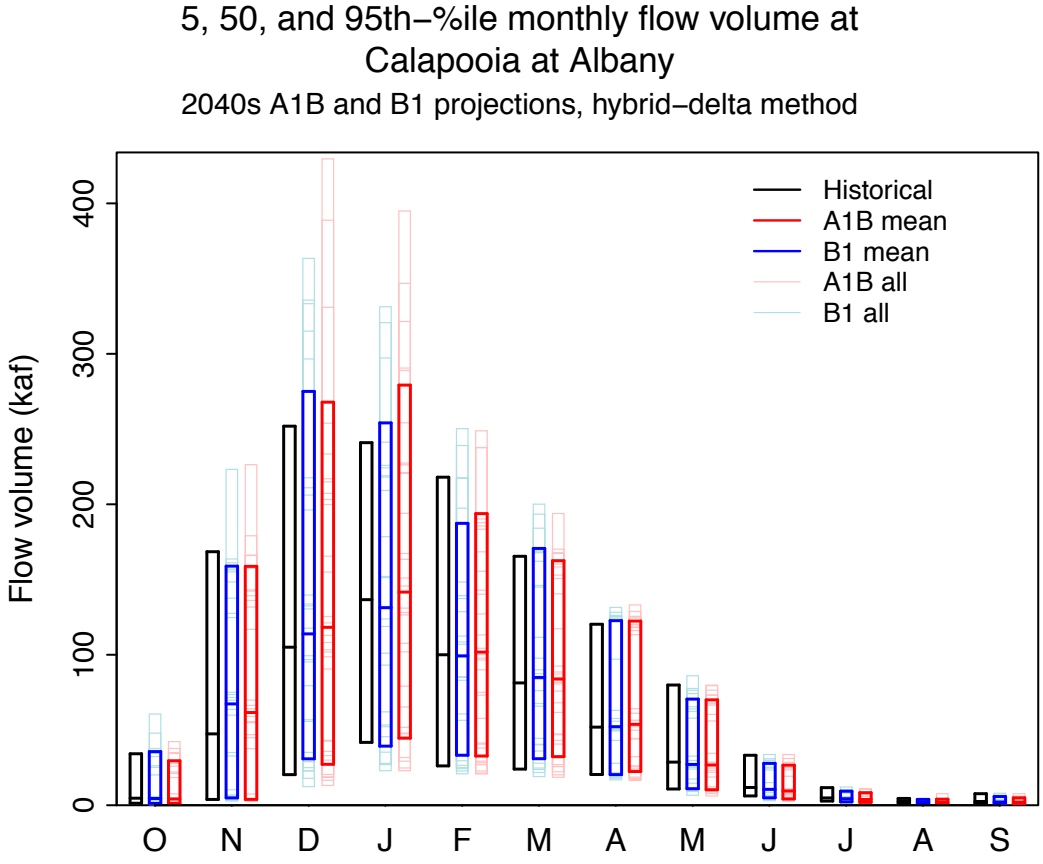

Figure F4. 5, 50, and 95th percentiles of winter (DJF) and summer (JJAS) simulated, bias-corrected, naturalized streamflow at Calapooia at Albany (CALAP 4038) for the historical period and hybrid-delta 2040s A1B and B1 future scenarios (upper panel) and change from historical to future (lower panel).

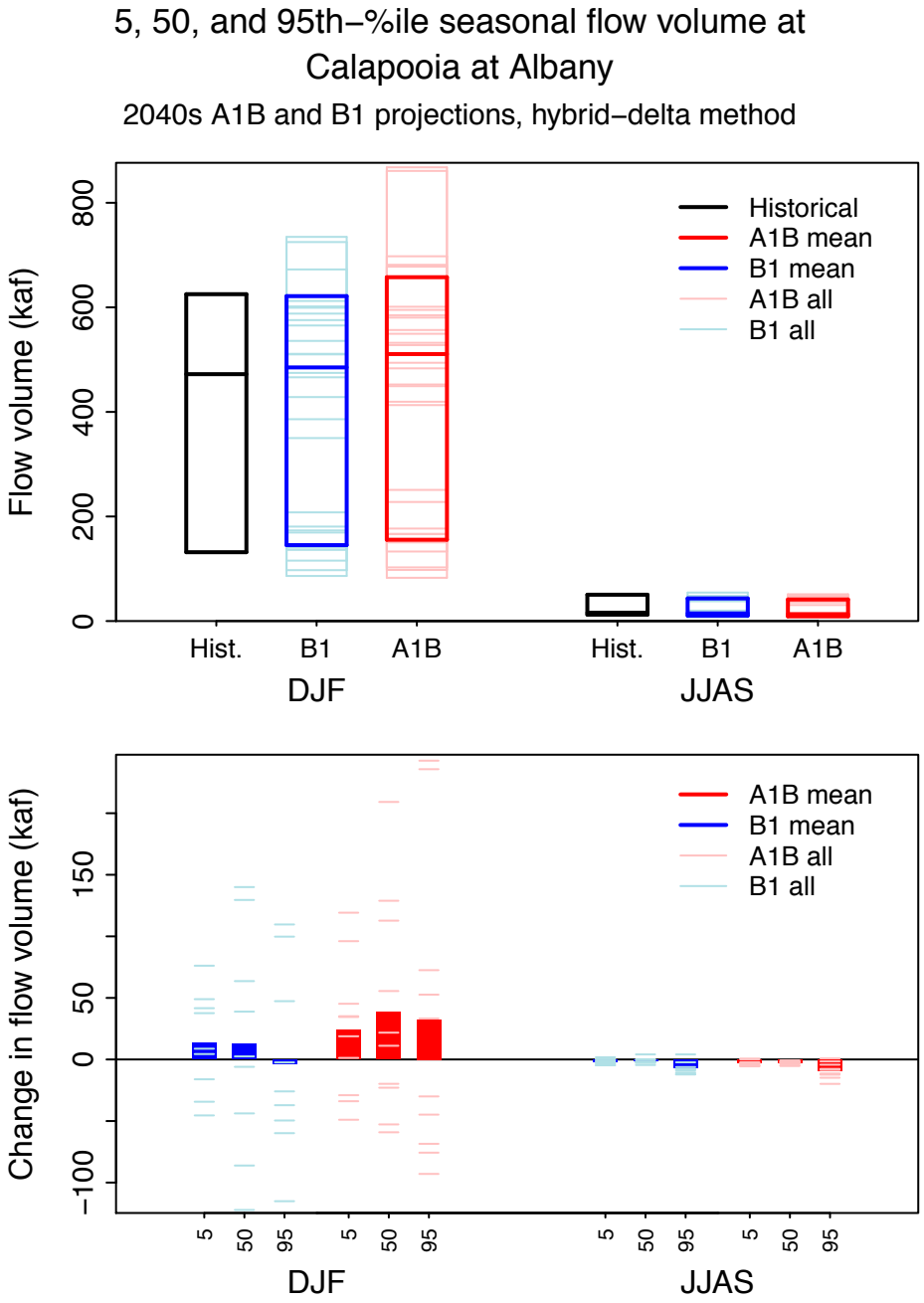

Figure F5. Mean annual hydrograph of daily simulated, bias-corrected, naturalized streamflow at Clackamas above Three Lynx Crk (CLKTH 4044). for the historical period and hybrid-delta 2040s A1B and B1 future scenarios (upper panel) and change in flow from historical to future (lower panel).

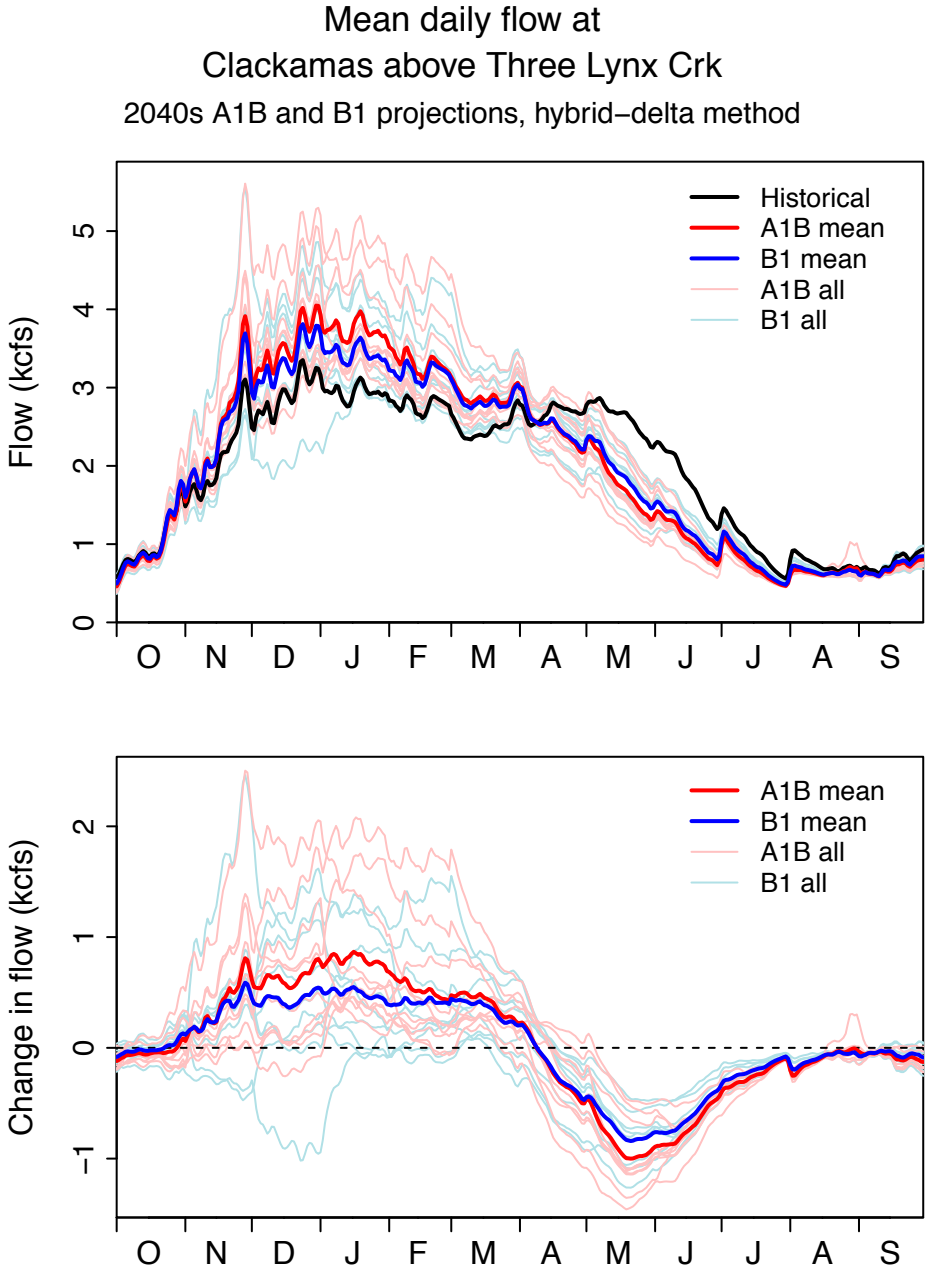

Figure F6. Mean annual hydrograph of monthly simulated, bias-corrected, naturalized streamflow at Clackamas above Three Lynx Crk (CLKTH 4044) for the historical period and hybrid-delta 2040s A1B and B1 future scenarios (upper panel) and change in flow volume from historical to future (lower panel).

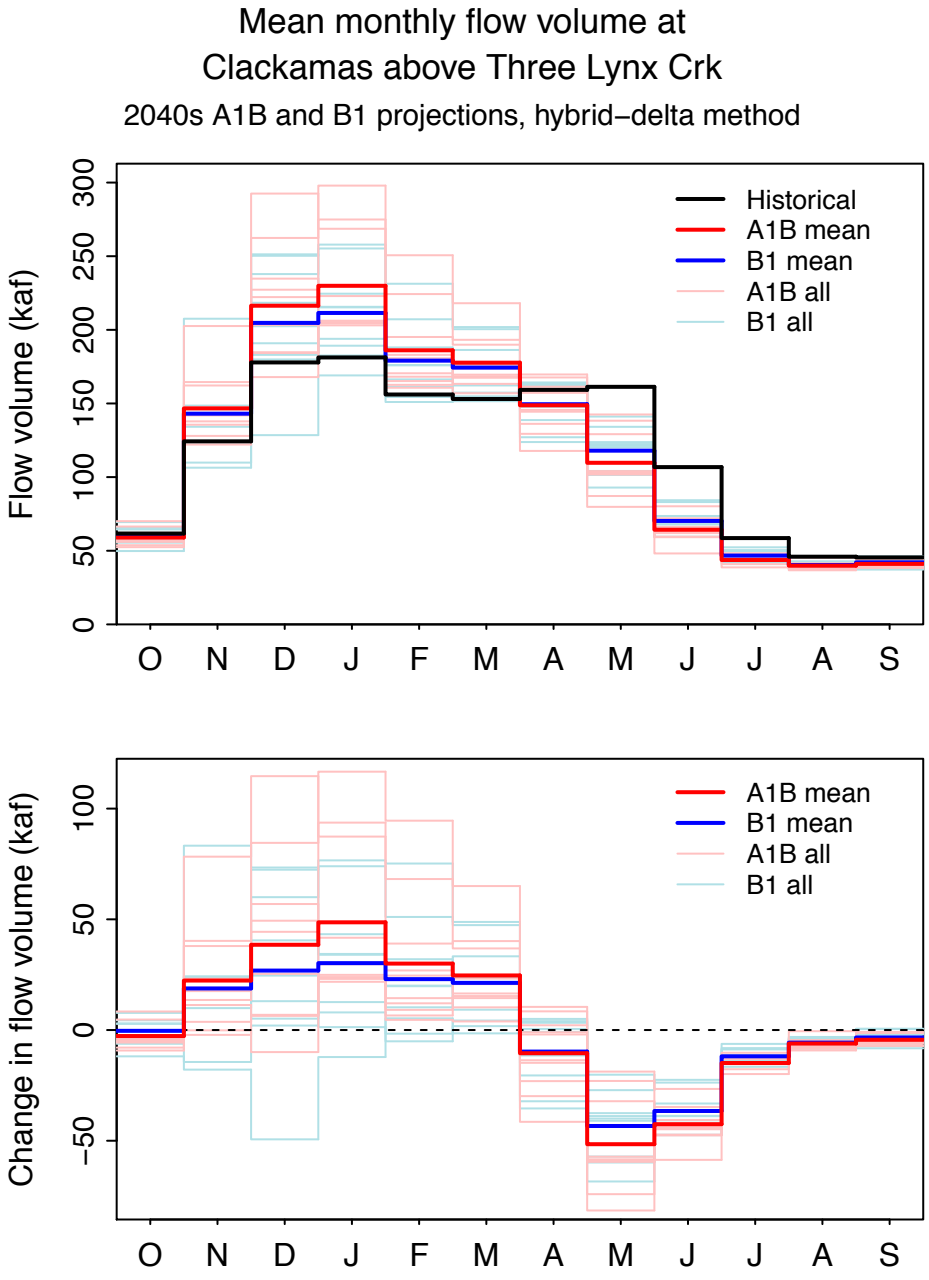

Figure F7. 5, 50, and 95th percentiles of monthly simulated, bias-corrected, naturalized streamflow at Clackamas above Three Lynx Crk (CLKTH 4044) for the historical period and hybrid-delta 2040s A1B and B1 future scenarios.

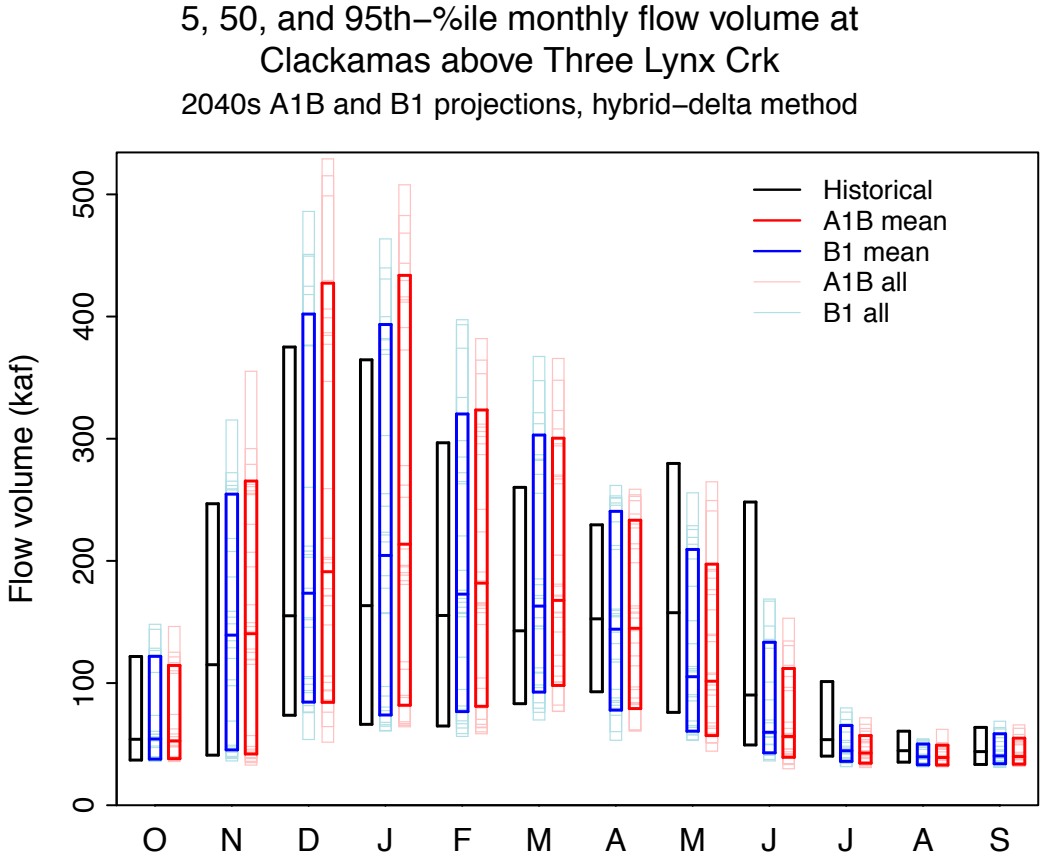

Figure F8. 5, 50, and 95th percentiles of winter (DJF) and summer (JJAS) simulated, bias-corrected, naturalized streamflow at Clackamas above Three Lynx Crk (CLKTH 4044) for the historical period and hybrid-delta 2040s A1B and B1 future scenarios (upper panel) and change from historical to future (lower panel).

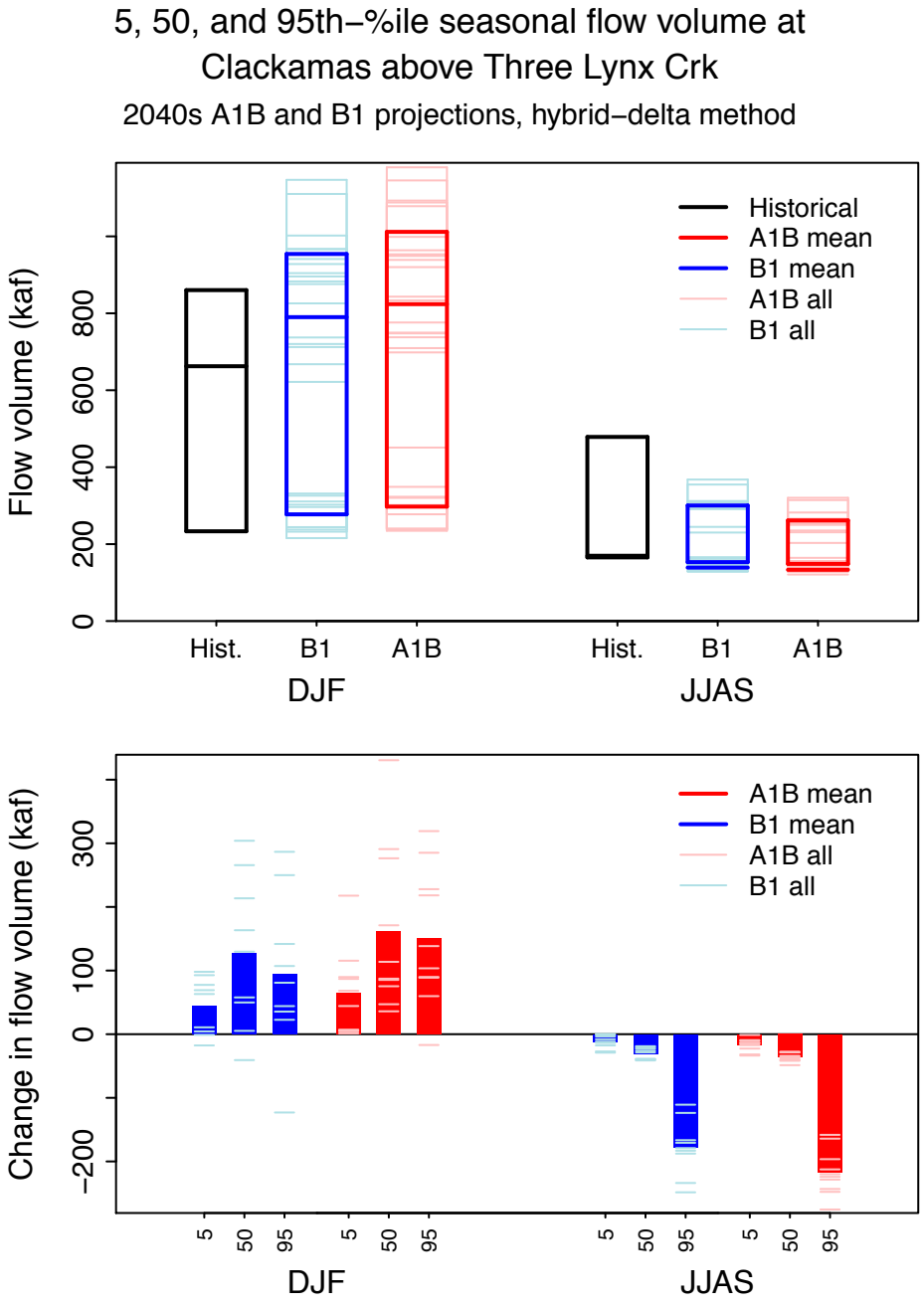

Figure F9. Mean annual hydrograph of daily simulated, bias-corrected, naturalized streamflow at McKenzie nr Vida (MCKVI 4036). for the historical period and hybrid-delta 2040s A1B and B1 future scenarios (upper panel) and change in flow from historical to future (lower panel).

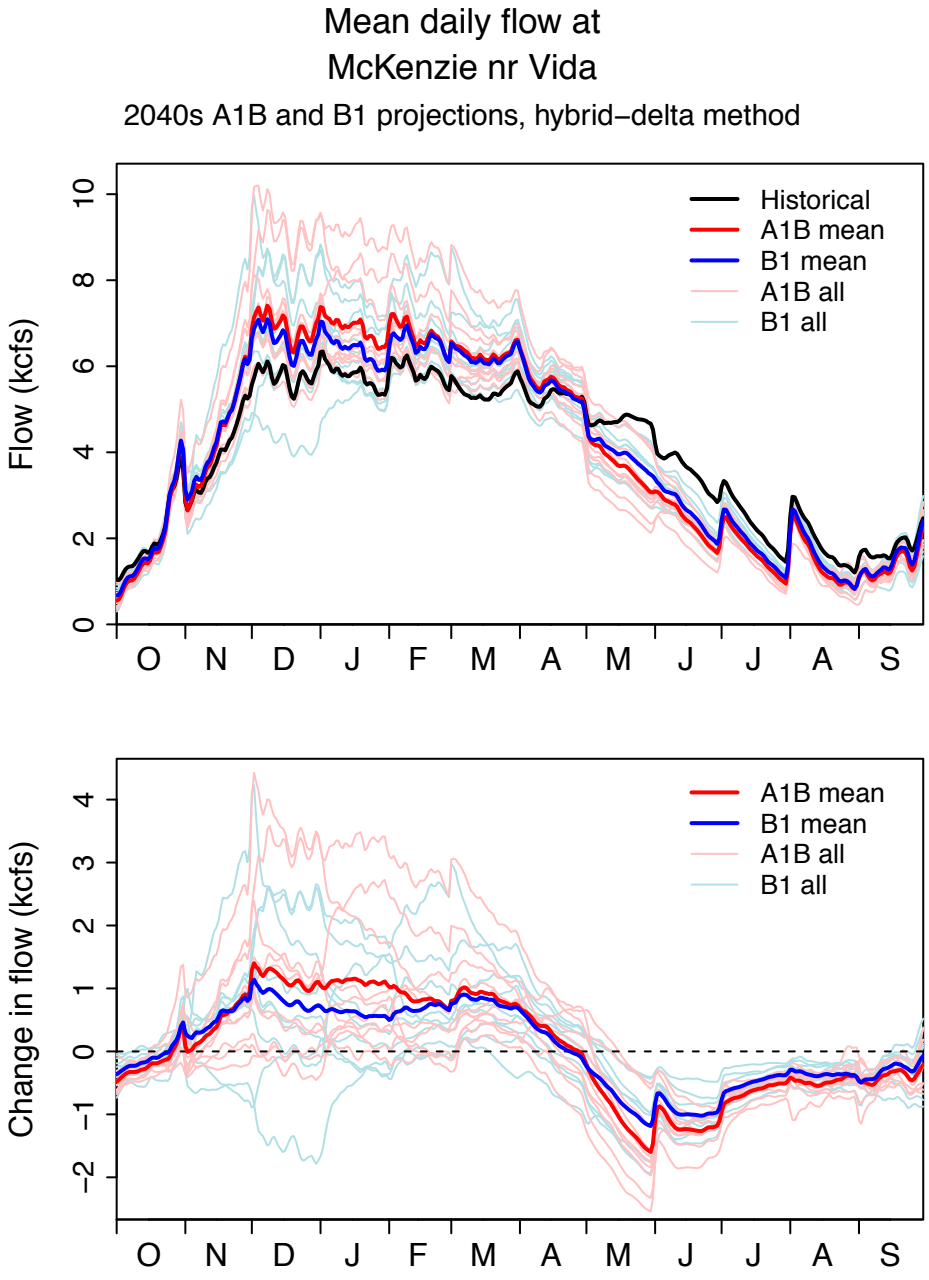

Figure F10. Mean annual hydrograph of monthly simulated, bias-corrected, naturalized streamflow at McKenzie nr Vida (MCKVI 4036) for the historical period and hybrid-delta 2040s A1B and B1 future scenarios (upper panel) and change in flow volume from historical to future (lower panel).

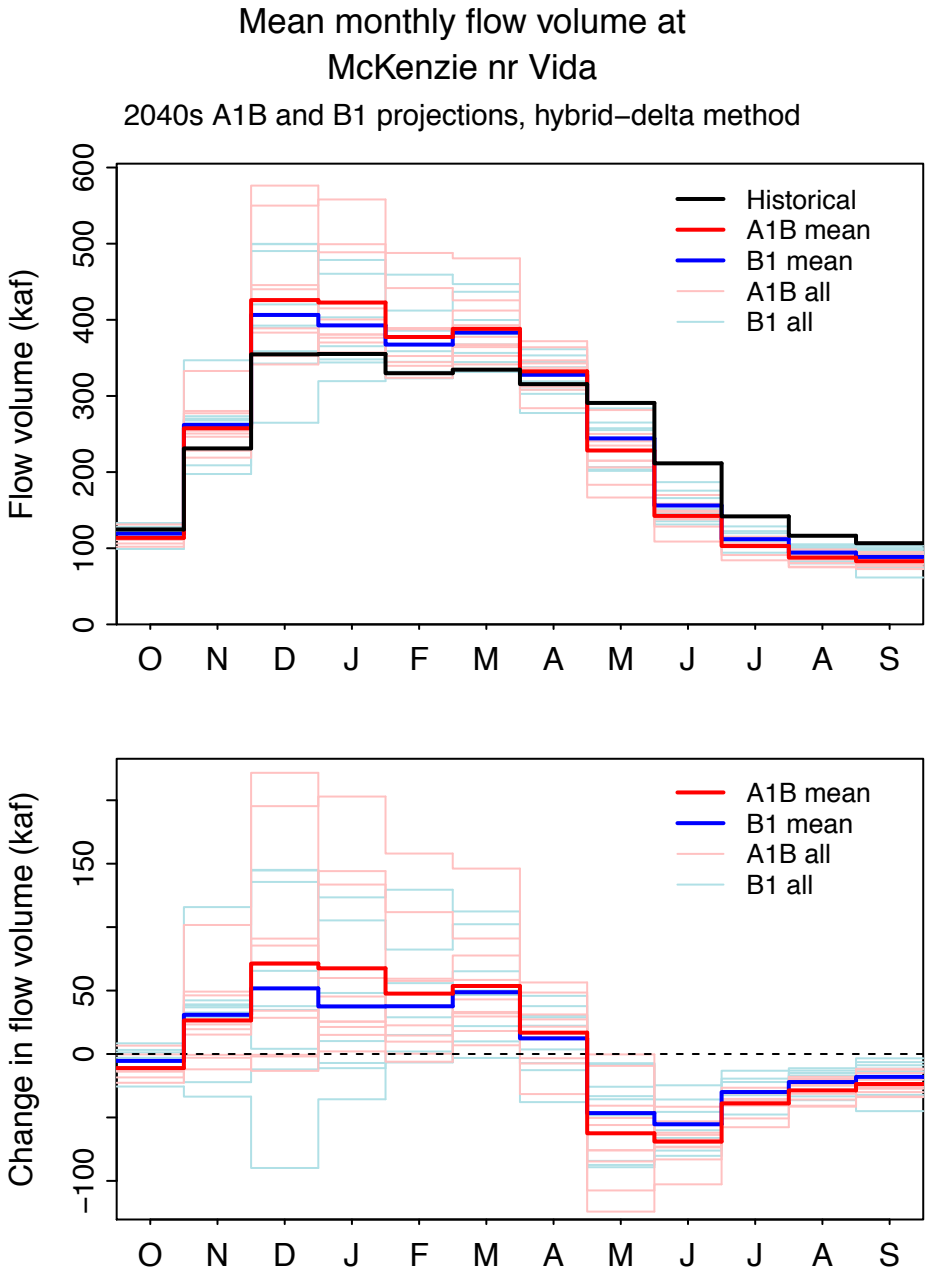

Figure F11. 5, 50, and 95th percentiles of monthly simulated, bias-corrected, naturalized streamflow at McKenzie nr Vida (MCKVI 4036) for the historical period and hybrid-delta 2040s A1B and B1 future scenarios.

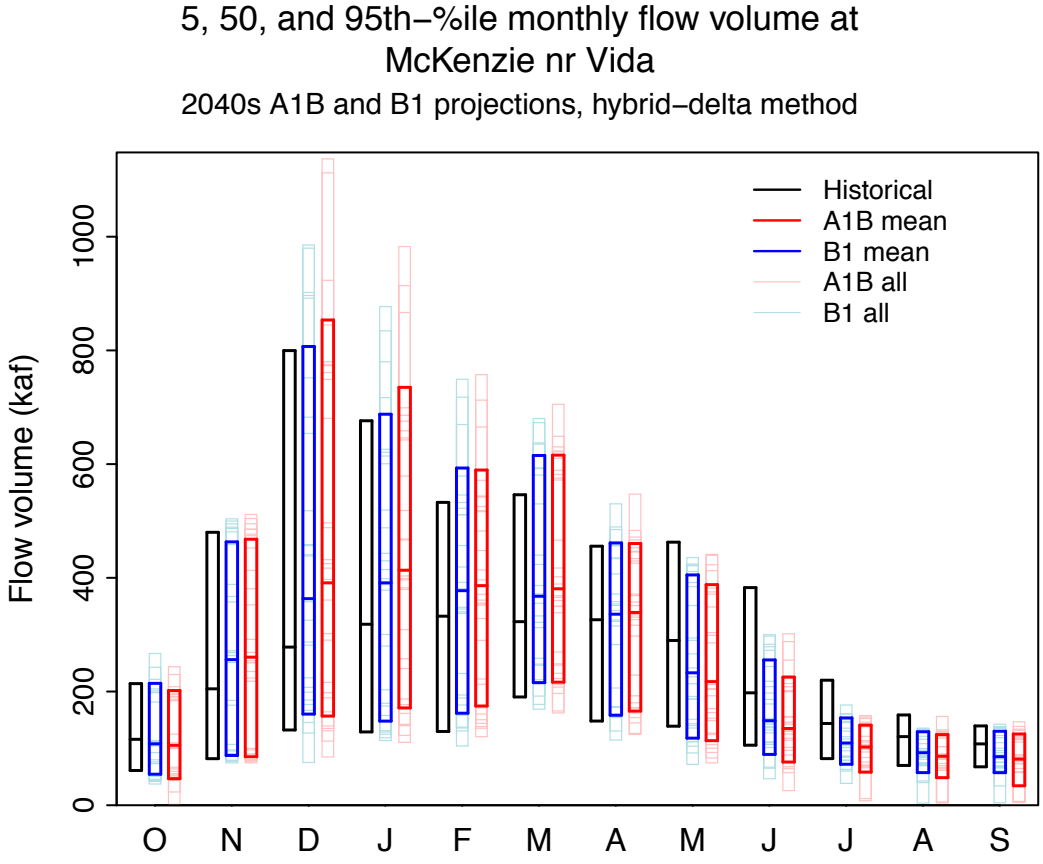

Figure F12. 5, 50, and 95th percentiles of winter (DJF) and summer (JJAS) simulated, bias-corrected, naturalized streamflow at McKenzie nr Vida (MCKVI 4036) for the historical period and hybrid-delta 2040s A1B and B1 future scenarios (upper panel) and change from historical to future (lower panel).

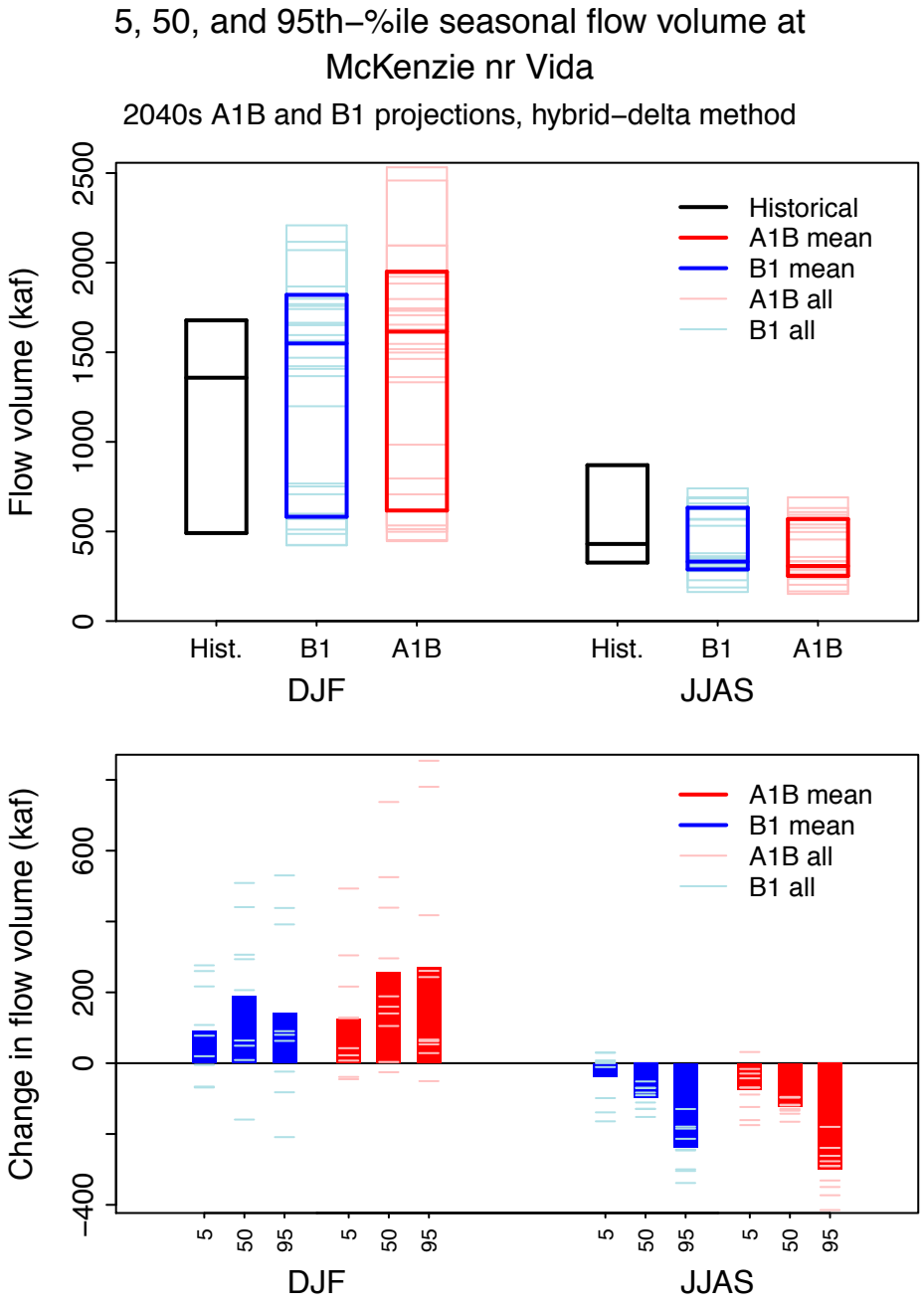

Figure F13. Mean annual hydrograph of daily simulated, bias-corrected, naturalized streamflow at Molalla nr Canby (MOLAL 4043). for the historical period and hybrid-delta 2040s A1B and B1 future scenarios (upper panel) and change in flow from historical to future (lower panel).

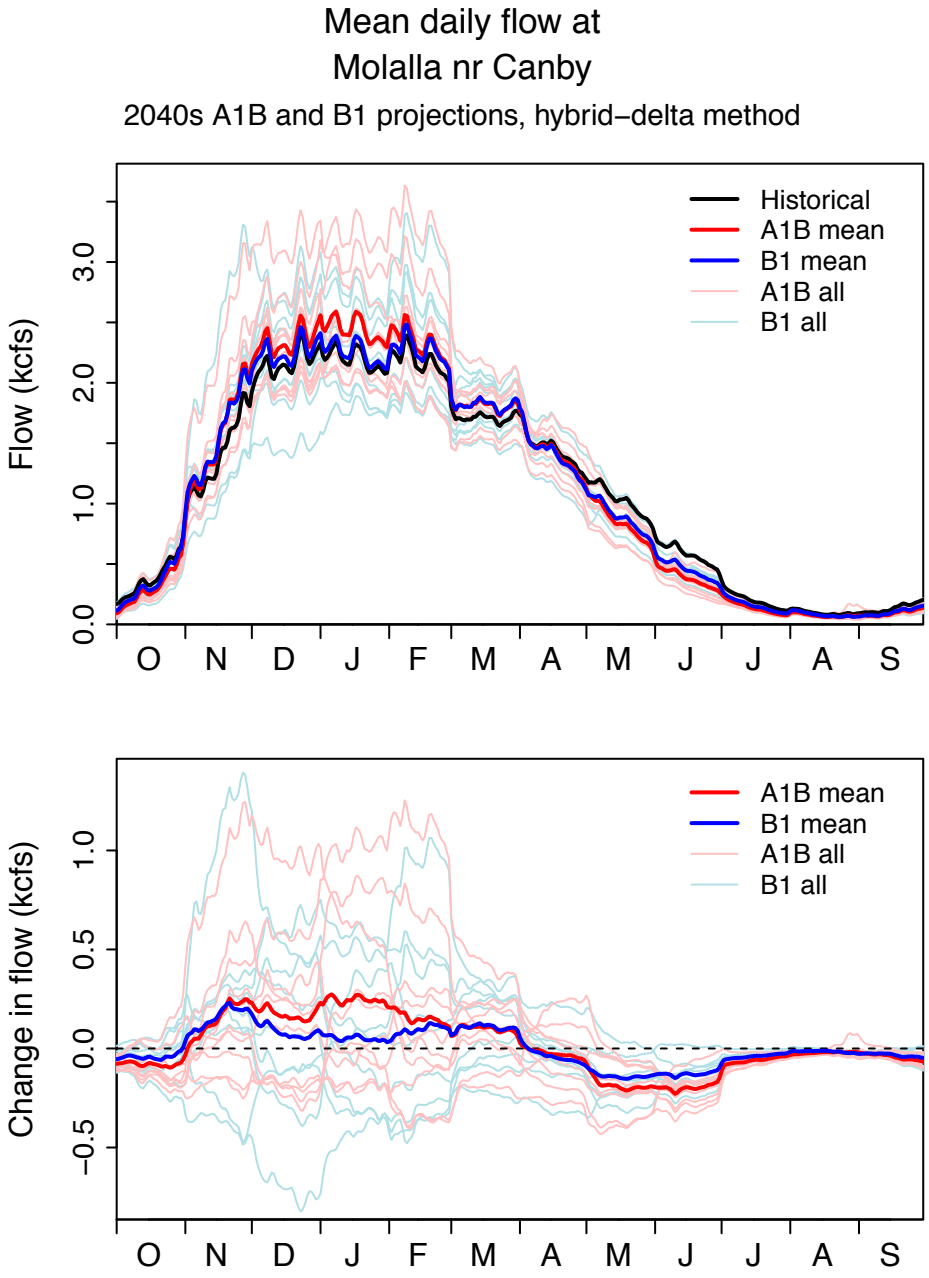

Figure F14. Mean annual hydrograph of monthly simulated, bias-corrected, naturalized streamflow at Molalla nr Canby (MOLAL 4043) for the historical period and hybrid-delta 2040s A1B and B1 future scenarios (upper panel) and change in flow volume from historical to future (lower panel).

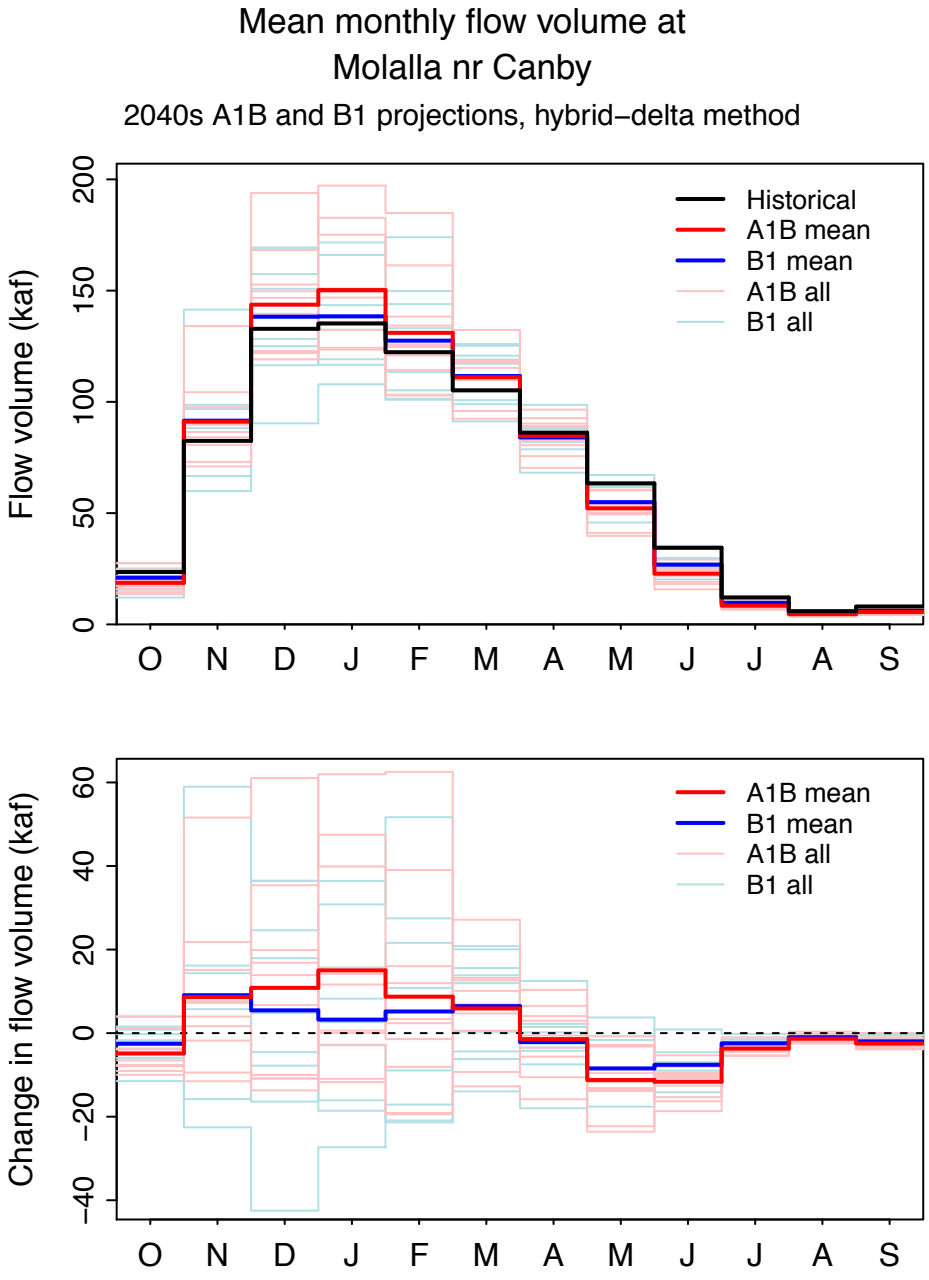

Figure F15. 5, 50, and 95th percentiles of monthly simulated, bias-corrected, naturalized streamflow at Molalla nr Canby (MOLAL 4043) for the historical period and hybrid-delta 2040s A1B and B1 future scenarios.

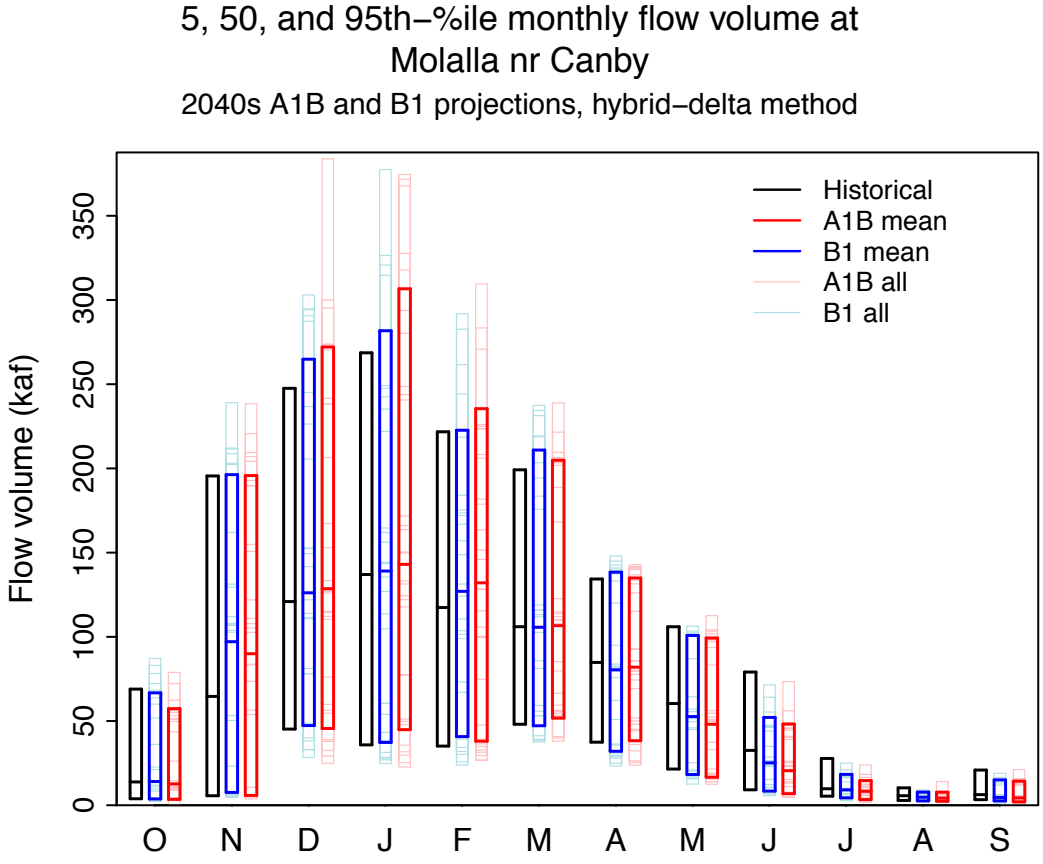

Figure F16. 5, 50, and 95th percentiles of winter (DJF) and summer (JJAS) simulated, bias-corrected, naturalized streamflow at Molalla nr Canby (MOLAL 4043) for the historical period and hybrid-delta 2040s A1B and B1 future scenarios (upper panel) and change from historical to future (lower panel).

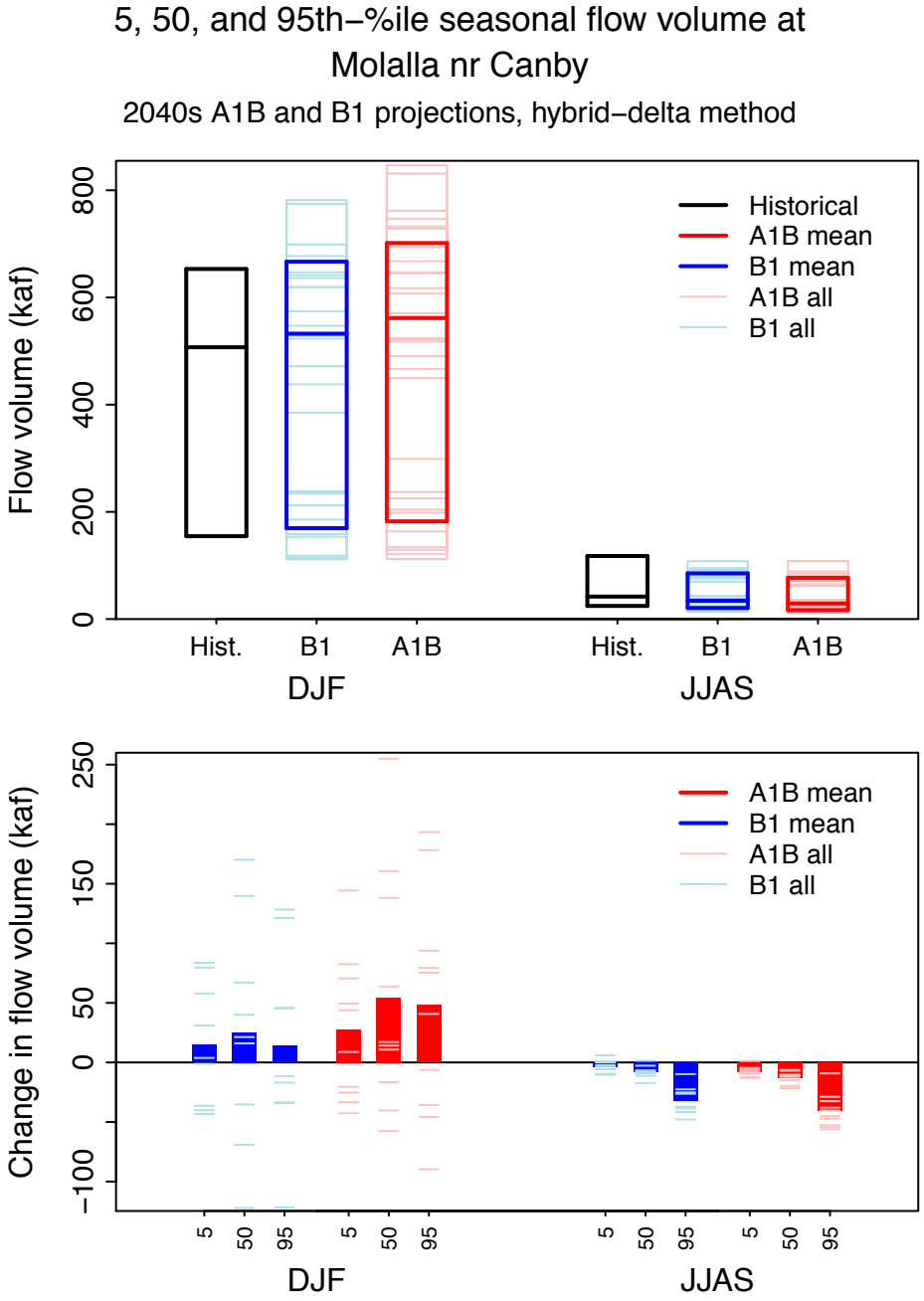

Figure F17. Mean annual hydrograph of daily simulated, bias-corrected, naturalized streamflow at N Santiam blw Boulder Crk nr Detroit (NOSAN 4056). for the historical period and hybrid-delta 2040s A1B and B1 future scenarios (upper panel) and change in flow from historical to future (lower panel).

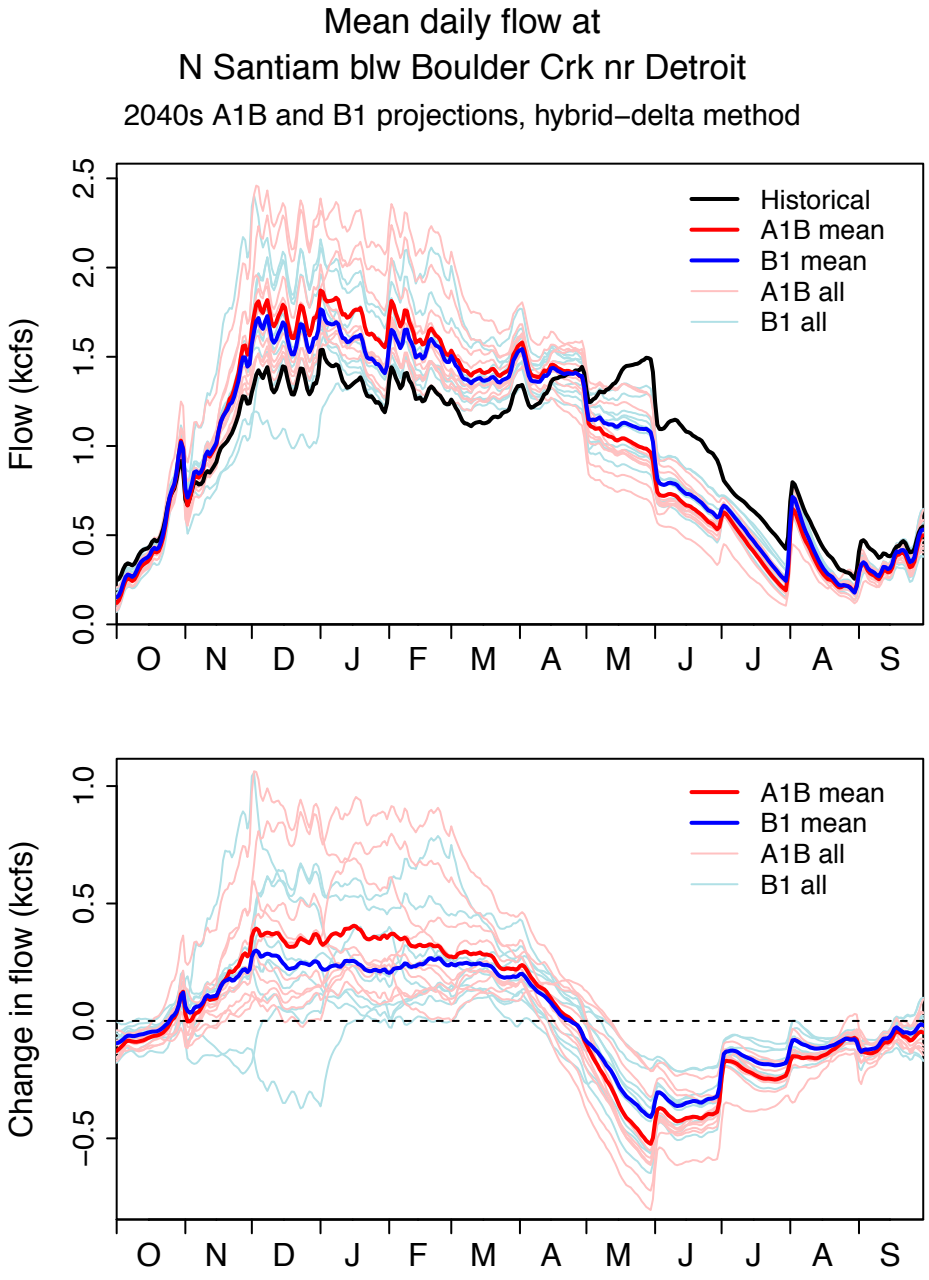

Figure F18. Mean annual hydrograph of monthly simulated, bias-corrected, naturalized streamflow at N Santiam blw Boulder Crk nr Detroit (NOSAN 4056) for the historical period and hybrid-delta 2040s A1B and B1 future scenarios (upper panel) and change in flow volume from historical to future (lower panel).

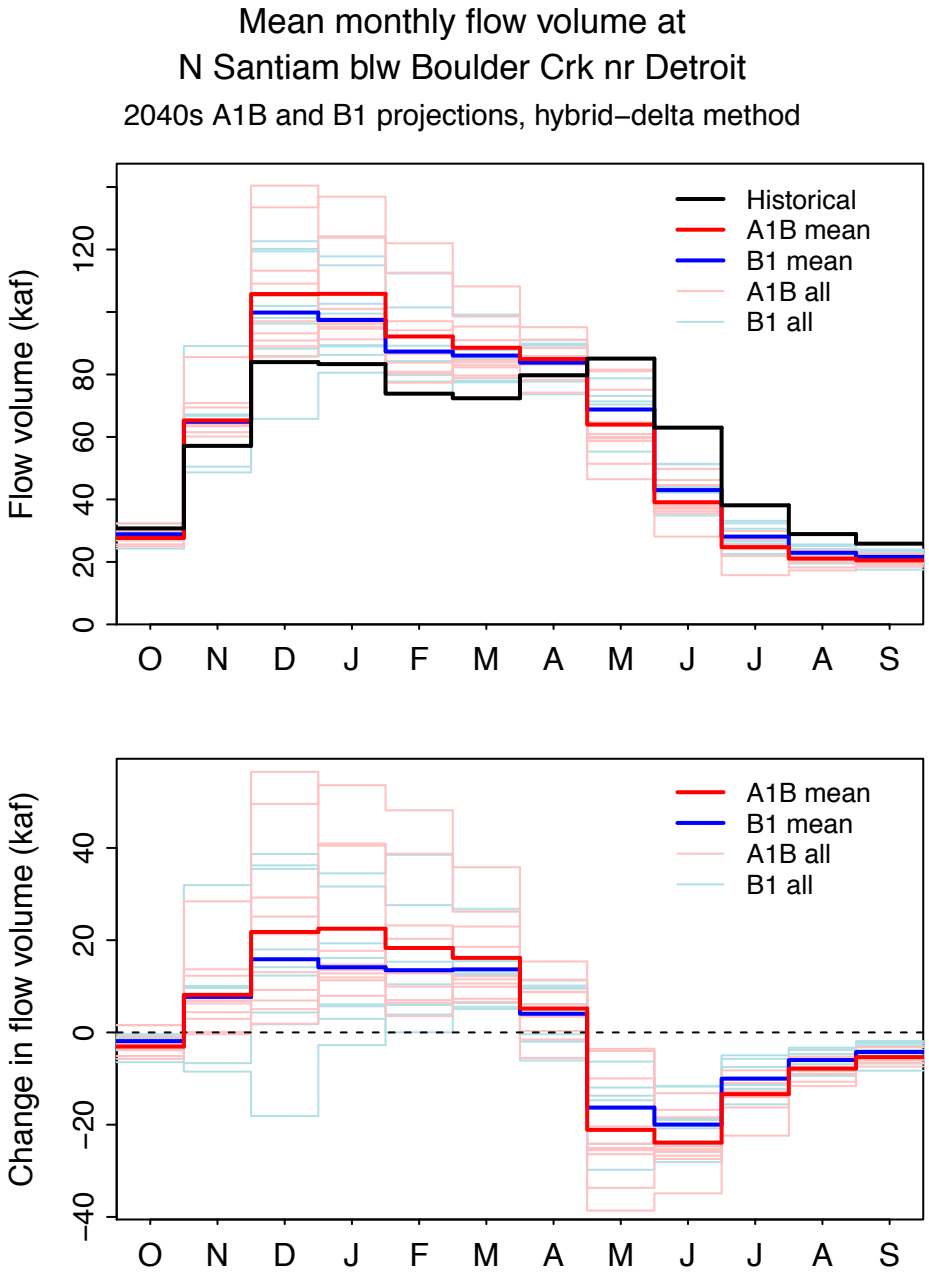

Figure F19. 5, 50, and 95th percentiles of monthly simulated, bias-corrected, naturalized streamflow at N Santiam blw Boulder Crk nr Detroit (NOSAN 4056) for the historical period and hybrid-delta 2040s A1B and B1 future scenarios.

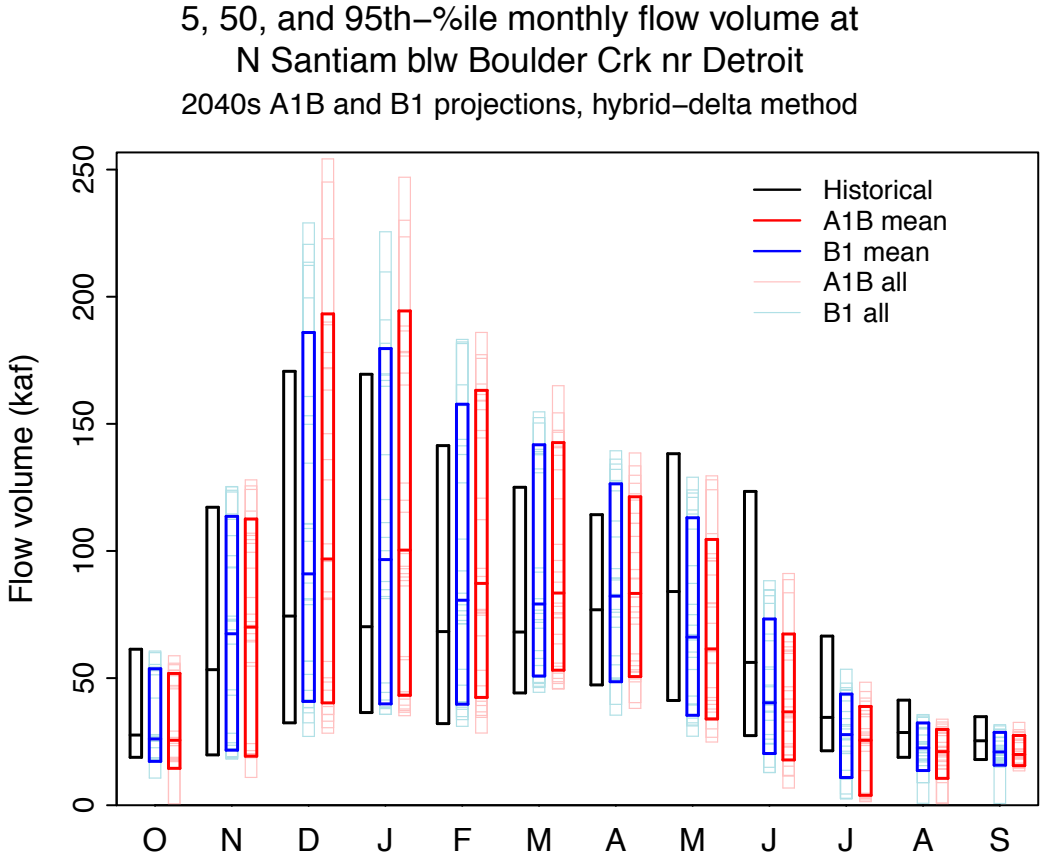

Figure F20. 5, 50, and 95th percentiles of winter (DJF) and summer (JJAS) simulated, bias-corrected, naturalized streamflow at N Santiam blw Boulder Crk nr Detroit (NOSAN 4056) for the historical period and hybrid-delta 2040s A1B and B1 future scenarios (upper panel) and change from historical to future (lower panel).

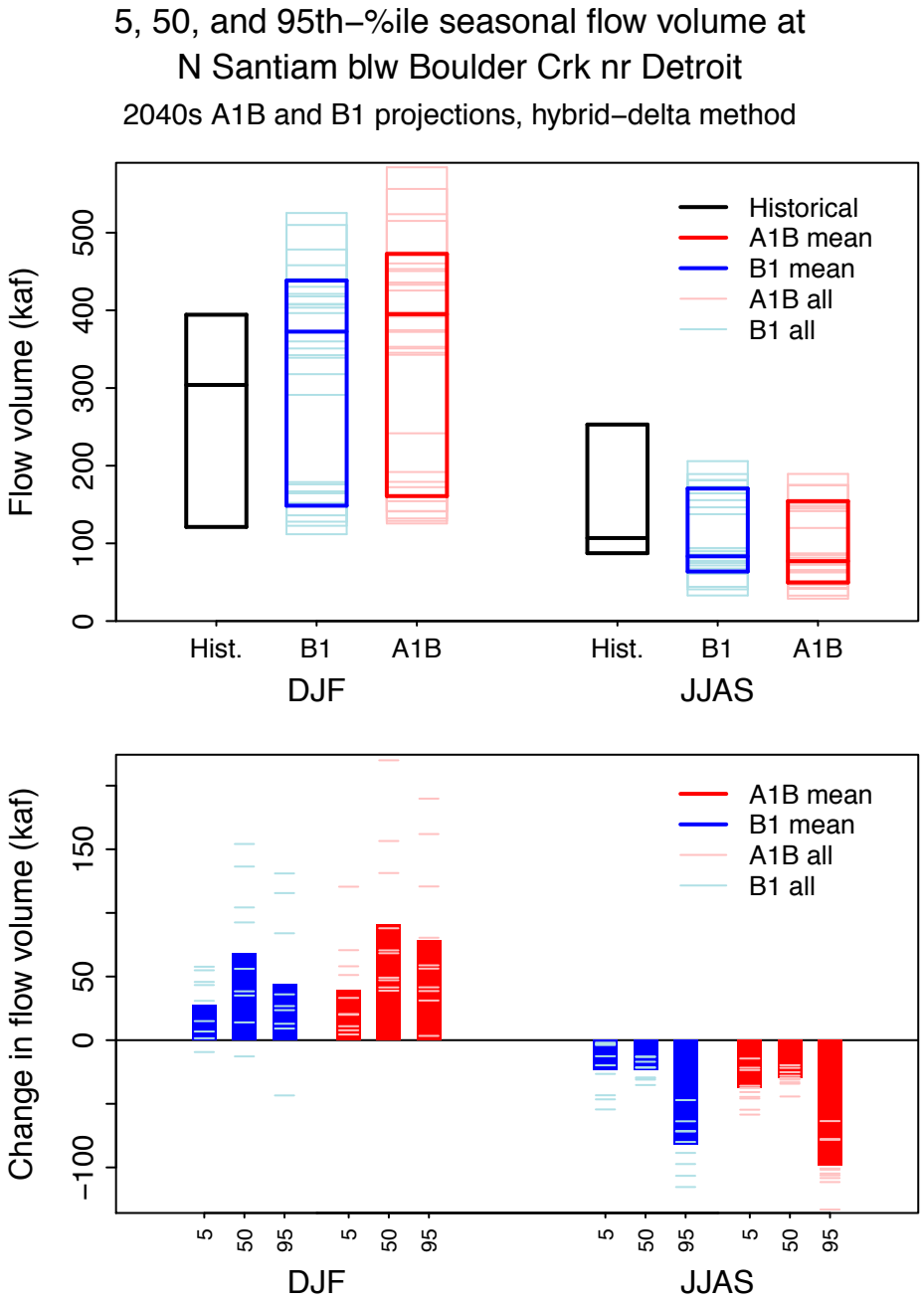

Figure F21. Mean annual hydrograph of daily simulated, bias-corrected, naturalized streamflow at Clackamas at River Mill Dam (RMILL 4046). for the historical period and hybrid-delta 2040s A1B and B1 future scenarios (upper panel) and change in flow from historical to future (lower panel).

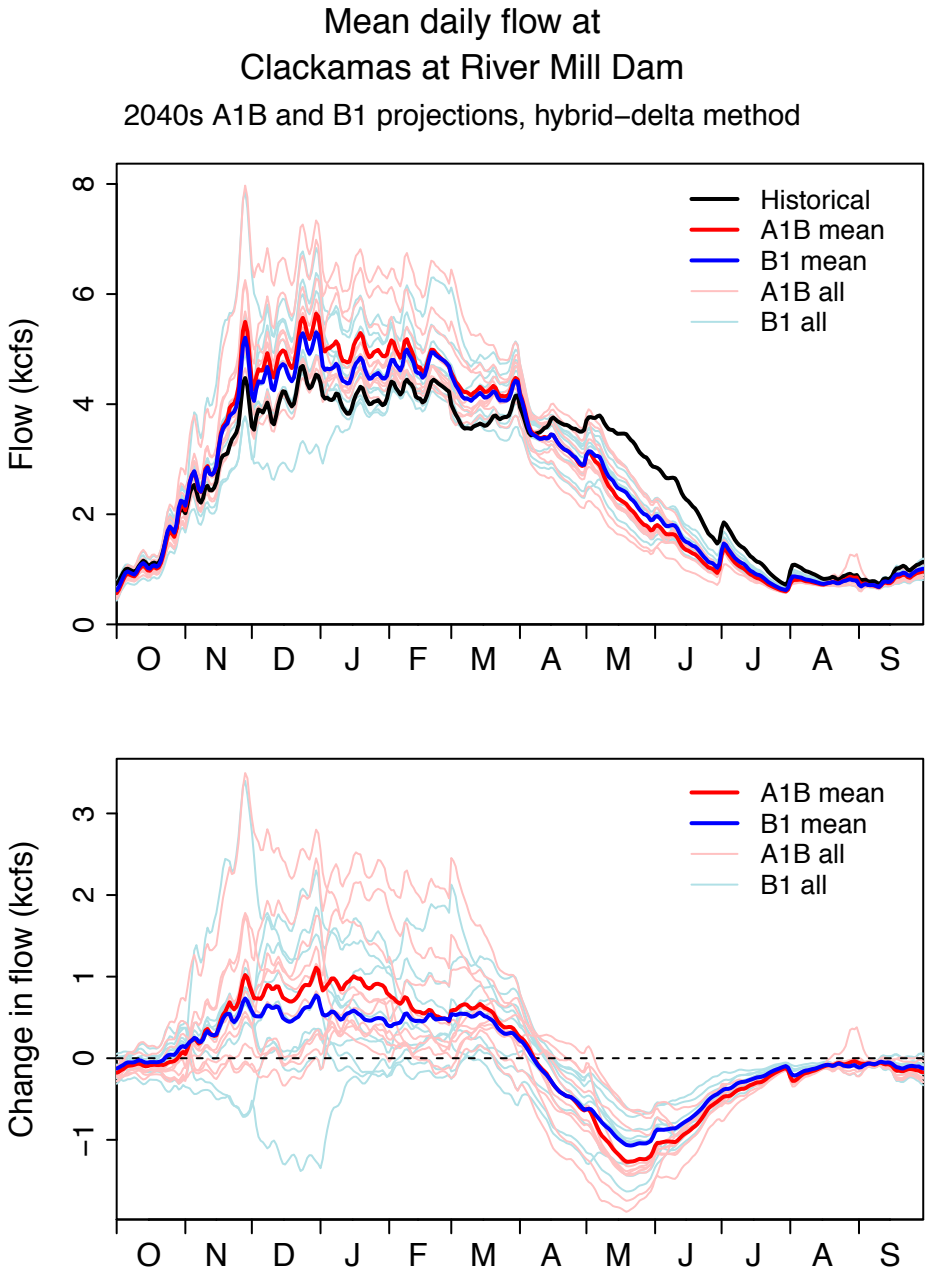

Figure F22. Mean annual hydrograph of monthly simulated, bias-corrected, naturalized streamflow at Clackamas at River Mill Dam (RMILL 4046) for the historical period and hybrid-delta 2040s A1B and B1 future scenarios (upper panel) and change in flow volume from historical to future (lower panel).

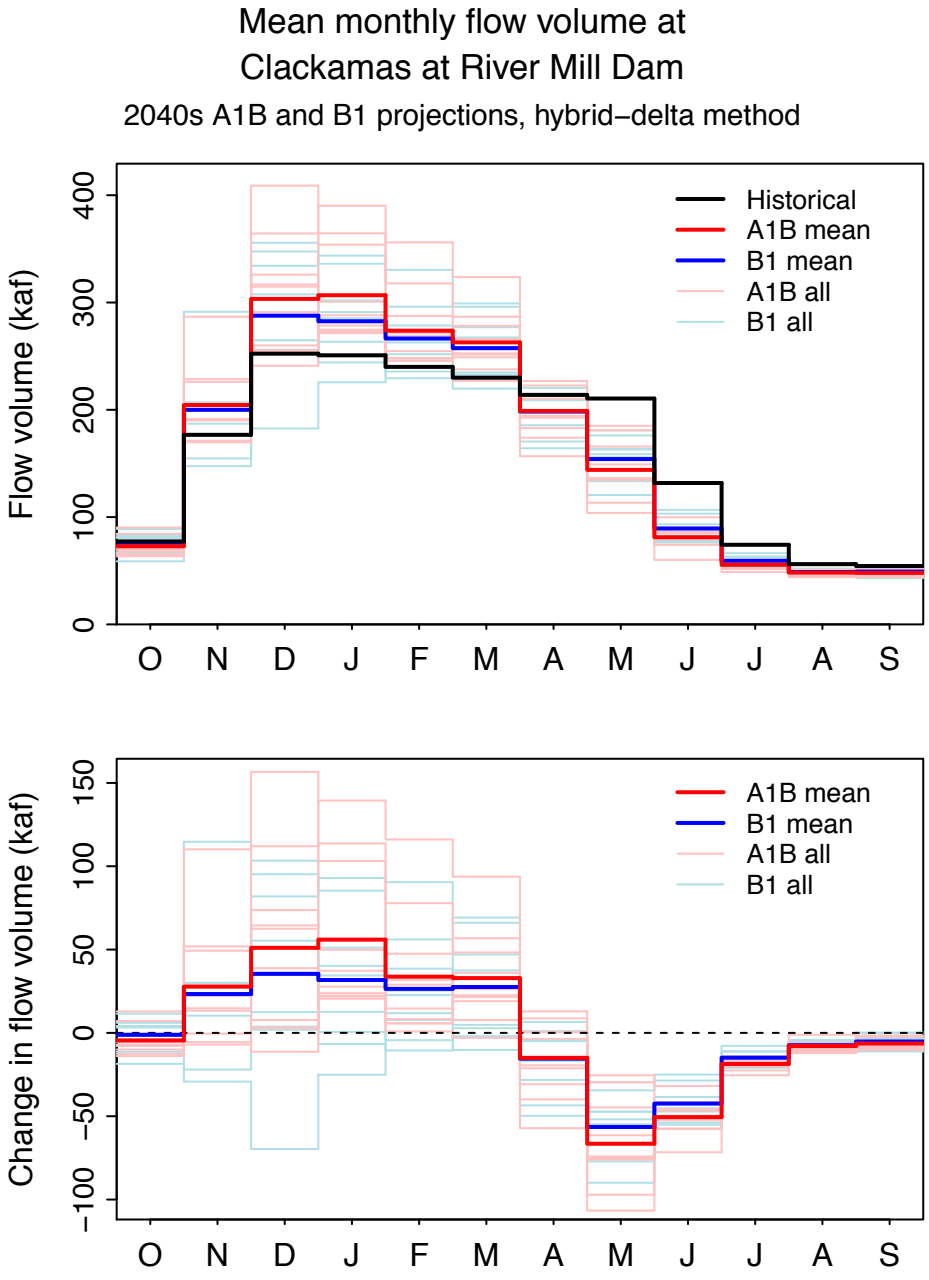

Figure F23. 5, 50, and 95th percentiles of monthly simulated, bias-corrected, naturalized streamflow at Clackamas at River Mill Dam (RMILL 4046) for the historical period and hybrid-delta 2040s A1B and B1 future scenarios.

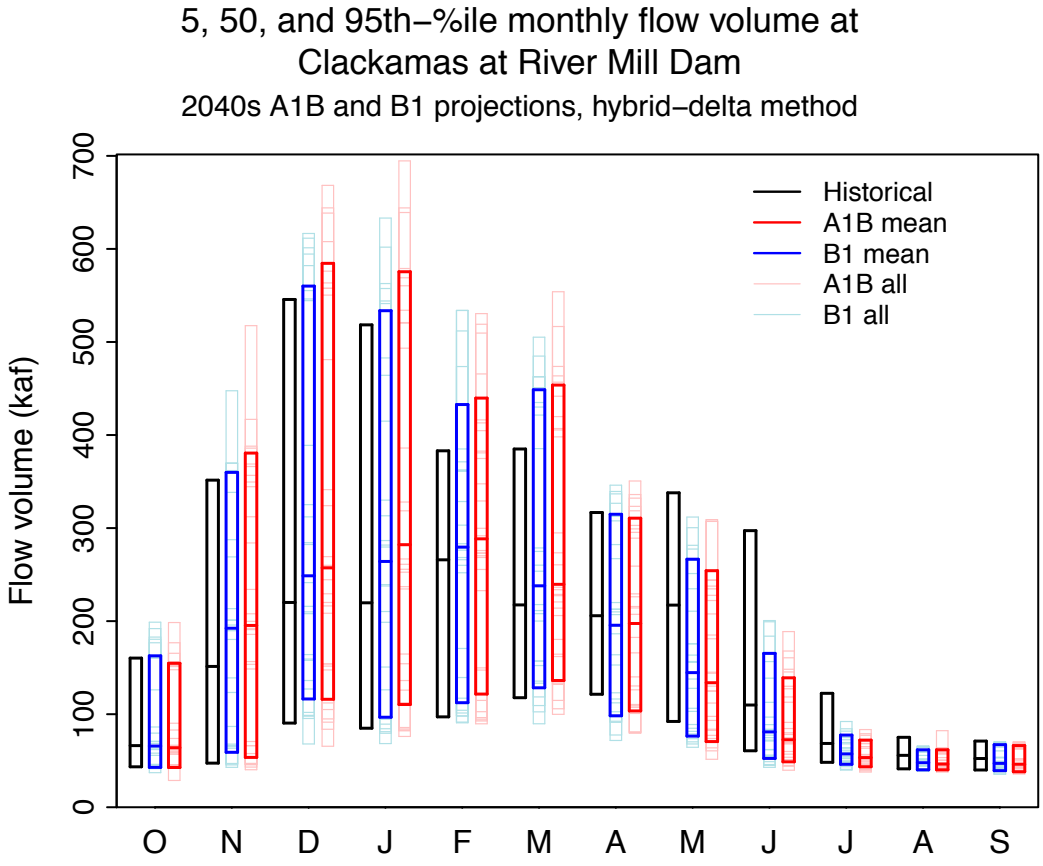

Figure F24. 5, 50, and 95th percentiles of winter (DJF) and summer (JJAS) simulated, bias-corrected, naturalized streamflow at Clackamas at River Mill Dam (RMILL 4046) for the historical period and hybrid-delta 2040s A1B and B1 future scenarios (upper panel) and change from historical to future (lower panel).

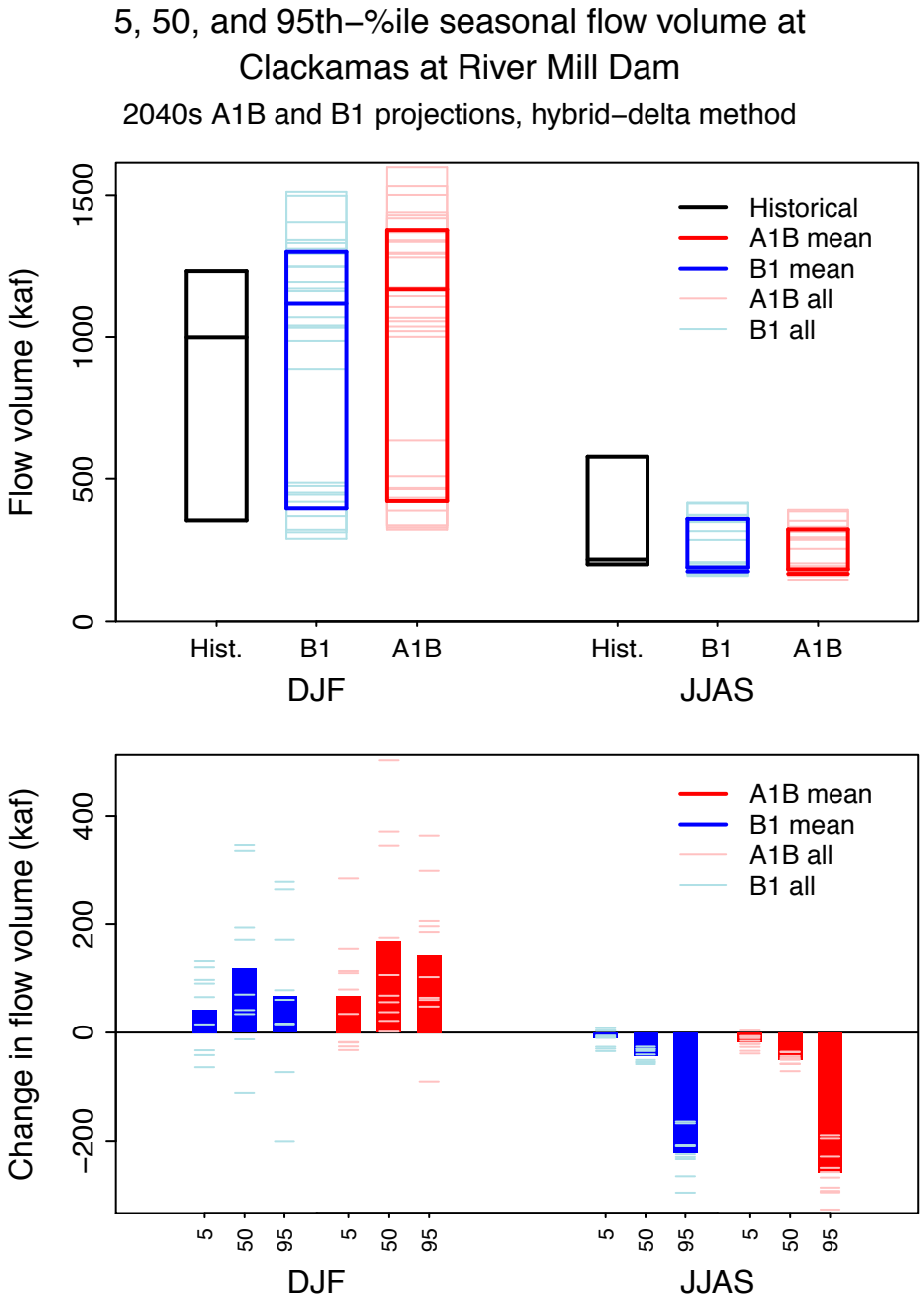

Figure F25. Mean annual hydrograph of daily simulated, bias-corrected, naturalized streamflow at Row above Pitcher Crk nr Dorena (ROPIT 4035). for the historical period and hybrid-delta 2040s A1B and B1 future scenarios (upper panel) and change in flow from historical to future (lower panel).

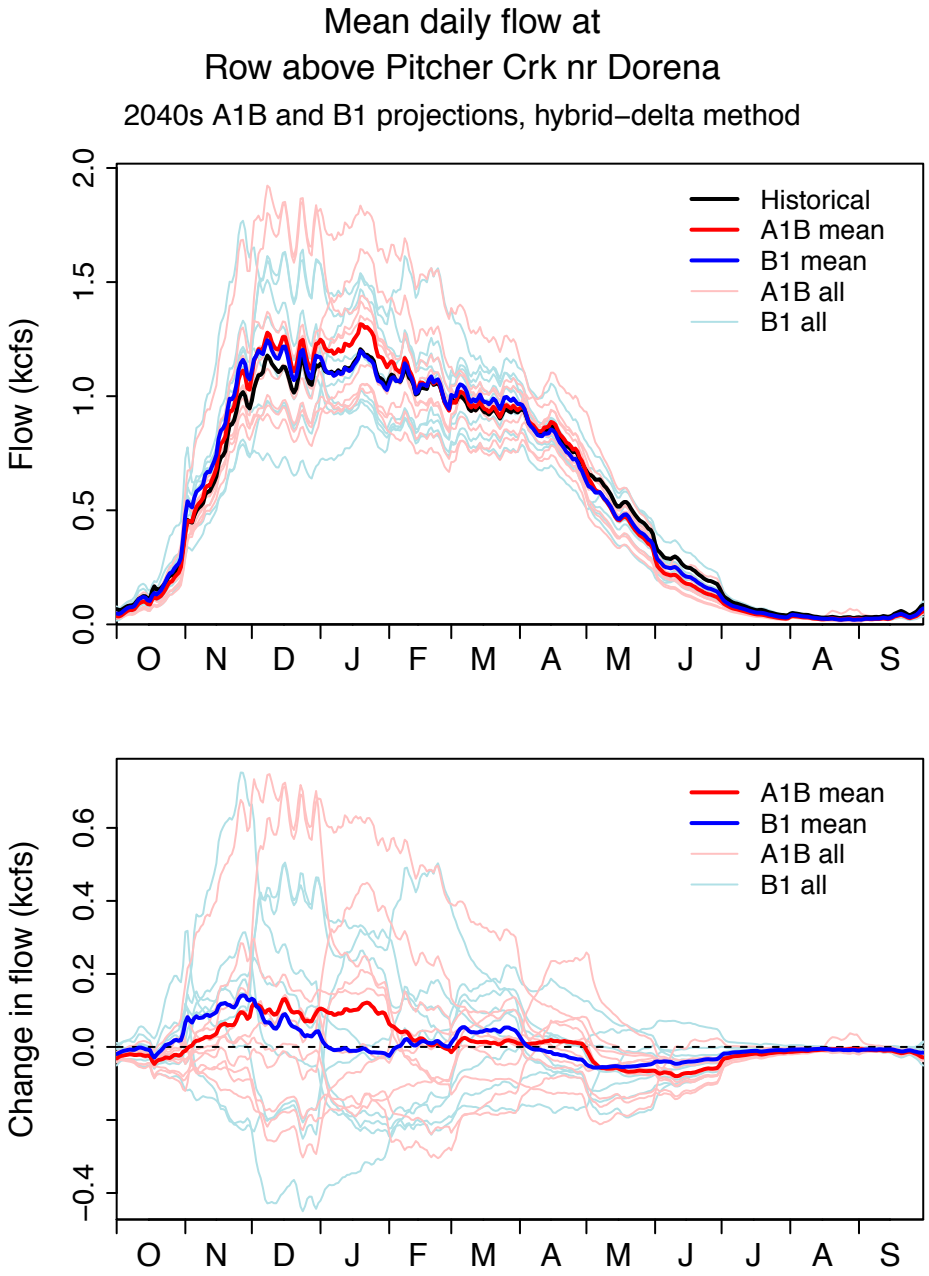

Figure F26. Mean annual hydrograph of monthly simulated, bias-corrected, naturalized streamflow at Row above Pitcher Crk nr Dorena (ROPIT 4035) for the historical period and hybrid-delta 2040s A1B and B1 future scenarios (upper panel) and change in flow volume from historical to future (lower panel).

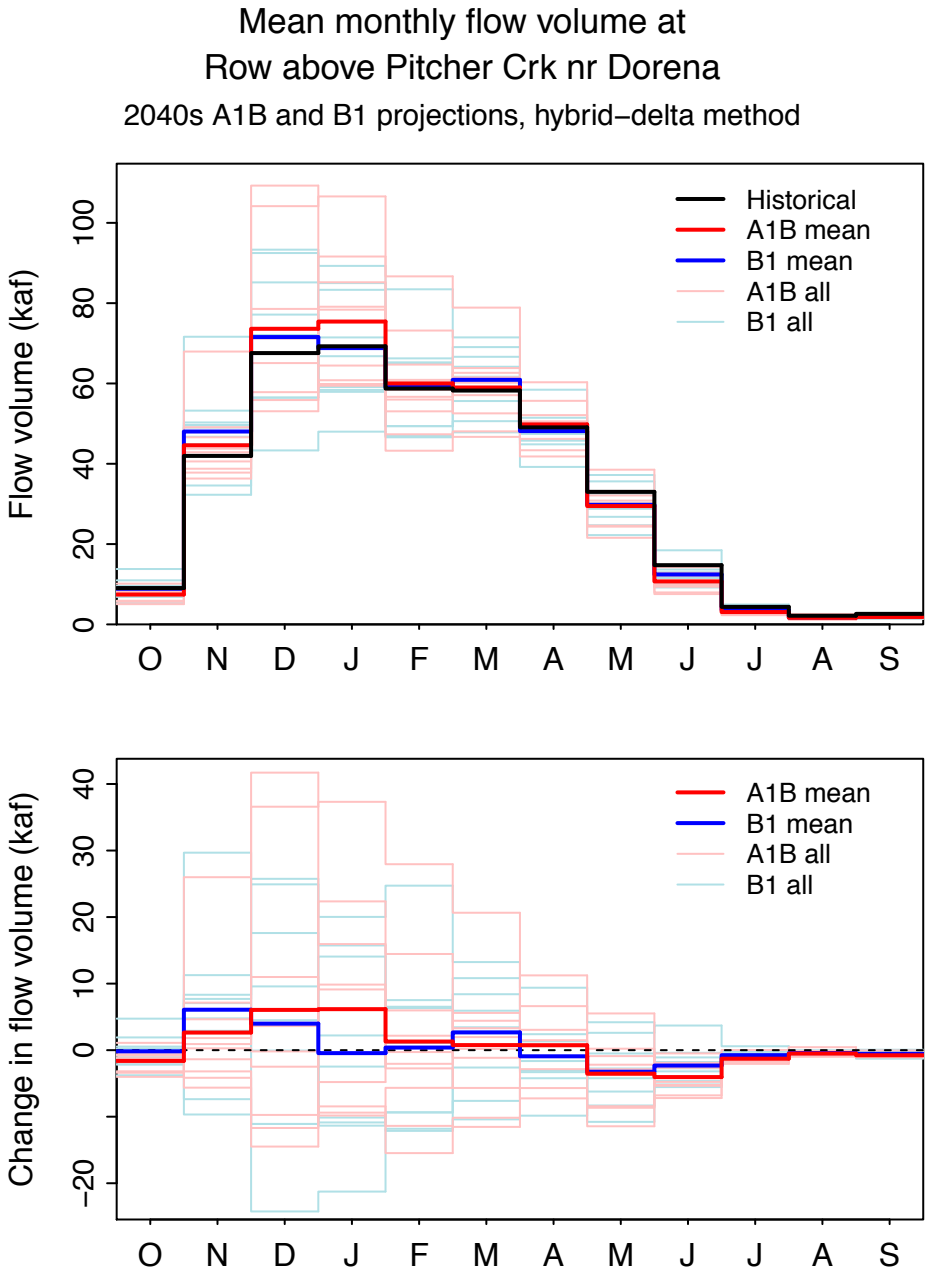

Figure F27. 5, 50, and 95th percentiles of monthly simulated, bias-corrected, naturalized streamflow at Row above Pitcher Crk nr Dorena (ROPIT 4035) for the historical period and hybrid-delta 2040s A1B and B1 future scenarios.

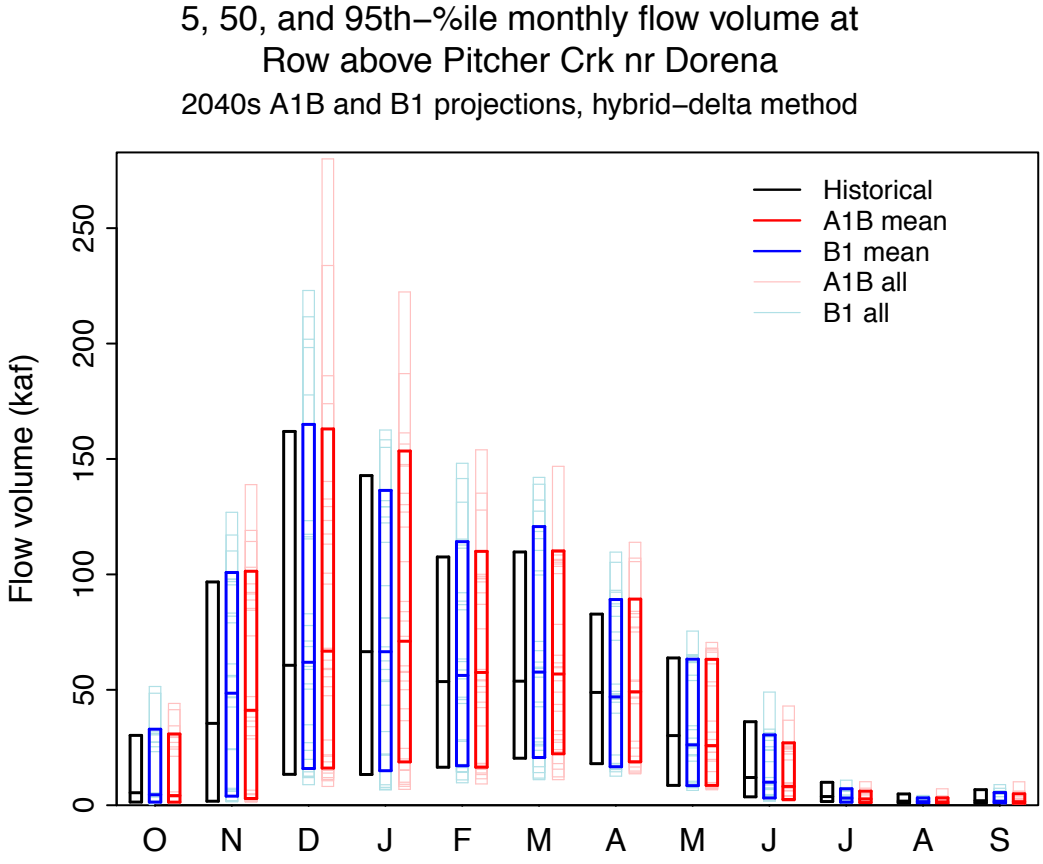

Figure F28. 5, 50, and 95th percentiles of winter (DJF) and summer (JJAS) simulated, bias-corrected, naturalized streamflow at Row above Pitcher Crk nr Dorena (ROPIT 4035) for the historical period and hybrid-delta 2040s A1B and B1 future scenarios (upper panel) and change from historical to future (lower panel).

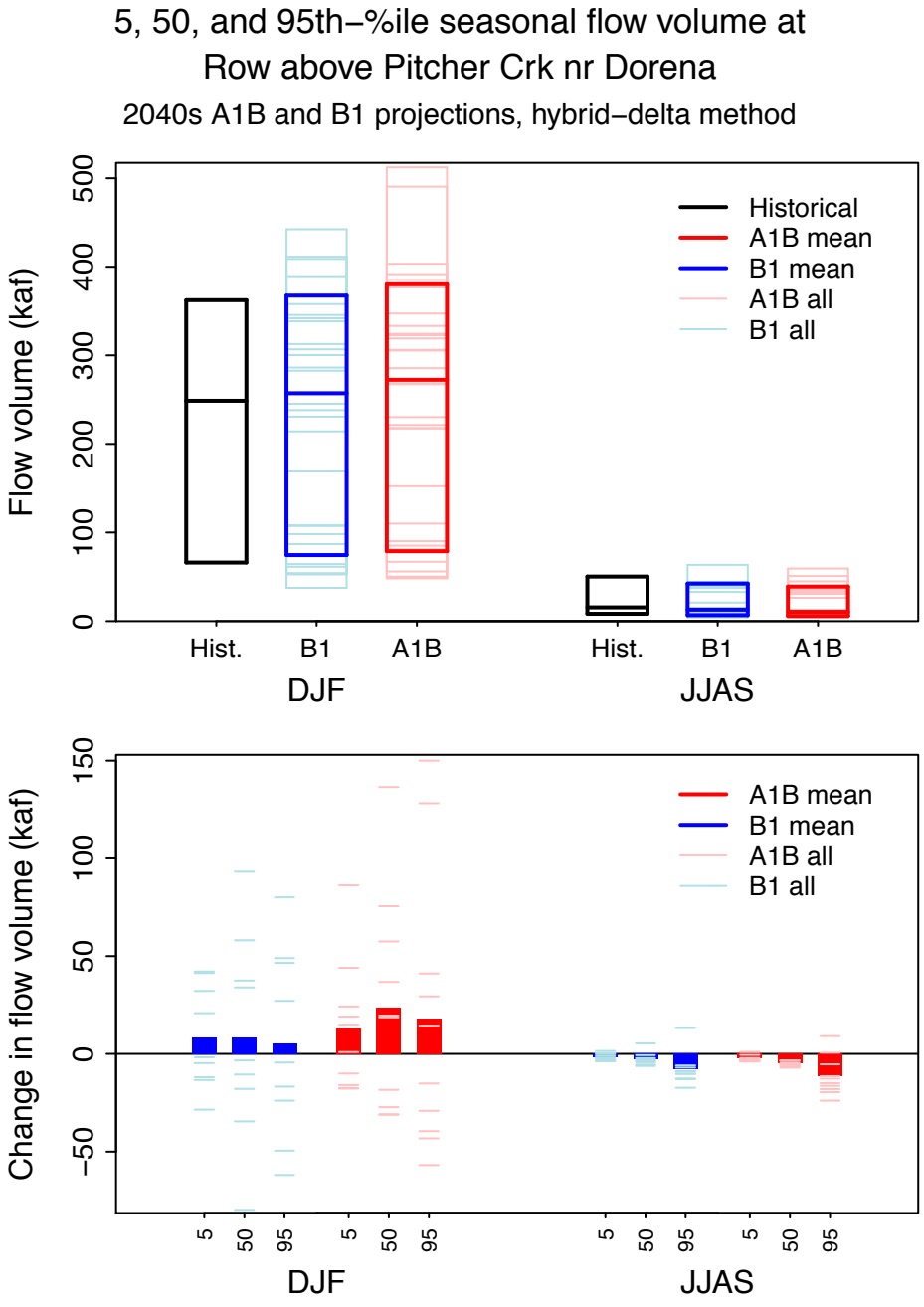

Figure F29. Mean annual hydrograph of daily simulated, bias-corrected, naturalized streamflow at N Santiam at Mehama (SANME 4039). for the historical period and hybrid-delta 2040s A1B and B1 future scenarios (upper panel) and change in flow from historical to future (lower panel).

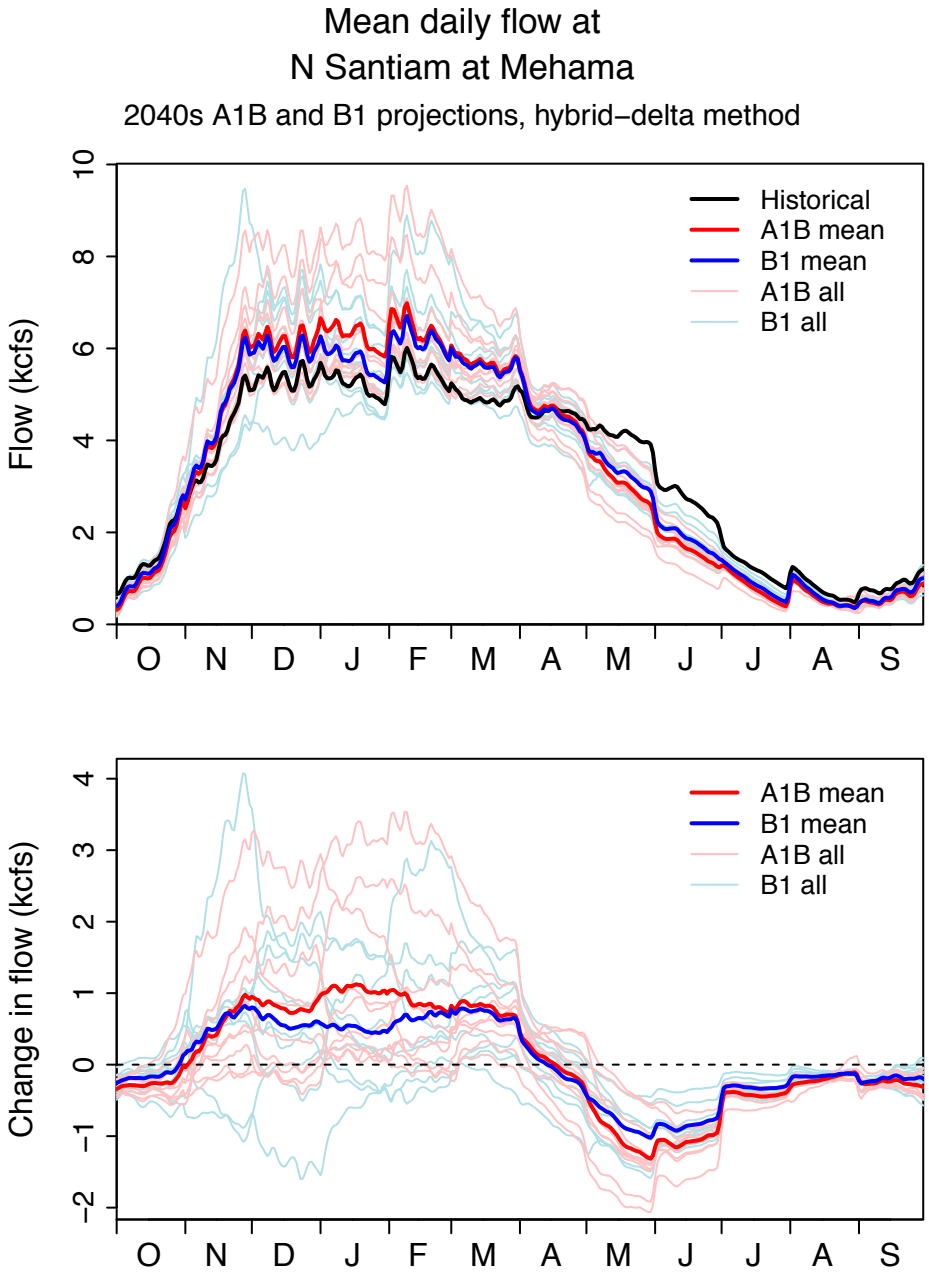

Figure F30. Mean annual hydrograph of monthly simulated, bias-corrected, naturalized streamflow at N Santiam at Mehama (SANME 4039) for the historical period and hybrid-delta 2040s A1B and B1 future scenarios (upper panel) and change in flow volume from historical to future (lower panel).

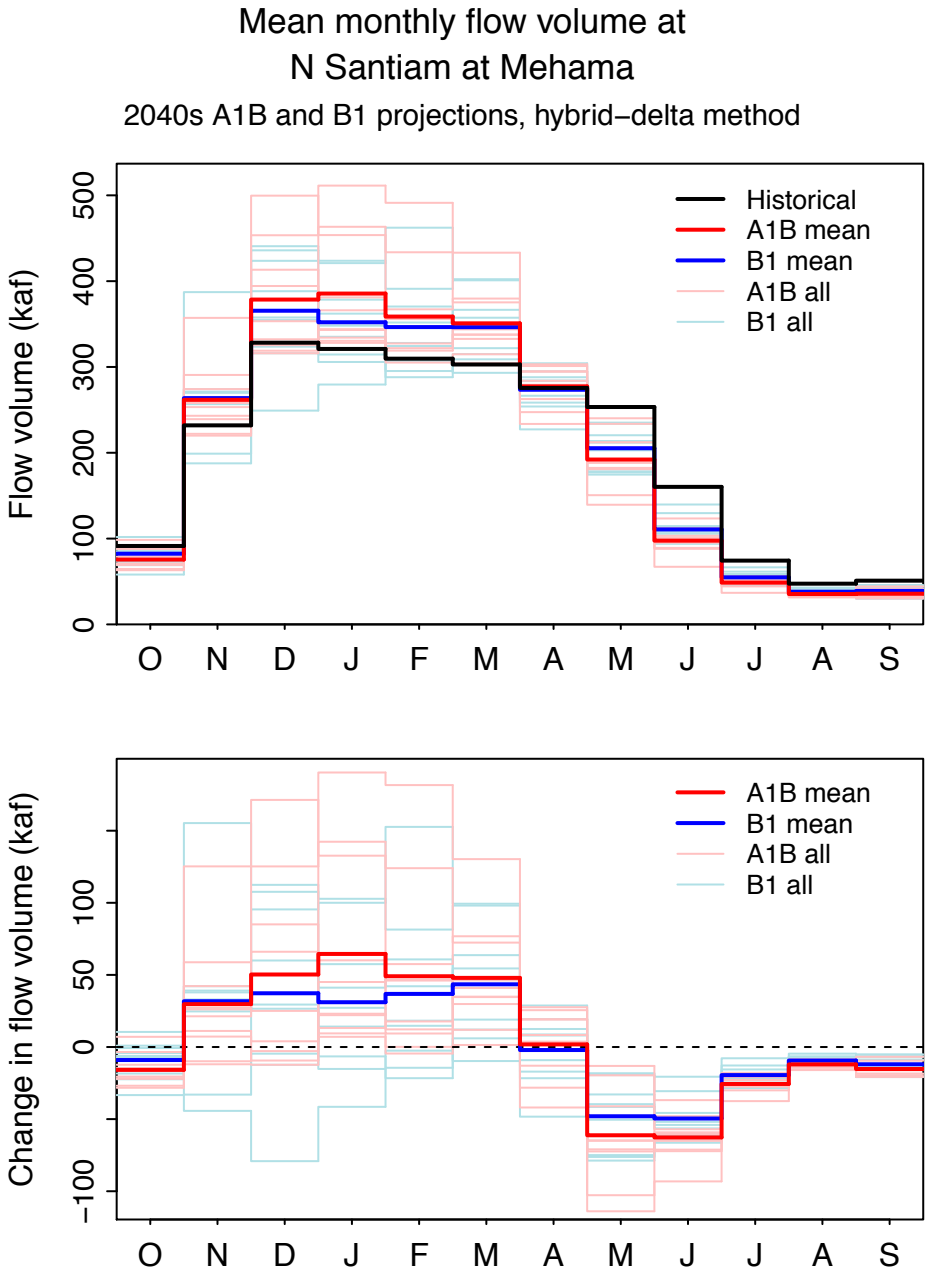

Figure F31. 5, 50, and 95th percentiles of monthly simulated, bias-corrected, naturalized streamflow at N Santiam at Mehama (SANME 4039) for the historical period and hybrid-delta 2040s A1B and B1 future scenarios.

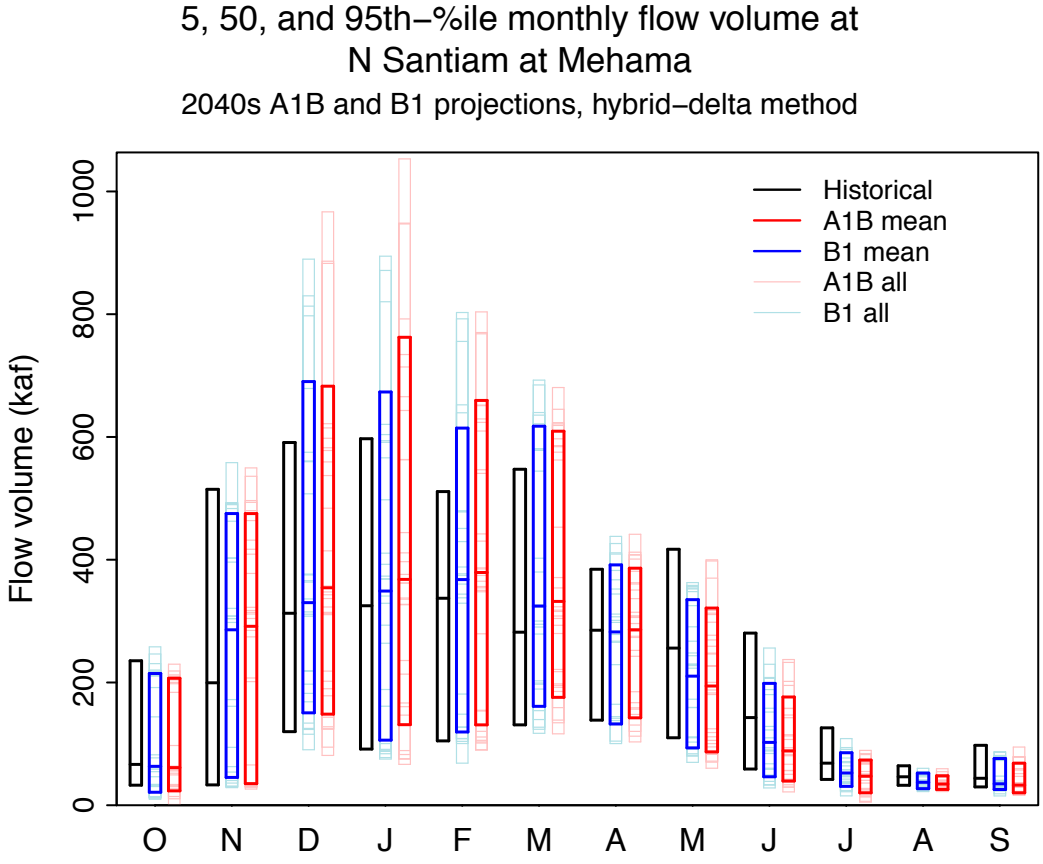

Figure F32. 5, 50, and 95th percentiles of winter (DJF) and summer (JJAS) simulated, bias-corrected, naturalized streamflow at N Santiam at Mehama (SANME 4039) for the historical period and hybrid-delta 2040s A1B and B1 future scenarios (upper panel) and change from historical to future (lower panel).

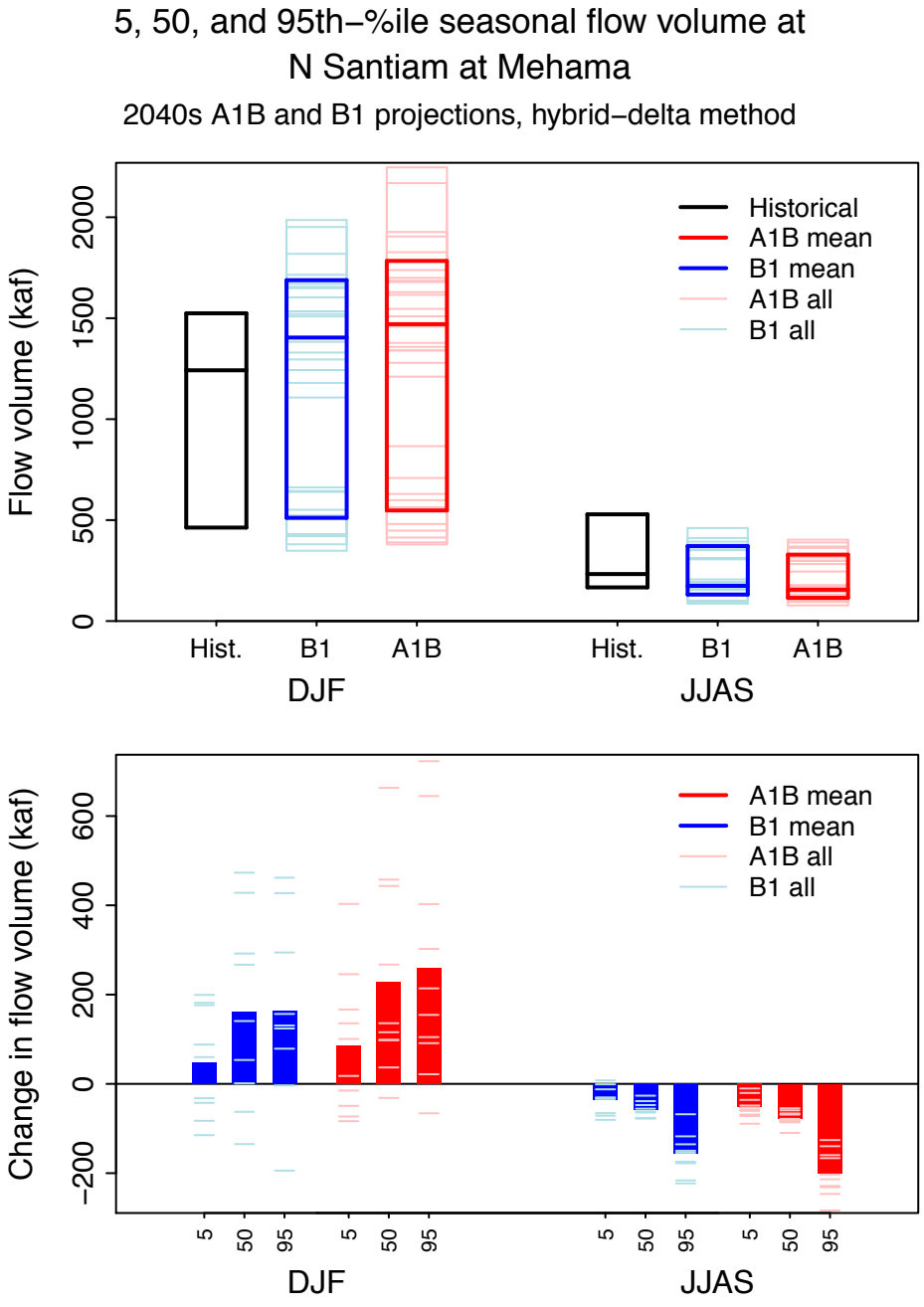

Figure F33. Mean annual hydrograph of daily simulated, bias-corrected, naturalized streamflow at S Santiam at Waterloo (SANWA 4059). for the historical period and hybrid-delta 2040s A1B and B1 future scenarios (upper panel) and change in flow from historical to future (lower panel).

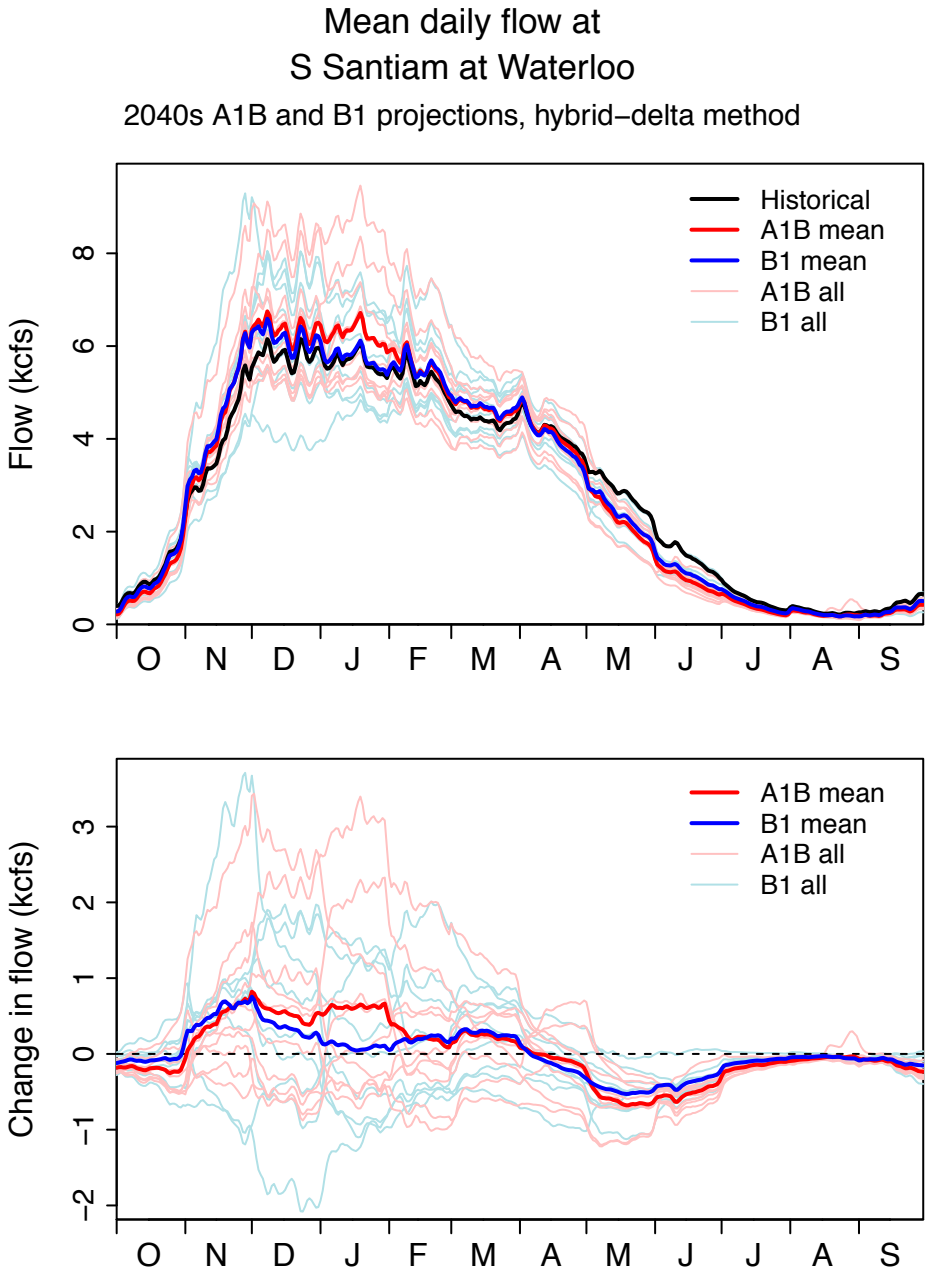

Figure F34. Mean annual hydrograph of monthly simulated, bias-corrected, naturalized streamflow at S Santiam at Waterloo (SANWA 4059) for the historical period and hybrid-delta 2040s A1B and B1 future scenarios (upper panel) and change in flow volume from historical to future (lower panel).

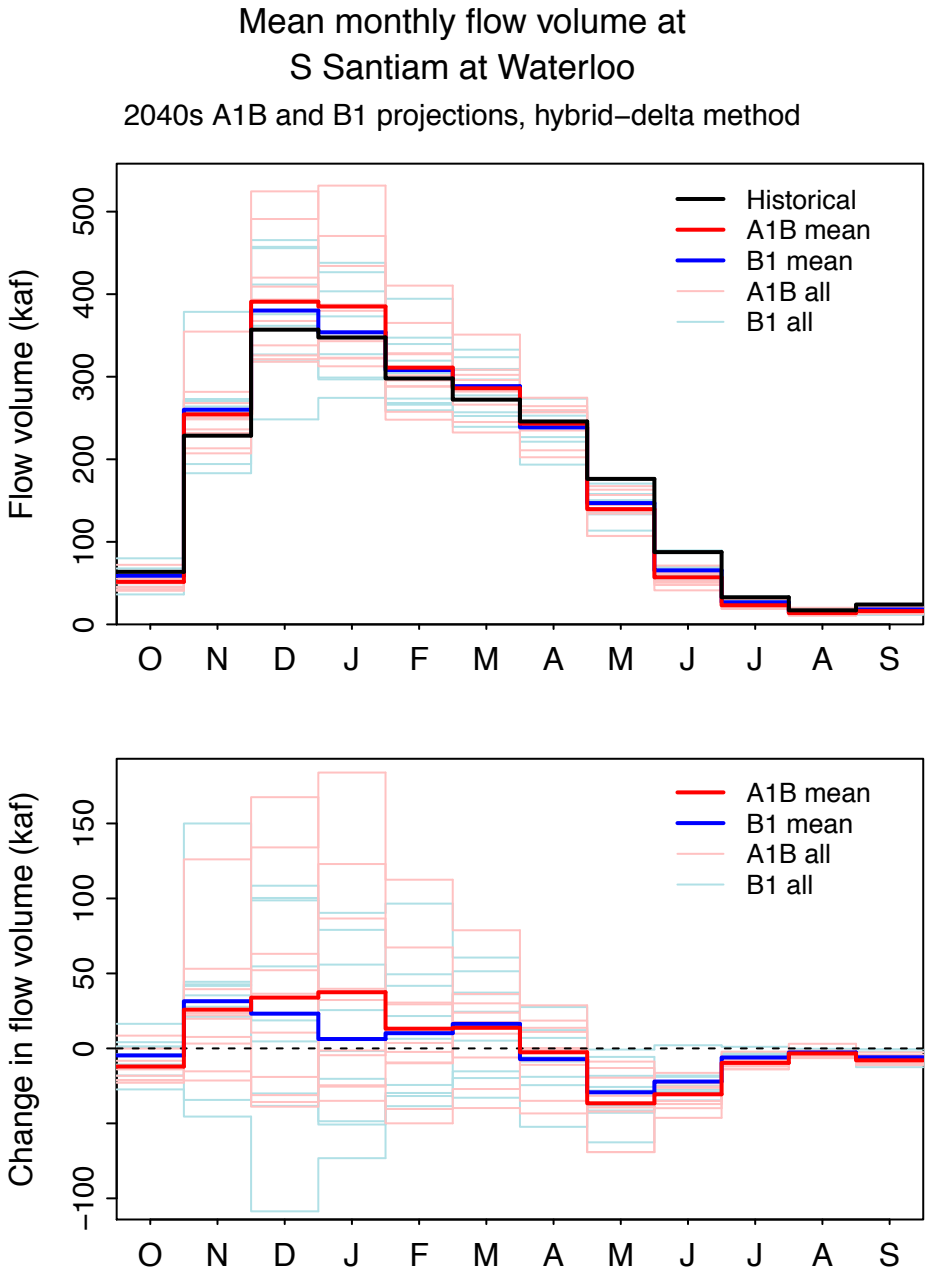

Figure F35. 5, 50, and 95th percentiles of monthly simulated, bias-corrected, naturalized streamflow at S Santiam at Waterloo (SANWA 4059) for the historical period and hybrid-delta 2040s A1B and B1 future scenarios.

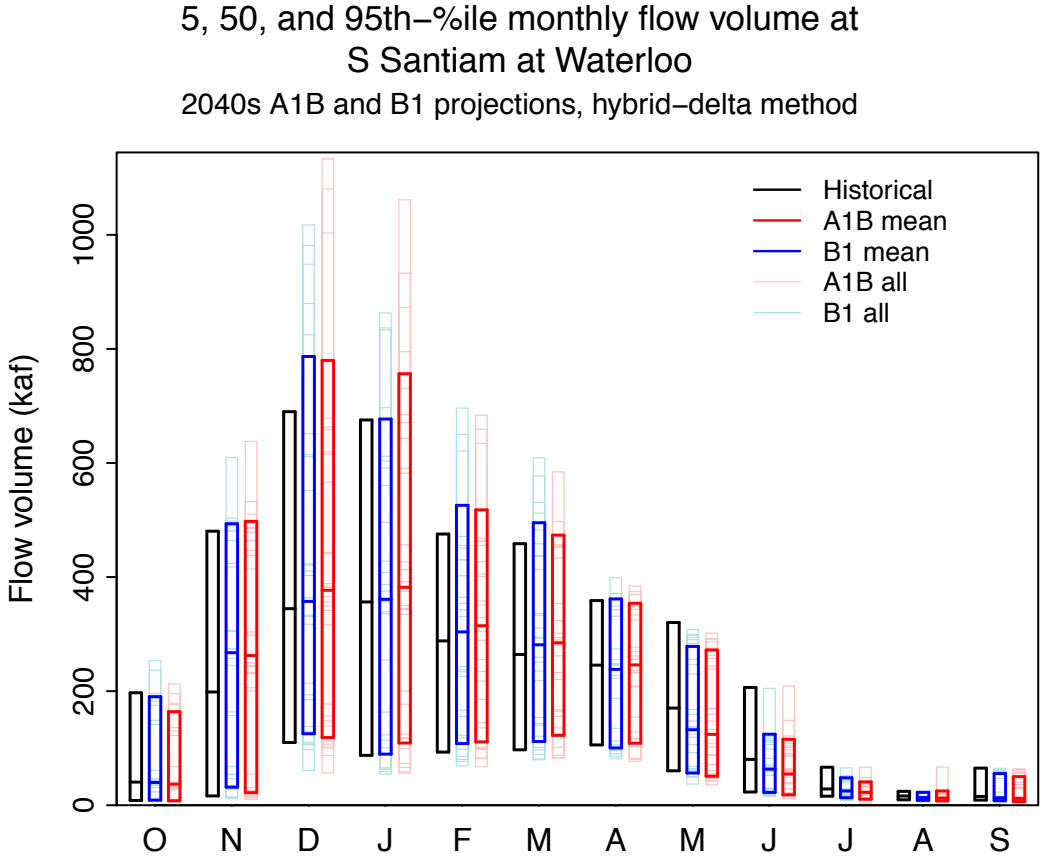

Figure F36. 5, 50, and 95th percentiles of winter (DJF) and summer (JJAS) simulated, bias-corrected, naturalized streamflow at S Santiam at Waterloo (SANWA 4059) for the historical period and hybrid-delta 2040s A1B and B1 future scenarios (upper panel) and change from historical to future (lower panel).

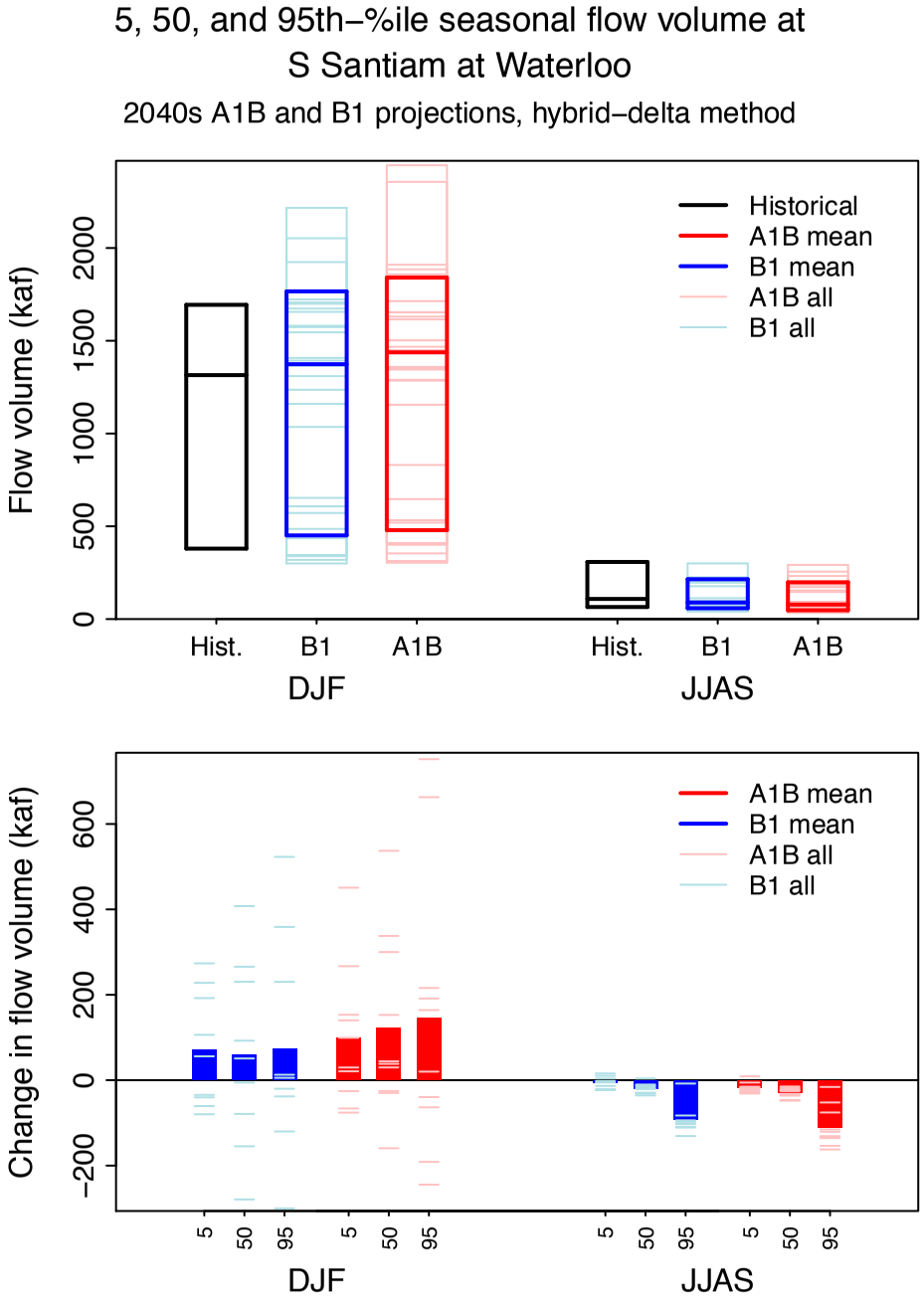

Figure F37. Mean annual hydrograph of daily simulated, bias-corrected, naturalized streamflow at Willamette abv Falls at Oregon City (WILFA 4064). for the historical period and hybrid-delta 2040s A1B and B1 future scenarios (upper panel) and change in flow from historical to future (lower panel).

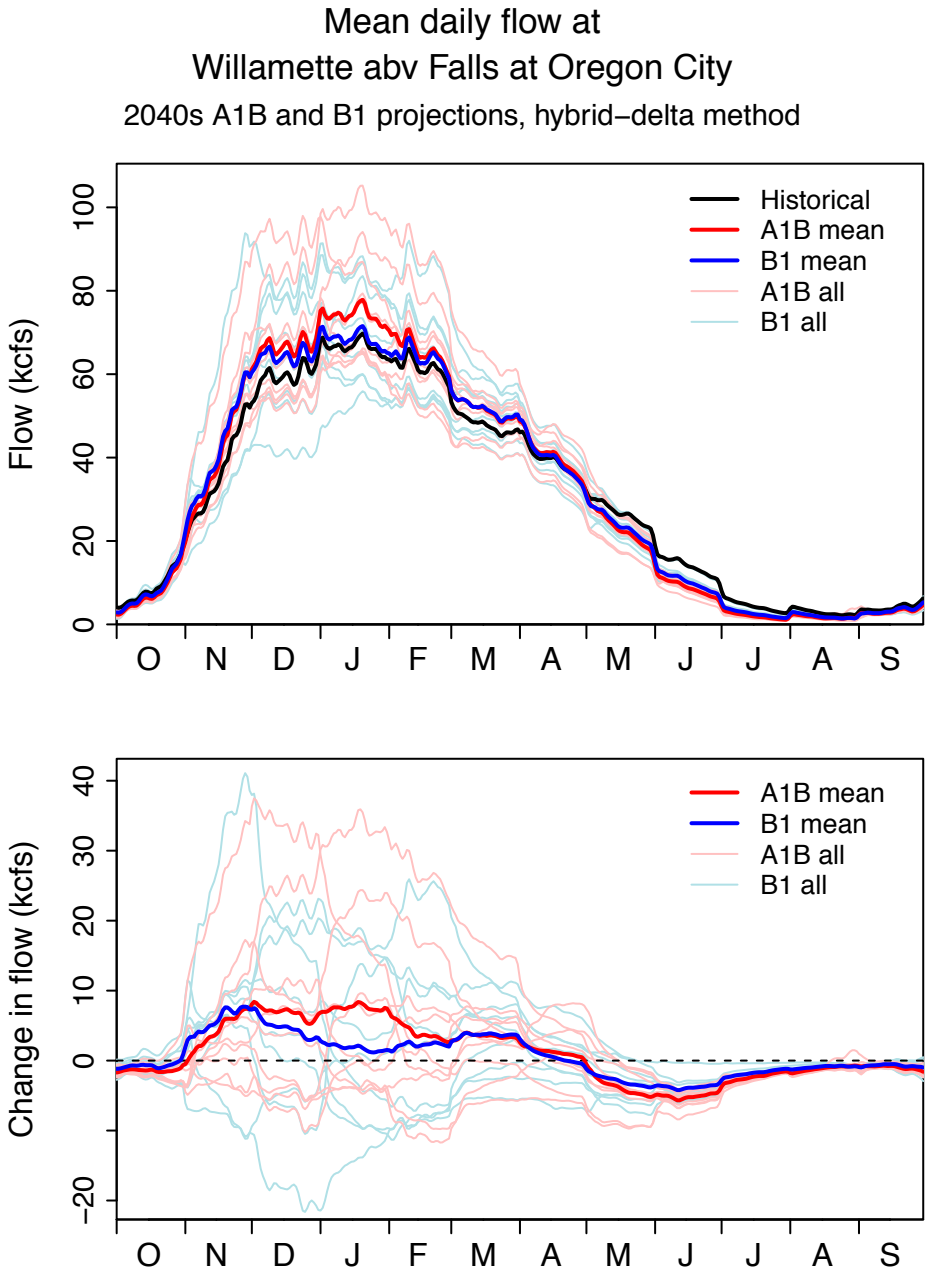

Figure F38. Mean annual hydrograph of monthly simulated, bias-corrected, naturalized streamflow at Willamette abv Falls at Oregon City (WILFA 4064) for the historical period and hybrid-delta 2040s A1B and B1 future scenarios (upper panel) and change in flow volume from historical to future (lower panel).

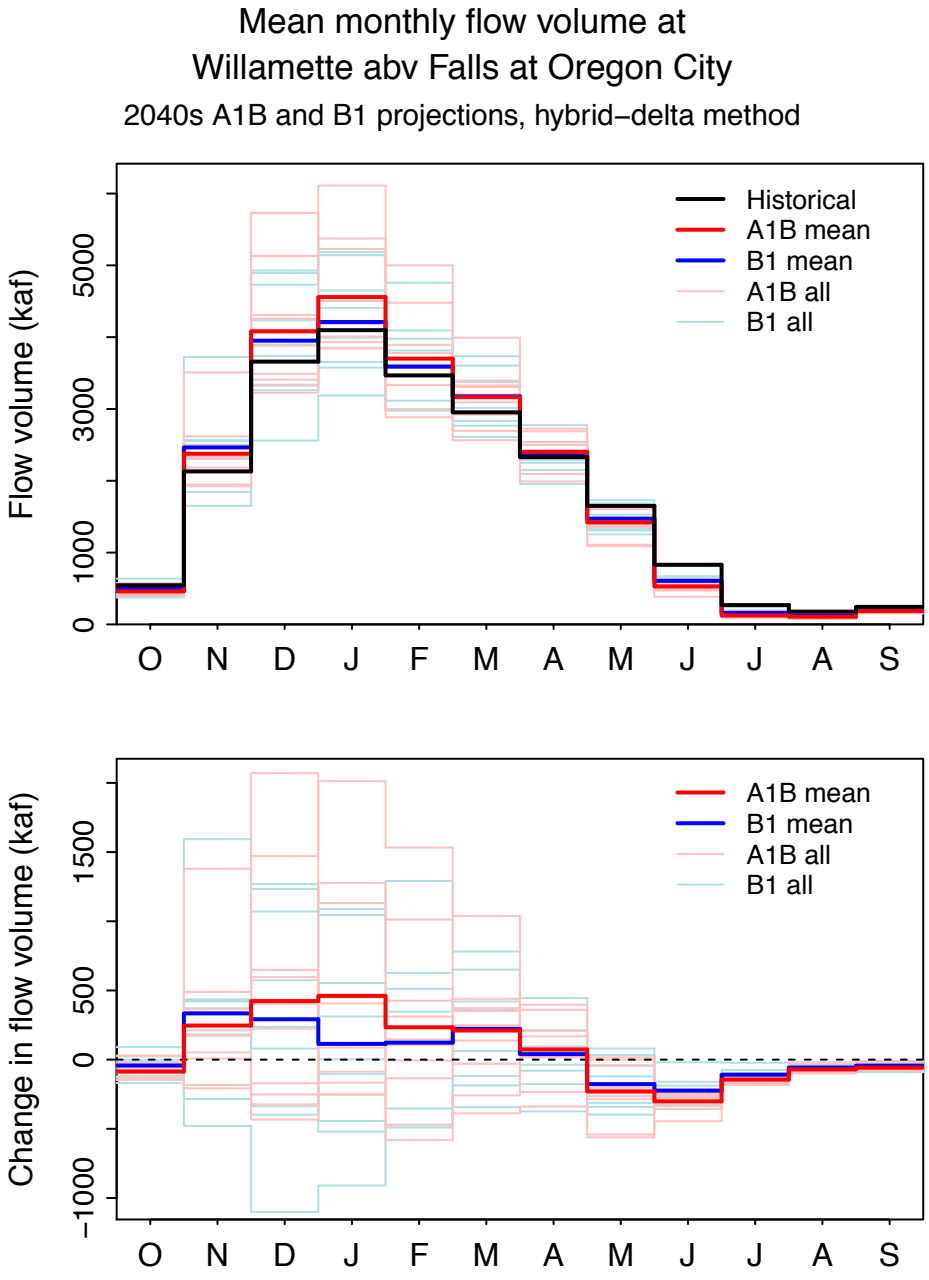

Figure F39. 5, 50, and 95th percentiles of monthly simulated, bias-corrected, naturalized streamflow at Willamette abv Falls at Oregon City (WILFA 4064) for the historical period and hybrid-delta 2040s A1B and B1 future scenarios.

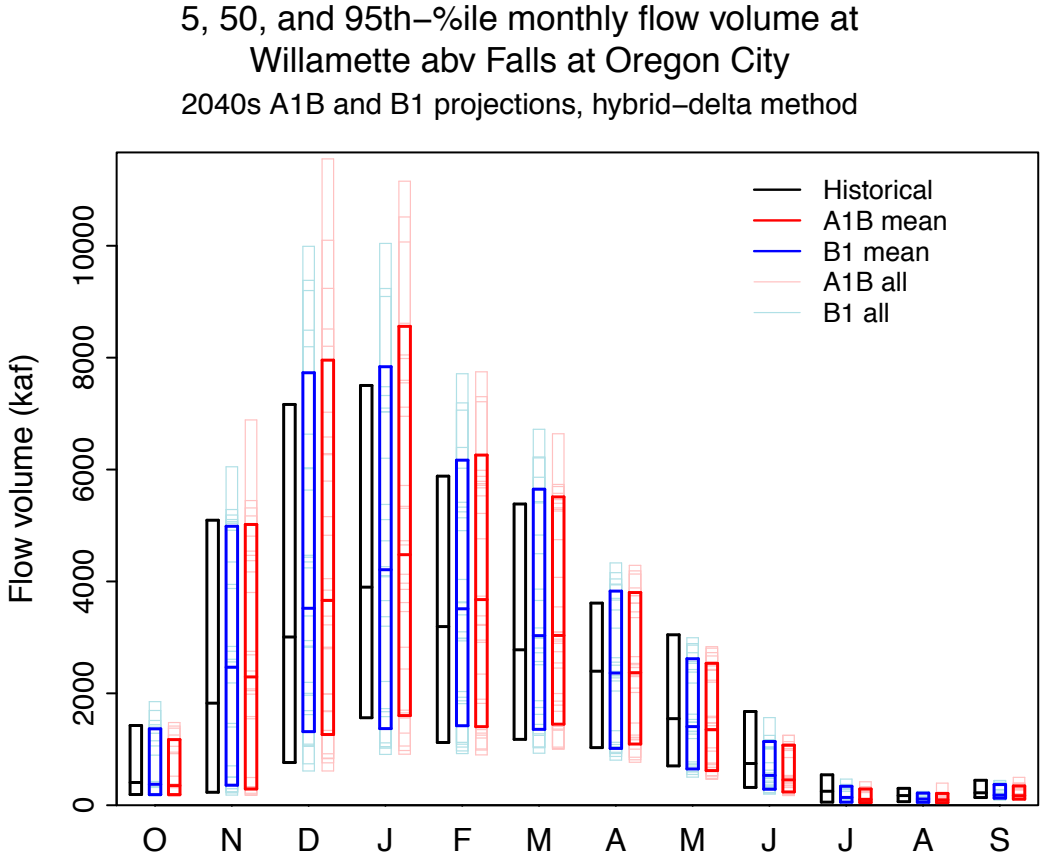

Figure F40. 5, 50, and 95th percentiles of winter (DJF) and summer (JJAS) simulated, bias-corrected, naturalized streamflow at Willamette abv Falls at Oregon City (WILFA 4064) for the historical period and hybrid-delta 2040s A1B and B1 future scenarios (upper panel) and change from historical to future (lower panel).

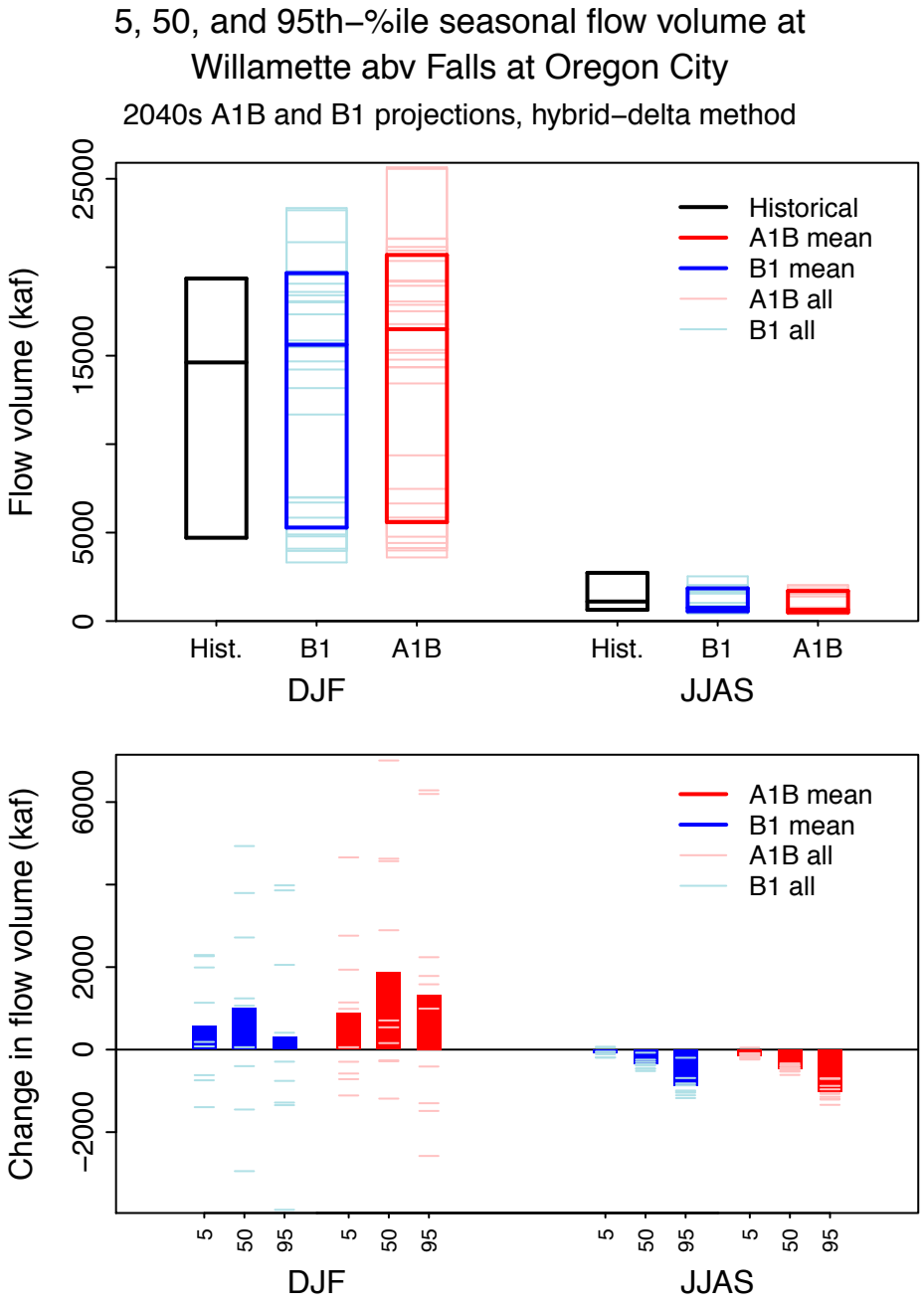

Figure F41. Mean annual hydrograph of daily simulated, bias-corrected, naturalized streamflow at Middle Fork Willamette blw N Fork nr Oakridge (WILNF 4048). for the historical period and hybrid-delta 2040s A1B and B1 future scenarios (upper panel) and change in flow from historical to future (lower panel).

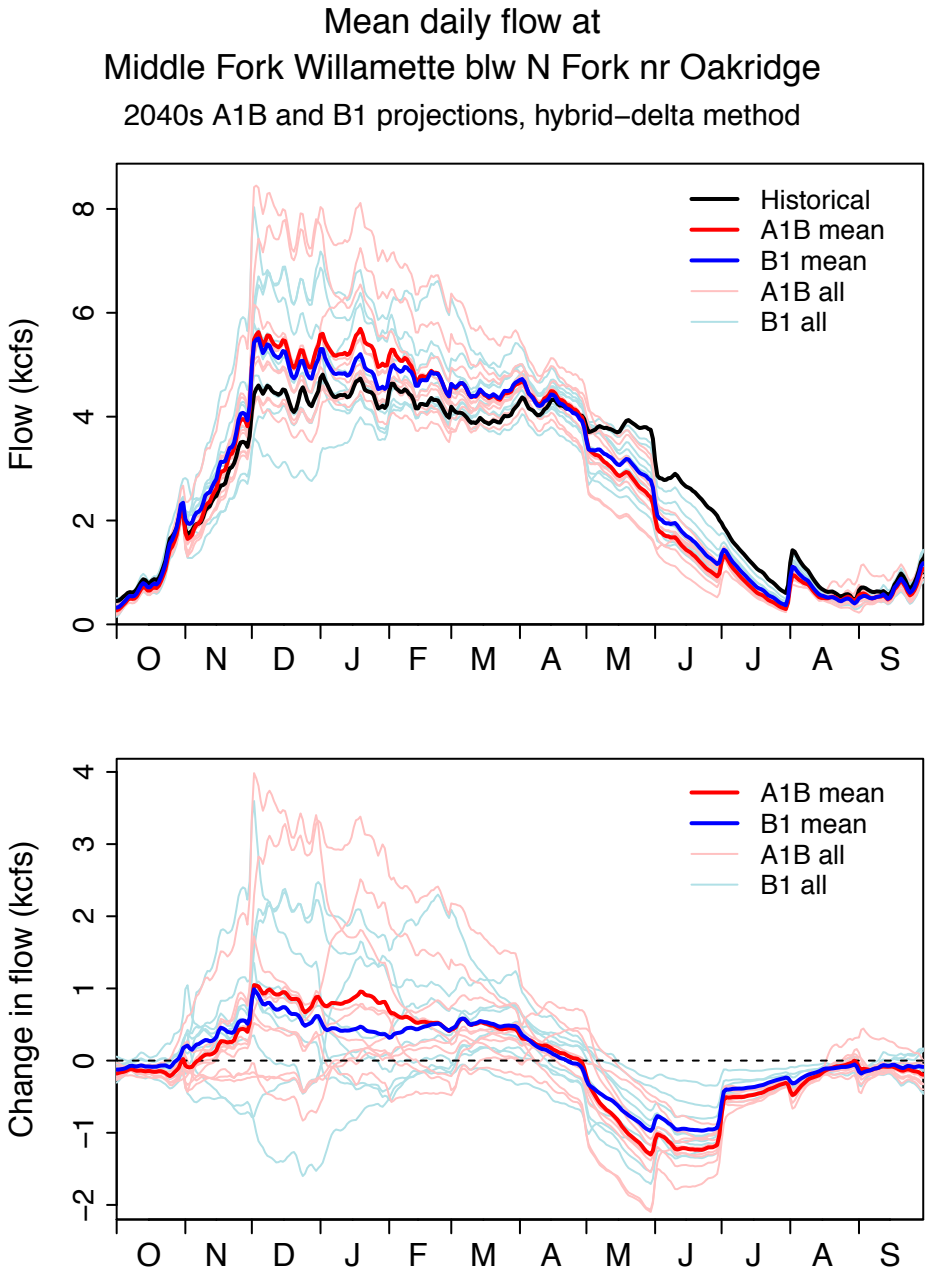

Figure F42. Mean annual hydrograph of monthly simulated, bias-corrected, naturalized streamflow at Middle Fork Willamette blw N Fork nr Oakridge (WILNF 4048) for the historical period and hybrid-delta 2040s A1B and B1 future scenarios (upper panel) and change in flow volume from historical to future (lower panel).

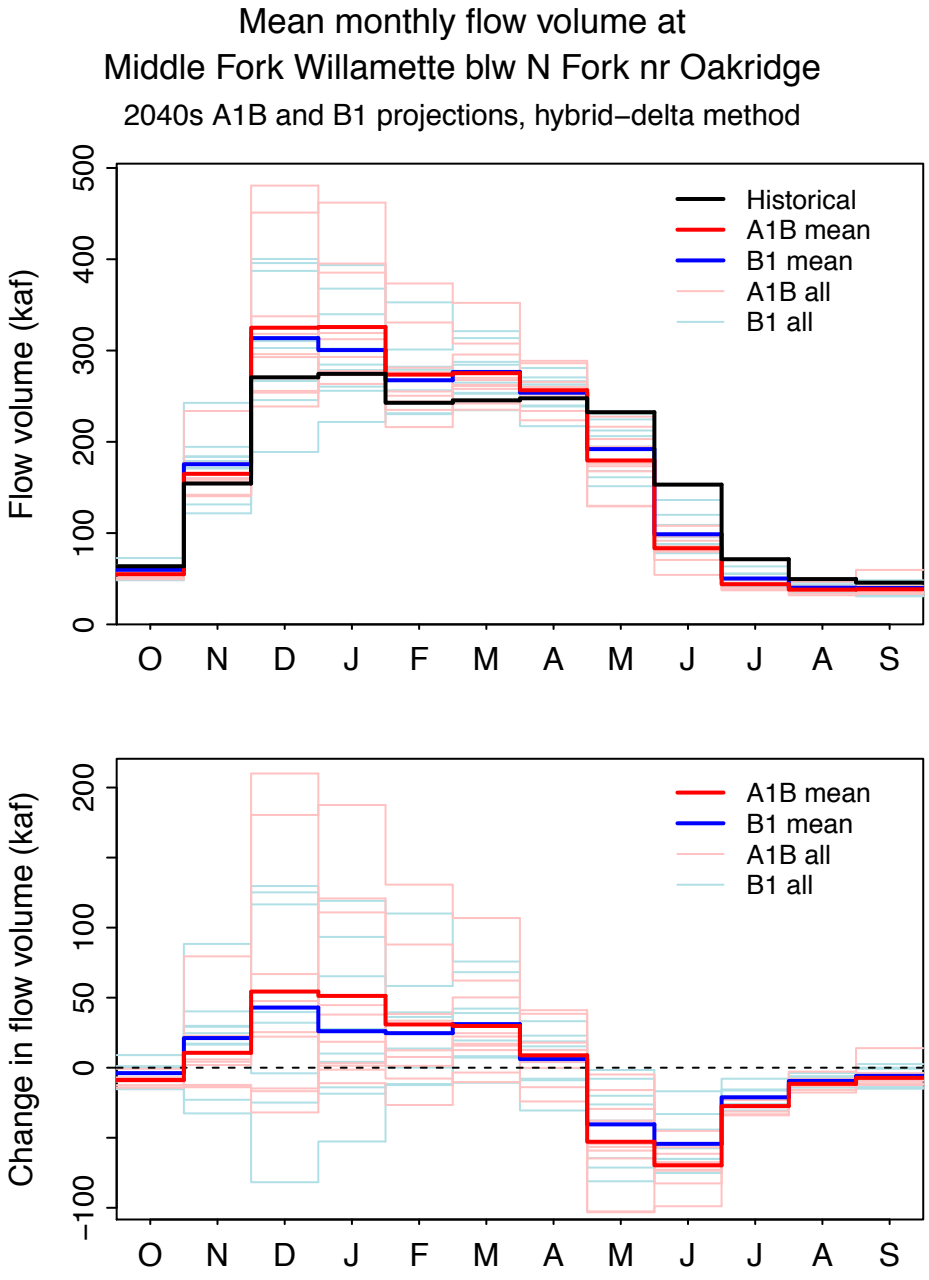

Figure F43. 5, 50, and 95th percentiles of monthly simulated, bias-corrected, naturalized streamflow at Middle Fork Willamette blw N Fork nr Oakridge (WILNF 4048) for the historical period and hybrid-delta 2040s A1B and B1 future scenarios.

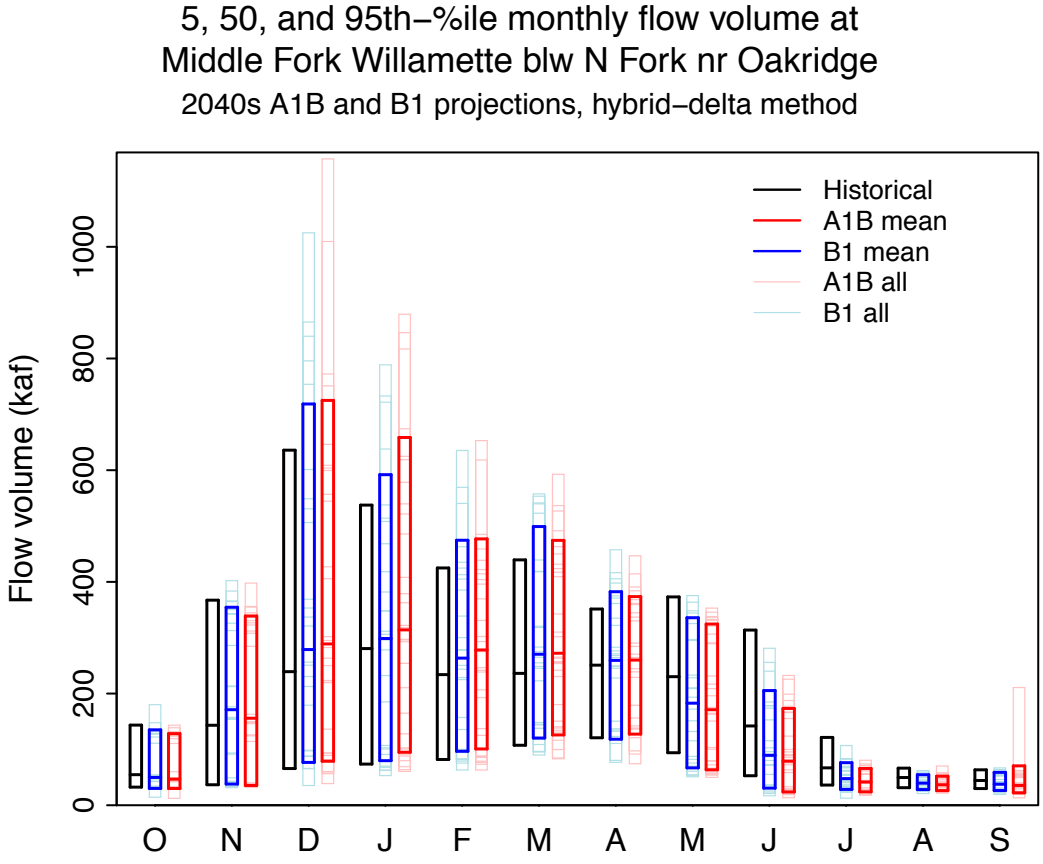

Figure F44. 5, 50, and 95th percentiles of winter (DJF) and summer (JJAS) simulated, bias-corrected, naturalized streamflow at Middle Fork Willamette blw N Fork nr Oakridge (WILNF 4048) for the historical period and hybrid-delta 2040s A1B and B1 future scenarios (upper panel) and change from historical to future (lower panel).

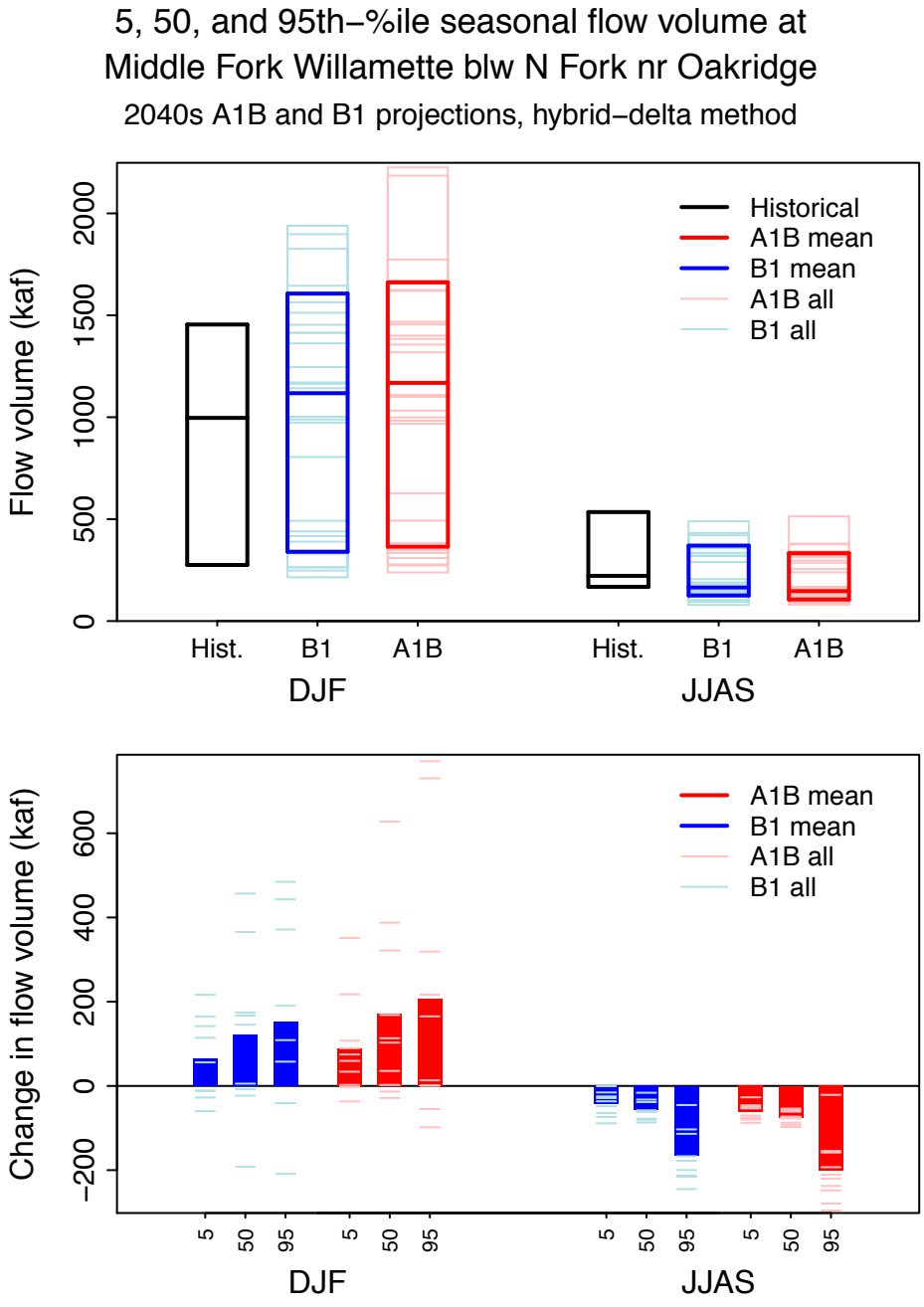

Appendix G. Projected Changes to Flow-Duration-Frequency Curves of Annual Maximum Flows

Figure G1. Flow-duration-frequency curves for annual maxima streamflow of 1-, 3-, 5-, 7-, and 15-day durations for the historical period and future periods (2040s A1B and B1) at Calapooia at Albany (CALAP 4038).

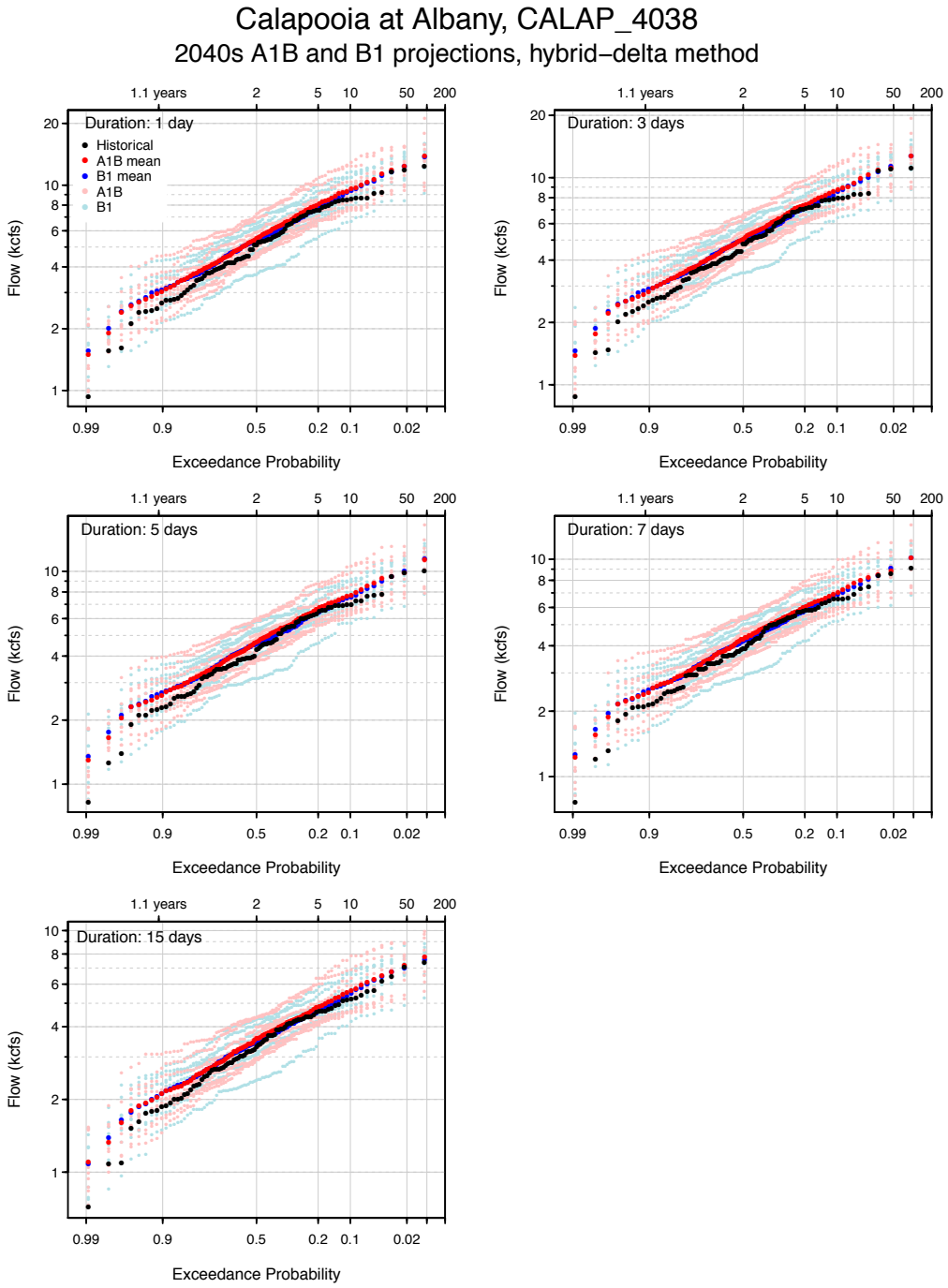

Figure G2. Relative change in flow-duration-frequency curves by annual maximum flow from the historical period and future period (2040s A1B and B1) at Calapooia at Albany (CALAP 4038).

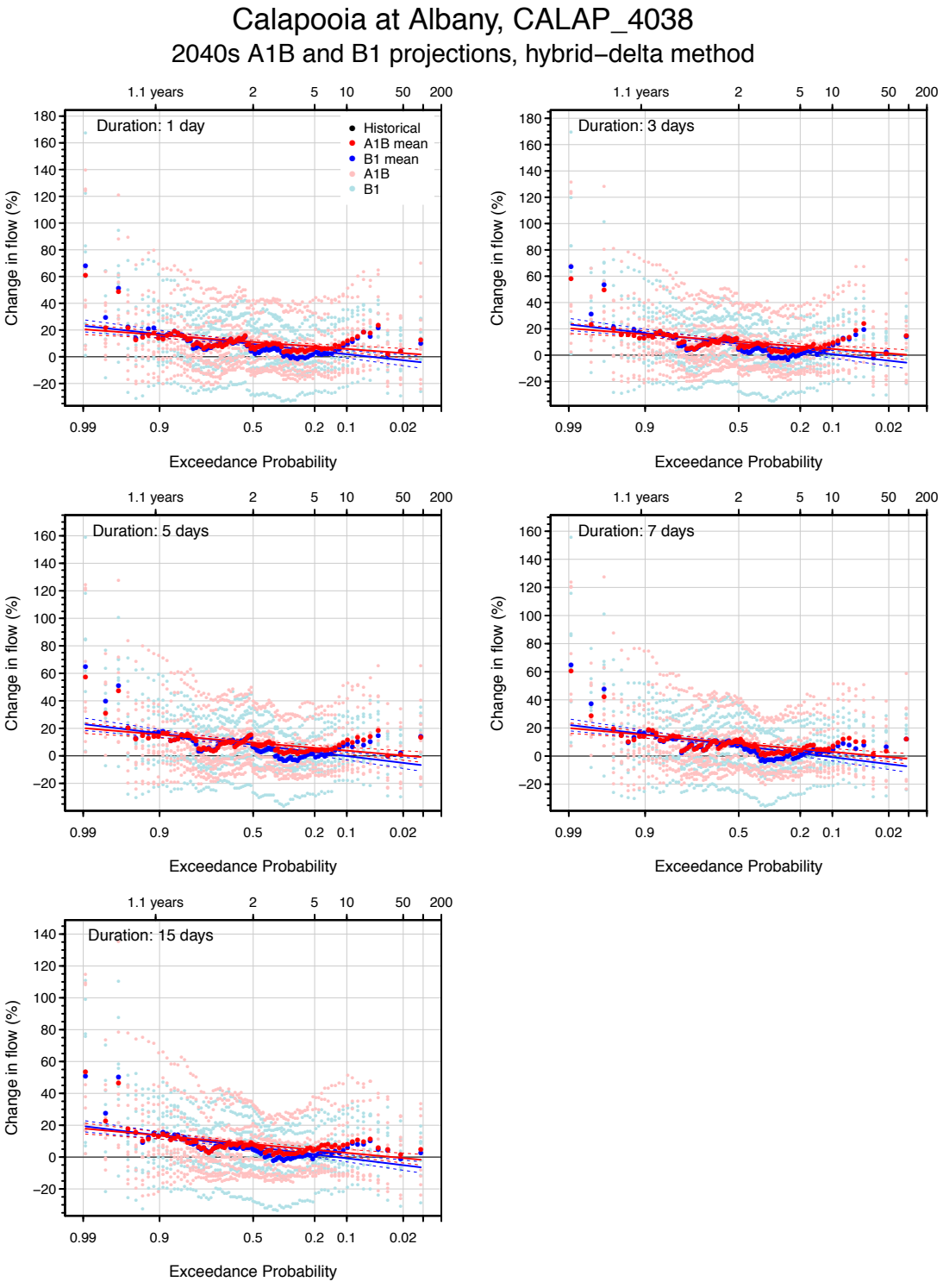

Figure G3. Flow-duration-frequency curves for annual maxima streamflow of 1-, 3-, 5-, 7-, and 15-day durations for the historical period and future periods (2040s A1B and B1) at Clackamas above Three Lynx Crk (CLKTH 4044).

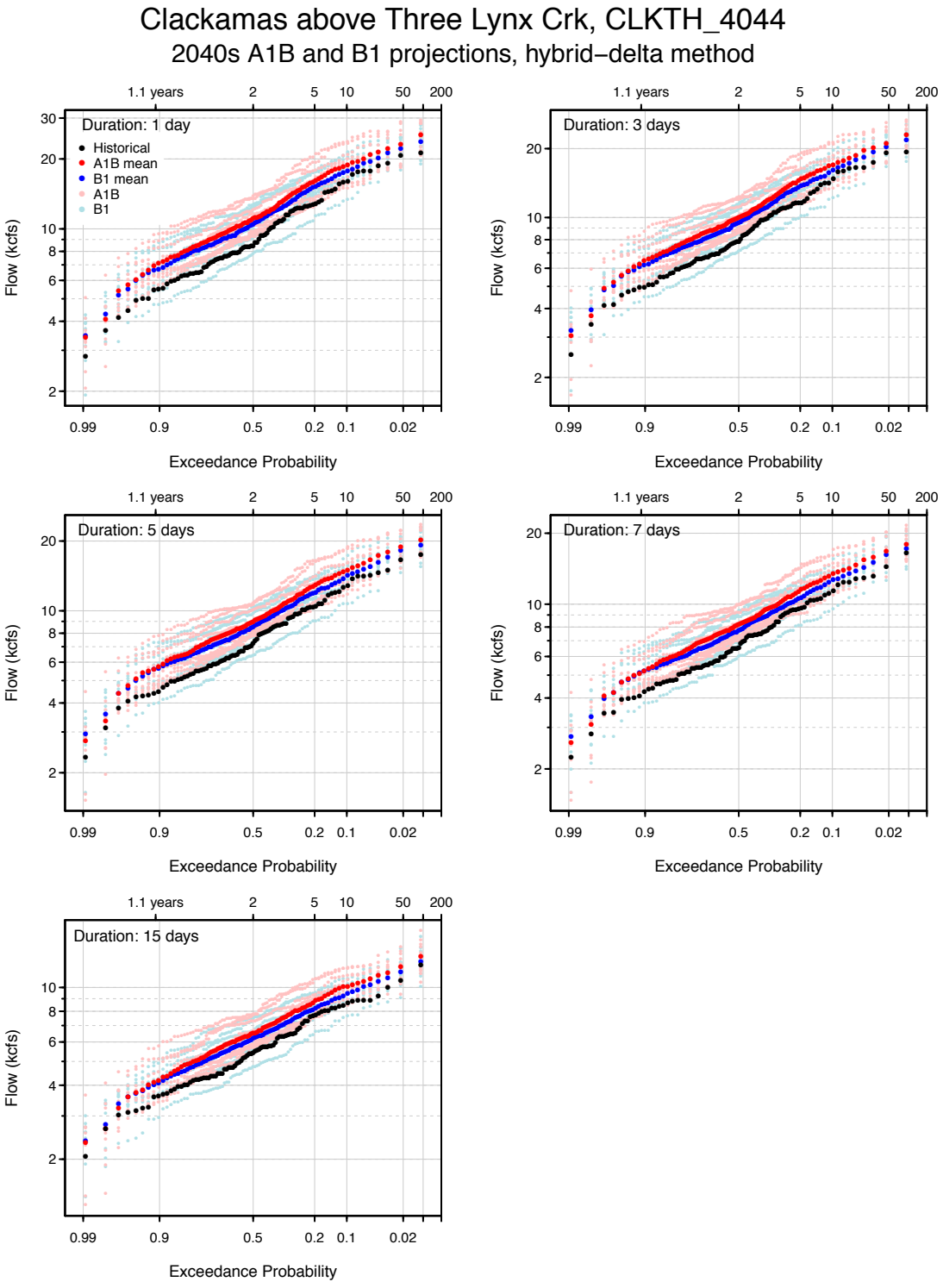

Figure G4. Relative change in flow-duration-frequency curves by annual maximum flow from the historical period and future period (2040s A1B and B1) at Clackamas above Three Lynx Crk (CLKTH 4044).

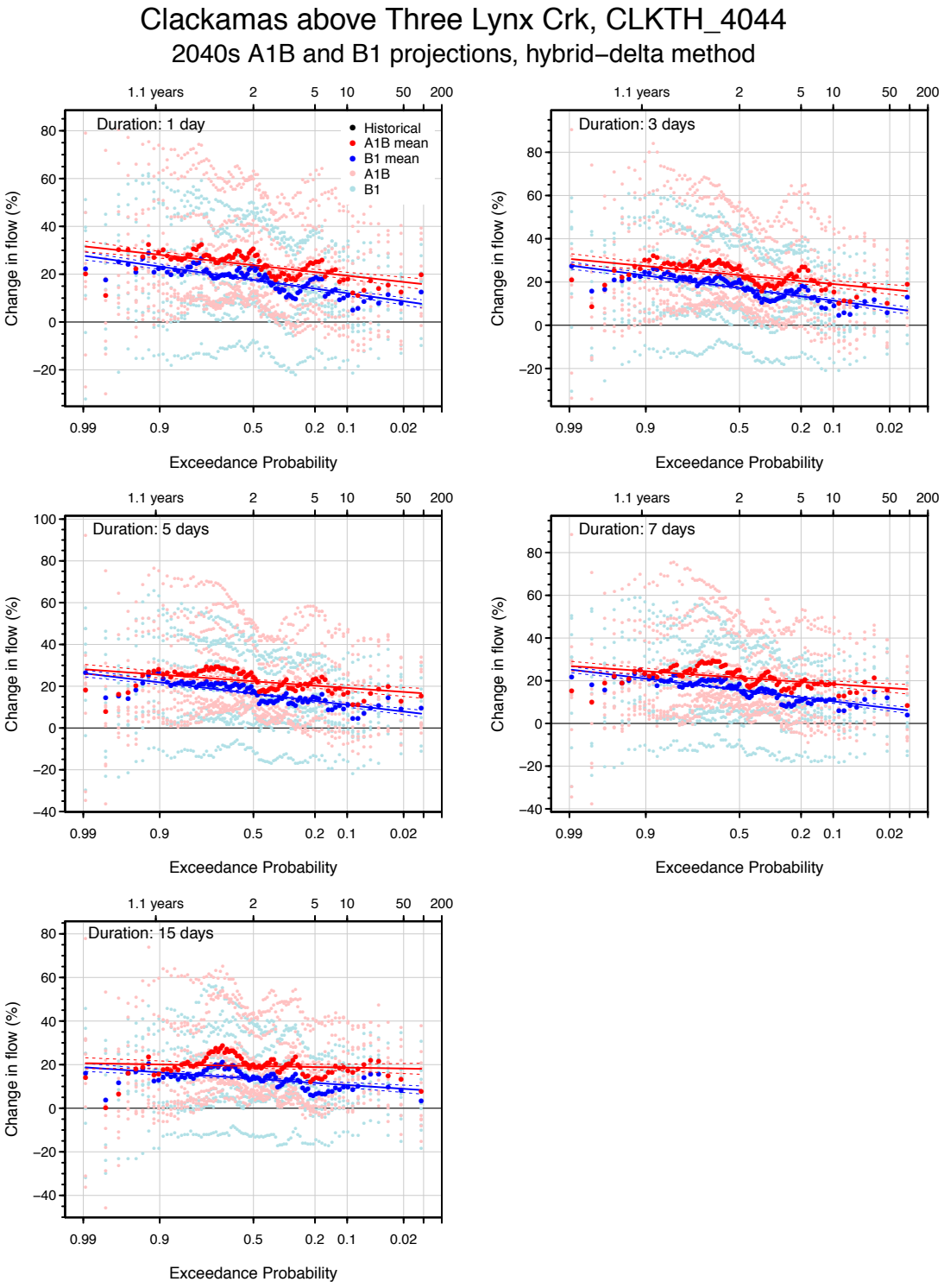

Figure G5. Flow-duration-frequency curves for annual maxima streamflow of 1-, 3-, 5-, 7-, and 15-day durations for the historical period and future periods (2040s A1B and B1) at McKenzie nr Vida (MCKVI 4036).

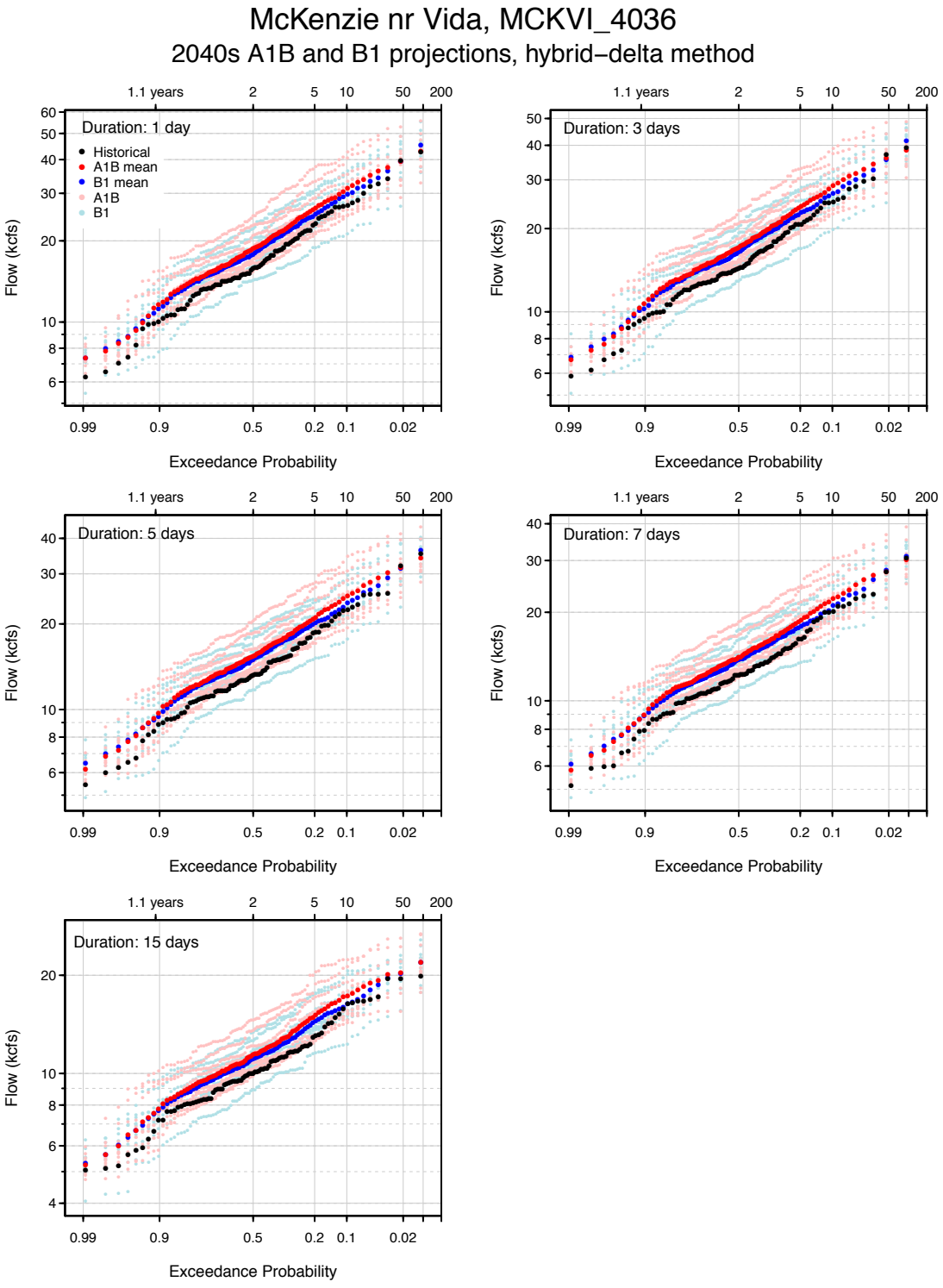

Figure G6. Relative change in flow-duration-frequency curves by annual maximum flow from the historical period and future period (2040s A1B and B1) at McKenzie nr Vida (MCKVI 4036).

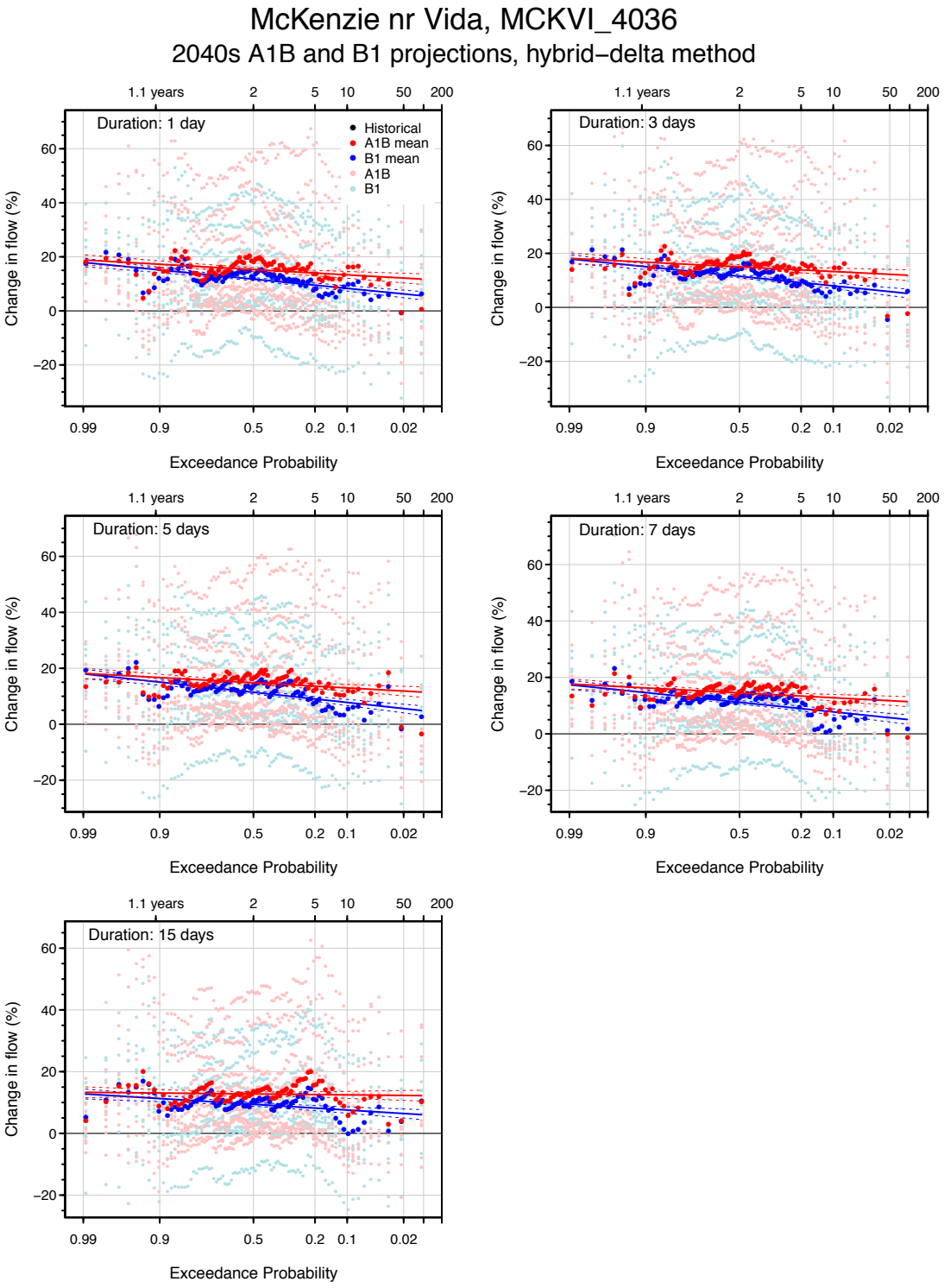

Figure G7. Flow-duration-frequency curves for annual maxima streamflow of 1-, 3-, 5-, 7-, and 15-day durations for the historical period and future periods (2040s A1B and B1) at Molalla nr Canby (MOLAL 4043).

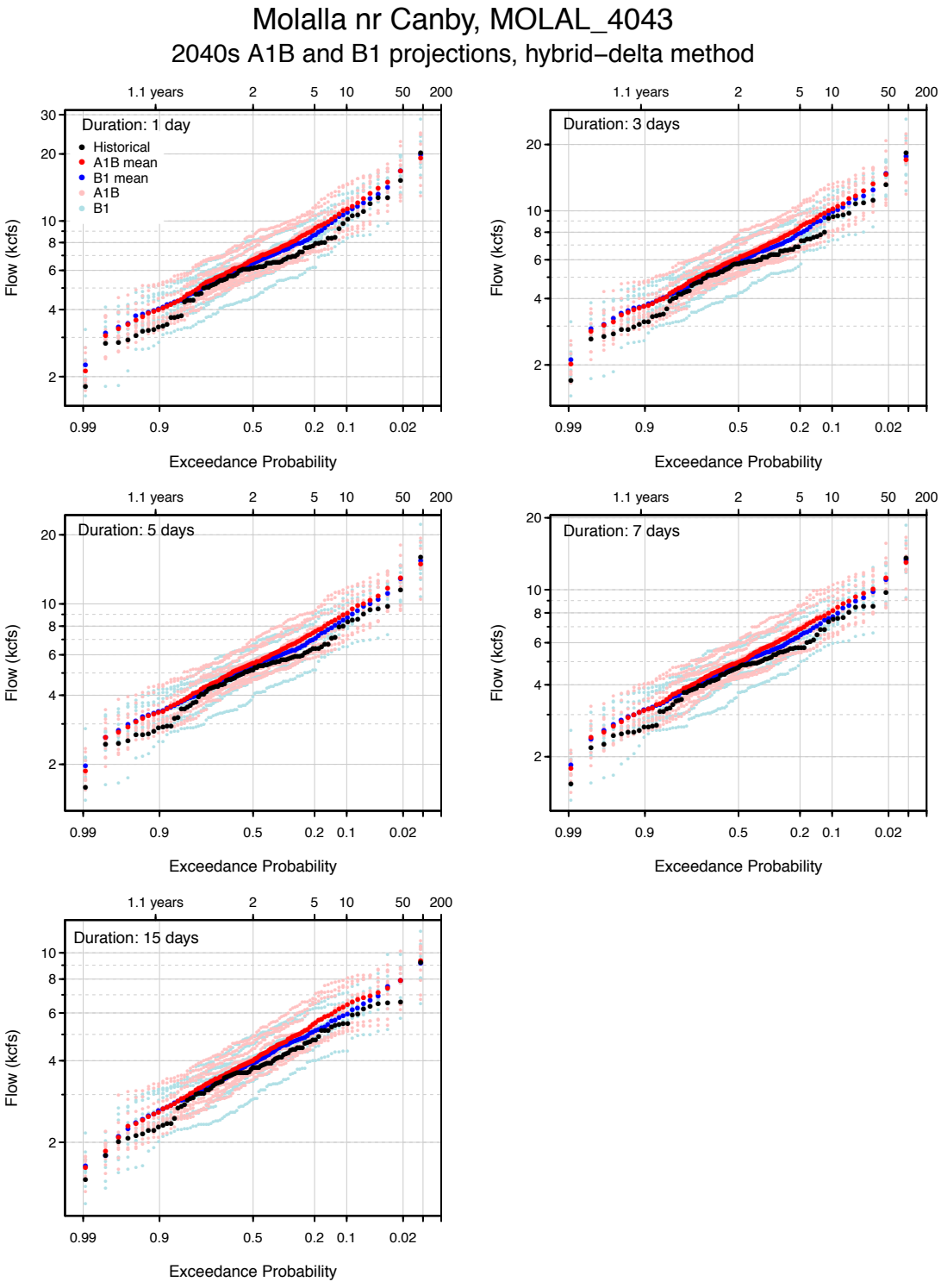

Figure G8. Relative change in flow-duration-frequency curves by annual maximum flow from the historical period and future period (2040s A1B and B1) at Molalla nr Canby (MOLAL 4043).

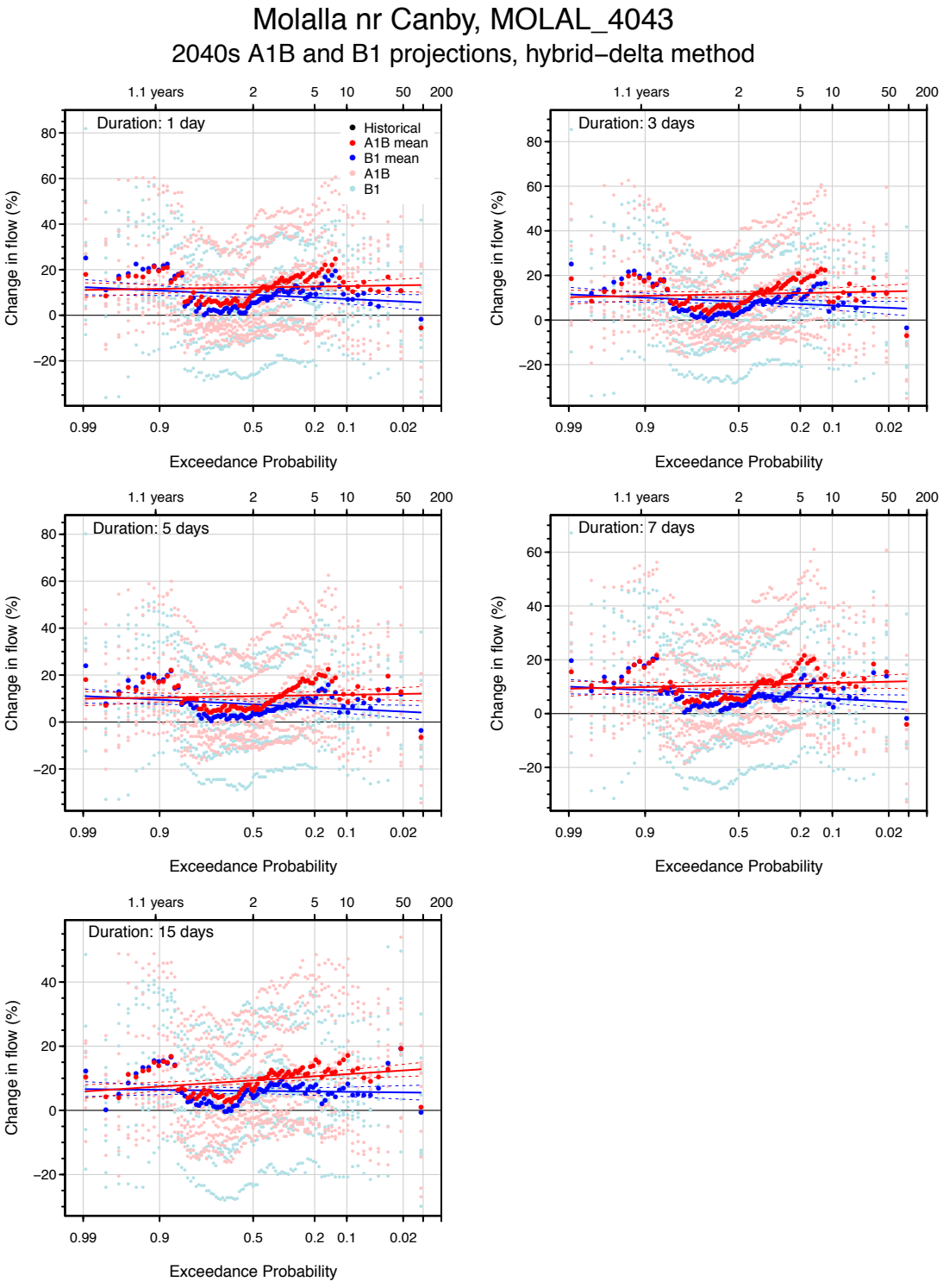

Figure G9. Flow-duration-frequency curves for annual maxima streamflow of 1-, 3-, 5-, 7-, and 15-day durations for the historical period and future periods (2040s A1B and B1) at N Santiam blw Boulder Crk nr Detroit (NOSAN 4056).

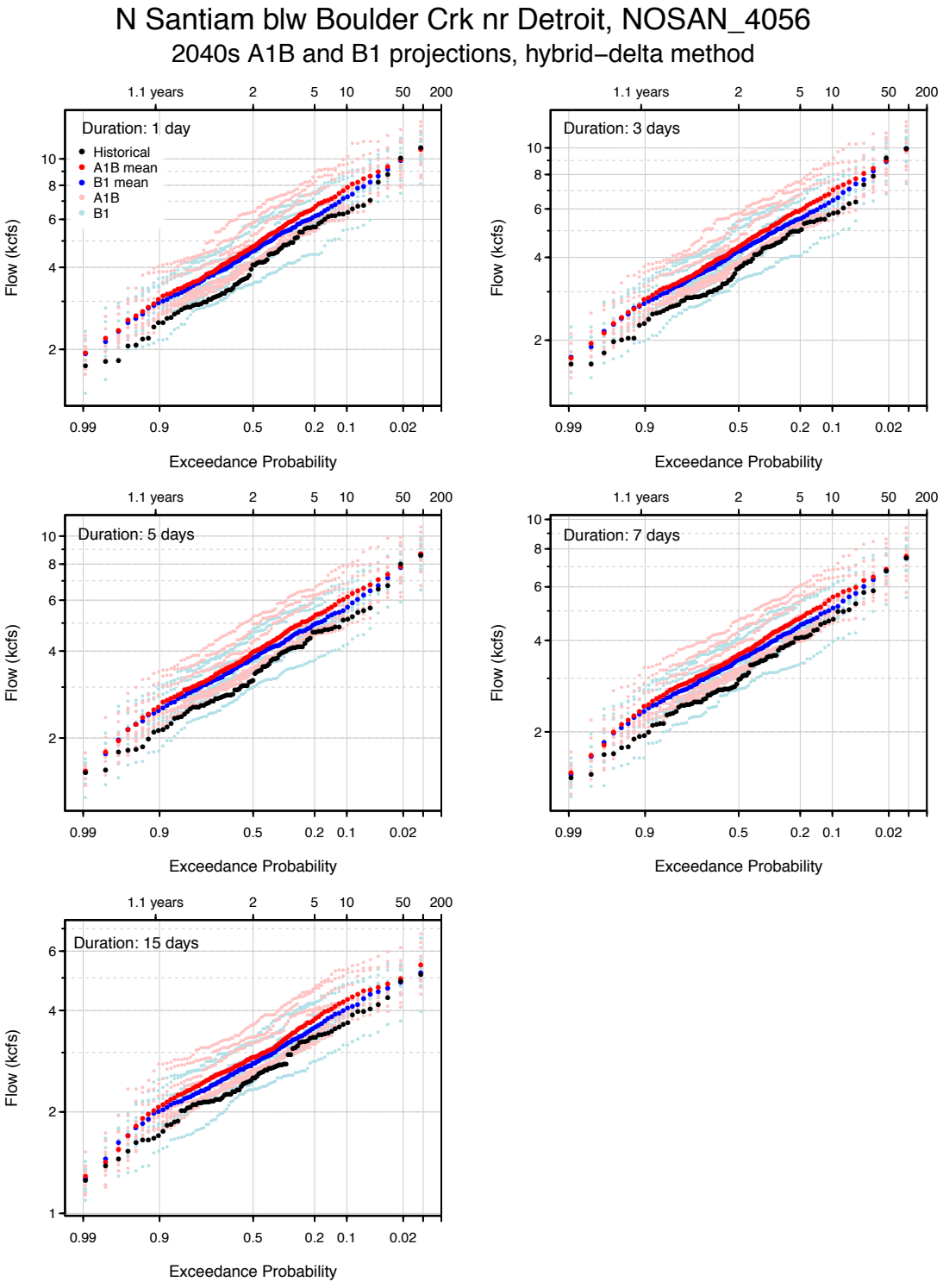

Figure G10. Relative change in flow-duration-frequency curves by annual maximum flow from the historical period and future period (2040s A1B and B1) at N Santiam blw Boulder Crk nr Detroit (NOSAN 4056).

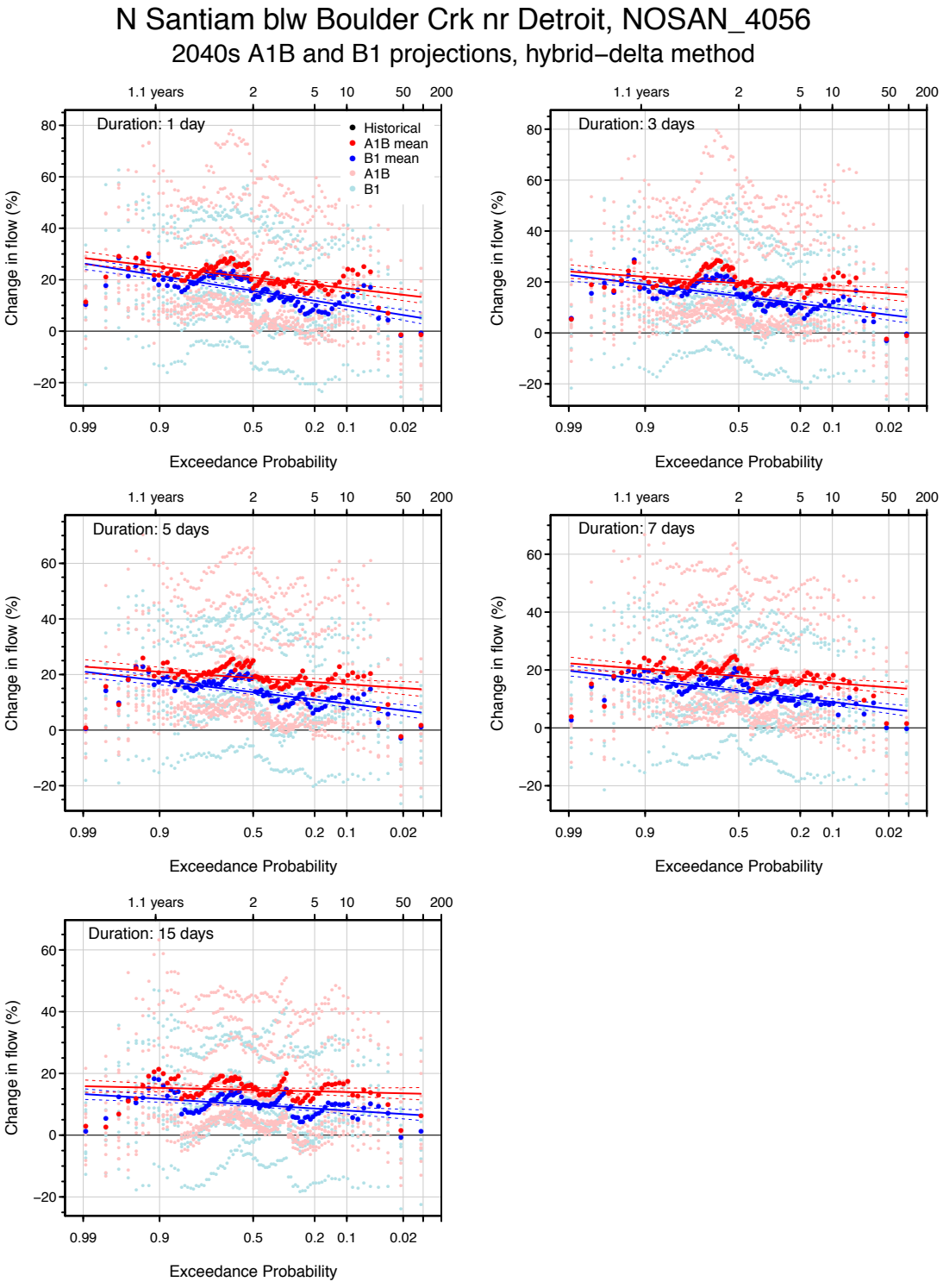

Figure G11. Flow-duration-frequency curves for annual maxima streamflow of 1-, 3-, 5-, 7-, and 15-day durations for the historical period and future periods (2040s A1B and B1) at Clackamas at River Mill Dam (RMILL 4046).

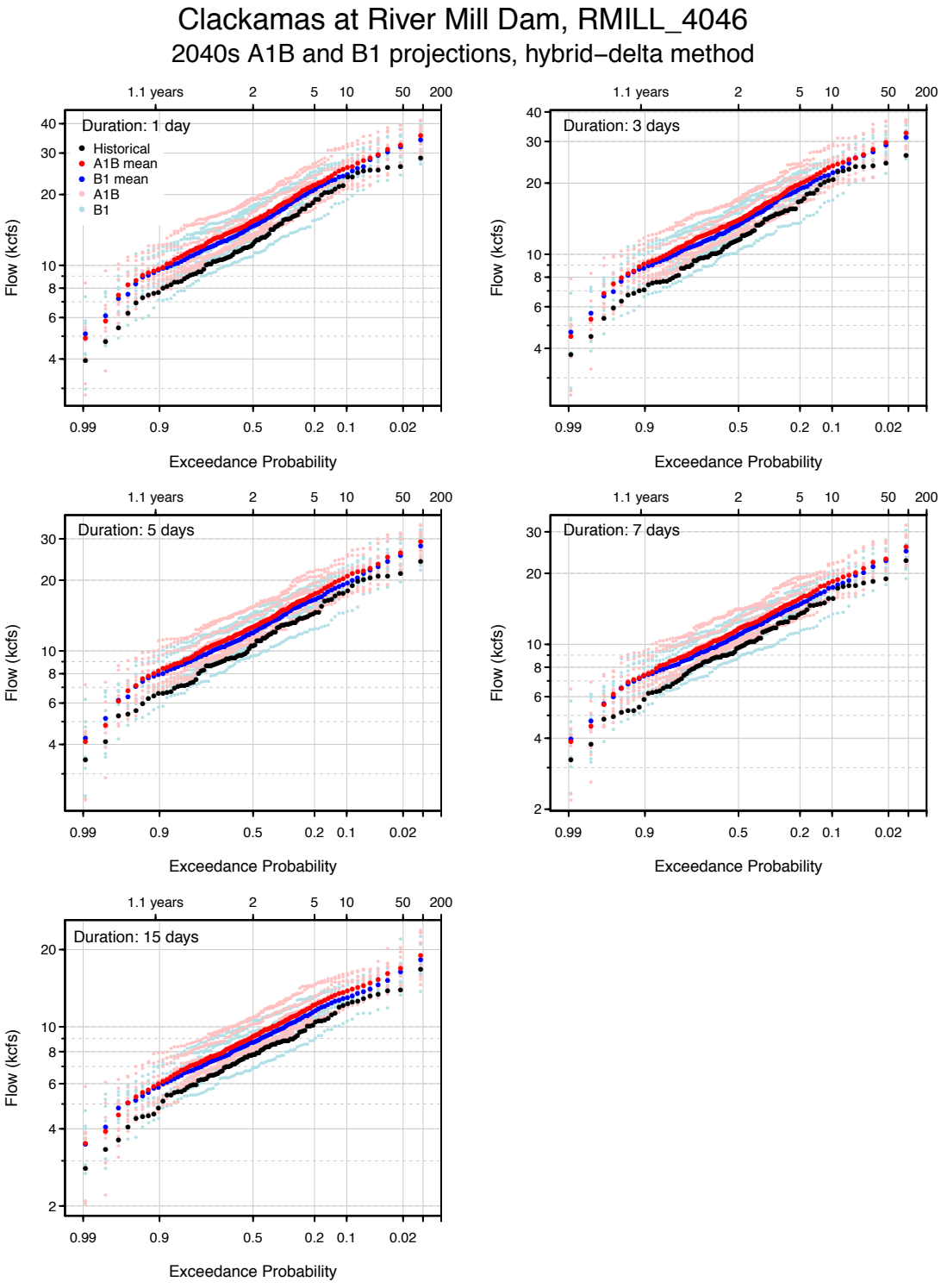

Figure G12. Relative change in flow-duration-frequency curves by annual maximum flow from the historical period and future period (2040s A1B and B1) at Clackamas at River Mill Dam (RMILL 4046).

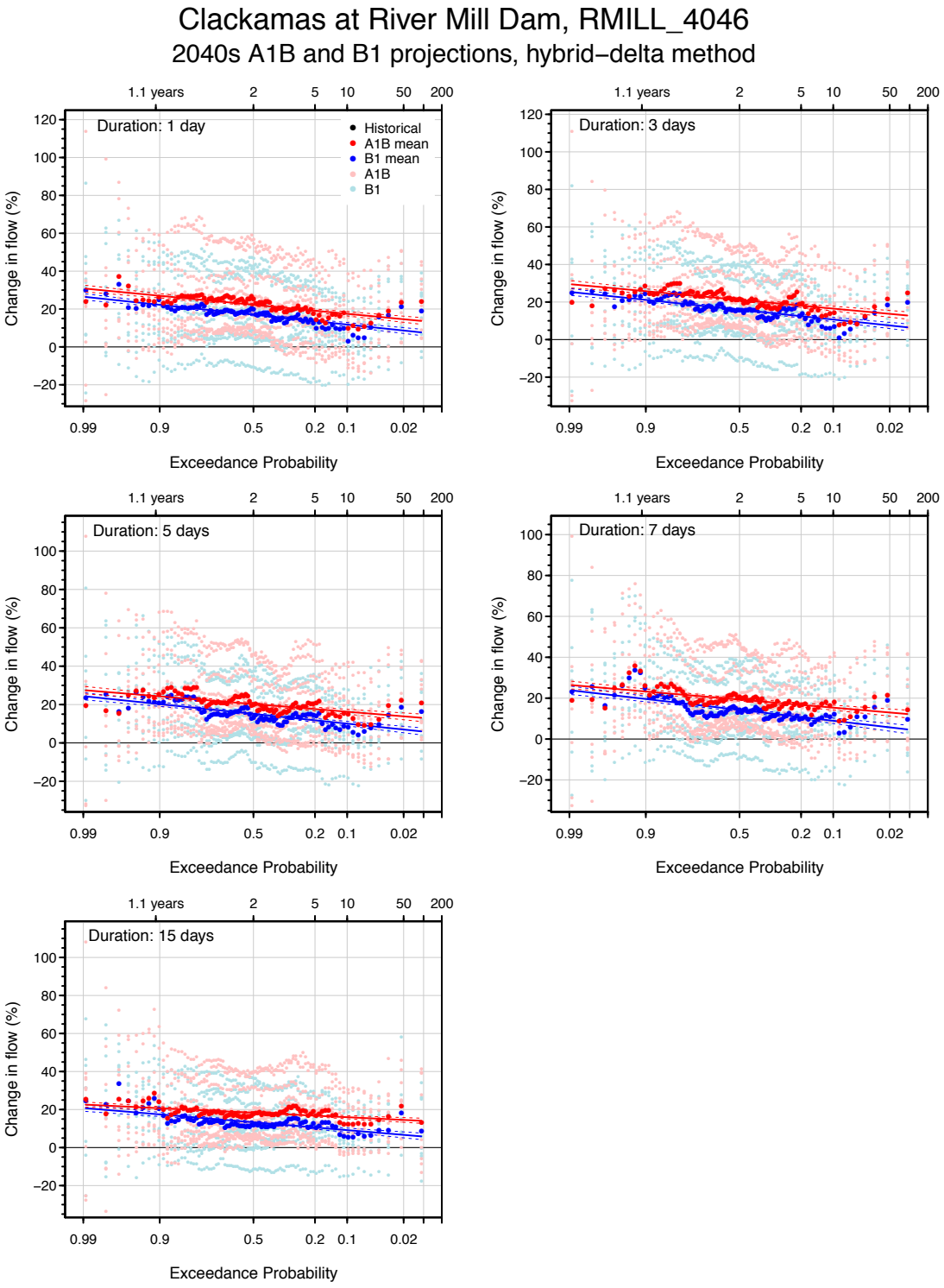

Figure G13. Flow-duration-frequency curves for annual maxima streamflow of 1-, 3-, 5-, 7-, and 15-day durations for the historical period and future periods (2040s A1B and B1) at Row above Pitcher Crk nr Dorena (ROPIT 4035).

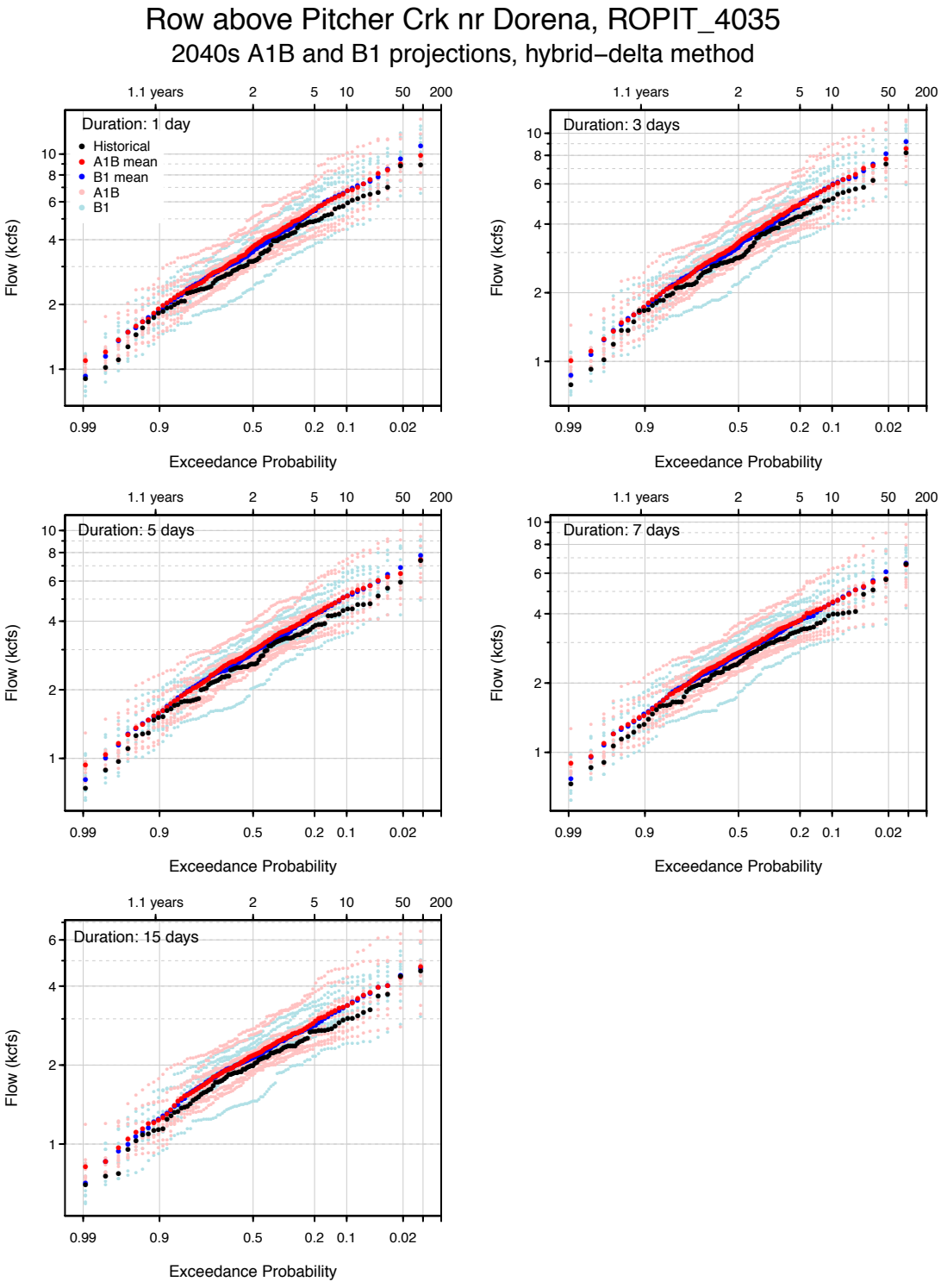

Figure G14. Relative change in flow-duration-frequency curves by annual maximum flow from the historical period and future period (2040s A1B and B1) at Row above Pitcher Crk nr Dorena (ROPIT 4035).

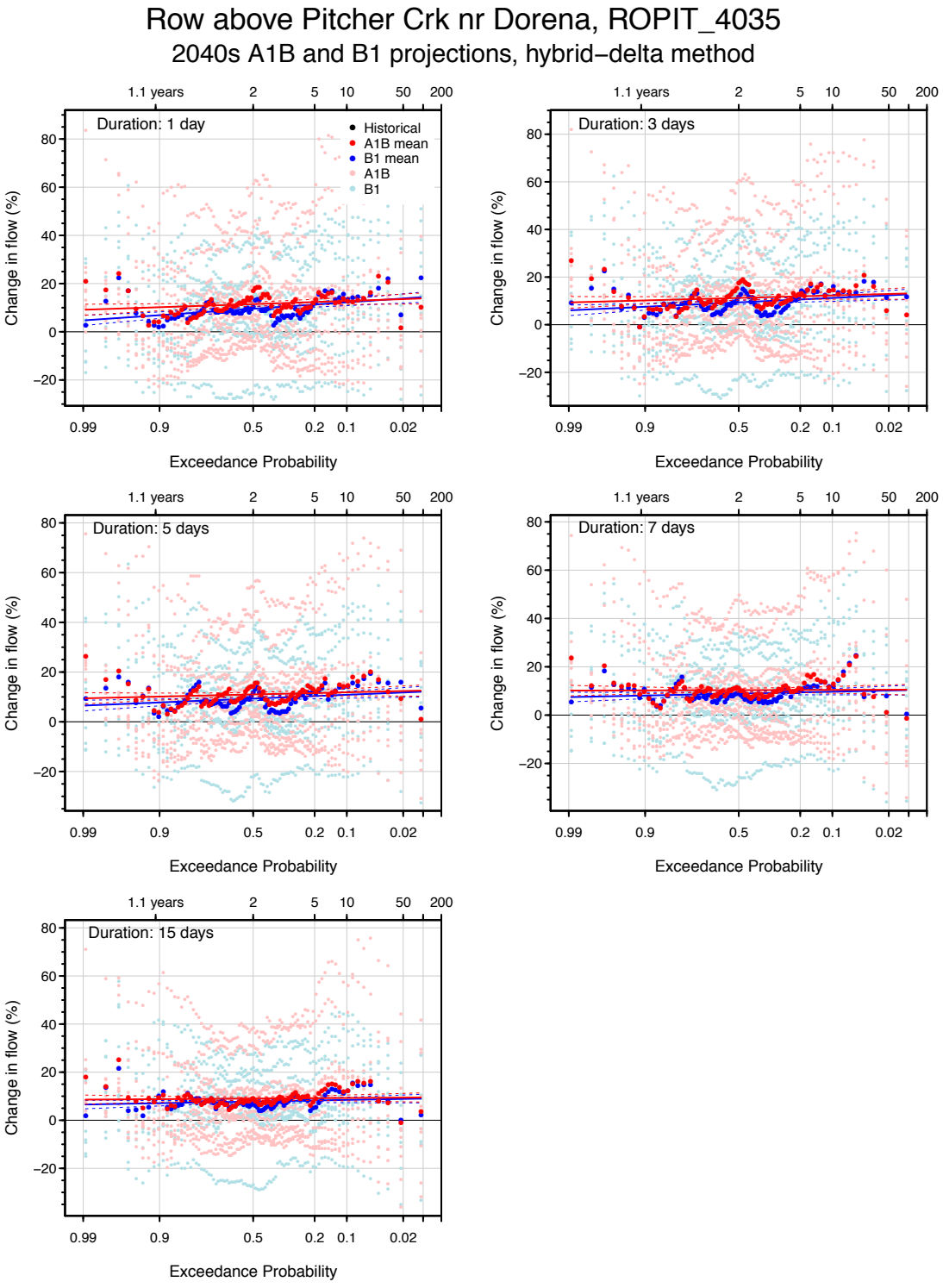

Figure G15. Flow-duration-frequency curves for annual maxima streamflow of 1-, 3-, 5-, 7-, and 15-day durations for the historical period and future periods (2040s A1B and B1) at N Santiam at Mehama (SANME 4039).

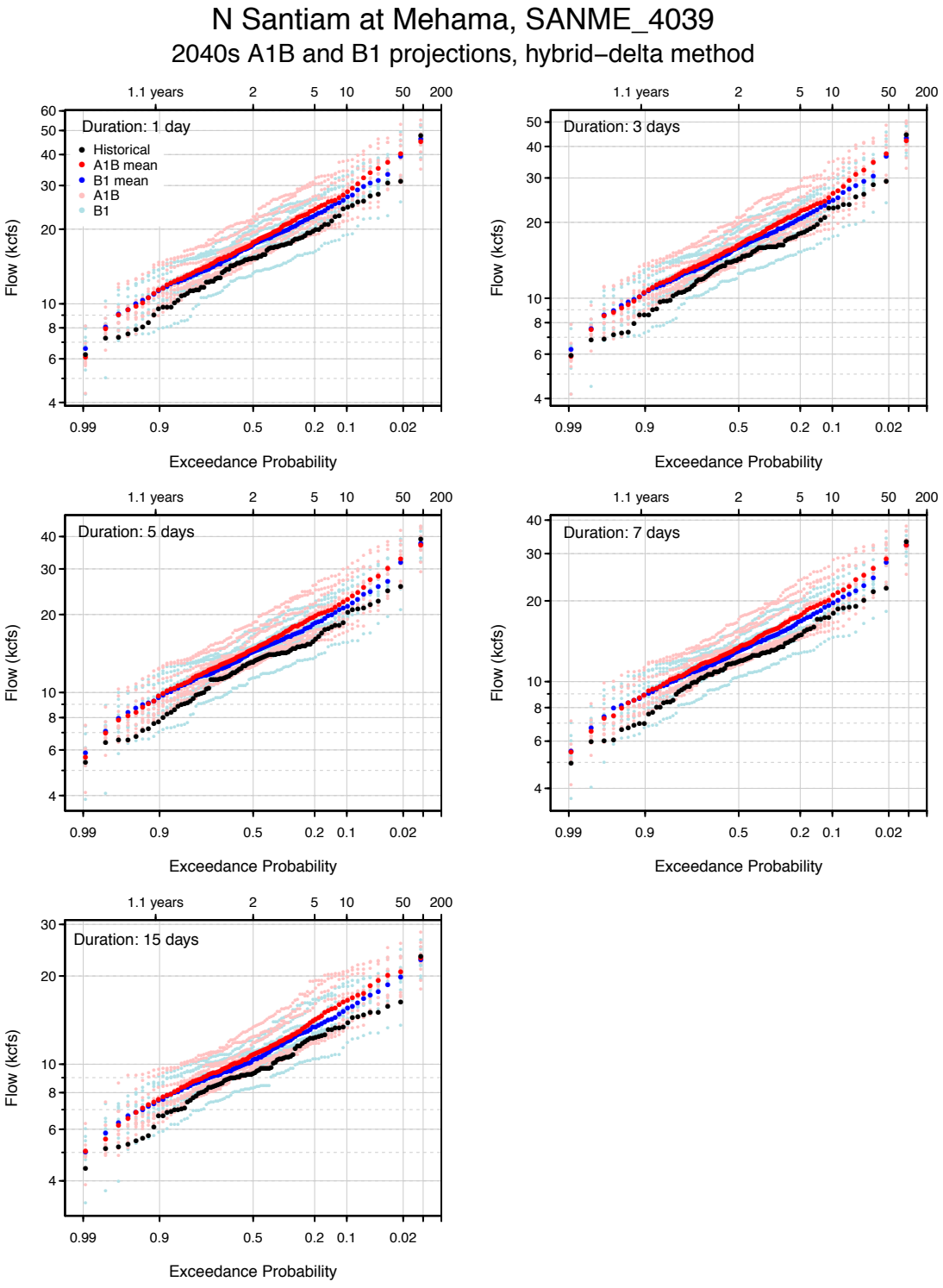

Figure G16. Relative change in flow-duration-frequency curves by annual maximum flow from the historical period and future period (2040s A1B and B1) at N Santiam at Mehama (SANME 4039).

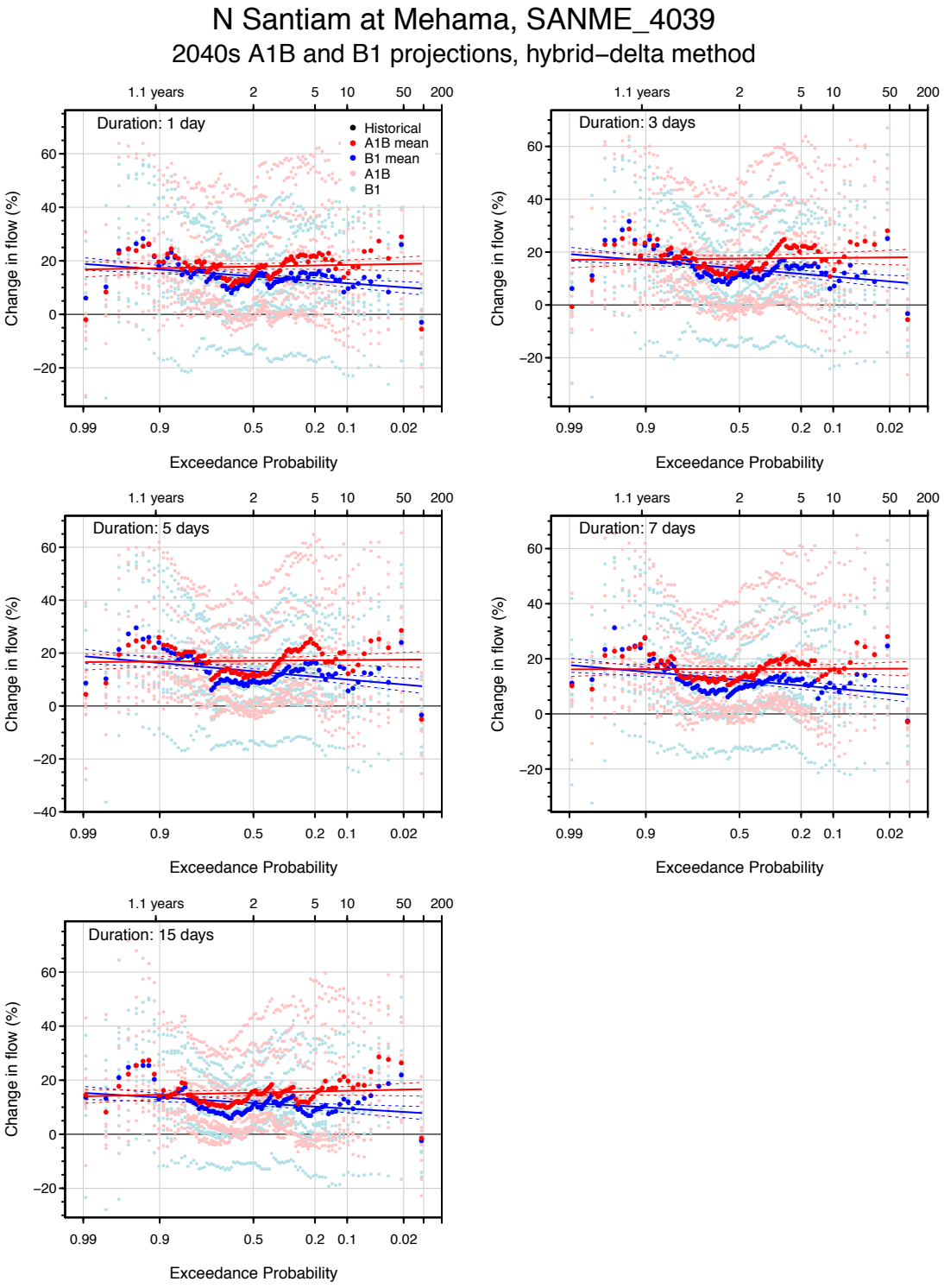

Figure G17. Flow-duration-frequency curves for annual maxima streamflow of 1-, 3-, 5-, 7-, and 15-day durations for the historical period and future periods (2040s A1B and B1) at S Santiam at Waterloo (SANWA 4059).

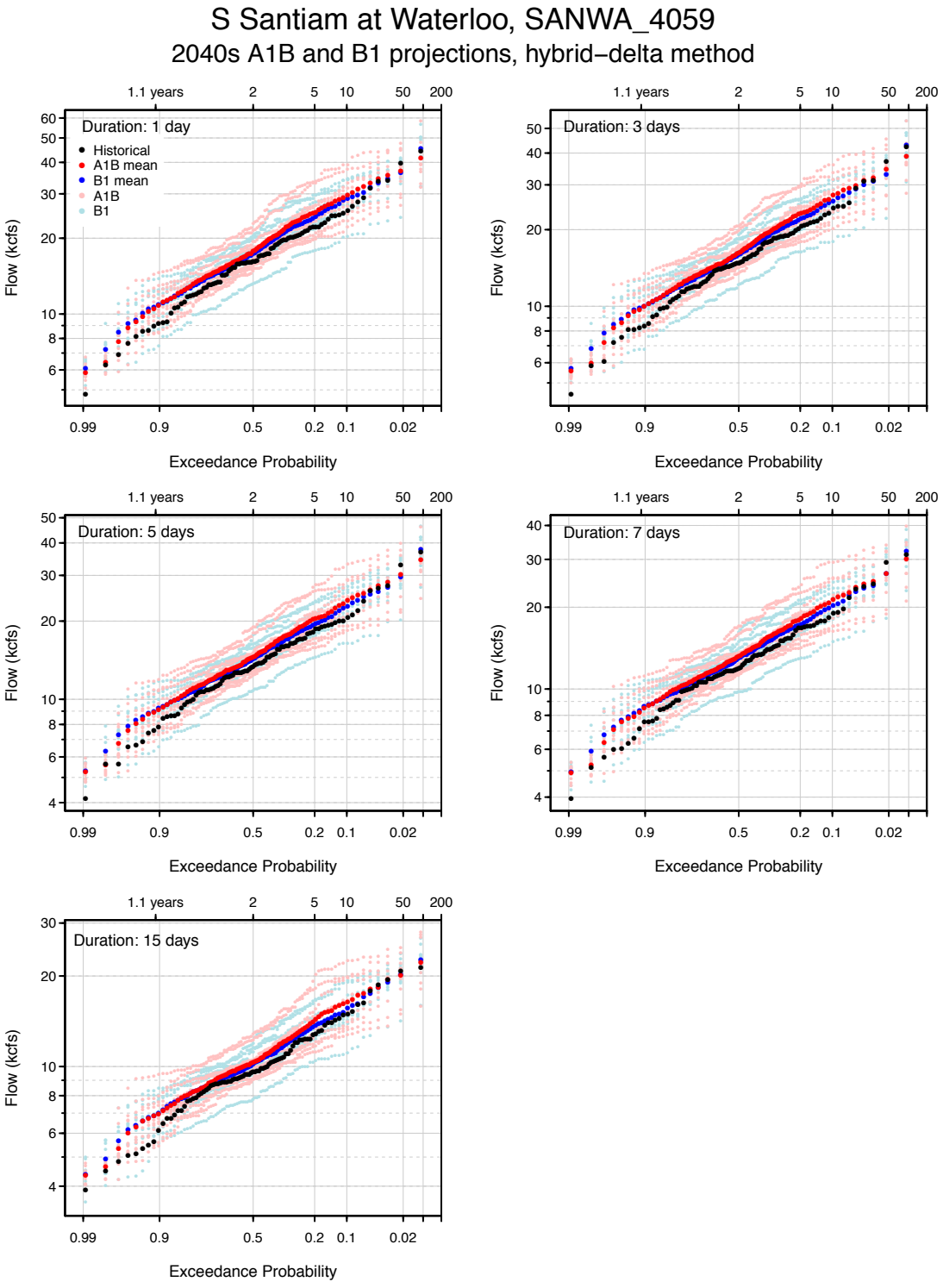

Figure G18. Relative change in flow-duration-frequency curves by annual maximum flow from the historical period and future period (2040s A1B and B1) at S Santiam at Waterloo (SANWA 4059).

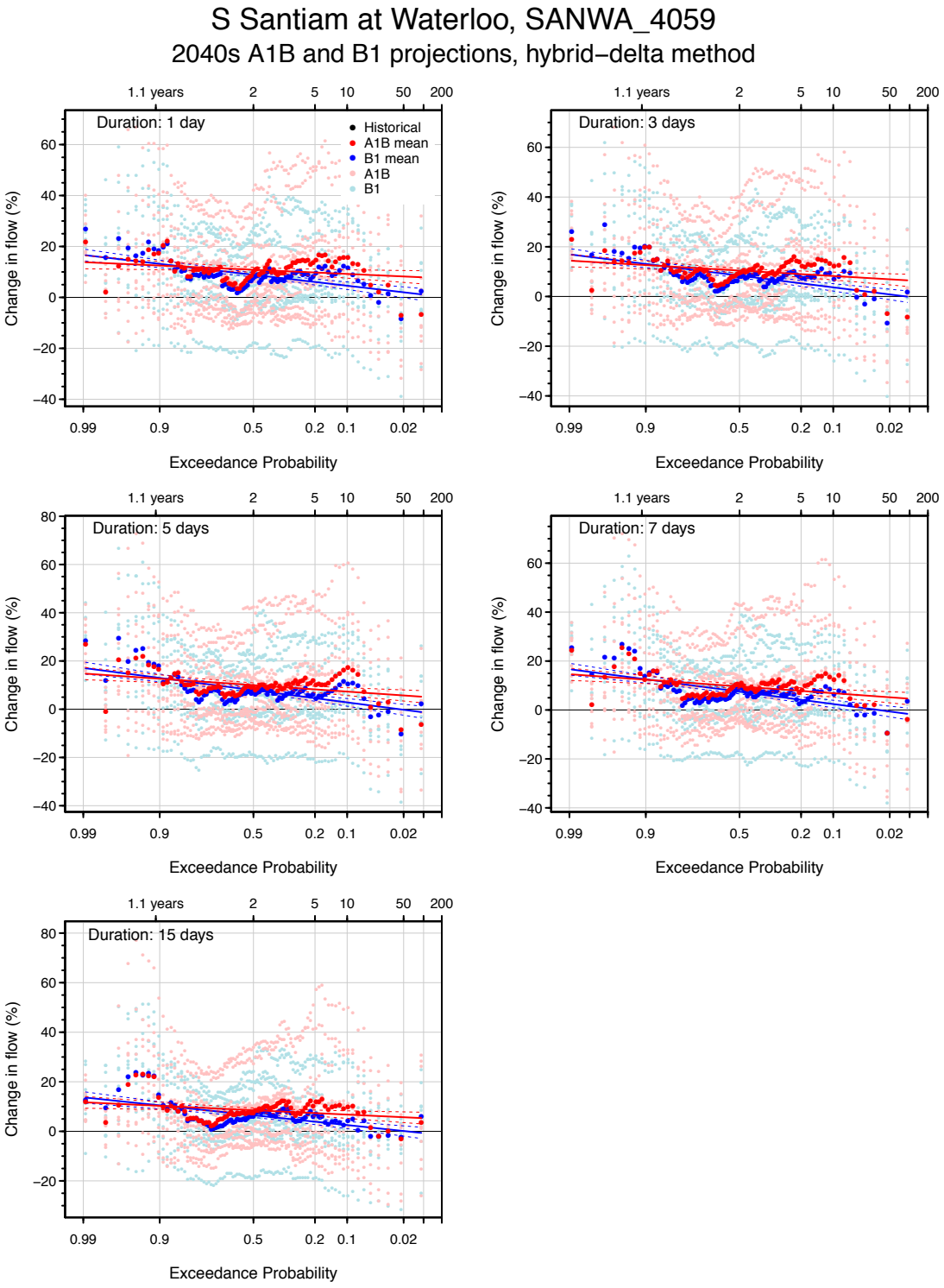

Figure G19. Flow-duration-frequency curves for annual maxima streamflow of 1-, 3-, 5-, 7-, and 15-day durations for the historical period and future periods (2040s A1B and B1) at Willamette abv Falls at Oregon City (WILFA 4064).

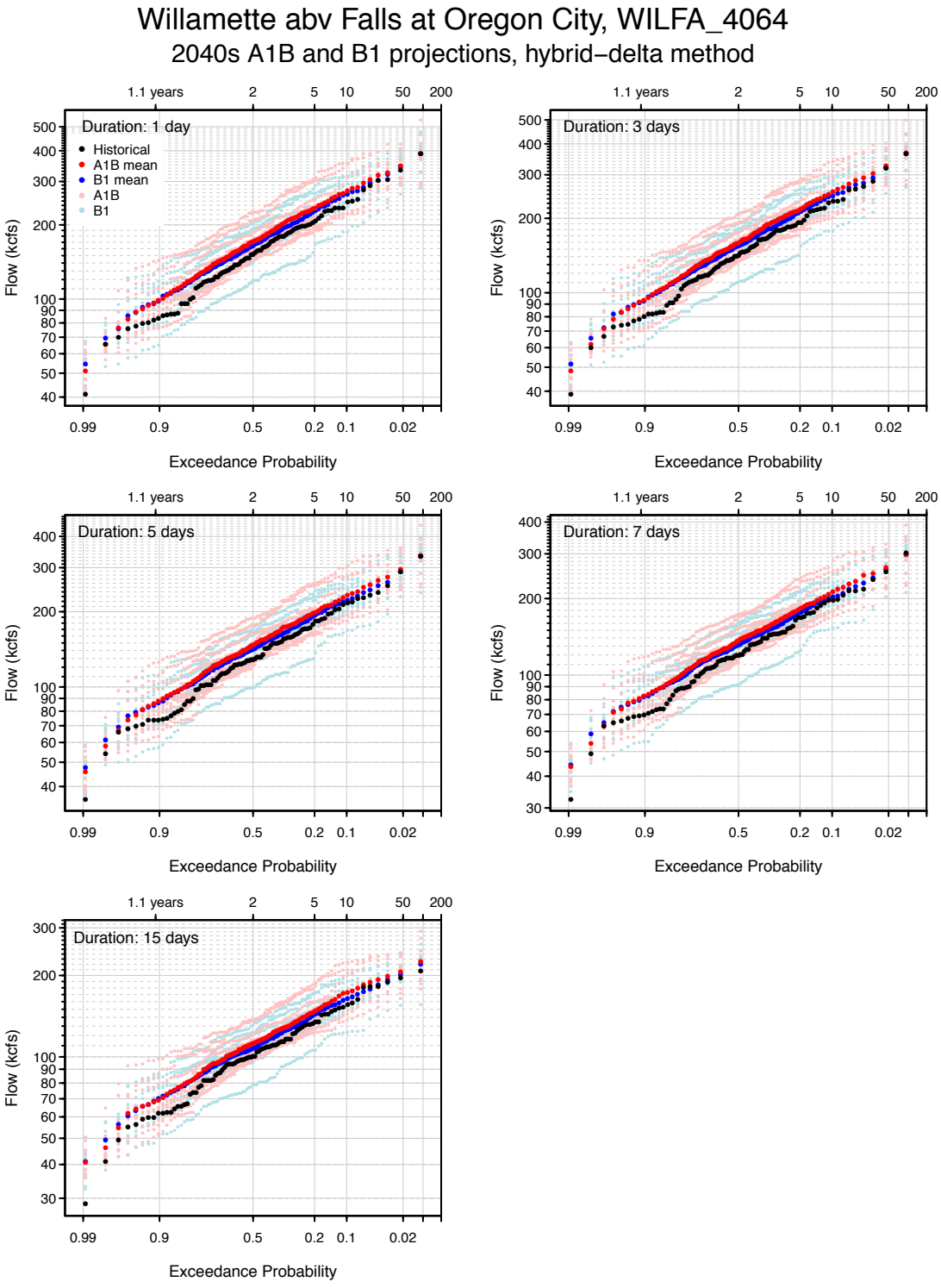

Figure G20. Relative change in flow-duration-frequency curves by annual maximum flow from the historical period and future period (2040s A1B and B1) at Willamette abv Falls at Oregon City (WILFA 4064).

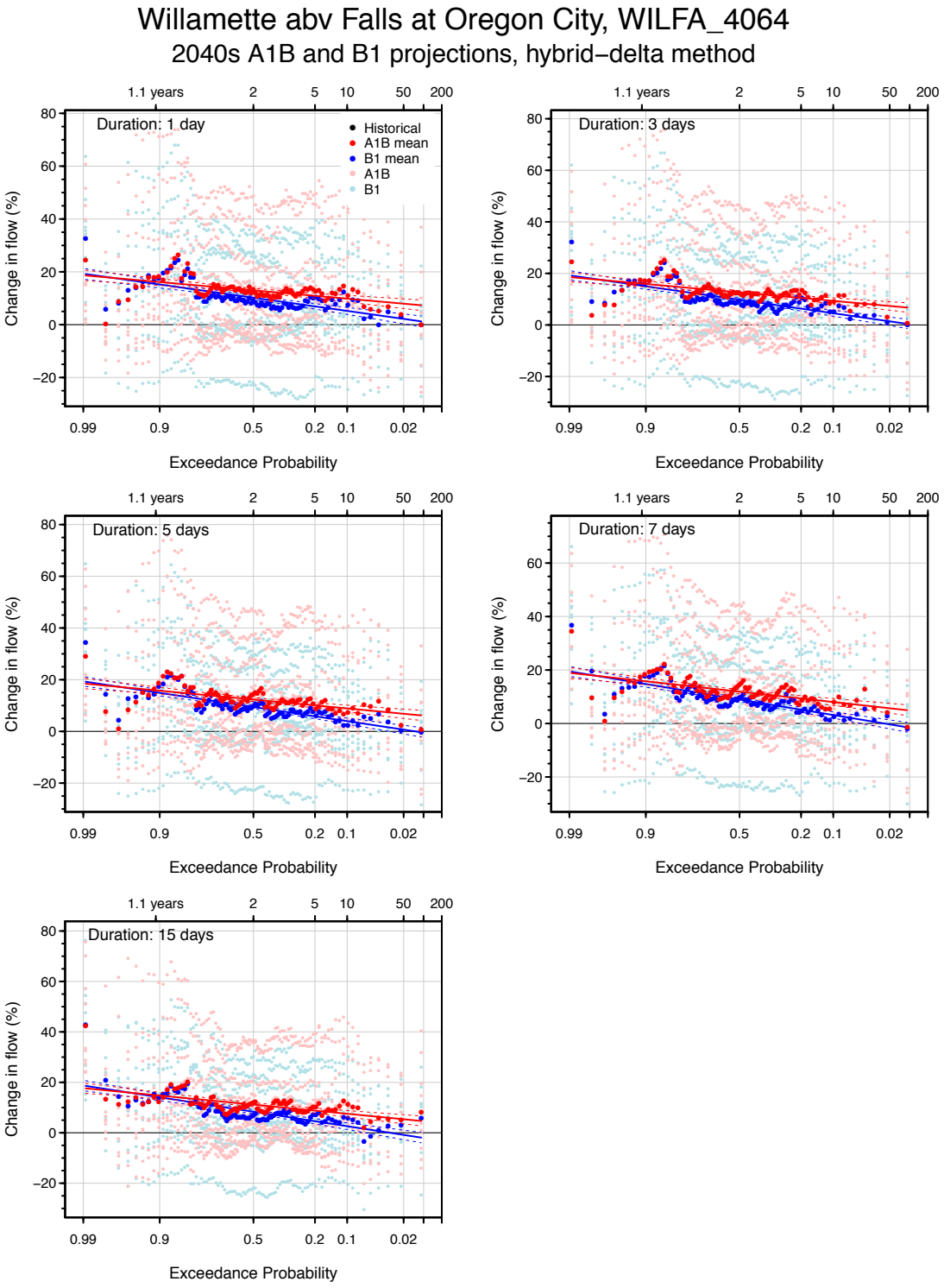

Figure G21. Flow-duration-frequency curves for annual maxima streamflow of 1-, 3-, 5-, 7-, and 15-day durations for the historical period and future periods (2040s A1B and B1) at Middle Fork Willamette blw N Fork nr Oakridge (WILNF 4048).

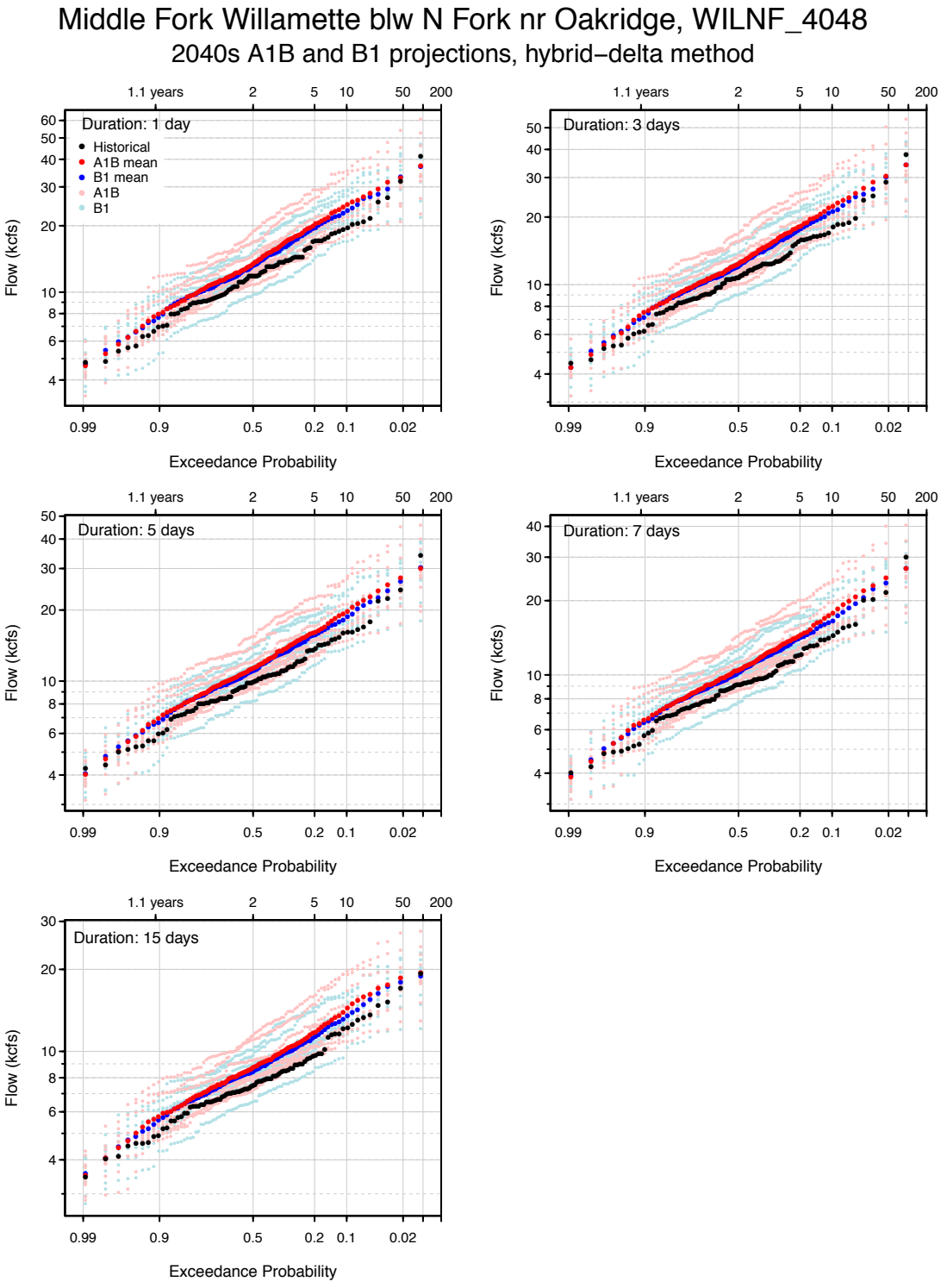

Figure G22. Relative change in flow-duration-frequency curves by annual maximum flow from the historical period and future period (2040s A1B and B1) at Middle Fork Willamette blw N Fork nr Oakridge (WILNF 4048).

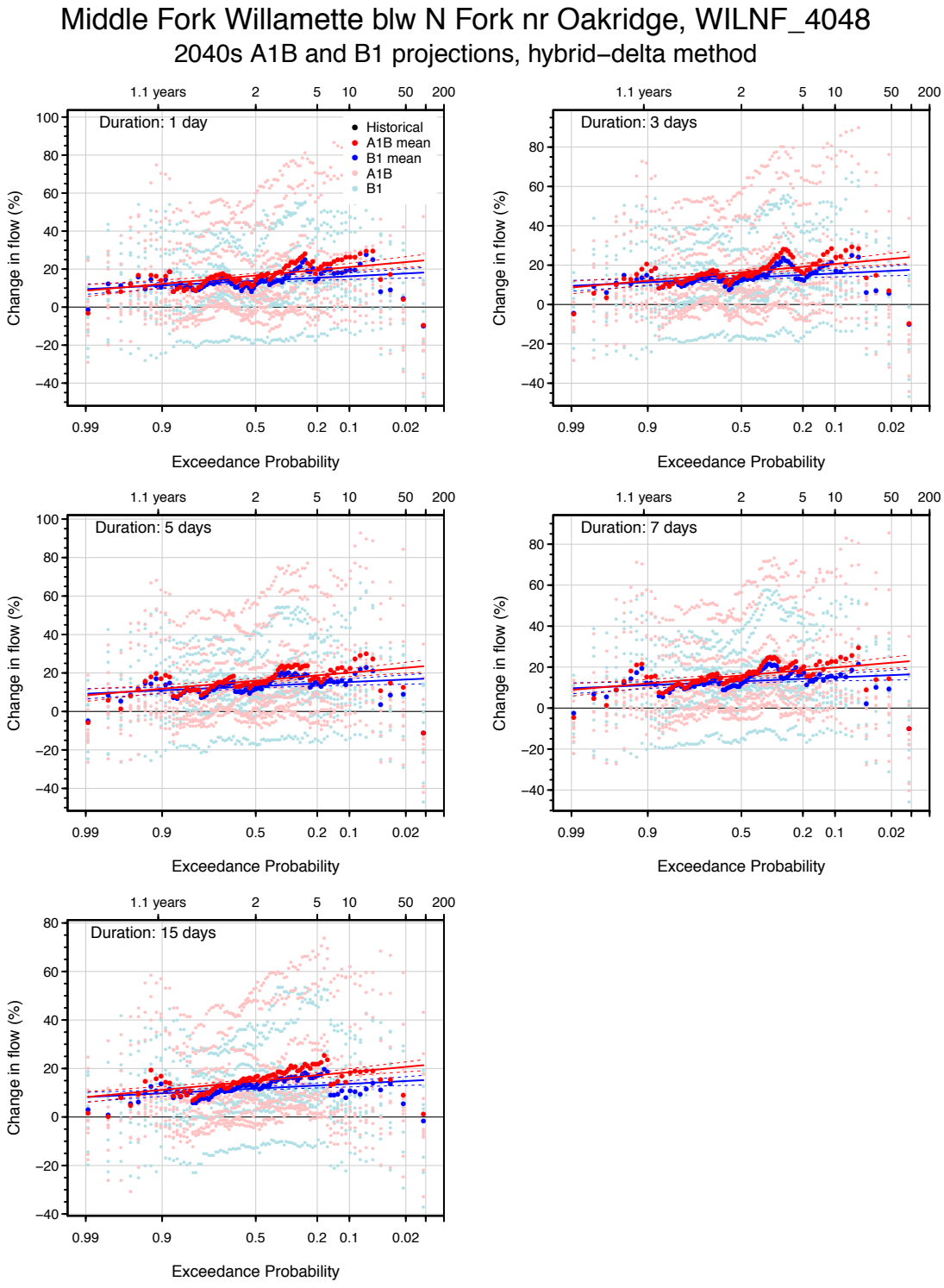

Figure G23. Mean change in date of annual maximum flow from historical period to future periods (2040s A1B and B1) for flow durations of 1, 3, 5, 7, and 15 days.